Ph.D 13175

THE EROSION OF DUCTILE METALS BY SOLID PARTICLE IMPACT

ALAN KENNETH COUSENS
FITZWILLIAM COLLEGE

UNIVERSITY
LIBRARY
CAMBRIDGE

(DISSERTATION FOR THE DEGREE DOCTOR OF PHILOSOPHY)

FEBRUARY 1984

Alan K. Cousens

Fitzwilliam College

Thesis title : The erosion of ductile metals by solid particle impact.

Erosion is a wear process, in which surface damage is caused by the repeated application of high localised stresses. Erosion by solid particle impact is a problem of great practical significance which can result in component failures in, for example, turbines and energy conversion systems.

This dissertation describes experiments in which ductile metal surfaces were eroded with abrasive particles (size range 40 - 600μm) under controlled conditions. Damage to the surface was characterised by weight loss measurements, and also by microscopical examination. Surface and subsurface damage was studied using optical microscopy and also scanning electron microscopy.

As a result of this experimental work a new model of the erosion process, for ductile metals eroded by spherical particles, at normal impingement, is proposed. Analytical techniques were used to investigate the observed surface deformations, and also the energy requirements of the proposed model.

Further experiments were conducted to investigate the effect of erodent particle shape on the erosion of mild steel. A literature survey was completed, which identifies methods which may prove useful in quantifying the shapes of abrasive particles.

A study of the effect of nitrogen ion implantation on the erosion resistance of mild steel was completed. An investigation of indentation parameters provided an explanation for the minimal effects recorded.

The technique of cross correlation has been applied to the problem of measuring the velocity of the erodent particles. A device has been developed to measure the time of flight of particles over a known distance. Data from this device was analysed on a micro-computer.

PREFACE

This dissertation is the result of my own work and includes nothing which is the outcome of work done in collaboration. No part of my dissertation has already been or is being concurrently submitted for any degree, diploma or other qualification. Where the work of others is referred to, the date of publication is stated in parentheses, and full details are listed in a bibliography.

I would like to express my thanks to those who have helped me in the course of my research: to my Supervisor Dr I M Hutchings for his guidance and encouragement (and for supplying the specimens referred to in Table 6.2): to Prof. R W K Honeycombe for the provision of laboratory facilities: to the Science and Engineering Research Council for financial support: and to Mr K Page and Mr R Home of the Dept. of Metallurgy and Materials Science for help with the design and construction of the electronic circuitry described in Chapter 5.

Special thanks are expressed to Mrs B E Cousens for typing this dissertation, and to Mr and Mrs N Davis for help with the proof-reading.

Finally, thanks are especially due to my wife for the long hours spent helping to prepare this dissertation.

A K Cousens

A K Cousens
February 1984

PREFACE

This dissertation is the result of my own work and includes nothing which is the outcome of work done in collaboration. No part of my dissertation has already been or is being concurrently submitted for any degree, diploma or other qualification. Where the work of others is referred to, the date of publication is stated in parentheses, and full details are listed in a bibliography.

I would like to express my thanks to those who have helped me in the course of my research: to my Supervisor Dr I M Hutchings for his guidance and encouragement (and for supplying the specimens referred to in Table 6.2): to Prof. R W K Honeycombe for the provision of laboratory facilities: to the Science and Engineering Research Council for financial support: and to Mr K Page and Mr R Home of the Dept. of Metallurgy and Materials Science for help with the design and construction of the electronic circuitry described in Chapter 5.

Special thanks are expressed to Mrs B E Cousens for typing this dissertation, and to Mr and Mrs N Davis for help with the proof-reading.

Finally, thanks are especially due to my wife for the long hours spent helping to prepare this dissertation.

A K Cousens

A K Cousens
February 1984

C O N T E N T S

CHAPTER 1 : INTRODUCTION AND LITERATURE SURVEY OF EXPERIMENTAL STUDIES

1.1 INTRODUCTION

In common use the word 'erosion' describes a wear process, for example the process by which the landscape is shaped by the wearing away of rocks. The root of the word is the latin verb 'rodere', which means 'to gnaw'. In the disciplines of materials science and engineering the term 'erosion' is used to describe a specific type of wear.

Finnie (1967) stated 'The removal of material from a solid surface by the action of impinging solid or liquid particles is known as erosion'. This definition is however too specific, and excludes processes which can correctly be termed erosion.

Tabor (1979) spoke in more general terms, addressing a conference on erosion. 'Erosion usually involves the repeated application of high local stresses. In many cases the individual stresses are applied for very short intervals of time'.

With characteristic thoroughness the American Society for Testing and Materials (1977) defined erosion as 'progressive loss of original material from a solid surface due to the mechanical interaction between that surface and a fluid, a multicomponent fluid, or impinging liquid or solid particles'. A.S.T.M. chooses its words carefully in order to include all three of the fundamentally different types of erosive wear : erosion by solid particle impingement, erosion by liquid drop impingement, and erosion by cavitating liquids. The expression 'mechanical interaction' is chosen to isolate erosion from the chemical

UNIVERSITY
LIBRARY
CAMBRIDGE

interaction of corrosion; however in the great majority of instances erosion will occur in conjunction with corrosion. The types of erosive wear can be further subdivided; for instance, erosion by solid particle impingement includes wear by dust particles entrained in gas streams and also slurry erosion (wear by particles suspended in a liquid). These two subtypes will differ greatly in the actual mode of wear. The former will in general involve much higher particle velocities, while the latter may be accompanied by significant corrosion and cavitation erosion.

The removal of material by an erosive process can lead to component failures, and thus the study of erosion can be motivated by the need to increase a material's erosion resistance. Conversely the same process of wear may be utilised for cutting or cleaning materials. In this instance the study of erosion will be directed towards controlling and maximising the removal of material.

Limited world resources have necessitated vast changes in energy extraction methods in industry. Erosion problems occur at all stages in the extraction of energy from mineral resources, from mining or drilling through to energy conversion systems. Oil cracking involves the transport of a catalyst which is deposited on the surface of finely divided, inert and also abrasive powders. Extraction of energy from coal involves the transport both of the pulverised fuel, before combustion, and also its ash after combustion.

The present study is limited to erosion by solid particle impact, and concentrates on the erosion of ductile metals by particles entrained in gas streams. Mechanisms of erosion which occur only in brittle materials, for example ceramics, are outside the scope of this study and are not discussed.

This dissertation commences by presenting a survey of the relevant literature; for clarity this survey is divided into three sections. The remainder of this chapter is devoted to an overview of the literature describing experimental studies of erosion. Several mechanisms of the erosion process have been proposed; these are reviewed in Chapter 2. The third chapter presents more detailed literature surveys on the specific topics which were selected as subjects for the present study. In this way the first two chapters introduce the erosion of ductile materials in general terms, whilst Chapter 3 provides a detailed introduction to the present work.

1.2 LITERATURE SURVEY

1.2.1 Erosion Testing

The majority of experiments reported in the literature involve the use of an erosion test apparatus. This apparatus will project a single particle, or a stream of particles onto a flat specimen : impact angle, particle size, and particle velocity are controlled during the experiment. Field or service trials are sometimes conducted; Goodwin (1968) reported details of field trials on helicopter engines, and Mills and Mason (1979) reported service trials on pipework sections. This type of trial is especially suitable for materials selection, but provides limited fundamental information. In Chapter 5 full details are presented of the types of erosion test apparatus in common use.

Experimental studies commonly involve the measurement of specimen mass or volume change. Figure 1.1 shows a cumulative mass loss plot, which records the specimen's mass change with increasing exposure to the

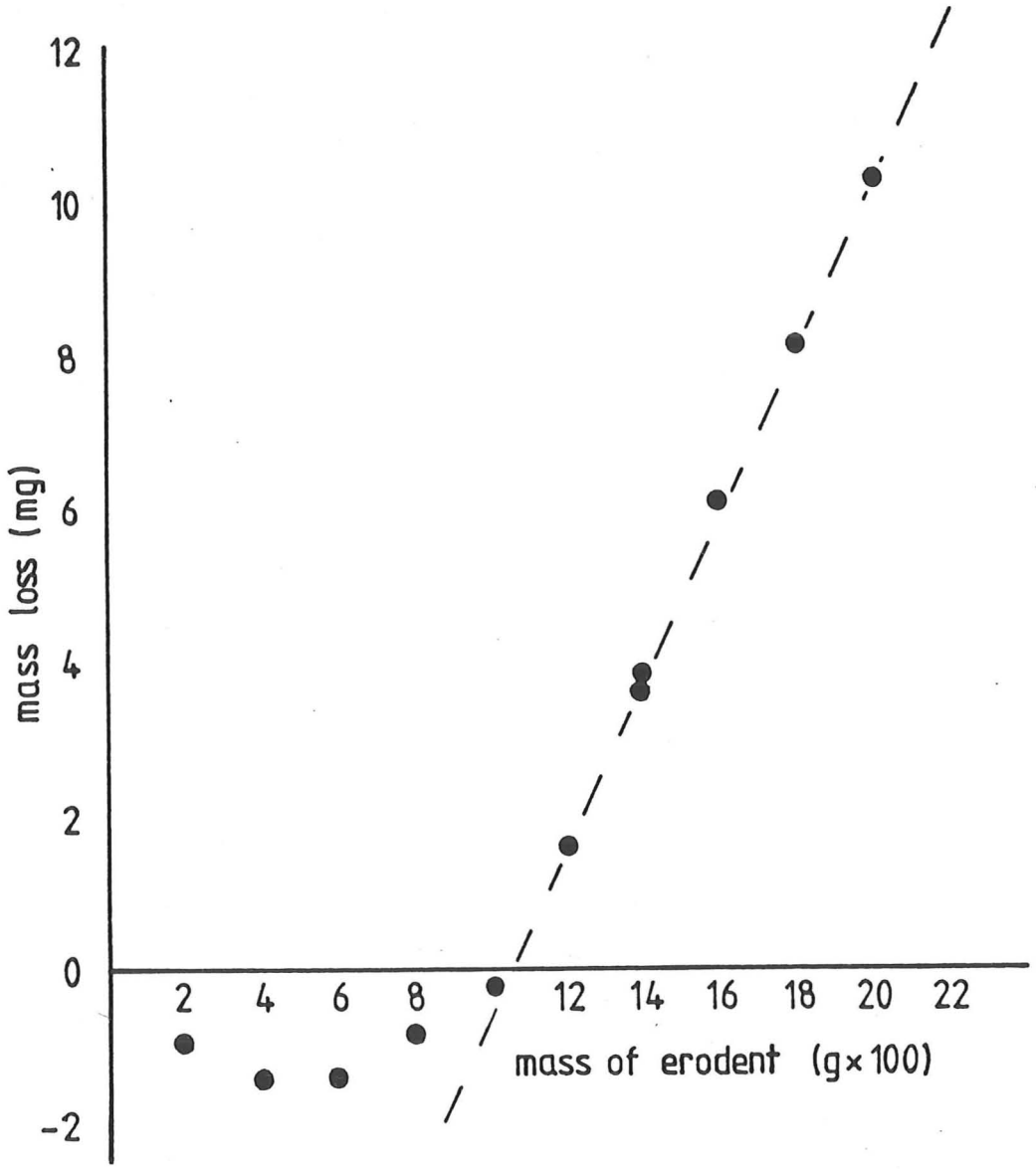

Figure 1.1 : Cumulative mass loss curve for precipitation hardened aluminium alloy (HE15) eroded by 400-600μm spherical glass beads at normal impingement. (Dotted line indicates steady state erosion.)

abrasive particle stream. Initially the rate of material removal from the surface is very low. Some specimens, as shown in Figure 1.1, may first gain mass initially, before mass loss occurs, at an increasing rate. The mass loss rate increases until a steady rate of wear is established; this is shown by the straight line in Figure 1.1. The initial behaviour, before steady state erosion is established, is known as 'incubation'.

It is common to quote the slope of the steady state region of the cumulative mass loss curve as a value of erosion rate. This slope is a dimensionless value, being mass loss per unit mass of abrasive. Occasionally, alternative expressions for erosion rate are used, for example volume removed per unit volume of abrasive or volume removed per unit mass of abrasive (Sheldon (1977)). Other measurements of erosion resistance have been suggested which are specific to an erosion test method. An example of such a measurement, dependent upon the geometry of the experiment, is the midpoint recession rate quoted by Sherman et al (1979); this value has units of ms^{-1}. A knowledge of the mass of abrasive impinging per unit time on unit area of the specimen, together with the specimen's density, will allow the conversion of this 'midpoint recession value' to the more conventional, dimensionless value. The dimensionless erosion value allows meaningful comparisons to be readily made between erosion tests conducted by different experimenters, and, because mass loss is a relatively simple measurement to make, this value is generally favoured.

1.2.2 Experimental Variables

(a) Angle of attack

For all types of material it is found that the erosion rate depends on the angle between the target surface and the stream of particles, known as the angle of attack. Figure 1.2, taken from Finnie et al (1967), is frequently reproduced in the literature. It shows schematically the typical response of ductile and brittle materials to varying angles of attack. The brittle response is found in the erosion of ceramics and glasses, but is also reported for certain metals. Wellinger (1949) reported that hard steels behaved in a brittle manner, as defined by the angular response in Figure 1.2. Softer steels behaved in the ductile mode. The A.S.T.M. standard terminology (A.S.T.M. (1977)) states that 'With brittle erosion the maximum volume removal occurs at an angle near 90 degrees, in contrast to approximately 25 degrees for ductile erosion behaviour'.

Neilson and Gilchrist (1968) reported the dependence of erosion on angle of attack for a range of materials. They too found brittle and ductile responses, but also reported that certain materials, for example graphite and polymethylmethacrylate (Perspex) behave in a more complex manner. They interpreted this behaviour by decomposing the response curves into brittle and ductile components. Their work was a development of that of Bitter (1963), details of which are presented in Chapter 2.

Gulden (1979) used the variation of erosion rate with angle of attack to investigate the behaviour of certain high-carbon martensitic steels. She reported a transition from ductile to brittle behaviour as a result of heat treatment, or at a critical size of impacting particle.

1.2.2 Experimental Variables

(a) Angle of attack

For all types of material it is found that the erosion rate depends on the angle between the target surface and the stream of particles, known as the angle of attack. Figure 1.2, taken from Finnie et al (1967), is frequently reproduced in the literature. It shows schematically the typical response of ductile and brittle materials to varying angles of attack. The brittle response is found in the erosion of ceramics and glasses, but is also reported for certain metals. Wellinger (1949) reported that hard steels behaved in a brittle manner, as defined by the angular response in Figure 1.2. Softer steels behaved in the ductile mode. The A.S.T.M. standard terminology (A.S.T.M. (1977)) states that 'With brittle erosion the maximum volume removal occurs at an angle near 90 degrees, in contrast to approximately 25 degrees for ductile erosion behaviour'.

Neilson and Gilchrist (1968) reported the dependence of erosion on angle of attack for a range of materials. They too found brittle and ductile responses, but also reported that certain materials, for example graphite and polymethylmethacrylate (Perspex) behave in a more complex manner. They interpreted this behaviour by decomposing the response curves into brittle and ductile components. Their work was a development of that of Bitter (1963), details of which are presented in Chapter 2.

Gulden (1979) used the variation of erosion rate with angle of attack to investigate the behaviour of certain high-carbon martensitic steels. She reported a transition from ductile to brittle behaviour as a result of heat treatment, or at a critical size of impacting particle.

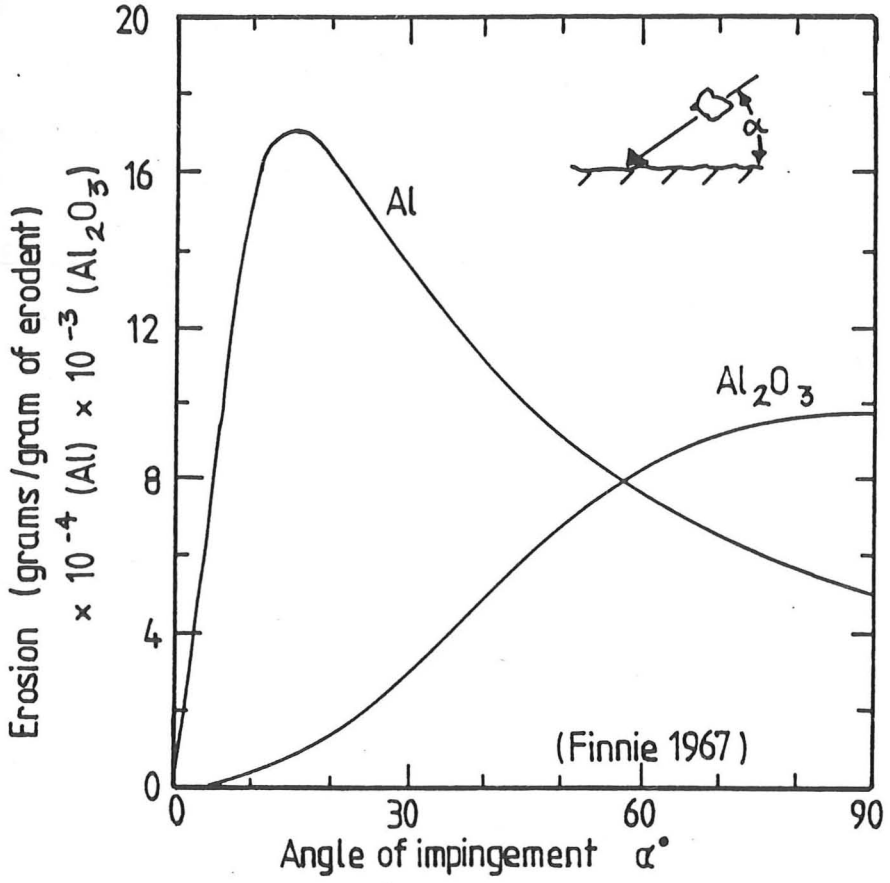

Figure 1.2 : Erosion vs angle of impingement. (After Finnie et al (1967))

In Chapter 8 a study is presented of the erosion response of mild steel. A transition from ductile to brittle erosion behaviour, as defined by the dependence of erosion on impact angle, is investigated using optical and scanning electron microscopy.

(b) Particle velocity

Figure 1.3 (taken from Ives and Ruff (1979)) shows a typical set of erosion test results. For a given angle of attack, it can be seen that increasing the particle velocity greatly increases the slope of the linear region of the cumulative mass loss curve (the steady state erosion rate). (Note : the erosion rate for an attack angle of 20^{o} is higher than that at 90^{o}, for both velocities. Following the convention described in section (a) above, this material displays ductile erosion behaviour.)

It is generally accepted that there exists an empirical relationship between erosion E (expressed by the dimensionless mass loss/mass erodent) and particle velocity V, such that

$$E \propto V^{n}$$

Experiments reveal that n is greater than the value of 2, which simple energy balance considerations would predict.

Velocity exponents have been measured for a variety of materials and experimental conditions, but the true significance of the exponent has not been determined conclusively. It appears not to depend solely on the type of material (Goodwin (1968)), but is sensitive to particle size (Goodwin (1968), Scattergood et al (1981)), attack angle (Ives and Ruff (1979)) and temperature (Ruff and Wiederhorn (1979)).

In Chapter 8 a study is presented of the erosion response of mild steel. A transition from ductile to brittle erosion behaviour, as defined by the dependence of erosion on impact angle, is investigated using optical and scanning electron microscopy.

(b) Particle velocity

Figure 1.3 (taken from Ives and Ruff (1979)) shows a typical set of erosion test results. For a given angle of attack, it can be seen that increasing the particle velocity greatly increases the slope of the linear region of the cumulative mass loss curve (the steady state erosion rate). (Note : the erosion rate for an attack angle of 20^{o} is higher than that at 90^{o}, for both velocities. Following the convention described in section (a) above, this material displays ductile erosion behaviour.)

It is generally accepted that there exists an empirical relationship between erosion E (expressed by the dimensionless mass loss/mass erodent) and particle velocity V, such that

$$E \propto V^{n}$$

Experiments reveal that n is greater than the value of 2, which simple energy balance considerations would predict.

Velocity exponents have been measured for a variety of materials and experimental conditions, but the true significance of the exponent has not been determined conclusively. It appears not to depend solely on the type of material (Goodwin (1968)), but is sensitive to particle size (Goodwin (1968), Scattergood et al (1981)), attack angle (Ives and Ruff (1979)) and temperature (Ruff and Wiederhorn (1979)).

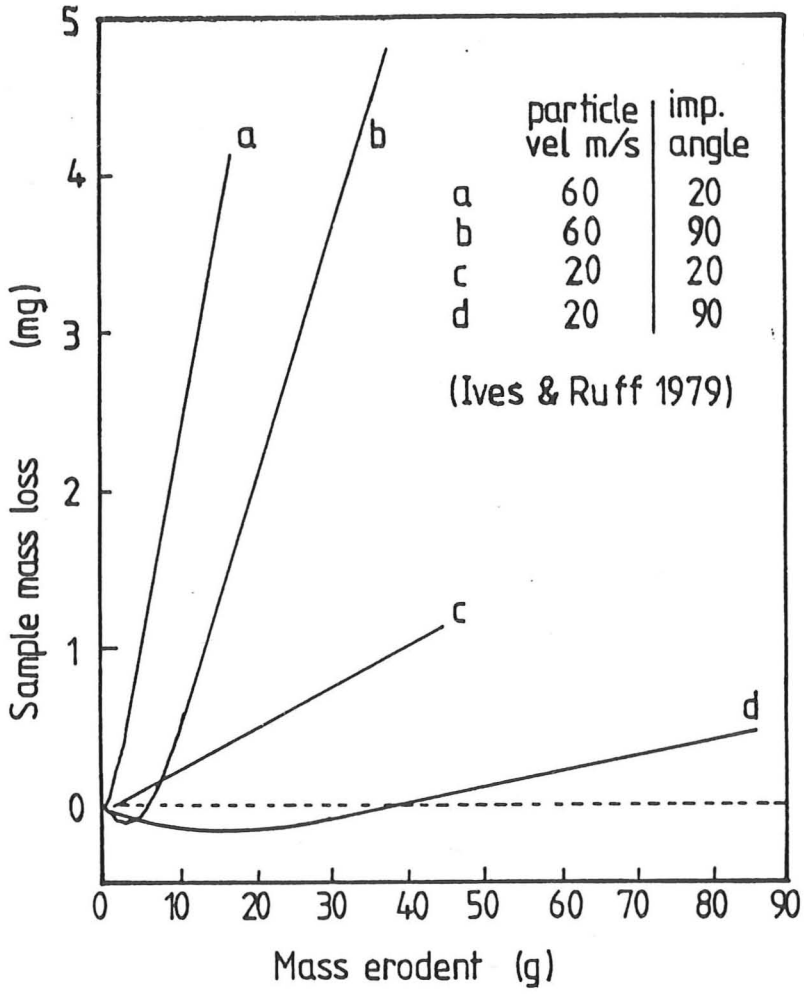

Figure 1.3 : Erosion vs particle velocity for copper eroded at two different angles of impingement. (After Ives and Ruff (1979))

In their general review Preece et al (1977) reported values of velocity exponents for metals of between 2.0 and 3.4. For glasses, ceramics, polymers and polymeric composites the range 2.0 - 6.5 was reported.

Several proposed mechanisms of erosive wear are discussed in Chapter 2. The velocity exponent predicted by any theoretical model for erosion should be compared with the average value of 2.4 found empirically for ductile metals.

(c) Environment

Erosive environments commonly involve both high temperatures and corrosive conditions, as is the case in gas turbines and coal gasification and liquefaction processes. While a study of corrosion is outside the scope of this investigation, it is recognised that the process of corrosion will alter the surface properties of materials. The form of the oxide layer on the surface of a metal, for instance, will greatly influence the rate of surface removal by erosion, and even the operating mechanism of erosive wear. Vyas (1979) can be consulted for a review of the erosion-corrosion literature.

High temperatures will both increase corrosion rates and alter the mechanical properties of materials. It is clear from the literature that there is no simple relationship between erosion rate and temperature. This may reflect the poor understanding of the importance of a material's mechanical properties, which is discussed in a later section. It may also be due to an inability to separate the effects of erosion and corrosion. Finnie (1972) suggested that the impact event produces large local

temperature rises. He proposed that the material being removed may therefore be close to its melting point and thus concluded that testing at elevated ambient temperatures may not significantly alter the local conditions unless the melting point is reached. The question of target melting is discussed in section 7 of Chapter 2, where the significance of thermal properties and their correlation with erosion are reviewed.

1.2.3 Properties of the target material

(a) Hardness

It is instructive to examine the role of specimen hardness in abrasive wear, and to consider the results of erosion studies in this light.

Figure 1.4 shows Khruschov's results correlating abrasive wear with indentation hardness (Khruschov (1974)). It can be seen that for annealed metals a linear relationship holds between a metal's hardness and its resistance to abrasive wear, defined as the reciprocal of the abrasive wear rate. The results for steels show that as the hardness is increased by heat treatment, the abrasive wear resistance also increases linearly; however, the slope is much less than that for annealed materials. Thus, in abrasive wear the selection of a material is more important in achieving wear resistance, than modifying the hardness by heat treatment.

Figure 1.5 presents the results of Finnie et al (1967) correlating erosive wear and indentation hardness. Figure 1.6 gives details of the effects of work hardening and thermal treatments on erosion resistance under the conditions of Finnie's experiments. These results are very similar to Khruschov's results for abrasion. As with the abrasion study

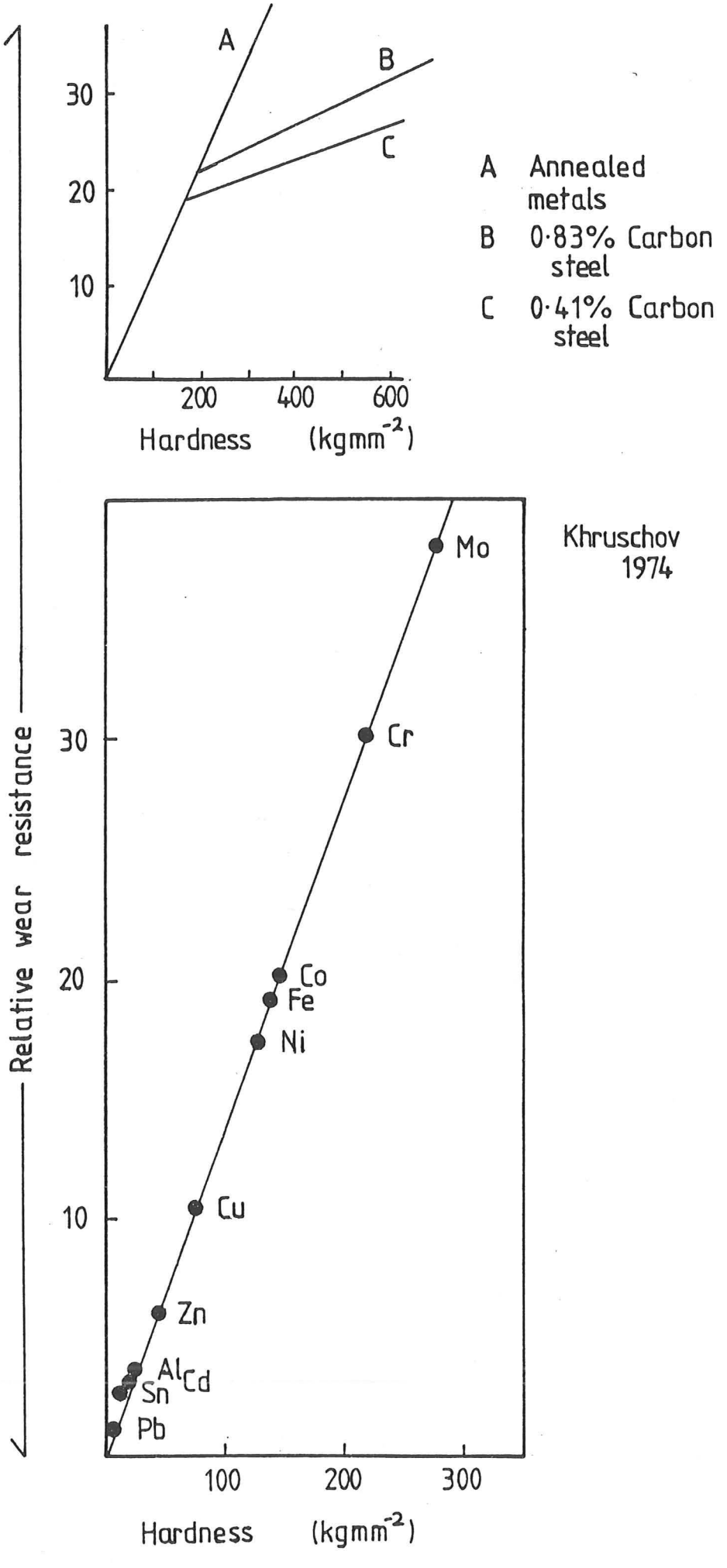

Figure 1.4 :

Hardness vs wear resistance (After Khruschov (1974))

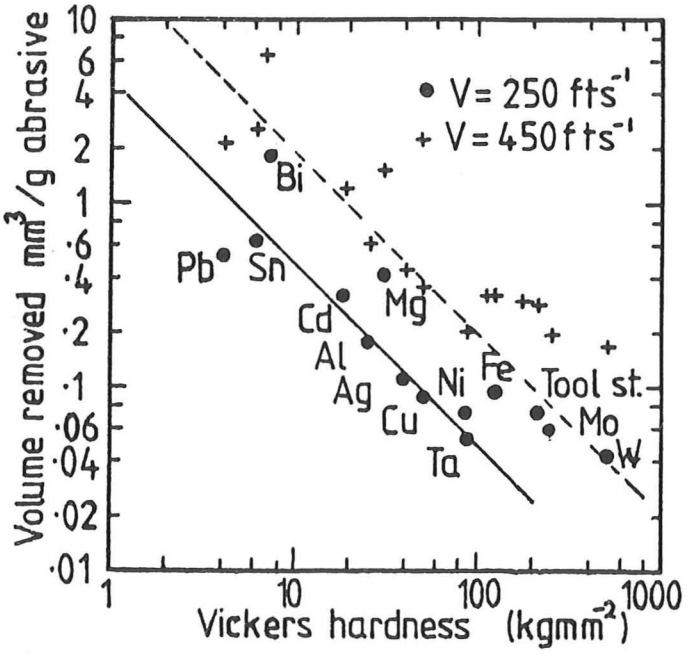

Figure 1.5 : Erosion vs hardness (annealed metals eroded by 60 mesh silicon carbide at 20° impact). (After Finnie et al (1967))

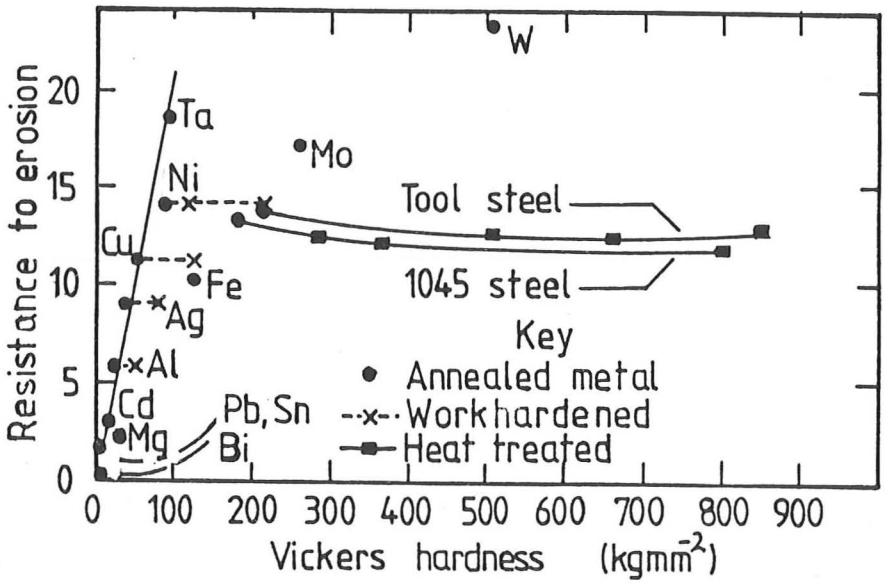

Figure 1.6 : Erosion vs hardness (eroded by 60 mesh silicon carbide at 20° impact, velocity 250 ft/sec). (After Finnie et al (1967))

it is found that the annealed hardness of a metal correlates with its erosion resistance, but that little improvement in erosion resistance can be achieved by heat treatment.

Wellinger (1949) reported the results of the erosion testing of steels of various hardnesses. He found that the variation of erosion rate wih angle of impingement depended upon the hardness of the steel. His results (as discussed in section 1.2.2 above) showed a transition from what is conventionally described as 'ductile' erosion, to 'brittle' erosion behaviour as the hardness increased.

Gulden (1979) also found a transition in behaviour in the erosion of high carbon martensitic steels, dependent on both the steel's heat treatment and also the size of the erodent particles. She tested five high carbon steels, each of which were heat treated to five martensitic conditions : untempered, tempered to maximum hardness, tempered to maximum fracture toughness, and tempered to the specific Rockwell hardnesses RC50 and RC30 (equivalent to 542 and 278, $kgfmm^{-2}$ Vickers hardness respectively). She reported that for low angles of impingement, increasing the hardness by heat treatment resulted in little or no change in erosion rate. However, at normal impingement the fully hardened martensitic steel had an erosion rate some four times greater than that tempered to the RC30 hardness. If Figure 1.2 is consulted, it can be seen that it will be at normal impingement that the greatest difference occurs in the erosion rates of materials demonstrating each of the two modes of behaviour (assuming the maximum erosion rates are of similar magnitude). It is significant that the results of Finnie et al (1967) reproduced in Figure 1.5 and Figure 1.6 are for metals eroded at a 20 degree impact angle.

The work of Wellinger (1949) and Gulden (1979) illustrates two important factors. First it is of little value to compare the behaviour of materials tested at different angles of impingement. If the angular dependence of erosion is different a test at normal impingement might lead to the opposite conclusion from one conducted at glancing angles of impingement.

The second factor illustrated by this work is that changing the hardness of a material almost invariably alters other mechanical properties of that material. This is displayed in the transition of modes of erosive behaviour, from a mode requiring high ductility to a mode reflecting low ductility. Increasing a material's hardness generally decreases its ductility. This effect is discussed by Gane and Murray (1979). They reported that as their hardness was increased, some steels became more susceptible to erosion losses. As the hardness of their specimens was increased the volume of material displaced by each impact was observed to decrease. However the proportion of the displaced material which was removed from the surface increased as the hardness increased. The conclusion that the balance of hardness and ductility is important in determining the erosion rate is also reached by Jones and Lewis (1979), Levy (1979) and Hutchings (1981), the latter stressing dynamic hardness.

Heat treatment can increase the hardness of alloys by several different mechanisms. Salik and Buckley (1981a) reported that the increase in hardness caused by solution treating an annealed aluminium alloy (6061) is accompanied by an increase in erosion resistance. However, precipitation treatment to further increase the hardness results in a slight lowering of the erosion resistance. Salik and Buckley also investigated the effects of different heat treatments in the erosion of a medium carbon steel (1045 - 0.46%C, 0.8% Mn, 0.04%P, 0.05%S). When

the steel was eroded with glass beads heat treatment was found to have a profound effect on its erosion resistance; however the same steel eroded by crushed glass showed little or no effect of heat treatment.

The hardness of metals can also be increased by mechanical treatments. Salik and Buckley (1981a,b) studied the effects of various surface treatment on the erosion behaviour of an aluminium alloy (6061). The treatments included cold rolling, grinding, sand blasting and shot peening. They concluded that during initial erosion a complex surface layer is established. This layer is subsequently maintained independently of the initial surface condition, and thus the steady state erosion behaviour will not be modified by surface mechanical treatments. Levy (1979) published results showing the effect of cold working on spheroidised 1075 steel (a near eutectoid, plain carbon steel 0.75%C) and showed that the initial erosion rate increased with the increased hardness developed by cold working. The steady state erosion rate was however constant regardless of the amount of prior cold working. These results suggest that the rate at which the surface layer is modified to its steady state condition depends upon the extent of prior cold working, but that the final form of this layer is independent of the cold working.

Sheldon (1977) investigated the modifications to the surface properties of metals caused by erosion. He measured micro-indentation hardness on eroded surfaces (after light chemical polishing). Figure 1.7 reproduces his results. Comparing Figures 1.6 and 1.7, we see that the work hardening caused by erosion is indeed greater than the work hardening treatments carried out by Finnie et al (1967). Sheldon claims that Figure 1.7 shows a better correlation between erosion rate and hardness measured after erosion than between erosion rate and the hardness of the annealed metal.

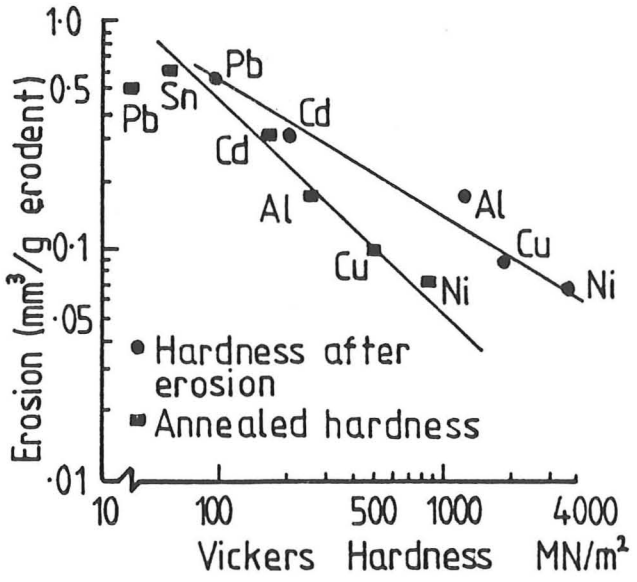

Figure 1.7 : Volume erosion vs hardness of annealed surface and of surface after erosion. (Eroded by 60 mesh silicon carbide at $75ms^{-1}$, 20^{o} impingement.) (After Sheldon (1977))

The general conclusions which can be drawn from the literature are :

(i) Changing a material's hardness will in general, affect other mechanical properties, for example ductility.

(ii) Heat treatment of an alloy usually does not produce a significant increase in erosion resistance; the gains achieved by any increase in hardness are offset by the loss due to decreased ductility.

(iii) The hardness of a pure metal in its fully annealed state can be used as an indicator of its likely erosion resistance.

(iv) Mechanical treatments can affect the rate at which the initial surface of a metal is modified by erosion, but will not in general affect the steady state erosion rate. The steady state erosion rate will depend upon the mechanical properties of the material after erosion, rather than those of the undeformed material. The surface, under steady state erosion conditions, is mechanically deformed to the point of failure, and therefore prior mechanical treatments are not significant.

(b) Other mechanical properties

A number of parameters have been investigated in an attempt to correlate a metal's erosion response with readily available data in the form of mechanical properties. Before considering these parameters in detail it is useful to put into perspective the range of erosion responses of

Table 1.1 (From Tilly (1979))

Erosion values for common materials tested with 125 - 150μm quartz particles at 250m/sec and 90° impingement.

Material	Diamond pyramid hardness (kg/mm^2)	Erosion (cm^3/kg)
Hot pressed silicon nitride	1800	0.2
11% chromium steel	355	0.6
Forged nickel alloy	207	0.6
0.05mm plated tungsten carbide	1050	0.85
Titanium alloy, sheet	340	1.0
Aluminium alloy, sheet	155	2.0
Cast cobalt alloy	600	2.2
Type 66 Nylon	-	2.3
Polypropylene	-	3.1
30% glass-reinforced nylon	-	7.0
25% carbon-reinforced nylon	-	7.0
Extruded magnesium alloy	37	13.0
70% glass-reinforced expoxy	-	53.0
Annealed soda glass	450	100

ductile materials. If all types of material are considered, the volume erosion (cm^3/kg) under a specific set of testing conditions may vary by three orders of magnitude. Table 1.1 (taken from Tilly (1979)) illustrates this for common materials tested at normal impingement. However, Tilly stated 'In all studies of the types of material commonly used for compressor blading in aero gas turbine engines, it has been found that as a 'rule of thumb' it can be assumed that the erosion expressed as specific weight loss is the same for all these materials. This simplification includes steels and the common types of aluminium, titanium and nickel alloy.' The same conclusion was reached by Smeltzer et al (1970) and Goodwin (1968). In the previous section the negligible effects of heat treatment and mechanical treatments on erosion resistance were reported. Thus we must expect, when investigating the class of metals, not to find any great sensitivity to an individual material parameter.

Sheldon (1977) systematically tested a series of copper/nickel alloys, and concluded that there was poor correlation between erosive wear and elastic modulus or density. C D Wood (1966) reported that gross mechanical properties (as determined from tensile tests) showed little correlation with his erosion test results. His measurements included Knoop hardness, density, ultimate tensile strength, yield strength, elongation and reduction of area, and Young's modulus. Wood concluded that 'Erosion is influenced by undetermined properties of the very thin surface layer, rather than by commonly used gross properties.'

In agreement with the conclusions drawn from the literature relating hardness with erosion (section (a) above), Smeltzer et al (1970) stated 'It is apparent that specimen flow strength, which is related to hardness and metallurgical structure, has little bearing on the inherent erosion resistance of a specific target material.'

Rickerby (1983) correlated the mechanical energy density required to cause failure in a tensile test, with volume erosion. He computed the maximum strain energy density in the material from the product of the strain at failure in a tensile test, and the arithmetic mean of the yield stress and ultimate tensile stress. His results are reproduced in Figure 1.8 (data points labelled A). Rickerby used data from Finnie et al (1967); his mechanical energy density data is presented for annealed materials. If Rickerby's strain energy density calculation is examined, the strain term is found to be almost constant for all the metals (except magnesium, which does not fit the general trend of the data). In Figure 1.8 the mean of yield stress and ultimate tensile stress is also plotted versus volume erosion. This results in a straight line (line B) of almost identical slope to Rickerby's line A, with similar scatter of the points about the line. If the numerical value for the mean of yield stress and ultimate tensile stress is expressed as a multiple of the yield stress for these materials, in each case the factor is found to be approximately 1.5 (Table 1.2 presents all the relevant data, taken from Rickerby (1983) and Finnie et al (1967)). Indentation hardness in metals is similarly related by a numerical factor to yield stress (Tabor (1951)) and is known to correlate with volume erosion, for annealed metals. Finnie et al's results of indentation hardness versus volume erosion are reproduced in Figure 1.8 (lines C and C'); again we find a straight line of similar slope, and scatter of the points. (The points for magnesium, iron and molybdenum lie on a separate line, the possible reasons for this effect are discussed by Finnie et al (1967)). In conclusion, Rickerby's proposed mechanical energy density can be shown to be simply an alternative presentation of previously published correlations of hardness, or yield stress, with erosion resistance.

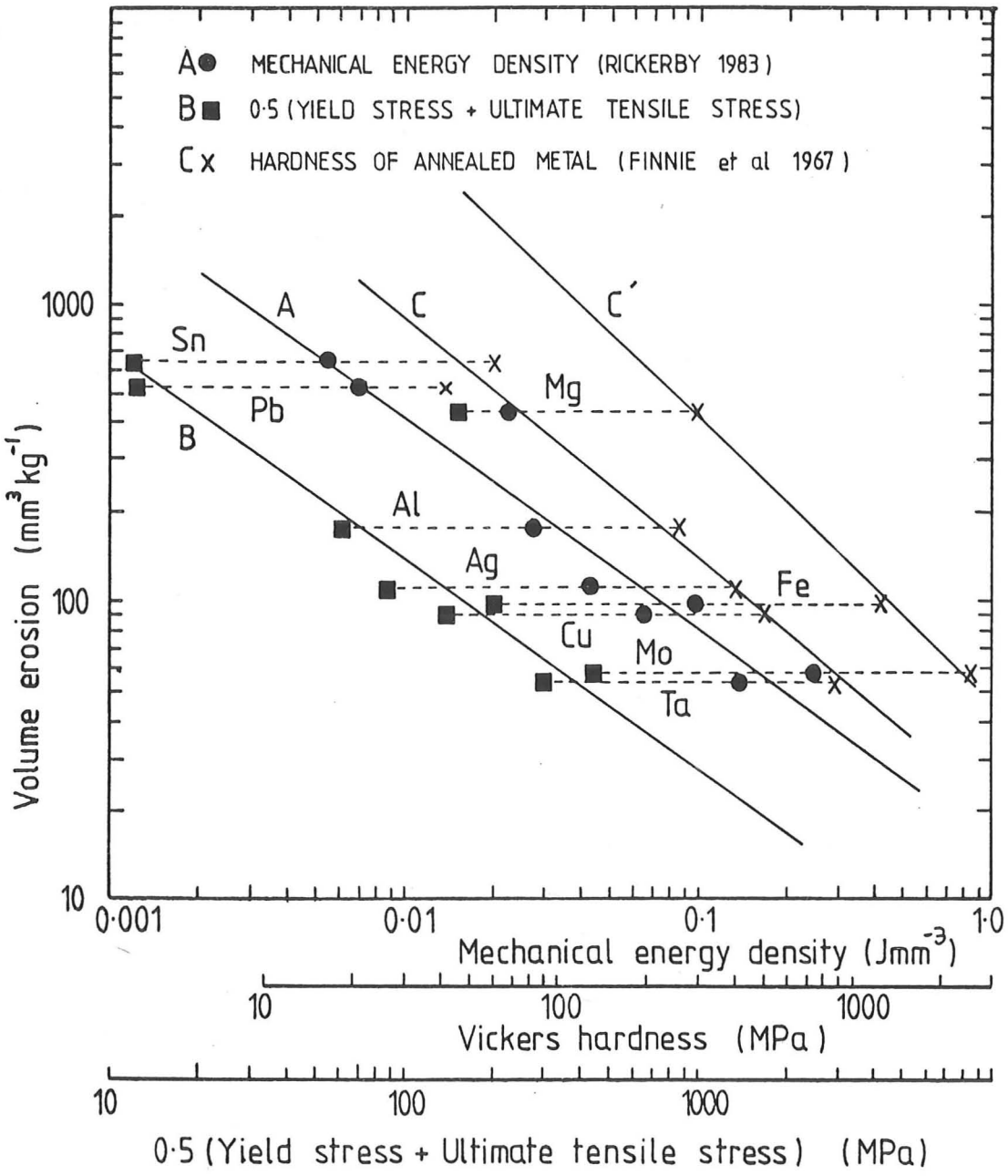

Figure 1.8 : Erosion vs mechanical properties.

Table 1.2 : Mechanical Properties of Annealed Metals

Material	Volume erosion $mm^3 kg^{-1}$ (Finnie et al (1967))	Elongation % ε_f	Yield stress MPa σ_y	Ultimate tensile stress MPa σ_u	$\frac{\sigma_y+\sigma_u}{2}$ MPa σ_m	Mechanical energy density $Jmm^{-3} \times 10^{-2}$ *	$\frac{\sigma_m}{\sigma_y}$	Vickers hardness MPa (Finnie et al (1967))
Al	169	45	35	90	62.5	2.8	1.79	265
Ag	108	48	55	125	90	4.32	1.64	392
Cu	88	45	69	220	144.5	6.50	2.09	505
Fe	96	47	126	283	204.5	9.61	1.62	1280
Mg	426	15	103	193	148	2.22	1.44	305
Mo	58	55	345	549	447	2.46	1.30	2600
Pb	513	52	9	17	13	0.676	1.44	41.8
Sn	636	45	9	15	12	0.54	1.33	62.0
Ta	54	45	271	343	307	13.8	1.13	900

* Rickerby uses the following expression to compute the maximum stress energy density

$$W = \frac{1}{2}(\sigma_y + \sigma_u)\varepsilon_f$$

(The values of ε_f, σ_y and σ_u listed in this table are those quoted by Rickerby (1983); he cited as sources :

'Metals Handbook' Vol 1 ASM, Metals Park, OH, 8th edn. 1961
L Northcott, 'Molybdenum, Butterworths, London, 1956, p.59
G L Miller, 'Tantalum and Niobium', Butterworths, London, 1959, p.398)

Rickerby proposed that data for alloys should be tested by this approach, in order for its predictive capabilities to be evaluated. The mechanical energy density will alter with heat treatment, and to some extent with mechanical treatment, but not in a simple manner. Erosion is known to be insensitive to these treatments, and thus the mechanical energy density correlation proposed by Rickerby would not be expected to hold.

An alternative correlation between erosion and a characteristic energy term is presented by Vijh (1976). Figure 1.9 presents the results of his correlation between interatomic bond energy and volume erosion rate. Vijh explained that high binding energies signify that the atoms of a metal are held together quite strongly, and will not leave the lattice easily in any attempt to dislodge them, e.g. during impact erosion. The approach of Vijh is over-simplistic, and does not take into account the actual mechanisms of deformation that will occur during erosion. It is known that energy requirements for plastic deformation are not dependent upon bond energies. The correlation, as illustrated by Figure 1.9 (a) and (b), is not good. Vijh claims merely to show a trend.

There are several possible reasons why erosion rate does not correlate with the mechanical properties of a material. First, as discussed above and also in the previous section, the mechanical properties of the surface layer of an eroded specimen are as yet undetermined. It is evident that the properties differ from the bulk material, although they will in some way be related to the bulk properties.

In a similar manner, there is evidence that the microstructure of the target material will influence its erosion behaviour. If the scale of

UNIVERSITY
LIBRARY
CAMBRIDGE

Figure 1.9 : Erosion vs bond energy (after Vijh (1976))

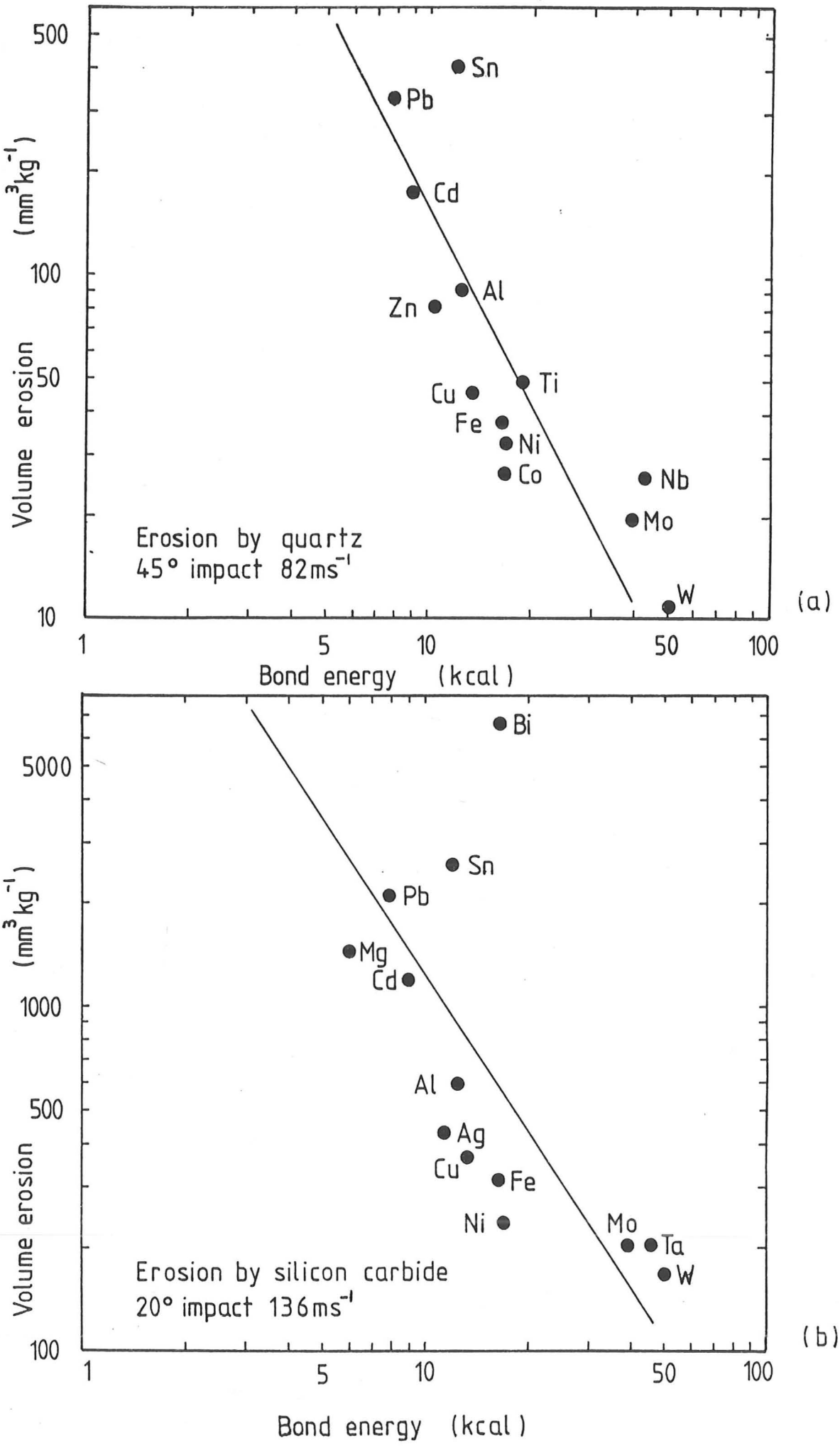

interaction during erosion is of the same order as the microstructural scale, bulk properties may be less significant than, for example, the properties of the matrix and precipitate phases. Green et al (1981) discussed the erosion of plain carbon steels, with reference to microstructural features, while Levy (1979) reported similar work on pearlitic steels.

Finally, as pointed out by Hutchings (1977), extremely high strain rates are experienced by targets impacted by submillimetre particles travelling at velocities of the order of tens of metres per second. Such high strain rates are not reached in conventional testing apparatus, and thus bulk properties measured at low strain rates need not necessarily be relevant to erosion testing.

(c) Correlation of thermal properties with erosion resistance.

Energy balance considerations for an inelastic impact show that at least eighty percent of the kinetic energy of the impacting particle will be dissipated as heat (Hutchings (1981)). Clearly this will lead to some temperature rise in the area of impact. Ascarelli (1971) introduced the concept of 'thermal pressure' to describe a material's response to heating caused by impact. Ascarelli assumed that in the immediate region of the tip of the impacting particle intense heating occurs. Moreover, the bulk of the target material constrains the heated region of the crater to remain at the same fixed density throughout the impact. He thus defined the thermal pressure to be the pressure due to the atomic thermal vibrations of the target material. A change in thermal pressure occurs during the impact process. This change in thermal pressure is the change in pressure experienced by a fixed volume of the target material which is

raised in temperature whilst being constrained to a constant volume. Ascarelli defined the thermal pressure (Pt) of a material by the following relationship :

$$Pt = \frac{\alpha_t (Tm - Tr)}{\Psi}$$

where α_t = coefficient of expansion
Tm = melting temperature
Tr = room temperature
Ψ = isothermal compressibility

(N.B. Ascarelli does not take the variations of both α_t and Ψ with temperature into account).

Figure 1.10 reproduces Ascarelli's results, showing that the erosion resistance of pure metals may be predicted with some accuracy from their thermal pressures.

Hutchings (1975a) considered the influence of thermal softening on a proposed mechanism of material removal. This mechanism involved the formation of fragile lips of metal at the edge of impact craters. He concluded that the product $\rho Cp\Delta T$ should correlate with erosion resistance. (ρ is the density, Cp in the specific heat at constant pressure and ΔT is the difference between the melting point and ambient temperature.) Figure 1.11 is reproduced from this work. Hutchings is careful to emphasise that the value of this parameter as an indicator of erosion resistance is based solely on the evidence of the empirical data. In a similar manner Malkin (1981) related the kinetic energy per unit volume of metal removed to the melting energy per unit volume of the target metal. (Melting energy is defined as the difference in enthalpy between the liquid state at the melting point and the ambient condition.) A discussion is

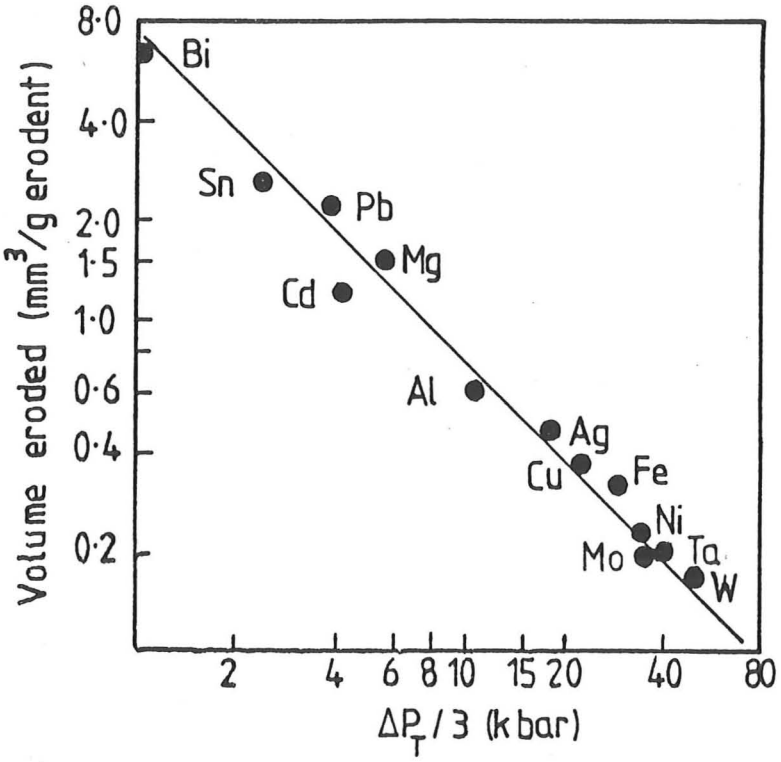

Figure 1.10 : Thermal pressure vs erosion (after Ascarelli (1971))

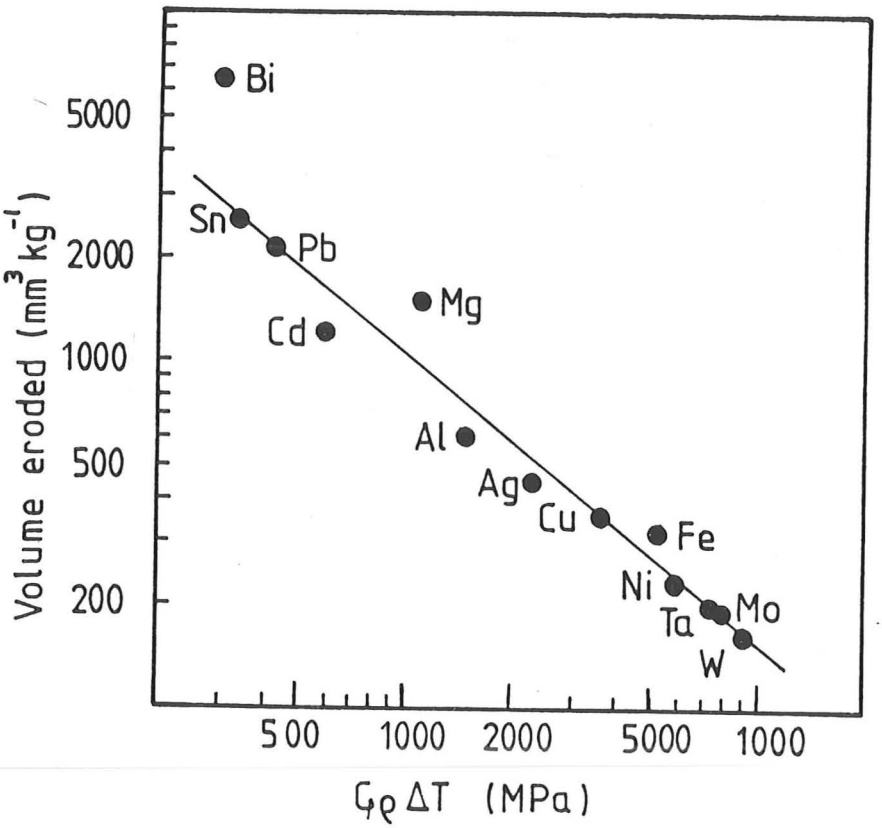

Figure 1.11 : Volume erosion rates (after Finnie et al (1967)) plotted against Hutchings' thermal factor (Hutchings (1975a))

included in section 8 of Chapter 2 of the significance of the localised heating which occurs during erosion.

In conclusion, the results presented in the literature suggest that there is good correlation between certain thermal properties and the erosion resistance of metals. However, these correlations have been reported only for pure metals, and have yet to be extended to alloy systems. While there is little agreement on the interpretation of these correlations, it can be observed that in general they are at least as good as those reported for mechanical properties and erosion resistance.

1.2.4 Particle Characteristics

(a) Particle size

It is generally accepted that the erosive wear process becomes less efficient as the abrasive particle size decreases below about 100 μm. This effect is also noted in other wear processes, for example two and three body abrasion of ductile metals (Misra and Finnie (1981)). The so called size effect is fortunate, from a practical point of view, because small particles are not so easily removed from the environment (for example by filtration) as large particles.

Figure 1.12 presents the results of Tilly et al (1970), and shows an initial increase in erosion with particle size, until above a certain size erosion becomes independent of particle size. Tilly warned that in gas blast rigs the effect is complicated by the fact that small particles may be deflected by the gas flow. As a result of this deflection they either fail to impact against the target, or do so at modified angles and velocities. This effect

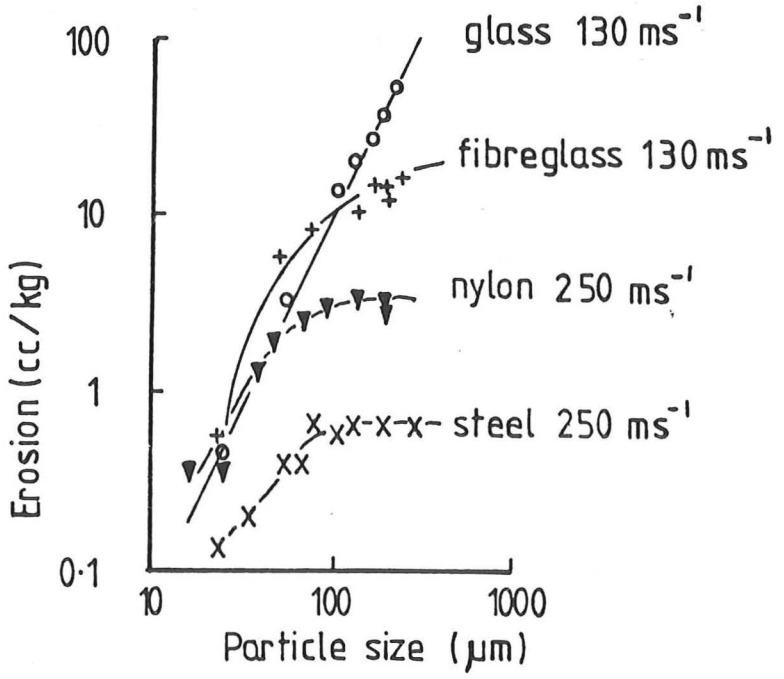

Figure 1.12 : Effect of particle size on erosion of ductile and brittle materials (after Tilly and Sage (1970))

may indeed be a contributory factor to the dependence of erosion on particle size, when testing with this type of erosion rig. However, the bulk of evidence gained from tests with a variety of types of apparatus, together with the observation of similar size effects in other forms of wear, indicates that there is a 'true' size effect in erosion. Tilly offered a further explanation of the size effect in erosion which was based on his model of a two stage erosion process (Tilly (1973)). This model is discussed in detail in Chapter 2, section 2.3. Essentially Tilly suggested that the erosion process can be considered in terms of primary and secondary impact events, the total mass of material removed from the target is therefore the sum of that removed in the primary and secondary stages. The primary impact is simply the impact of the erodent particle with the target. The erodent particle may or may not fragment as a result of this impact. Secondary erosion will occur after fragmentation, and arises when the fragments subsequently strike the target. This model is discussed fully in Chapter 2. Relevant to the present discussion is Tilly's proposal that the particle size effect is a result of reduced secondary erosion. Tilly suggested that smaller particles are less susceptible to fragmentation, and as a consequence of reduced secondary erosion, cause less erosive wear. Tilly's model has been the subject of much discussion and criticism (e.g. by Kleis et al (1975)), in particular, the importance and indeed occurrence of secondary erosion is challenged. These criticisms are detailed in Chapter 2.

There are two weaknesses in Tilly's model, which are exposed by experimental study of the particle size effect. First, the size effect in erosion is not confined to erosion with frangible abrasive. Second, Tilly's model suggests that the critical size below which erosion becomes less efficient is a function of erodent type. This has not been reported in the literature.

Misra and Finnie (1981) studied the particle size effect in erosive and abrasive wear. Their work contained a review of much of the literature in this field. They isolated two possible mechanisms which may explain the size effect in these forms of wear.

First, it is possible that a thin surface layer preferentially work hardens. The thickness of this layer is dependent on the properties of the target material. Small impacting particles interact with material contained in this surface layer. Thus the material subject to erosive wear has a flow stress significantly higher than the bulk material, and consequently lower erosion rates than expected are recorded.

Second, it is possible that there is a true physical size effect such that regions below a certain size show an increase in strength values. This proposal is based on experiments by Gane and Cox (1970) where indentation hardness was measured with indenters of differing sizes. Indentation hardness was found to increase to two or three times the macroscopic value when very small regions, of approximately $1\mu m^2$, were indented. Thus it is suggested that small particles will cause less erosive wear, because the volume of metal deformed by an individual impact is significantly harder than the bulk. This proposal is also reported by Finnie (1972).

Hutchings (1977) discussed the work of Gane and Cox. He pointed out that the critical size, below which erosive wear falls rapidly in efficiency, is of the order of $100\mu m$. Particles of this size will produce indentations much larger than $1\mu m^2$ in area. Hutchings concluded that while the mechanism of Gane and Cox may be important in erosion with submicrometre particles, it cannot account for the size

effect in erosion. Hutchings, in the same paper, used both Hertzian (elastic) and plastic theories to estimate the contact times and strain rates involved in the impact of spherical particles on to metals. His work suggests that the impact durations for 1mm and 1μm spheres striking a target are of the order of 1μs and 1ns respectively. The corresponding strain rates are very high, and depend on the impact velocity. A 1mm sphere striking mild steel at 100ms^{-1} will deform the target at a strain rate of approximately $10^{5}s^{-1}$; for a 1μm sphere the strain rate would be about $10^{8}s^{-1}$. Hutchings suggested that although little is known of the behaviour of metals at such high strain rates, the indication is that yield stress increases with strain rate. Thus small particles will give rise to higher strain rates, and correspondingly higher yield strengths will be experienced. In this way Hutchings suggested that the strain rate sensitivity of metals may at least partially account for the particle size effect in erosion.

Shewmon (1981) suggested a fourth mechanism by which small impacting particles interact with material with a flow stress significantly higher than that involved in erosion with larger particles. Shewmon suggested that generally erosion will involve localised temperature rises which in turn lead to intense localised deformation and the detachment of surface metal. In soft metals extreme local plasticity leads to extruded lips, in hard alloys adiabatic shear localisation occurs. If the deformation is slow, or on a very fine scale heat conduction will make it effectively isothermal. Consequently material involved in the impact work hardens rather than thermally softens, and the volume detached reduces.

It must be concluded that the particle size effect in erosion is at present poorly understood. Of the mechanisms suggested the most plausible involve an apparent or actual increase in hardness of the surface layers. However, as discussed earlier in section 1.2.3 (a), the role of hardness in erosion is also poorly understood. There is much evidence that an increase in hardness due to work hardening will not result in increased erosion resistance. The proposed mechanisms are expressed in terms of a pristine metal surface which is impacted with a single particle, or a small number of particles. However, it has been experimentally established that in the case of normal and near normal impact several thousand impacts on a small area are required before any material is removed. It is not known how such severely deformed metal will behave at high strain rates. It is not clear either if the results of studies involving fine scale deformation of pristine metal surfaces can be applied to models of the deformation of eroded surfaces. More work is required to determine a conclusive mechanistic explanation for the particle size effect.

(b) Particle shape

It is generally accepted that sharp erodent particles will cause more erosive wear than will rounded particles. A search of the literature for experimental studies investigating the effects of particle shape reveals that this is an area which at present is poorly inderstood.

Goodwin (1968) was among the first to point out that comparisons between results from different workers are meaningless, unless the abrasive particle shapes are similar. He attemped to use only naturally occurring sands 'such as regularly find their way into engines' in his work on the erosion of turbine components, and contrasted his results with those of workers using silicon carbide and alumina.

Kleis (1969) eroded mild steel with angular and spherical iron shot and reported appreciably more erosion with angular particles. He also found that the angle of particle impact for maximum erosion was lower with angular particles than with round shot.

Raask (1979) investigated the erosion of steels and refractory materials using pulverised coal. He concluded that the abrasive property of pulverised coal depends mainly on the quantity of hard sharp-edged quartz and pyrites particles. Pulverised coal ash consists largely of spherical glassy particles which Raask found comparatively non-abrasive.

Salik and Buckley (1981a) eroded 6061 aluminium and 1045 steel with crushed glass and glass beads. They reported that the crushed glass produced an erosion rate an order of magnitude higher than that caused by glass beads. Significantly, they also suggested that the mechanism of erosion is dependent upon particle shape. They reported that erosion with crushed glass was not sensitive to the microstructure of the target material, whereas erosion with glass beads was found to be very sensitive to microstructure.

Shewmon and Sundararajan (1983) suggested that irregularly shaped abrasive particles will embed in the target surface, and spin out leaving a tip behind; this process will give rise to a composite layer of abrasive fragments and base metal. Kosel et al (1978) and Sheldon and Kanhere (1972) also found particle embedding when eroding metals with alumina and silicon carbide respectively. Both reported that no embedding occurs with spherical particles tested under similar conditions. Neither Sheldon nor Kosel et al drew the conclusion that this effect is due simply to particle shape. (In Chapter 6 of this work it is shown that erosion by spherical particles can give rise to a composite layer similar to that described by Shewmon.)

Gonzalez-Rivas (1981) investigated the effects of particle shape and sharpness on the slurry erosion of copper. He characterised the shape of abrasive sands using many shape factors. His work highlights the many problems involved in measuring shape factors of abrasive grits. He reported some correlation between slurry erosion (at 30^{o} impingement) and Wadell's Roundness and Lees' Angularity factors. (Details of these factors are presented in Chapter 4). Gonzalez-Rivas' results are inconclusive, his experimental techniques and erosion parameters non standard. (He quoted Rabinowicz wear coefficient, rather than non-dimensional erosion rate - see Chapter 7, section 7.2.4.)

In addition to the experimental work reviewed above, there have also been attempts to incorporate shape descriptions into expressions describing erosion. Shewmon and Sundararajan (1983) produced an expression which described erosion as inversely proportional to a shape factor. They were not able, however, to describe this shape factor fully, but suggested its form for a spherical particle.

Ratner and Styller (1981) accounted for particle shape in their fatigue-based model of the erosion of polymeric materials by defining an apparent particle density : the total mass of a particle is said to be contained within a sphere of radius equal to that of a sharp projection on its surface.

From this survey it can be concluded that little is known of the effect of particle shape on erosion by solid particles. Experimental details published suggest that the mechanism of material removal is sensitive to particle shape, however this is not reflected in the theoretical expressions describing erosive wear which attemptto include a shape factor.

(c) Particle hardness

Intuitively it would be expected that for erosive wear to occur the erodent particles must be harder than, or at least as hard as, the target material. Most of the analyses of static indentation assume that the indenter is rigid and does not deform, and this approach is carried over to the analyses of deformation during erosion. Particle hardness can be related to particle shape : soft materials will in general tend to form more rounded particles than hard materials. For a given material hardness, the particle shape will reflect the way the particle was produced : for example wind blown quartz will tend to be more rounded than quartz sand produced by crushing. Care must be taken, therefore, to isolate the effects of particle shape and particle hardness.

Goodwin et al (1969) reported a correlation between erosive wear and the hardness of the erodent particles. They concluded however that in their experiments it was not possible to fully isolate the effects of particle shape and particle hardness.

The studies of Raask (1979) on the erosive properties of pulverised coal and its ash have been mentioned in the previous section. He concluded that the amount of erosive damage is determined by the proportion of hard (and sharp) quartz and pyrites particles. In British coal these particles account for approximately 1% to 3% of the total weight.

The most controversial study in this field is that of Head et al (1973). They eroded 302 stainless steel and 6061-T6 aluminium alloy, with alumina and fluorite particles. The hardnesses of these materials are listed in Table 1.3.

Table 1.3

Material	Vickers Hardness ($kgf\ mm^{-2}$)
302 stainless steel	250
6061-T6 aluminium alloy	80
Alumina	2000
Fluorite	150

(Head et al (1973))

Head et al found, surprisingly, that the fluorite was more erosive than alumina, for both 302 stainless steel and 6061-T6 aluminium alloy.

Tilly (1973) and Maji and Sheldon (1979) reported on the effects of brittleness or frangibility of the erodent particles. Tilly suggested a two stage mechanism of erosion, with primary erosion being caused by the initial impact of the erodent particles. Secondary erosion is caused by the glancing impacts of fragments of the original particle which fly out radially from the primary impact site. Tilly and Maji and Sheldon examined eroded surfaces by scanning electron microscopy, and claim to have found evidence that a significant amount of erosive wear is caused by the secondary mechanism. Tilly's work is discussed in more detail in section 2.3 of Chapter 2.

It is concluded that the effect of the particle hardness in the erosion of metals is at present poorly understood. The literature indicates that the erodent particles must be harder than the target material for significant wear to occur. The work of Head et al (1973) has yet to be reproduced by others and unless they can be reproduced their results

must be considered anomalous. Tilly's suggestion that the particle hardness will determine the degree of fragmentation, which in turn will determine the erosion rate, also requires further experimental verification. The significance of secondary erosion is at present open to question, a discussion of the criticisms advanced is included in Chapter 2, section 2.4. Further, the effect of strain rate on the hardness and frangibility of the erodent particle is not known. It is possible that angular, hard particles may fragment more than expected under the high strain rate conditions occurring during impact in erosion, thus making the relationship between hardness and fragmentation and secondary erosion more complex than Tilly suggests. The literature survey indicates that more work is required to isolate the effects of particle shape and particle hardness in erosion. Until it is possible to quantify the shape of an erodent particle, difficulties will exist in designing experiments to investigate the effect of particle hardness. Shape quantification is essential if particles of different hardness but identical shape are to be selected for use in erosion experiments.

CHAPTER 2 : LITERATURE SURVEY : MECHANISMS OF EROSION

2.1 INTRODUCTION

The preceding chapter has introduced some of the important factors in the erosion process. It has also revealed something of the complexity of the mechanisms by which material is removed from a surface by erosion. This chapter presents an introduction to the proposed mechanisms of erosion. It is not possible here to present an exhaustive discussion of each model; further details are provided, where appropriate, in the body of this dissertation. First, three of the most influential of the proposed mechanisms are presented, these are among the earliest suggested mechanisms and provide a useful background to this topic. The later work is then presented, classified by type of mechanism.

It is interesting to note that none of the early models were based on microscopical observations of eroded surfaces. The development of electron microscopy has provided an important tool in the study of erosion. The use of both scanning electron microscopy, and transmission electron microscopy is frequently reported in the more recent literature in this field.

2.2 FINNIE'S CUTTING MODEL

Some 25 years ago, Finnie (1958), drawing on his experience in the analysis of metal cutting, proposed one of the first and most successful models of the erosion of ductile metals. His analysis applied for grazing angles of impingement, a condition which frequently occurs in erosive situations and which is known to result in the maximum rate of material removal in ductile metals.

Finnie drew an analogy between material removal by a rigid tool tip, and the cutting action of a sharp-cornered abrasive particle grazing a plane surface. To estimate the rate of material removal in erosion, Finnie solved the equations of motion of the particle as it impacted the surface. By predicting the trajectory of the tip of the particle as it swept through the metal, Finnie arrived at an estimate of the volume of metal removed during each impact. He made various assumptions (fully detailed in Finnie (1972)) to simplify the geometry of the impact, and also to allow the results from cutting and grinding tests to be incorporated in the model. Amongst the most significant of these assumptions are: first, that the particle only rotates very slightly during the impact and second, that the volume of material swept out by the particle tip is the volume of material removed. Figure 2.1 shows details of the geometry of impact, and the results of Finnie's analysis compared with experimental data for the erosion of aluminium by angular silicon carbide grit.

The expression Finnie obtains for the volume of material swept out by the tip of the particle is :

$$V = \frac{cMU^2}{4p(1 + \frac{mr^2}{I})} \left(\cos^2\alpha - \left(\frac{\dot{X}'t}{U}\right)^2\right) \qquad .. 2.1$$

where :

V = volume removed from surface

M = mass of eroding particles

m = mass of individual particle

I = moment of inertia of a particle about its centre of gravity

r = average particle radius

α = angle of impact

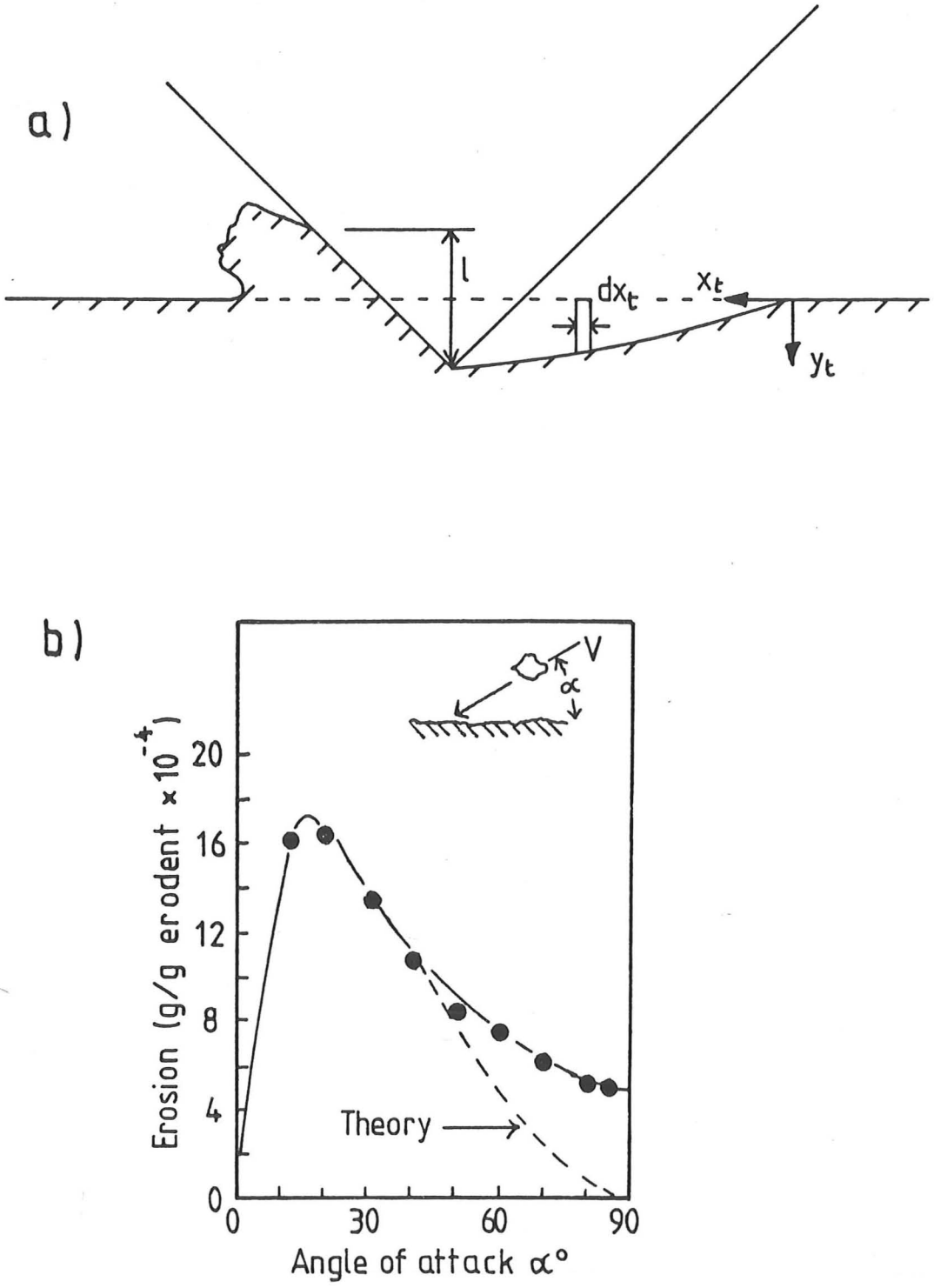

Figure 2.1 : Finnie's analysis of ductile erosion :

(a) Geometry of impact

(b) Experimental results show aluminium eroded by 120 mesh silicon carbide at approximately 170ms^{-1}

(After (a) Finnie (1960), (b) Finnie (1967))

U = particle velocity

p = horizontal component of flow stress (which Finnie found to approximate to the Vickers hardness of the metal)

c = fraction of particles cutting in idealised manner

$\dot{X}'_t$ = horizontal velocity of tip of particle when cutting ceases

Experimental results show good agreement with prediction for the angle of impact for maximum erosion.

The factor c had to be introduced because the theoretical treatment was found to greatly overestimate erosion rates. Values of c must be taken which allow for approximately 90% of the impinging particles not cutting in an idealised manner, and consequently not removing material.

Finnie's analysis predicts a velocity exponent of 2, that erosion is inversely proportional to 'flow pressure' and that no material is removed by particles striking the surface normally. As discussed in Chapter 1 section 1.2.2 (b), velocity exponents of approximately 2.3 to 2.4 are generally found experimentally. 'Flow pressure' and indentation hardness are simply related; however, as discussed in Chapter 1 section 1.2.3 (a), erosion is <u>not</u> found to be inversely proportional to indentation hardness. Finally, as shown in Figure 2.1, significant erosion is found to occur at normal incidence (in this example, for aluminium eroded by silicon carbide at approx 170m/sec, the erosion at normal incidence is some 30% of the maximum erosion).

In spite of these problems, Finnie's work has added greatly to the understanding of the erosion process. It is now generally accepted that cutting mechanisms are the major source of material removal in the erosion of ductile metals by angular particles at glancing angles. Scanning electron microscope investigations carried out since Finnie's early work

(Hutchings (1979b), Bellman and Levy (1981) and Carter et al (1980)) have provided ample evidence of cutting processes. Much work has been done since Finnie first proposed his model to investigate the correlation of erosion with material flow strength, as well as the velocity exponent. Most simple approaches, analysing erosion in energy terms or as a dynamic indentation process, make similar, incorrect, predictions (these are discussed later in this chapter). The breakdown of Finnie's mechanism of cutting, at near normal impingement, has stimulated much work investigating erosion mechanisms under conditions unfavourable for cutting. (Hutchings (1981) etc)

2.3 BITTER'S MODELS

Bitter (1963a,b) defines two types of erosive wear. At low impact angles he suggests that a cutting wear process operates. Like Finnie he generates mathematical descriptions of erosion by solving the equations of motion of the impacting particle. His basic equation is :

$$W_c = \frac{m}{2}\left(\frac{V^2 - v^2}{\varepsilon}\right) \qquad .. 2.2$$

where :

W_c = wear due to cutting, expressed as volume removed by a particle of mass m

m = the particle mass

V = particle velocity parallel to surface on impact

v = particle velocity, parallel to surface, as it leaves the target

ε = energy needed to scratch out a unit volume from the surface

This equation is not significantly different from that of Finnie (equation 2.1).

Bitter proposed that at high angles of impact 'deformation' wear predominates. Bitter generates an equation governing this form of erosion from Hertzian expressions describing elastic contact stresses, and expressions describing the partition of the particle's kinetic energy during deformation of the target. The result is :

$$Wd = \frac{m(V\sin\alpha - K)^2}{2\varepsilon'} \qquad .. 2.3$$

where :

Wd = wear due to 'deformation', expressed as volume removed by a particle of mass m

α = angle of attack

ε' = deformation wear factor $\left(\frac{\alpha \text{ yield strength}}{\text{Elastic modulus}}\right)$

K = maximum particle velocity at which collision is purely elastic

Neilson and Gilchrist (1968) described Bitter's theoretical work as 'exhaustive and extremely intricate, accounting... for the elastic as well as for the plastic properties of the particle and specimen materials'. Others are not so enthusiastic. Finnie (1972) dismissed Bitter's analysis as curve fitting, in which K and ε' are treated as disposable constants.

Bitter does not attempt to describe his deformation wear mechanism, apart from its theoretical derivation. This derivation is based on Hertzian analyses of stress fields for purely elastic contact, and it is clear that erosive impacts resulting in material removal (by processes other than cutting) will involve plastic deformation. Bitter's assumption is that the deformation wear mechanism is some form of brittle fracture process.

It is not clear how the cutting and deformation wear processes are summed. While Bitter stresses the importance of the target material's hardness in the cutting processes, and the recrystallisation temperature in the deformation processes, the roles of other material properties are not described. Chapter 1 details the complex roles of material properties and microstructure in erosion, and also the variation of erosion with experimental conditions. In the light of the experimental evidence available it is clear that Bitter's work is over simplistic: most significant is his inability to describe a physical basis for what he terms 'deformation wear'.

2.4 TILLY'S TWO STAGE EROSION MECHANISM

Tilly (1973) proposed a two stage erosion mechanism. Cutting erosion, as described by Finnie, forms 'primary erosion'. 'Secondary erosion' occurs when the original impacting particles break up and project fragments radially out from the primary impact sites. Tilly provided evidence for this secondary process in the form of high speed photographs of fragmenting particles, and also scanning electron micrographs of secondary 'scars' around a primary impact site.

Tilly developed expressions for primary and secondary erosion using energy balance considerations, similar to Bitter's work. He introduced concepts of threshold particle size and threshold particle velocity into his expression for primary (cutting) erosion.

Tilly produced evidence of the fragmentation of strong erodent materials, such as silicon carbide, and concluded that his mechanism can be applied to all types of solid particle erosion. He stated that this mechanism

successfully accounts for the dependence of erosion on impact angle, with primary erosion being dominant at glancing angles, and secondary dominant at near normal impingement.

Maji and Sheldon (1979) also produced evidence of two stage erosion. They reported the results of erosion tests on a hardened aluminium alloy (Al-6061 T6) using annealed, ductile, steel shot and also a heat treated brittle steel shot. They found that ductile shot removed considerably less material than brittle, more frangible steel shot.

Kleis et al (1975) raised several objections to Tilly's theory. They disputed Tilly's energy calculations, and pointed out that in general the fragments will be smaller than the experimentally determined 'threshold' size below which erosive wear becomes negligible. Moreover, Kleis claimed, even if secondary erosion were energetically feasible, it would involve particles impacting at very small angles of impingement. It is generally accepted that erosion at such small angles of incidence, far from being a major contribution to surface removal, is in fact almost insignificant.

It must be concluded that even though fragmentation may occur in some cases, secondary erosion cannot explain the experimentally observed rates of wear when erosion involves near normal impact. Further, it is suggested that the method of material removal during secondary erosion is essentially the same as that caused by primary impact, and is a cutting process involving small particles impacting at glancing angles. At present the experimental evidence does not confirm this, and in certain cases (especially of normal impact with rounded particles) there is much

to support the contrary view that different mechanisms of material removal occur as the impact angle approaches 90^{o}. This evidence is discussed more fully in section 2.7 of this chapter.

2.5 CUTTING MECHANISMS

Hutchings (1976, 1979b) used a similar approach to that of Finnie in developing a model for glancing angle erosion. He used a computer to solve numerically the equations of motion of a square-sectioned rigid particle as it impacts the metal. In this way Hutchings was able to make fewer assumptions about the geometry of the impact than Finnie. Finnie's treatment averages the orientations of the impacting particles. Hutchings assumed that the force acting on the particle results from a uniform pressure acting over the area of contact: this pressure is a measure of the hardness of the metal.

By computing the motion of the particle during impact Hutchings identifies three types of behaviour. Ploughing occurs when the angle between the leading face of the particle and the target is very small (or when spherical particles impact a flat surface).

Two types of cutting behaviour are identified, depending upon the angle between the leading face of the particle and the target, and the consequent rotation of the particle during impact. Figure 2.2 illustrates these cutting modes. Type I machining results in forward rotation of the particle, and leaves triangular indentation with a raised lip. Type II machining involves the backward rotation of the projectile and leads to the removal of a machined chip of material. There is experimental evidence for each of these deformation modes. The analysis also provided

to support the contrary view that different mechanisms of material removal occur as the impact angle approaches 90^{o}. This evidence is discussed more fully in section 2.7 of this chapter.

2.5 CUTTING MECHANISMS

Hutchings (1976, 1979b) used a similar approach to that of Finnie in developing a model for glancing angle erosion. He used a computer to solve numerically the equations of motion of a square-sectioned rigid particle as it impacts the metal. In this way Hutchings was able to make fewer assumptions about the geometry of the impact than Finnie. Finnie's treatment averages the orientations of the impacting particles. Hutchings assumed that the force acting on the particle results from a uniform pressure acting over the area of contact: this pressure is a measure of the hardness of the metal.

By computing the motion of the particle during impact Hutchings identifies three types of behaviour. Ploughing occurs when the angle between the leading face of the particle and the target is very small (or when spherical particles impact a flat surface).

Two types of cutting behaviour are identified, depending upon the angle between the leading face of the particle and the target, and the consequent rotation of the particle during impact. Figure 2.2 illustrates these cutting modes. Type I machining results in forward rotation of the particle, and leaves triangular indentation with a raised lip. Type II machining involves the backward rotation of the projectile and leads to the removal of a machined chip of material. There is experimental evidence for each of these deformation modes. The analysis also provided

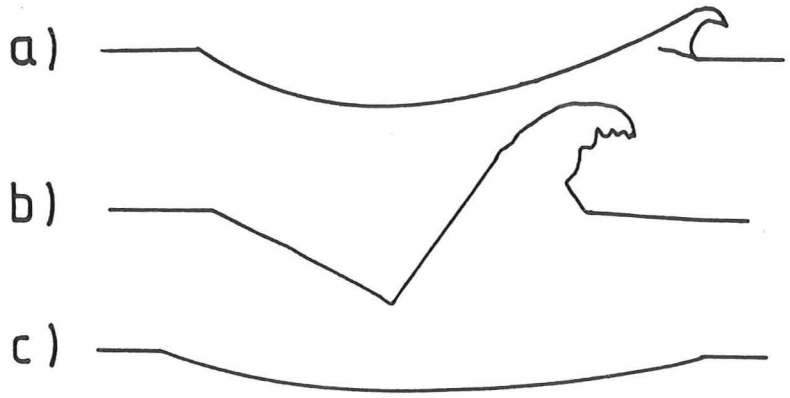

Figure 2.2 : Sections through impact craters, showing typical shapes (After Hutchings (1979b))

(a) Plowing deformation by a sphere

(b) Type I cutting

(c) Type II cutting

predictions of indentation volume and particle energy losses, which were confirmed by experiment.

2.6 FATIGUE MECHANISMS

Hutchings (1979a) discussed the possibility of near normal impingement erosion being a fatigue process. He cited experimental evidence that under these conditions material is removed in relatively large fragments after very many impacts, rather than in very small fragments after few impacts. The Coffin-Manson law (describing low cycle fatigue in metals) is used to derive an expression for near normal impingement erosion. Hutchings concluded that experimental results are compatible with this treatment of erosion, and thus further evidence for a fatigue mechanism should be sought.

In a later paper (Hutchings (1981)) he proposed a theory of critical strain. This states that fragments are removed from an eroded surface when the maximum plastic strain within the surface reaches a critical value. He suggested that the critical strain is a property of the material, and is a measure of its ductility under erosion conditions. A simple argument drawing on random-walk theory showed that an expression similar to the Coffin-Manson law is generated by the application of the critical strain failure criterion.

Hutchings proceeded to develop an expression for erosion based on this principle. This expression involved the density, dynamic hardness and erosion ductility of the target material. He also examined the ability of his model to estimate the duration of the incubation period of erosion. Experimental evidence was examined in the light of this theory.

Hutchings' conclusions were that this approach allows several features of the erosion of metals by normal impact of spherical particles to be explained. It predicts that high values of dynamic hardness and ductility are required for erosion resistance. Several problems exist; for example, the model predicts a velocity exponent of 3.0 which is higher than is commonly reported. In addition, conventional measurements of hardness and ductility in general will not apply at the strain rates experienced during erosion. Before this model can be used in a predictive manner, these properties must be investigated under conditions more relevant to erosion.

Follansbee et al (1981) also considered erosion at high impact angles as a low cycle fatigue process. They used finite element analysis to examine the strain reversals occurring under a single impact. From this analysis of a single impact they inferred the effects of multiple impacts, using the Coffin-Manson approach. Their theoretical study was carried out in conjunction with a programme of experiments. The experimental results correlated well with theoretically predicted erosion rates.

Fatigue mechanisms will only become dominant under conditions of erosion which prevent the more effective cutting and gouging mechanism, for example,erosion by rounded particles at near normal impact angles. The work of Follansbee et al is marred by a conflict in the progression of their hypothesis. Initially the impact of a single particle on a pristine surface is analysed. However, the results of this analysis are incorporated in a description of a process which requires a vast number of impacts to operate. It is not possible at present to analyse in detail the dynamic indentation of an already severely damaged surface; it is clear from experimental studies that erosive weight loss, under conditions

of normal impingement of rounded particles, does not occur until the surface has suffered several thousand impacts. While the fact that a large number of strain reversals occur in an eroding surface encourages speculation of a fatigue process, there is as yet insufficient experimental evidence that this is the case.

2.7 FORGING AND EXTRUSION MECHANISM

Examination of eroded surfaces by scanning electron microscopy reveals the presence of flakes or platelets. Many workers have proposed that the removal of these platelets constitutes the major mechanism of erosive weight loss. Platelets have been reported on surfaces eroded by particles at all angles of impact; it is generally agreed that they are most significant in erosion by rounded particles at normal impingement.

Levy and others (Levy (1982), Bellman and Levy (1981)) proposed a model for the formation of surface platelets which involves the establishment of three zones beneath the eroded surface. It was suggested that a thin surface layer remains soft, due to the heating which occurs during impact. This heating prevents any work hardening of the surface layer, and may indeed stress-relieve or even anneal material that had become work hardened. Immediately beneath the soft surface is a cooler zone of work hardened material. The hardness increases with distance from the heated surface region to a maximum level, and then decreases. Below the work hardened zone the bulk material is unaltered.

Levy (1982) proposed that the incubation period is the time required to establish these zones fully. Particles impact the soft surface and deform it producing craters, smeared regions and platelets. The stronger, work hardened layer beneath acts as an anvil on which the

platelets are 'forged and extruded'.

The heating effects of particle impact will be discussed in the following section. Levy's model requires that this surface heating must be sufficient not only to relieve the strains in the surface layer accompanying impact, but also to relieve the upper surface of the underlying work hardened zone as it becomes exposed by material removal. It is not clear from Levy's model how the work hardened zone is established by deformation which occurs principally in the softened surface zone.

Salik et al (1981a,b) reported experimental measurements showing that the surfaces of aluminium alloys become work-hardened, in spite of a degree of recrystallisation. Rickerby and Macmillan (1980) reported that the surface material was hardened, and assumed that platelets are formed by extrusion of the hardened surface material between the particle and the softer substrate.

Carter et al (1980) proposed a mechanism which is based on the observation that a stable hill and valley surface topography is established when ductile metals are eroded. They suggested that these surface patterns are related fundamentally to the morphology of individual impact craters. A process of plastic flow is said to result in the build up of hills, which are collections of the extruded crater lips. Thus the hills are composed of substantially hardened material, and Carter suggested that the major erosive process occurs via removal of flakes from the embrittled hills. Once again, another model has been proposed which is in direct contrast. Brown et al (1981b) reported a hill and valley topography in the erosion of copper and iron targets by glass spheres at normal impingement. Material was removed from the hill sides by a ploughing process, but the major weight

loss mechanism was said to involve flake detachment from the valleys.

The situation is further complicated by the more recently reported phenomenon of erodent fragment embedding. A detailed survey of this literature is reported in Chapter 6.

It can be concluded that although it is generally accepted that the formation and removal of surface flakes or platelets is an important weight loss mechanism in erosive wear, this process is at present poorly understood. The accounts of soft surface layers on eroded surfaces are not backed by conclusive experimental evidence. Microhardness indentation measurements cannot give a reliable indication of the hardness of a very thin surface layer. If the surface itself is indented difficulties arise in ensuring that the deformation is confined to the surface layer in question.

Sheldon (1977) reported the results of microhardness indentation tests on a range of metals, and found that all metals tested 'appear to be work-hardened by (erosion) to a very high degree; higher in fact, than has been noted in other types of work-hardening process'. Sheldon's results are reproduced in Figure 1.7 (Chapter 1). He estimated that in these microhardness tests the depth of indentation was between 2 and 3μm. Clearly these results contradict the claims for a soft surface layer, even if allowances are made for the difficulties encountered in testing rough surfaces.

The ultramicrohardness technique has been used with some success by Pethica et al (1982) in the determination of hardness profiles of polished, treated surfaces. It cannot however be applied to a rough, eroded surface.

Attempts have been made to measure the variation of hardness with depth by indenting polished sections (Levy (1982) and Naim and Bahadur (1983)). Due to the requirement that the material deformed by the indenter must be fully contained by undeformed material, this technique can only reliably be used above a certain distance from the free surface. An indentation made within this distance will result in the buckling of the surface, or possible bursting, with a corresponding underestimate of the materials hardness. Samuels and Mulhearn (1957) discussed this problem and suggested that for 70:30 brass indented with a pyramidal diamond the minimum spacing from the centre of the impression to the edge of the specimen should be $1.8d_p$ (where d_p is the diagonal of the impression). They stressed that this factor is dependent upon both the yield point and work hardening characteristics of the material. Levy (1982) showed a plot of microhardness versus depth, and a micrograph of an indented specimen, for an aluminium alloy (Al 1100-0) eroded by silicon carbide particles. He stated that the test was carried out 'using a very light, 5gm, load so as not to cause false readings near the surface', and further that 'the evenness of the geometry of the indentation indicates that valid near-surface readings were obtained'. Levy's micrograph does show that the geometry of the indentation is uniform, even for indentations at a distance of d_p from the free surface. However, measurements from this micrograph indicate that the indentation diameter <u>increases</u> with distance from the surface. If all the indentations were made with the same, 5g, load as is reported, the evidence of the micrograph is at variance with the hardness results quoted in the same paper. Levy's micrograph shows that the aluminium specimen was mounted in some form of resin, to facilitate metallographic polishing. There appears to be fibrous material in the resin and thus Levy probably used a commercially available bakelite mixture containing chopped glass fibre. Such mixtures are recommended for edge

retention characteristics, and are considerably harder than conventional mounting compounds. If it is the case that Levy used such a compound, far from being a free surface the edge would in fact be supported and surface buckling or bursting prevented.

It must be concluded that the results of the microhardness testing reported by Levy require more detailed analysis and investigation. Further, the evidence in the literature that an individual impact by an erodent particle results in work hardening around the impact crater, is convincing. For a soft surface layer, as described by Levy, to be established each impact would have to generate sufficient heat to anneal the deformed material completely. Moreover, as the underlying work hardened 'anvil' material is exposed by the removal of the target surface, it will also require annealing if the soft layer is to be renewed. The literature describing the evidence of heat generation during impact, and its significance in erosion, is discussed in section 2.8 following. The evidence for a soft surface layer, and of a 'hammer and anvil' mechanism of platelet formation, is at present inconclusive. More work is required, involving the observation of eroded surfaces, the examination of debris removed from the surface during erosion and also an investigation of the subsurface features in eroded specimens.

2.8 THERMO-MECHANICAL MECHANISMS

Levy's model, reported in the previous section, involved the thermal softening and recrystallisation of the eroded surface. Many workers have reported the effects of heating caused by particle impact. These effects include surface melting, surface recrystallisation and the formation of adiabatic shear bands.

(a) Melting caused by particle impact

Smeltzer et al (1970) were among the first to suggest actual melting of the impact target surface. They reported that the effect was confined to within 1μm of the surface. They suggested that splattering of molten metal would be most likely to occur in erosion involving the impact of sharp cornered particles. In this case, they claim, the particle is decelerated most rapidly over the smallest total contact area. This situation, they conclude, should promote very intense heat build up and the maximum tendency to melting. They observed particles of colloidal size (0.1 - 2μm) which 'appeared metallic' floating in the test chamber, which were believed to be remnants of the liquid metal droplets. The evidence reported by Smeltzer et al is extremely subjective, and the theoretical basis of the mechanism proposed has been the subject of much criticism. In order to achieve target melting the available energy delivered by the particle must be concentrated into a very small area, and delivered at sufficiently high rate to make losses by thermal conduction within the target bulk insignificant. Thus, Smeltzer et al emphasise the need for maximum deceleration rates, resulting in maximum transfer rate of energy, as well as corner oriented impacts, to concentrate the energy into the smallest possible volume of target material. However, maximum deceleration will occur when the area of contact is maximised, as is the case when a face of the particle impacts the surface. Furthermore, there is now considerable evidence that the impact of sharp cornered particles results in material removal by micro-machining mechanisms, as proposed by Finnie and detailed in section 2 of this chapter. It is inconceivable that melting on the scale reported by Smeltzer et al could contribute significantly to target weight losses caused by the cutting and gouging actions of sharp erosive particles.

Finnie (1972) stated that the target temperature had little effect on erosion as 'material being removed is almost at its melting point'. Brown and Edington (1982a), Sarkar (1983) and Gulden (1979) all reported small globular particles, which were assumed to be resolidified ejected molten droplets. Gulden concluded, however, that the volume of the particles observed, compared with the volume of material lost per impact, indicated that the ejection of several hundreds of these particles from a single impact would be necessary to account for the measured erosion. Thus she concluded that melting was unlikely to be the only mechanism of material loss.

Melting is by no means accepted as a significant mechanism of erosive weight loss. Follansbee et al (1981) were careful to state 'there is no evidence of melting on the target surface'. Rickerby and Macmillan (1979) similarly stated 'the appearance of the crater lips formed in the metals suggest that these result from plastic extrusion rather than splashing of molten metal'.

Hutchings (1979b) pointed out that in order to arrive at a figure for the temperature rise, an estimate must be made of the volume of metal in which the heat energy is dissipated. He estimated that the deformed volume is about twice the indentation volume. His calculations produce temperature rises insufficient to produce melting. He concluded that some mechanism must be postulated by which the available energy is concentrated into volumes much smaller than that of the indentation. Adiabatic shear provides one possible mechanism, and is discussed below.

Bellman and Levy (1981) assumed that melting does not occur on the metal surface because the underlying bulk material acts as an efficient heat sink. Thus rapid conduction will prevent the concentration of heat in a small enough volume to result in target melting. Bellman and Levy did, however, find evidence of resolidified aluminium on the surface of silicon carbide erodent particles. They concluded that melting was possible against the erodent particle because the thermal conductivity and heat capacity of the silicon carbide was insufficient to remove heat from the contact area.

An extreme case of target melting in erosion has been reported by Brown and Edington (1981c). They eroded Gallium (melting point 29^{o}C) and Indium (melting point 156^{o}C) and found evidence of resolidified metal on the eroded surfaces.

It must be concluded that the evidence of target melting, in the erosion of engineering materials, does not substantiate the claims that it is a major mechanism of material removal. Much of the evidence produced is in the form of scanning electron micrographs showing spheroidal globules. It is possible that the high surface energy of such a small particle will drive surface diffusion, and result in a degree of spheroidisation at temperatures significantly less than the bulk melting point. The small size of the particles discovered on eroded surfaces prevents their collection and detailed examination. While it is possible that some material may be removed from the target surface in molten form, the evidence reported to date suggests that micro-machining, forging and extrusion mechanisms are considerably more efficient. Melting of the target in such a way as to promote the detachment of chips of material is a more feasible proposal than the simple ejection of microscopic globules. The role of adiabatic shear is discussed in this context in section (c) following.

(b) Recrystallisation caused by particle impact

The work of Levy has already been discussed; Brown et al (1981a,b and 1982b) also produce much evidence for surface recrystallisation. In their paper (1982b) they suggested that the presence of embedded particles in an eroded copper target contributed to this recrystallisation. They suggested that a continuous process of plastic deformation and dynamic recrystallisation occurs during erosion. Simultaneously, large plastic strains are imposed on the material and local heating effects are maximised owing to the low thermal conductivity of the embedded erodent. In their earlier paper (1981a) they reported recrystallisation of detached surface flakes, a process enhanced by poor thermal contact with the underlying bulk material.

Ives and Ruff have performed transmission electron microscopy and selected area electron channelling studies on eroded copper (1979) and 310 stainless steel (1978). They concluded that a high degree of strain exists in the immediate vicinity of the impact crater. Furthermore, they concluded that this strain 'would have a significant role in the erosion of ductile materials under repeated impact'. They provided microscopic evidence showing a zone of high dislocation density a few microns wide surrounding each impact crater. As discussed earlier, Levy's model requires not only that an individual impact on the surface is accompanied by sufficient transient heating to relieve any induced strain, but also that exposed, work hardened, metal is also annealed. In the light of the evidence of Ives and Ruff, this appears unlikely.

(c) Adiabatic shear bands caused by particle impact

As indicated in a previous section, one method of concentrating the available heat energy into a very small volume is the formation of adiabatic shear bands. Many metals, when deformed at high speed, display localised temperature increases and strain concentration. Examination of the microstructure of steels deformed by ballistic impact, for example, reveals narrow, white etching bands. Rogers (1979) has reviewed the literature describing adiabatic plastic deformation. He concluded that in most cases these bands of severely deformed material follow slip line trajectories. Two types of shear bands are identified: deformed bands which are regions of intense shear without structural transformation, and transformed bands which have more distinct boundaries, a well defined width and display a change in structure from the matrix. In neither case is it certain that the deformation is truly 'adiabatic', but it is clear that temperature plays a significant role in localising the deformation.

The role of adiabatic shear bands in erosion has been discussed by many workers (Hutchings (1975b), (1979b), Hutchings et al (1976), Shewmon (1979), Andrews and Field (1982) and Sundararajan (1983)).

As discussed in section 5 of this chapter, Hutchings impacted mild steel with single hard steel particles: balls 9.5mm in diameter and 5mm square plates. He reported that two forms of deformation occurred which resulted in lips of material being raised at the exit edge of the impact craters. Sections of these lips revealed that in both cases (Type 1 cutting, and ploughing deformation) bands of localised shear were present in the raised material. Hutchings concluded (Hutchings (1979b)) that although melting might occur along these shear bands, it would simply aid the detachment of lip material formed by a cutting or ploughing process. As such the

fundamental mechanism operating is, therefore, mechanical with melting playing a minor role in aiding the removal of heavily deformed metal.

Shear bands have also been detected within the bulk material, underneath impact craters (see Figure 2.3). Andrews and Field (1982) suggested that surface melting will occur where the shear band intersects the surface within the impact crater. This, they suggested, will result in the formation of small spherical globules which will contribute to the target weight loss. In this way it is proposed that melting, due to adiabatic shear localisation, will play a major role in material removal by erosion.

Sundararajan (1983), continuing the work of Shewmon (1979), proposed two mechanisms by which adiabatic shear in erosion can lead to material removal. Figure 2.3 is taken from his work. First, as proposed by Hutchings, the raised lip of material around an impact crater (Figure 2.3,I) may become detached by separation along an adiabatic shear band. Second, in the case of very hard materials, a network of shear bands (Figure 2.3, II) is formed at the base of the impact crater. Material is then removed in 'chunks' where the shear bands intersect.

The work reported above involved the projection of macroscopic (1 to 10mm) particles at metal surfaces. Timothy and Hutchings (1983) investigated the dependence of adiabatic shear band activity on particle size and found that there was a critical size of projectile below which no shear bands were formed. They fired steel shot, of sizes from 0.3mm to 6.35mm, at velocities up to $320ms^{-1}$ at normal incidence onto a titanium alloy. This alloy (Ti - 6% Al - 4%V) is known to be very susceptible to adiabatic shear band formation; the impact conditions were chosen to be extremely severe in comparison with common erosive conditions. They found that the

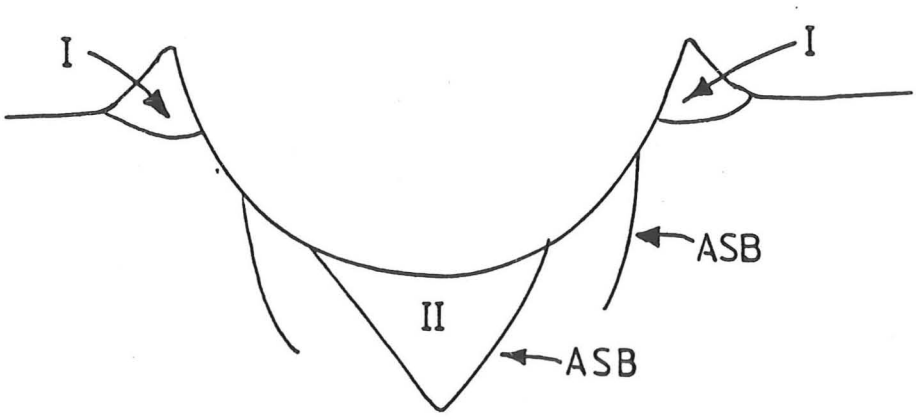

Figure 2.3 : Mechanisms of material removal proposed by Sundararajan (1983)

pattern of shear bands changes with projectile size, and that the shear band width, and depth of shear band damage both diminish more rapidly than the projectile size. They concluded that for a given velocity there will be a critical value of sphere diameter below which the deformation will fail to localise into adiabatic shear bands. Thus the role of adiabatic shear in erosion may be much less important than has previously been suggested.

CHAPTER 3 : INTRODUCTION TO THE PRESENT STUDY

3.1 EROSION BY SOLID SPHERICAL PARTICLES AT NORMAL INCIDENCE

It is generally found that the erosion rate of ductile materials is at a maximum at angles of incidence in the range 20^{o} - 30^{o}; the experimental evidence for this is reviewed in Chapter 1 section 1.2.2 (a). Early experimental and theoretical investigations of the erosion of metals consequently concentrated on wear at these shallow angles of incidence. The mechanisms which have been proposed for the erosion of metals at glancing angles of impact are discussed in Chapter 2, sections 2.2 and 2.5.

More recently, attention has turned to erosion at normal and near-normal impingement. Most workers agree that in the erosion of ductile materials by spherical or rounded particles the major mechanism of material removal involves the detachment of thin flakes of metal which are formed by multiple impacts. However, as concluded in Chapter 2 section 2.7, there is less agreement concerning the mechanism of formation of these flakes or platelets. Bellman and Levy (1981) proposed a combined forging-extrusion mechanism, with a soft (flaky) surface layer above a harder subsurface layer. In contrast Rickerby and Macmillan (1980) initially suggested a hard (flaky) layer above a softer bulk, but subsequently revised this, to propose an extrusion process involving a hard subsurface layer (Rickerby and Macmillan (1982)). Carter et al (1980) also suggested that the flakes were hard; their proposed mechanism involved the flow of metal from ductile troughs on a rippled eroded surface to embrittled wave crests.

The work described in Chapter 6 was carried out in an attempt to investigate the erosion process under conditions of normal impact by spherical particles.

The surface features of specimens eroded in this way are well documented, and include flakes and surface ripples. The present study concentrates on the examination of the subsurface structure developed by erosion, and attempts to interpret the surface features in the light of these observations.

In Chapter 7 consideration is given to the magnitude of the stresses and strains occurring in an erosion damaged surface. The erosion mechanism proposed in Chapter 6 is analysed in detail, using techniques developed for estimating forces in metal working operations. Experimentally observed deflections are analysed to provide estimates of the strains developed by erosion at normal angles of impingement.

The material in Chapter 6 has been published, (Cousens and Hutchings (1983a)).

3.2 PARTICLE VELOCITY MEASUREMENT

As reported in Chapter 1 (section 1.2.2(b)) it is generally found that erosion, E, (expressed as mass loss per unit mass of erodent) is related to the particle velocity, V, by the relationship :

$$E \propto V^{2.4}$$

Clearly the velocity of the erodent particle is an important factor in the erosion process. The velocity of the particle on impact is possibly the most difficult parameter to measure in an erosion experiment. Several velocity measurement techniques have been used in erosion research. These include photographic methods, laser doppler anemometry and a mechanical 'shutter' device. Chapter 5 describes in detail the methods available for

use, and concludes that all have significant limitations. As a consequence it was decided to develop a new particle velocity measurement technique specifically for use in erosion testing. The development of this device is described in Chapter 5. The measurement is based on the determination of the particle's 'time of flight' as it interrupts a pair of light beams which are set at a known distance apart. These interruptions are detected by photo-electric devices and the electronic signals generated are analysed by a cross-correlation method. Chapter 5 also presents full details of the experimental equipment and techniques.

3.3 THE EFFECT OF PARTICLE SHAPE ON EROSION

In a recent review, Finnie (1978) concluded that 'a weakness of most erosion research is that the properties of the particles except for size have received little attention'. It is generally agreed that along with size, hardness and strength, particle shape is an important factor influencing erosion. Chapter 1 (section 1.2.4(b)) presents a review of the literature reporting studies of the effects of particle shape and erosion. This review revealed that this aspect of the erosion of ductile materials is poorly understood. While itis clear that the mechanism of material removal is sensitive to particle shape, it has not been possible to describe this sensitivity theoretically.

Chapter 8 reports an experimental study into the effect of erodent particle shape on the erosion of mild steel. This work involved measurement of erosion at different angles of particle impingement, together with detailed observations of the surface features of eroded specimens.

The experimental study of Chapter 8 is complemented in Chapter 4 with a review of the literature describing shape measurement. Whilst it is discovered that shape measurement is a problem confronting a wide range of disciplines (from geography to chemical engineering) it is concluded that no simple solution is available. The methods most suitable for use in erosion studies are identified and possible developments outlined.

The material presented in Chapter 8 has been published (Cousens and Hutchings (1983(b)).

3.4 THE EFFECT OF ION IMPLANTATION ON THE EROSION RESISTANCE OF MILD STEEL

Ion implantation is a relatively new technique for introducing foreign species into the surface of a material, with the objective of modifying the mechanical, chemical or electrical behaviour of the material close to the surface.

Historically, ion-solid interaction was first recognised by physicists during the development of nuclear reactors. The effect of major interest was radiation damage. Ion implantation techniques were then initially developed for the production of semi-conductors. Low ion dose rates are used for doping semiconductors; essentially it is a technique for achieving controlled low concentrations of an impurity element. Most recently, higher dose rates, achieving higher concentrations have been used to modify surface mechanical properties.

A discussion of the ion implantation process is beyond the scope of this work; Dearnaley (1978) may be consulted for a detailed introduction.

Dearnaley and Hartley (1979) listed a number of important material properties which are controlled by the near-surface composition and physical state of a solid, including friction, wear, hardness, corrosion resistance, electro-

chemistry, catalysis, interfacial bonding, lubrication and adhesion. Potentially, they suggested, ion implantation can affect any or all of these properties.

The increase in wear resistance as a result of ion implantation is an area which has received much attention. Ion implantation has been attempted on a wide range of materials, for example; steels (Hartley (1975), Herman et al (1979), Pethica et al (1982), Dearnaley et al (1979)), iron (Pethica et al (1982), Shepard et al (1982), Ashworth et al (1977)), titanium (Pethica et al (1982), Shepard et al (1982)), aluminium (Ashworth et al (1977)), chromium (Pethica et al (1982)), copper (Shepard et al (1982)), phosphor bronze (Saritas et al (1982)), tungsten carbide (Dearnaley et al (1979) and silicon and silicon carbide (Roberts and Page (1982)).

Implanted species have included N, B, C, P, Cr, Fe, Ti, Al, Ni, Si, Zn, Y, La, Sr, Eu, Ce and Ba; most commonly however, the lighter elements N, B and C are used.

In his recent review paper Dearnaley (1982) collected evidence that ion implantation improves resistance to sliding wear, rolling contact fatigue, abrasive wear and corrosion. Shepard and Suh (1982) reported improved resistance to lubricated sliding wear achieved by ion implantation. Herman (1981) reported improvements in the fields of friction, wear, cavitation erosion and fatigue, and similarly Saritas et al (1982) reported 'significant and persistant beneficial effects' on sliding friction and wear.

chemistry, catalysis, interfacial bonding, lubrication and adhesion. Potentially, they suggested, ion implantation can affect any or all of these properties.

The increase in wear resistance as a result of ion implantation is an area which has received much attention. Ion implantation has been attempted on a wide range of materials, for example; steels (Hartley (1975), Herman et al (1979), Pethica et al (1982), Dearnaley et al (1979)), iron (Pethica et al (1982), Shepard et al (1982), Ashworth et al (1977)), titanium (Pethica et al (1982), Shepard et al (1982)), aluminium (Ashworth et al (1977)), chromium (Pethica et al (1982)), copper (Shepard et al (1982)), phosphor bronze (Saritas et al (1982)), tungsten carbide (Dearnaley et al (1979) and silicon and silicon carbide (Roberts and Page (1982)).

Implanted species have included N, B, C, P, Cr, Fe, Ti, Al, Ni, Si, Zn, Y, La, Sr, Eu, Ce and Ba; most commonly however, the lighter elements N, B and C are used.

In his recent review paper Dearnaley (1982) collected evidence that ion implantation improves resistance to sliding wear, rolling contact fatigue, abrasive wear and corrosion. Shepard and Suh (1982) reported improved resistance to lubricated sliding wear achieved by ion implantation. Herman (1981) reported improvements in the fields of friction, wear, cavitation erosion and fatigue, and similarly Saritas et al (1982) reported 'significant and persistant beneficial effects' on sliding friction and wear.

Experimental results have been published (Pethica (1982)) which indicate that the depth of the implanted layer is of the order of 0.1 to 0.2μm. Although this is small it was nevertheless felt worthwhile to examine the effect of ion implantation in steel on its resistance to solid particle erosion. To date there has been no such experimental study reported in the literature.

A small number of mild steel specimens ion-implanted with nitrogen were available. Chapter 9 reports the results of a study investigating the effect of nitrogen ion implantation on the erosion resistance of mild steel.

CHAPTER 4 : PARTICLE SHAPE ANALYSIS - A LITERATURE SURVEY

4.1 INTRODUCTION

A discussion of the effect of particle shape on the erosion of ductile metals was presented in Chapter 1, section 1.2.4(b). Chapter 8 presents the results of an experimental investigation in which mild steel is eroded by particles of different shapes. This chapter presents a literature survey of the methods available for analysing particle shape, with the aim of selecting methods which can be used to describe the shape of particles taken from erosive environments, or commonly used in erosion studies. There are several examples in the literature of attempts to control the erodent particle shape.

In single particle experiments it is possible to project a particle of well characterised morphology (sphere, disc, cube etc) at a known angle and orientation onto the test surface (Hutchings (1975b), (1979b)).

In multiparticle experiments the erodent is commonly a commercially available powder or abrasive grit. The use of spherical glass ballotini is one method of simplifying the geometry of erosion tests; the use of metal shot can also be successful provided care is taken with the method of its production (Exner and Linck (1977)). Experiments using angular abrasive grits raise the problem of defining the shape of the grit, measuring its size distribution and, if at all possible, arranging the orientation of the particles at impact.

It is hoped that the use of some measure of shape will allow greater control over erosion testing. Characterising grits and powders will allow

meaningful comparisons of results and enable laboratories to standardise testing methods. Measurements of the sensitivity of erosion rates to particle shape will provide information on mechanisms of material removal. Dust samples from industrial environments (such as coal gas converters) can be examined and the selection of erodent for laboratory tests facilitated.

Whilst acknowledging the importance of particle size measurement in erosion studies, and the close association between size and shape measurement, this survey concentrates on the literature describing shape measurement.

One of the striking features of the literature in this field is the range of disciplines embraced; Pohl and Redlinger (1977) suggested that the anatomist Henning initiated the development of quantitative microscopy in shape measurement. Mandelbrot (1977) developed an analysis from the work by Richardson on measurement of geographical features. Geology, petrology, chemical engineering, metallurgy and materials science, civil engineering and agricultural engineering are among the disciplines contributing in this field.

As an aid to presentation, two broad categories have been used: feature measurement and shape analysis.

Feature measurement combines a series of measurements or observations to produce a quantitative statement about one aspect of a particle's shape.

Shape analysis attempts to transform a large series of measurements mathematically to produce a complex statement about the relationships between many features of a given shape.

Table 4.1 : Extract from BS 2955 : 1958 'Glossary of terms relating to powders' British Standards Institution, London 1958.

Acicular	Needle shaped
Angular	Sharp-edged or having roughly polyhedral shape
Crystalline	Of geometric shape freely developed in a fluid medium
Dendritic	Having a branched crystalline shape
Fibrous	Regularly or irregularly thread-like
Flaky	Plate-like
Granular	Having approximately an equidimensional irregular shape
Irregular	Lacking any symmetry
Nodular	Having rounded irregular shape
Spherical	Global shape

4.2 FEATURE MEASUREMENT

4.2.1 Methods which use words to convey shape characteristics

From infancy we learn to classify objects by comparison, and descriptions such as 'plate-like' remain acceptable in the scientific literature. British Standard BS 2955 contains definitions of particle shape, and part of the standard is reproduced in Table 4.1.

The obvious problem with such a classification scheme is that although it is possible to describe certain idealised shapes, real particles will have shapes lying between classes.

It is important to recognise that at present the description of shape in the erosion literature is almost entirely at this level.

(a) Shape groups

In order to define more clearly descriptions such as those found in Table 4.1 several workers have suggested the use of shape groups. Figure 4.1 illustrates this concept. Ratios of breadth/length and thickness/length define an area divided into named regions.

The borders between the regions are chosen arbitrarily and the concept of such a sharp division has little practical bearing.

Later in this section the use of triaxial plots in feature-space representation of shape is discussed. The use of two (and three) dimensional plots to describe shape, and shape distributions can be seen as a development of this simple classification.

(b) Fuzzy sets

Under the discussion of shape groups, the relevance of sharp divisions between types of shape was questioned, especially in the context of continuously varying shape 'ratios'. Bezdek (1977) discussed the use of fuzzy sets in property representation (see also Beddow (1976b, 1980)).

In an ordinary set there are only two levels of 'belonging'; $\emptyset$ represents a non-member and 1 represents a member; Beddow described a fuzzy set as being 'a class in which there is graded membership'. He cited the example of the set of 'old men'. This is poorly represented by ordinary set theory, which assumes a sharp borderline dividing all men into old and not old. Fuzzy set theory gives each individual a grade in the set of 'old men'.

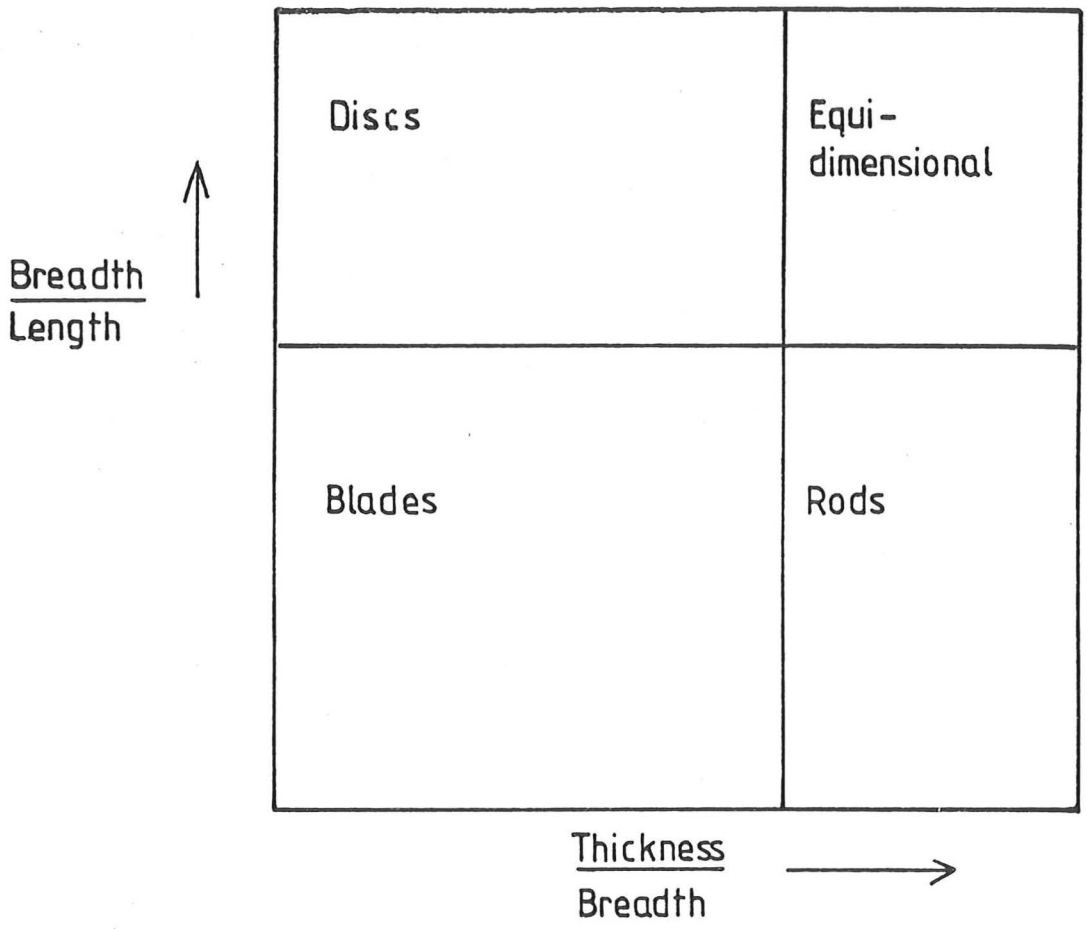

Figure 4.1 : Shape groups

In his article Beddow (1980) suggested the usefulness of the theory of fuzzy sets in constructing models for many situations. Clearly it is an attractive system for acknowledging the continuous spectrum which lies between extremes of shapes. As in ordinary set theory relationships between sets and subsets are defined, and the idea of an inexact inference is developed.

It remains to be shown how fuzzy set theory can be developed to provide a useful method for describing and manipulating shape descriptions and factors.

4.2.2 Shape measurements derived from bulk properties

The relationship between the shape of individual particles, and the behaviour of bulk powders, is the driving force behind the search for methods of describing and quantifying particle shape. Thus in an erosion study, to be able to describe the shape of the erodent and then to compare rates of erosion using erodents of differing shapes will add to our understanding of mechanisms of erosion. Shape description will enable more control of the variables in erosion experiments generally.

The use of bulk properties of powders to describe shape is to apply this principle in reverse. The measurement of sieving behaviour, compaction behaviour, porosity, flow rate, permeability and bouncing under controlled conditions have all been suggested (Beddow et al (1976a)).

The major problem with this method is that of finding a relevant bulk property to measure. A measurement of compaction behaviour will perhaps help define particle shape for sintering studies, but it is difficult

to see how anything short of quoting an erosion rate under controlled conditions would be of use in this field. Such a description hardly meets the needs mentioned above.

4.2.3 Methods using shape factors to describe particle shape

A shape factor represents an attempt to assign a number to a word describing a single feature of a shape.

Shape factors are calculated from measurements of individual particles, usually measurements on profiles of particles.

Before discussing specific factors, it is useful to list certain requirements that must be met by a shape factor for use in erosion studies.

(i) The measurements necessary to compute the factor must be easily and reliably made.

(ii) The shape factor must not be dependent on the size of the particle.

(iii) The shape factor must not be magnification dependent.

These requirements are outlined in detail below :

(i) The measurements necessary to compute the shape factor must be easily and reliably made.

A major factor in considering the ease of making measurements is the availability of such facilities as image analysing computers. A list of

measurements which can be readily made using such equipment follows this section. Any factor requiring measurements not on this list (for example Wadell's roundness factor involves measuring radii of curvature (Wadell (1932, 1933), Davies (1975)) will depend on the speed and skill of the technician. In some cases it may be possible to express a parameter in terms of combinations of the available measurements, but this will not always be the case. No attempt to compute Wadell's roundness factor from image analysing computer measurements has yet been reported.

The consideration of reliability must be made when investigating the experimental procedures leading to actual measurements. Most methods require a profile to be generated - this profile is then examined. Commonly a sample of the powder is spread on a microscope slide, magnified and viewed under transmitted light. The silhouette generated can then be photographed or viewed by a television camera connected to an image analysing computer.

Chernyavskii (1978a,b), among others, pointed out that this is not a random method of sampling. Particles will lie in 'a position of greatest stability'. Effectively this means that profiling by this method does not allow equiaxed flakes to be distinguished from equiaxed grits.

In order to apply a series of individual profile measurements to generating a description of an average particle, an assumption about particle shape must be made. The assumption that each particle's profile represents a random section through an average particle, demands that the sampling is truly random.

Other attempts to produce profiles are necessarily more complex. Work measuring grain shape, and pore shapes in castings (Pohl and Redlinger (1977)) illustrates the use of metallographic techniques. To apply such techniques to powder particle shape measurement the particles must be evenly dispersed in the mounting compound, avoiding alignment. A series of profiles for each particle is produced by carefully polishing and examining at a sequence of depths through the mount. It must be said that such a procedure would be difficult and tedious.

Davies (1975) described a microlathe microscopical system, in which particles are attached to a fine glass filament and rotated about this arbitrary axis under microscope examination. The profile which enclosed the maximum projected area was selected, measurements taken, then the particle rotated through a fixed angle and further profile measurements made.

Many complex shape factors have been suggested, and many complex systems of shape analysis developed, which are based on measurements taken from particle profiles.

Whilst recognising the difficulties involved in sampling, this literature survey reaches an early conclusion. It must be accepted that any shape description based on profile examination can only be as reliable as its method of particle profile generation.

(ii) The shape factor must not be dependent on the size of the particle

Measurements of size and shape are very closely related. In erosion studies the size of the erodent particle is recognised to be a very important parameter. It is therefore important that the description of shape be independent of size.

Fischmeister (1974) discussed this problem at length and rejected many suggested shape factors which could be shown to be either size dependent or to apply only to monosize systems. Monosize systems are exceptional in nature. Fischmeister warned against the use of average or assumed values to apply such factors to real systems. Consequently shape factors which are size dependent in either of these two ways are of little value in particle shape measurement in erosion studies.

(iii) The shape factor must not be magnification dependent

One of the earliest suggested shape factors, Wadell's roundness factor, was magnification sensitive (Wadell (1932, 1933), Davies (1975)) as he himself concluded. This factor involved the examination of a profile, and the measurement of the radii of curvature of the protrusions. Increased magnification will always reveal higher levels of texture for real profiles (not ideal geometric shapes).

Perimeter measurement, and also projected length in a given direction, will to some extent depend upon magnification. These observed facts are the genesis of the method of fractal analysis, and are discussed in detail later. It is sufficient at this stage to recognise that exact measurement of many features may not be possible for this reason, and so shape factor computations should not be highly sensitive to any single measurement.

(a) Measurements commonly used in shape factor determination

Fischmeister (1974) and Beddow et al (1976a) are useful sources for definitions of commonly used measurements.

Beddow (1976a) illustrated various dimensions which can be measured using a Quantimet image analysing computer. Figures 4.2 and 4.3 are reproduced from this reference. These figures define the dimensions clearly with the exception of Martin's diameter. There are two definitions of Martin's diameter in use, one illustrated by Figure 4.2, the other by Figure 4.3 (Beddow, (1976a), Chernyavskii (1978b)).

Figure 4.3 illustrates the definition 'Martin's diameter is the length of the chord which divides the profile area in two'.

This does not, however, uniquely define a length. On Figure 4.3 lines X', Y, Y', and X all contain chords satisfying this condition. Clearly the length of chords on X and Y are equivalent, but this length is different to those on lines X' and Y'.

As with the longest chord definition illustrated in Figure 4.2, it is important to define a direction in which the measurement is made. In a similar manner the direction of projection of Feret's diameter must be defined.

Fischmeister (1974) derived expressions which enabled, for example, area fraction to be related to volume fraction and line fraction. Such expressions will simplify calculation and measurement of features that can automatically be measured using image analysing computers, but are tedious to measure by hand.

Details of the types of computer analysis involved in image analysing computers can be found in a paper by Babu Rao et al (1982). Two methods

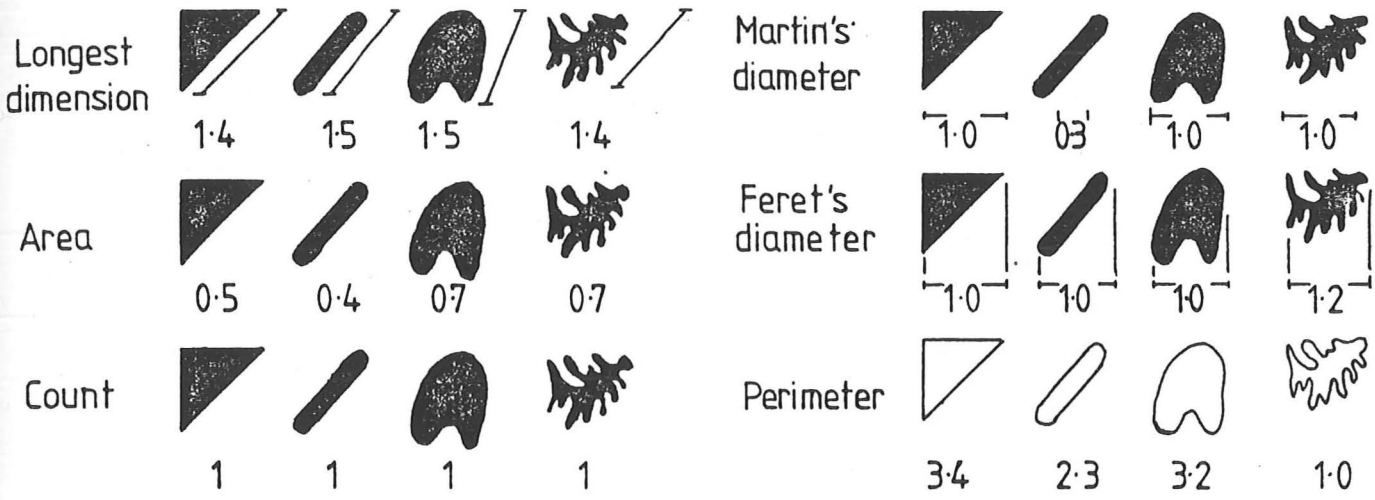

Figure 4.2 : Shape dimensions (after Beddow (1976a))

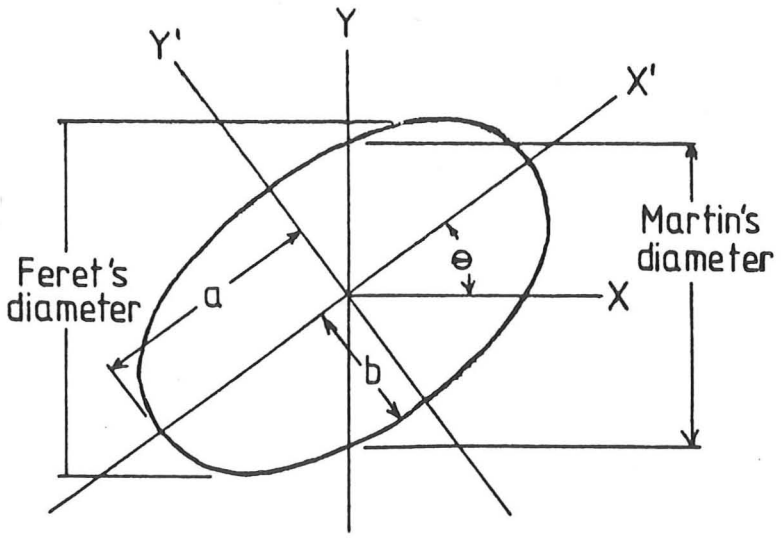

Figure 4.3 : Feret's and Martin's diameters (after Beddow (1976a))

were identified: Continuous Scan Method (CSM) and Feature Extraction Method (FEM). These methods differ in versatility, speed and memory requirements; CSM is recognised as quicker and requiring less memory, but suitable only for the computation of the simple parameters as listed above. FEM has great versatility; as Babu Rao stressed 'any parameter with an algorithm to obtain it can be computed'.

(b) Shape factors

Most commonly a shape factor attempts to show how a given shape deviates from an ideal geometric shape. Many examples of this type are available in the literature, some are mentioned below.

It is perhaps more satisfying, however, to develop a shape factor which does not measure how a given shape deviates from a standard, but rather quantifies positive aspects of shape. Fischmeister (1974) discussed this at length saying 'in this paper we shall examine how shape can be assessed without imposing a preconceived geometrical model. Such general shape factors, if they exist, will allow a more objective characterisation of shape: on the other hand we must not expect too much discriminating power from them'. This summarises the advantages and disadvantages of such factors - namely the lack of sensitivity outweighing the advantage of objectivity. The general factor he developed is related to mean average curvature and specific surface, or can be expressed alternatively in terms of mean surface, volume and diameter. His results suggested that the factor will not discriminate between grits as used in erosion studies: for example, the variation between a cube and a tetrahedron is very small.

(c) Comparative shape factors

To illustrate the use of comparative shape factors several references are summarised below.

(i) H Wadell (1932)

Sphericity is defined as the ratio of the surface area of a sphere having the same volume as the particle, to the actual surface area of the particle.

$$\Psi = \frac{\text{equivalent sphere surface area}}{\text{actual surface area}}$$

Roundness of a corner is the ratio of the radius of curvature of the corner to the radius of the maximum inscribed circle of the particle profile containing this corner. The total roundness of a solid in one plane is the arithmetic mean of the roundness of the individual corners.

Thus Wadell's factors compared a given shape with an equivalent sphere. Major problems exist with measuring and calculating these factors. Wadell (1933) suggested modifications for 'obtaining valid averages with economy of time', but still the treatment of large samples by his method is not practical. As mentioned earlier in this section, the roundness factor is magnification sensitive.

Wadell's factors are often quoted, and many shape factors are clearly developments of his basic ideas.

(ii) D Pohl and F Redlinger (1977)

In an investigation of pore shape measurement in sintered iron, the factor used was the 'true mean pore volume in relation to the apparent mean volume of equivalent spherical pores in the same specific surface'. The relationship between the shape of a pore, and the shape of a particle is obvious, and thus it can be seen that, as in Wadell's methods, we compare a given shape with an equivalent sphere.

A useful discussion of the method used to determine this factor is presented in their paper and the factor is shown to correlate with material properties.

(iii) H E Exner and E Linck (1977)

In an investigation of the shape distribution of lead powders, the factor

$$F = \frac{4\pi a}{u^2}$$

a = projected particle area

u = contour length

describes the deviation from a circle. (In the case of a circle F = 1).

Shape distributions are measured for lead powders produced by different methods and the shape factor is shown to be sensitive to the different degrees of roundness achieved. The value of semi-automatic image analysers, and desk calculators in data processing is stressed.

(iv) W C Krumbein (1941)

Krumbein developed Wadell's sphericity factor - improving the ease of measurement and calculation. He produced charts which yield values of sphericity for measured ratios of axes length. He specified orthogonal, but not necessarily intersecting axes, defining

$$\Psi^3 = (b/a)^2(c/b)$$

a, b and c are particle dimensions measured along the axes with a>b>c

Krumbein also suggested that visual inspection of profiles, and comparison with a selection of profiles of known roundness, enables this factor to be determined with reasonable accuracy.

(v) A I Medalia (1970)

Medalia proposed a dynamic method, based on the representation of an object as an ellipsoid with equivalent radii of gyration about the principal axes. This gives two types of dimensionless shape factors, the anisometry (elongation and flatness) and bulkiness, as well as the orientation.

In a very thorough account Medalia discussed methods of measuring his dynamic shape factors, and their interpretation. The measurements were readily carried out in two dimensions, but extension to the third is difficult, involving such techniques as

serial sectioning. He suggested 'these numerical shape factors were not intended to replace the usual qualitative descriptions of shape, such as 'dendritic', 'acicular', etc and should preferably be used in conjunction with such descriptions'.

Perhaps the most significant feature in this proposal is the attempt to compare a shape with a standard which will behave in a similar way - 'the ellipsoid is chosen so that it ... is dynamically equivalent to the particle; i.e. its motion in space, when subject to any force in proportion to its mass, is the same as that of the particle'. This, coupled with results which show a sensitivity to small changes in shape, and an ability to handle even re-entrant shapes, suggests that this may be a useful form of shape description in the study of erosion. (Medalia's work is an adaption of Hausener's in which he considers the dimensions of an enveloping rectangle of minimum area.)

(vi) G Lees (1964)

Lees discussed the problems which arise from using existing shape factors when trying to describe crushed or angular particles.

He defined a factor 'degree of angularity', which considered three major characteristics of angular particles.

(a) The angle existing between considered faces, measured in the plane normal to these faces.

(b) The 'relative projection' i.e. the projection of the tip of the corner from, and relative to the size of, the largest internal spherical mass of the particle.

(c) The number of angular corners.

The angularity of a single corner is defined as

$$A = (180^{o} - \alpha) \, x/r$$

Where α = measured angle

x = distance from the tip of the corner to the centre of the maximum inscribed circle

r = radius of the maximum inscribed circle

Lees factor will be magnification sensitive (he suggested projection of profile to a standard size as a way of normalisation) and also involves measuring three profiles per particle (the major axes must initially be discovered). The factor involves measurements which are not readily made by automatic image analysing methods.

These summaries illustrate the types of shape factors and the general principles of this form of shape representation. Numerous examples are given of factors involving ratios of various dimensions; Beddow et al (1976a), Davies (1975), Fischmeister (1974) and Underwood (1980) provide summaries of other, similar, factors.

4.2.4 Particle feature representation

Davies (1975, 1980) gave detailed accounts of how shape distributions can be represented by triaxial plots. Figure 4.4 is taken from Davies (1980) and illustrates how shape factors or particle dimensions can be used to distribute results of shape measurements across a triaxial plot. Davies showed how the distributions change to represent changes in particle morphology. The use of a third dimension was suggested as a way of allowing form and feature measurements to be combined in describing the distribution. An example of such a 'feature space representation' is to use a triaxial plot of thickness, length and breadth extended into the third dimension with an axis proportional to roundness.

4.3 SHAPE ANALYSIS

In the previous section methods of combining measurements, or observations, in order to obtain a description of shape, were discussed.

In this section mathematical methods which attempt to describe profiles exactly are discussed. Also included is a description of fractal analysis which although involving a feature measurement (perimeter), is more accurately described as an analysis of dimension.

4.3.1 The geometric signature waveform

In both Fourier and Walsh methods (see below) the starting point is to generate a 'geometric signature waveform' of the two dimensional profile of the fine particle.

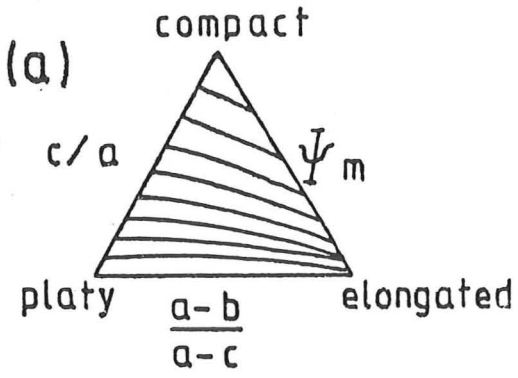

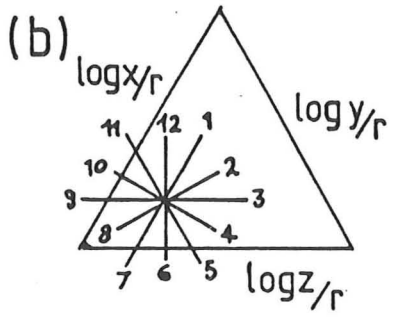

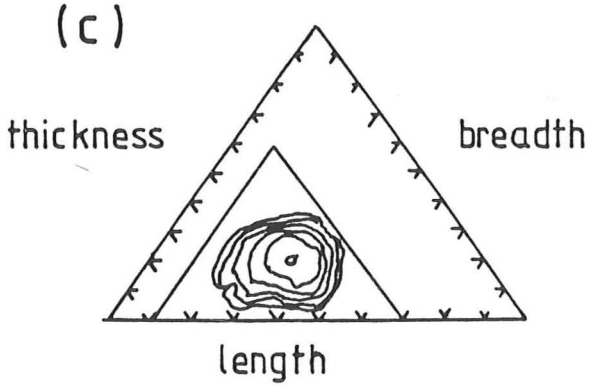

Figure 4.4 : (Taken from Davies (1975)) :

(a) Triangular plot, as used by Sneed and Folk
a = long diameter, b = intermediate diameter
c = short diameter, Ψ_m = maximum projection sphericity
($\Psi_m = 3\sqrt{c^2/ab}$)

(b) Types of transformation (a is X intercept, b is Y intercept, c is Z intercept and $r^3 = abc$). If we shape changes in the directions shown by the arrows the transformation is :

1,5,9 : constriction along Z,X,Y, respectively
3,7,11: flattening along Z,X,Y, respectively
2,8 : plane strain in ZX
4,10 : plane strain in YZ
6,12 : plane strain in XY

(c) Three-dimensional contour data for sharp silicon carbide

The problem of obtaining a representative profile, and the associated problems in constructing a three dimensional description from one or more profiles, have been discussed at length above. Analyses based on 'geometric signature waveforms' will necessarily be limited by the profile generating step.

Having obtained a profile, to generate a signature waveform the profile is swept by a rotating vector, and a plot of vector length versus angle is obtained. A second problem arises - the definition of an origin for the coordinates. Kaye (1978) discussed this problem. Some workers he reported, have used the centre of the smallest circumscribing circle as the pivot point for the rotating vector. Others used the centre of gravity which the profile would have if it were treated as a thin laminar fine particle (Meloy (1980)).

Kaye (1978) stated 'There is no a priori merit in either of these reference pivot points and many other reference points are possible'.

The Feret's diameter signature waveform is suggested as an attempt to overcome this problem. This describes the variations in the magnitude of the Feret's diameter of a profile for a systematic set of varying orientations. This waveform however describes a convex hull formed around the actual profile and as such does not accurately describe a profile with re-entrants.

The problems of re-entrants also arises with the rotating vector method of generating a signature waveform, for in this case there will be three possible values of vector length for given values of angle, as shown in Figure 4.5.

The problem of obtaining a representative profile, and the associated problems in constructing a three dimensional description from one or more profiles, have been discussed at length above. Analyses based on 'geometric signature waveforms' will necessarily be limited by the profile generating step.

Having obtained a profile, to generate a signature waveform the profile is swept by a rotating vector, and a plot of vector length versus angle is obtained. A second problem arises - the definition of an origin for the coordinates. Kaye (1978) discussed this problem. Some workers he reported, have used the centre of the smallest circumscribing circle as the pivot point for the rotating vector. Others used the centre of gravity which the profile would have if it were treated as a thin laminar fine particle (Meloy (1980)).

Kaye (1978) stated 'There is no a priori merit in either of these reference pivot points and many other reference points are possible'.

The Feret's diameter signature waveform is suggested as an attempt to overcome this problem. This describes the variations in the magnitude of the Feret's diameter of a profile for a systematic set of varying orientations. This waveform however describes a convex hull formed around the actual profile and as such does not accurately describe a profile with re-entrants.

The problems of re-entrants also arises with the rotating vector method of generating a signature waveform, for in this case there will be three possible values of vector length for given values of angle, as shown in Figure 4.5.

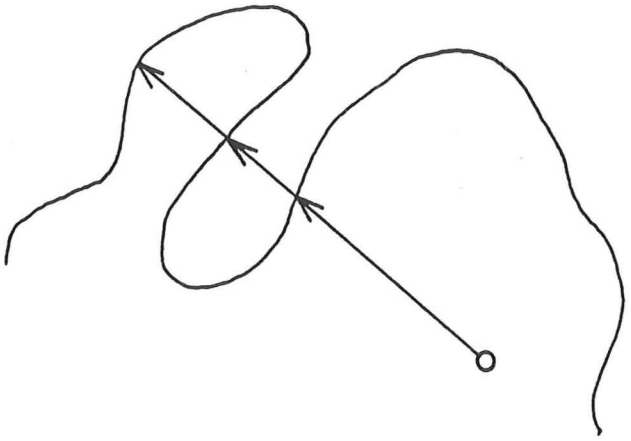

Figure 4.5 : The magnitude of the generating vector is not single valued as it crosses a re-entrant loop on the profile

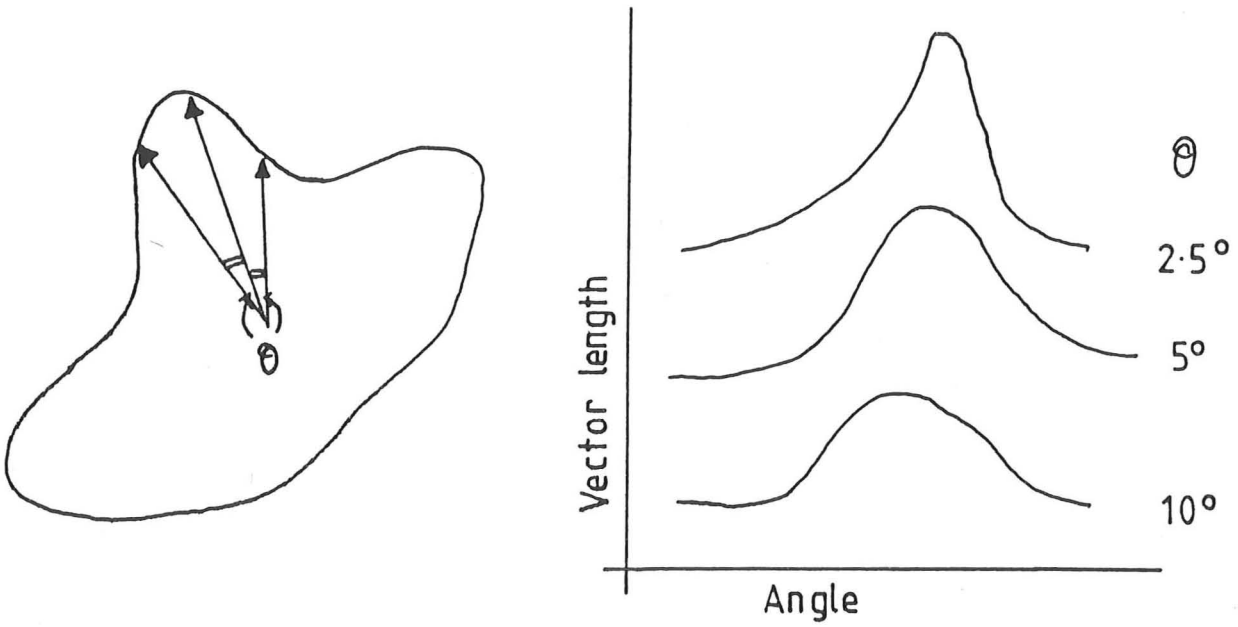

Figure 4.6 : As the angle between vector measurements, θ, is decreased the resolution greatly increases.

Kaye also demonstrated the need for high resolution in examination to detect sharp protuberances on the profile. Figure 4.6, reproduced from his paper, shows that as the angle between vector measurements is decreased the resolution greatly increases.

4.3.2 Fourier Methods

The technique of Fourier analysis can be applied to the geometric signature waveform to obtain a set of coefficients. These coefficients define the signature waveform, can be used to reproduce the profile, and also are in themselves a shape classification tool.

Mathematically, if the profile is expressed in polar coordinates (R, θ), the function $R(\theta)$ can be described in terms of a Fourier series of the general form :

$$R(\theta) = A_o + \sum_{n=1}^{\infty} A_n \cos(n\theta - \alpha_n)$$

α_n is the phase angle

Ideally the series is infinite; in practice it is possible to compare the profile generated by Fourier synthesis on a string of coefficients with the original. This will enable a decision to be reached concerning how many coefficients are necessary to define a given profile.

A profile with sharp protuberances will, as mentioned earlier, require a large number of polar coordinates. In turn a large number of coefficients will be required to describe such a profile, the sharp peaks on the signature waveform requiring high frequencies in the analysis.

It may be necessary to use large numbers of Fourier coefficients to describe a particle or to differentiate it from another particle. Meloy (1980) developed a concept of 'particle signature', a plot of log A_n vs log n (A_n is the coefficient of the nth term), and noted that gross shape differences yield differences in the first few Fourier coefficients. Finer features of the surface (sometimes called 'texture') were represented by higher order coefficients.

The 'particle signature' is a useful method of handling large numbers of coefficients, but unless some significance can be given to each coefficient the technique is of little value, merely substituting one shape, 'particle signature', for another, profile.

Meloy (1980) showed the significance of the coefficients by plotting them out in pairs. The zero coefficient A_0 simply represented particle size.

A combined plot of A_0 and A_1 shows A_1 to be the only asymmetrical term; Meloy stated that A_1 is thus a measure of the error in computing the centre of gravity (origin for the polar coordinates). A combined plot of A_0 and A_2 produces a dumb-bell shape, and thus A_2 is a measure of particle elongation.

A combined plot of A_0 and A_3 produces a triangular form with concave sides; thus, stated Meloy, A_3 shows the triangularity of the particle. If the profile is indeed triangular, the meaning of a large value of A_3 would be evident. Presumably a square will produce a large value of A_4. Being sharp cornered figures, we would also expect to have to use a large number of coefficients to fully describe and reconstruct them.

It is difficult however to interpret the significance of coefficients describing real, irregular particle profiles.

Referring again to Meloy's 'particle signature', the log A vs log n plots have slopes characteristic of particle profile shape. The values measured (Meloy (1980)) vary from -1.34 to -2.5 for a variety of particles, spherical bearing to long block respectively. From these results Meloy proposed the 'Law of morphological coefficients' :

'Fourier (and Walsh) coefficients are inversely proportional to a power of the frequency of the coefficient'.

Meloy developed his idea that the data are characterised by slope, intercept and scatter about the straight line. Figure 4.7 is taken from Meloy (1980) to illustrate this law.

The use of Fourier methods in erosion studies, for particle shape characterisation, will be discussed together with the application of Walsh analysis, after the next section.

4.3.3 Walsh methods

In Fourier methods, the use of the analysis to generate a series of coefficients was described. The general form of the series is :

$$R(\theta) = A_0 + \sum_{n=1}^{\infty} A_n \cos (n\theta - \alpha_n)$$

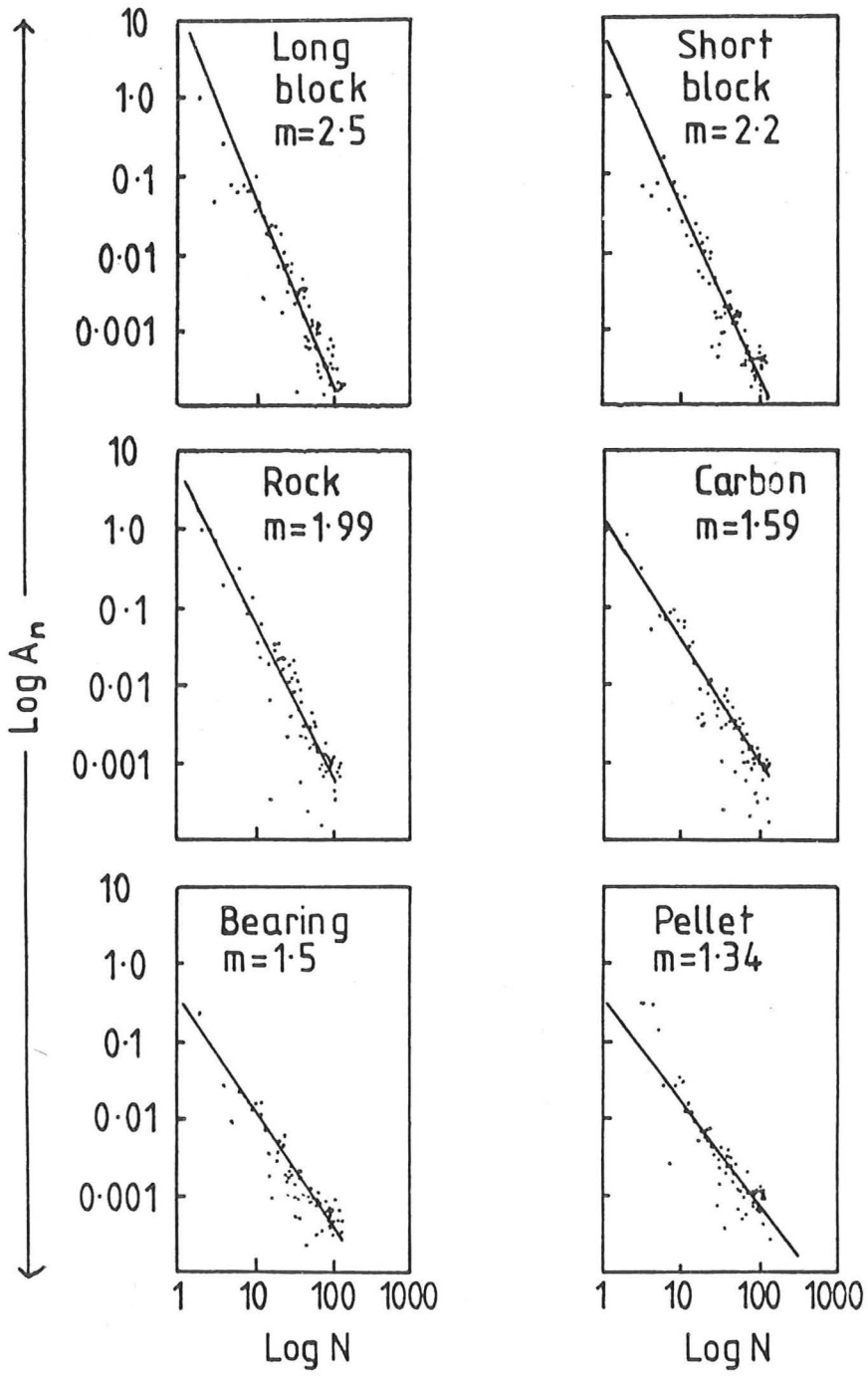

Figure 4.7 : Illustrating Meloy's 'Law of morphological coefficients', after Meloy (1980).

In a similar manner a Walsh series can be used to produce coefficients :

$$R(\theta) = A_0 + A_1 \, WAL(1,\theta) + A_2 \, WAL(2,\theta) + \ldots$$

In this equation A_0, A_1, A_2 ... are the Walsh coefficients. WAL (n,θ) where n=1, 2, 3 ... are Walsh functions.

Meloy plotted out values for the Walsh coefficients, as with the Fourier coefficients. The major difference is that whilst the variation in Fourier coefficients is smooth, sinusoidal, the Walsh coefficients vary as a block wave. Phase information is lost during Walsh analysis, and it is not possible to uniquely define a sum of coefficients as with the Fourier series. Lew et al (1979) discussed a modified Walsh transform, known as the R-transform, which is independent of the phase of the input signal. Unfortunately, such a modification also makes the transform less sensitive to finer detail of the profile. In addition the original series cannot be recovered by an inverse transform, as can be achieved with the standard Walsh transform.

Meloy used the coefficient of the Walsh transform to compute morphological characteristics such as excess surface area and edge length, number of corners and volume of positive blocks (Lew et al (1979), Meloy (1980)).

The great advantage of Walsh transforms compared with Fourier is that using Fourier coefficients it is extremely difficult to calculate even the simplest surface properties. Walsh coefficients can be readily used, because superposition can be assumed.

It is not possible in this survey to discuss at length the derivation of Meloy's equations and Walsh transforms generally. Meloy (1980) can be consulted for his thorough discussion on coefficients and feature measurement. Lew et al (1979) demonstrated the use of Walsh coefficients in characterising four different metal powders.

4.3.4 The use of Walsh and Fourier methods in erosion studies

In both forms of analysis, it is difficult to imagine how a simple list of coefficients could be used to characterise particles as used in erosion studies. The profiles in general will be irregular, and far from geometric.

If Figure 4.7 is examined, it would appear that the slope of Meloy's log A_n vs log n plots is not sensitive enough to enable, for instance, the difference between a sharp and a blunt grit to be quantified. The range of -1.34 to -2.5 describes the difference between a spherical bearing and a block. The large scatter of points suggests that only the first decimal point can be quoted with confidence.

Beddow (1980) suggested the use of various shape factors which are calculated from Fourier coefficients (centroid aspect ratio, lumpiness, roughness and assymmetry). Their plots, however, suggested that this method was also lacking in the sensitivity required.

Walsh methods would appear to be more useful but the literature suggests that there are certain areas of weakness. The modified Walsh transform, the R-transform, has been proposed as the only form suitable for morphological analysis (Lew et al (1979)). However, this lacks sensitivity being unable to represent accurately the finer details of particle profiles.

It is also felt that the significance to erosion studies of the various morphological characteristics needs careful investigation. The distributions for the quoted measurements appear to be very large and the variety of shapes within each particle type measured would appear to be the cause.

In order to implement either method, a method of digitising profiles, and data processing must be developed. Only by developing this technique using an image analysing computer would it be possible to collect and process the vast amount of data necessary for each profile. Lew measured only 50-100 particles for each of the four sets; certainly it would be hoped that the technique of data collection and analysis could be improved to allow much larger samples to be processed.

The general conclusion is that the adoption of either technique for shape classification in erosion studies will require time and effort that could more usefully be spent in developing other methods. It would be valuable to check the literature for further work in developing the Walsh method, especially work involved with measurements on varieties of real powders.

4.3.5 The SHADOW system

Kaye (1978) detailed this system; the name comes from the acronym Shape Analysis by Diffraction Originated Waveform. In this system a silhouette of the fine particle is used to generate a Fraunhofer diffraction pattern using laser light. This diffraction pattern is interrogated using a disc from which a V-shaped sector has been cut, which rotates in front of a photocell. The resultant wave generated in one revolution of the interrogation disc is treated as a signature waveform for the description of the fine particle profile. As with other forms of analysis the overall shape of the particle contributes part of the signature waveform

and the texture edges contribute the rest.

To quote Kaye: 'In some situations, the fact that some of the optical information is coming from the edges of the profile can be exploited to give a measure of the presence of sharp edges in a powder which is to be sintered'.

Thus the SHADOW system would seem to be of some relevance. Actual measurements of types of grits used in erosion studies would indicate the usefulness of the system. An obvious and significant drawback, however, is the complexity of the system. In order to process large numbers of particles, an automated method of producing a silhouette, the diffraction pattern and the resultant signature waveform must be developed, with, of course, a complementary data processing system.

Once again, the conclusion must be a recommendation to explore simpler systems initially, whilst watching the literature for further progress.

4.3.6 Fractal methods in shape analysis

It is only possible to provide a brief introduction to fractal analysis; Mandelbrot (1977) is recommended for a more rigorous mathematical treatment of the subject.

As mentioned in the introduction, the development of fractal methods in shape analysis stems from the early work of Lewis Fry Richardson on measurement of coastlines.

In introducing the concept of fractal dimension, Mandelbrot considered Brownian motion. A traditional experiment considers the motion of a fine smoke particle in air. The random path is generally represented by a string of vectors which show the displacement of the particle after a fixed time interval. If a far smaller time interval for inspection is chosen, then the vector representing one displacement previously must now be replaced by a randomised zigzagging trajectory. In fact as progressively smaller inspection intervals are chosen, the path will always be similar - the vector at the low level of scrutiny being replaced by a trajectory in every way similar to the total route at that low level.

Kaye (1978) summed up by saying 'From an intuitive point of view, the fractal dimension of a self-similar fractal curve actually corresponds to the ability of that curve to cover an area with a dense array of points. Again, in a non-rigorous sense, one can picture a fractal curve of higher fractal dimension covering a plane with points more quickly and/or densely. Thus Brownian motion has a fractal dimension of 2, in that given a long enough time, the staggering colloidal particle will entirely cover a Euclidian two-dimensional area'. (The topological dimension of the Brownian curve is 1.) Thus the fractal dimension refers to a space or surface filling ability of a given curve.

In order to see how this concept is of value in shape representation we must look to Richardson's work with coastline measurements. One possible method of obtaining an estimate of the length of the coastline of Britain is to take the largest scale map available and walk along the coastline with a pair of dividers. For a given opening X the dividers will measure out a length L(X). If the opening is then reduced, a new estimate will be produced, L(X) increasing as X decreases. It would be expected that L(X) would converge to a limit, this being a true measure of the coastline length. In most cases however L(X) increases without limit.

Other methods of making such a measurement are available. We could imagine a man walking around the coastline, keeping away from it no more than a prescribed distance X, always taking the shortest possible path.

Another method is to consider enlarging every point on the coastline into a patch of radius X. The coastline is thus transformed into a tape of width 2X - the length of the coastline can be estimated by dividing the tape area by 2X.

A fourth similar method would be to replace the coastline with patches of radius X. Rather than insisting, as before, that every point along the coastline be replaced by a circle, we could state that the coastline be completely covered but with a string of circles, and using the smallest number possible. Again the circles have radius X, and the total area divided by 2X provides this estimate of length.

Whichever method is chosen, the general finding is always the same. As X decreases, L(X), the estimated length, increases, tending to infinity.

Richardson completed a series of such measurements, and found that for coastlines, this trend was always repeated. He also attempted to measure the circumference of a circle, using the dividers method, and discovered that this measurement did indeed converge on the expected value.

The conclusion Richardson drew was that the number of steps, for divider spacing X was approximately Q^{-D} where Q and D are constants associated with a given coastline. The estimated length is thus approximately $L(X) = Q^{1-D}$.

D is the fractal dimension, and for a true fractal curve will equal 2 (e.g. the Brownian motion path fills the plane); for a Euclidian line D is equal to 1 (equivalent to the observation that the length estimate of a circle's circumference tends to the expected value).

A value for D may be obtained from a plot of log (length estimate) vs log (step length) which should yield a straight line of slope 1-D.

Mandelbrot (1977) discussed the value of this concept in the description of other real phenomena, such as cloud shapes and the shape of carbon black aggregates. Schwartz and Exner (1980), Flook (1978, 1979) and Kaye (1978) discussed the use of fractal methods in particle shape analysis.

Kaye (1978) first discussed existing methods of shape specification, then introduced the concept of fractal dimensions. As a conclusion to his paper he reported some experimental results which indicated the potential usefulness of fractal methods in particle profile characterisation. He suggested that crushed particles will be describable as fractals, as well as various flocks and crystal agglomerates. He discussed the need for an automatic analysing method and suggested that it may be possible to develop a method of grid intersection to evaluate the fractal dimension. He adopted a convention of normalising the stride magnitude (X), expressing this as a fraction of the maximum Feret's diameter of the profile. Similarly, the perimeter was expressed as a multiple of the maximum Feret's diameter. The exact measurement of Feret's diameter is also sensitive to magnification and this must be borne in mind when accepting this convention. The slope, and thus fractal dimension, is independent of measuring unit. Provided that, for each particle, one measurement of Feret's diameter is made, the normalisation will be valid.

Flook (1978, 1979) published work on the problem of the automatic measurement of fractal dimension. Flook's method was based on the third of those suggested by Mandelbrot (see above). Flook used a Quantimet 720 to obtain perimeter estimates as a function of increasing stride length by dilating each point on the boundary with an octagonal structuring element. As detailed earlier, this allows an area measurement to be carried out by the image analysing computer; the perimeter estimate is calculated by dividing area by tape thickness (2X). The dilation is effected using a 2D Amender module.

Flook discussed the interpretation of the two part curves that this method generates. He said 'At low dilation the fractal dimension is dominated by the structure of the subunits; at higher dilation it is due to the coarser structure of the agglomerate'. Kaye (1978) made the suggestion that the smaller step generates a dimension characterising the texture of the profile while the larger steps characterise the overall boundary. Flook suggested that his results illustrate this.

The method of Schwartz and Exner (1980) attempted to automate Mandelbrot's 'dividers' method. They used a semi-automatic image analyser, the video-plan. The profile was followed with a cursor, to generate a string of coordinates of equal spacing. This data was stored and the profile length estimate was calculated for all coordinate points, giving the largest value for the length estimate. Schwartz and Exner discussed the need for careful choice of cursor width, to avoid superfluous data collection and to ensure adequate resolution. The next estimate of length used every second pair of coordinates, the third estimate used every third pair and so on. See Figure 4.8.

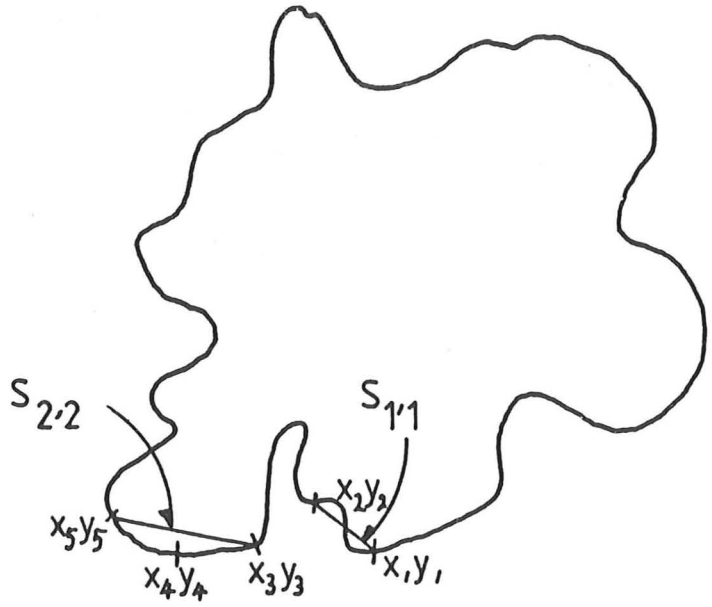

Figure 4.8 : Automatic measurement of fractal dimension. (After Schwarz and Exner (1980)).

$$\bar{S}_j = \sum_{i=1}^{k} S_{j,i}/k$$

$$P_j = \sum_{i=1}^{k} S_{j,i} + S_{j,1}$$

$\bar{S}_j$ = mean stride length

P_j = profile length estimate

In general the stride length will not be constant (except for stage 1, when the largest estimate is generated), therefore a mean stride length S is defined as the ratio of the profile length estimate to the number of distances counted. (Schwartz and Exner also discussed the problems involved with the last interval - the spacing between the first and last data points).

An anonymous reviewer makes a valuable contribution and suggests some reasons for the scatter found with this method. The choice of starting point for both this, and the simpler divider method, will in fact influence the estimate of perimeter length.

4.3.7 The use of fractal methods in erosion studies

The literature indicates that fractal methods enable the texture and general shape of a profile to be described in terms of fractal dimensions. Whilst such a simple description may not carry as much information as, for example,a string of Walsh coefficients, it may well prove adequate for ranking similar profiles. In this way,perhaps,it may be possible to describe and differentiate between two sets of grits, with regular sharp grits approximating to geometric profiles (and thus low dimensions) and blunt irregular grits approximating to fractal profiles (with fractal dimensions approaching 2). As yet there has been insufficient work on measurements of profiles relevant to erosion studies. Kaye's general remarks are encouraging.

The availability of a Quantimet image analysing computer with a 2D Amender module will encourage the adoption of Flook's method. The review suggested that this is not only more rapid than the Videoplan, but also produces results with less scatter, and so allows the collection of more reliable data from large samples.

4.4 CONCLUSIONS

The objective of this survey was to discover if a measurement of shape, or a shape analysis,existed which could be used to classify the erodent in erosion studies.

In the present chapter certain criteria, such as ease of gathering data, ease of calculation and sensitivity of the factor or measurement have been discussed.

No single method has been found which exactly fulfills the requirements and no report of measurements made on grits commonly used in erosion studies appears.

It is possible, however, to select a few methods which, with limited further investigation, may prove suitable.

4.4.1 Feature measurement

Of all the shape factors Medalia's dynamic method appeared most useful. It is the only comparative factor which attempts to discriminate shape by a relevant test.

The shape of various grits can be compared by Medalia's factors (ratios of the axes of the ellipses), as can the distribution of particle shape within samples of a given erodent.

Since Medalia's method produces an ellipsoid which has equivalent dynamic properties, it may be useful in theoretically modelling impacts of individual particles.

Problems do exist in three dimensional representations, and work must be done to test the speed of producing the relevant measurements (utilising a Quantimet 720 or similar image analysing computer).

The measurement of angularity proposed by Lees may prove suitable, but must either be adapted or used in conjunction with another shape factor (possibly Medalia's). Lees' factor considers only the angle between faces, and so maximum angularity would be assigned to a spiky particle. Intuition would suggest that the mass contained by an angular projection would prove to be a significant parameter in the area of erosion studies.

4.4.2 Shape analysis

General conclusions have been presented in the body of this chapter. In summary it is felt that either the complexity and difficulty of measurement, or the doubtfulness of the relevance, suggests that Fourier, Walsh and Shadow methods will not repay further investigation. Future developments in the literature concerning Walsh methods may prove interesting.

Fractal analysis, utilising an image analysing computer and the 2D Amender module, is thought to be promising. It should prove possible to ascertain quickly whether the method is sensitive in discriminating between types of erodent grits, and if, as hoped, the measure of dimension will in some way convey information about particle profile angularity.

Postscript

It has not been possible in the time available to attempt to measure the shapes of particles used in the work reported in the later chapters. The application of some of the factors or shape analysis methods to the measurement of single particles has been demonstrated. In some cases larger numbers of particles have been analysed. In terms of the numbers of particles used in individual erosion experiments the samples have always been small. Future work must concentrate on adapting the methods which have been identified as most suitable for analysis by image analysing computer.

It is important to note that the indents produced in erosion tests are generally small compared with the diameter of the particles. The ideal factor will, like Medalia's, convey information about the dynamic behaviour of particles, and also describe and measure features of the particle's shape on a scale relevant to the indentations.

CHAPTER 5 : DESCRIPTION OF APPARATUS

5.1 INTRODUCTION

In its simplest form, an erosion experiment arranges a collision between the target material and an erodent particle. Ideally the erosion test apparatus will enable a wide range of collision parameters to be studied.

First, it is necessary to be able to vary the angle of impact of the particle onto the target surface from 0^{o} to 90^{o} (normal impact). For non-spherical particles it is useful to be able to control the orientation of the particle on impact.

Second, the erosion test apparatus must be able to project particles with a wide variety of shape and size onto the target surface. Sizes of particles commonly encountered in the erosion literature lie in the range of 10μm to 10mm and shapes vary from angular abrasive grit through regular shaped discs and cubes to spherical beads and shot.

Finally, the erosion test apparatus must be capable of varying the collision velocity over a wide range, whilst ensuring that for a given test the velocity is held constant. Velocities reported in the literature vary from about one to several hundreds of metres per second.

There are several types of erosion test rig designed to meet some, or all, of the above requirements. The erosion test rigs may be classified as allowing single impact or multiple impact experiments to be conducted.

5.1.1 Single impact experiments

The gas gun has been used extensively for single-impact experiments (Hutchings (1979b), Shewmon (1979), Ives and Ruff (1978), Figure 5.1 (a)). A sabot, acting as a freely sliding piston, is propelled along a cylindrical tube by compressed gas. The gas is released from a pressure chamber by the rupture of a metal foil, the thickness and bursting strength of which is selected to control the sabot velocity.

The sabot carries the impacting particle or particles; it is brought to rest a short distance from the target and the particle or particles released to impact the target. The sabot and/or particle velocity is commonly measured by allowing it to interrupt a series of light beams.

This apparatus permits careful control of the velocity of impact and the angle of impact. It is also possible to arrange the orientation of the particle at impact. Although it is possible to carry a charge of several particles on a single sabot, one experiment is unlikely to give a measurable weight loss for the target. (It is not unusual to impact several kilograms of erodent particles in the course of an experiment to establish a value of erosion resistance.)

Another apparatus which enables the impact angle, velocity and orientation to be carefully controlled is a modified form of lathe. Gane and Murray (1979), used a lathe with an eccentric workpiece to arrange impacts with a tool tip. Again this is essentially a single-impact experiment, useful for examining deformation modes but not for establishing erosion resistance.

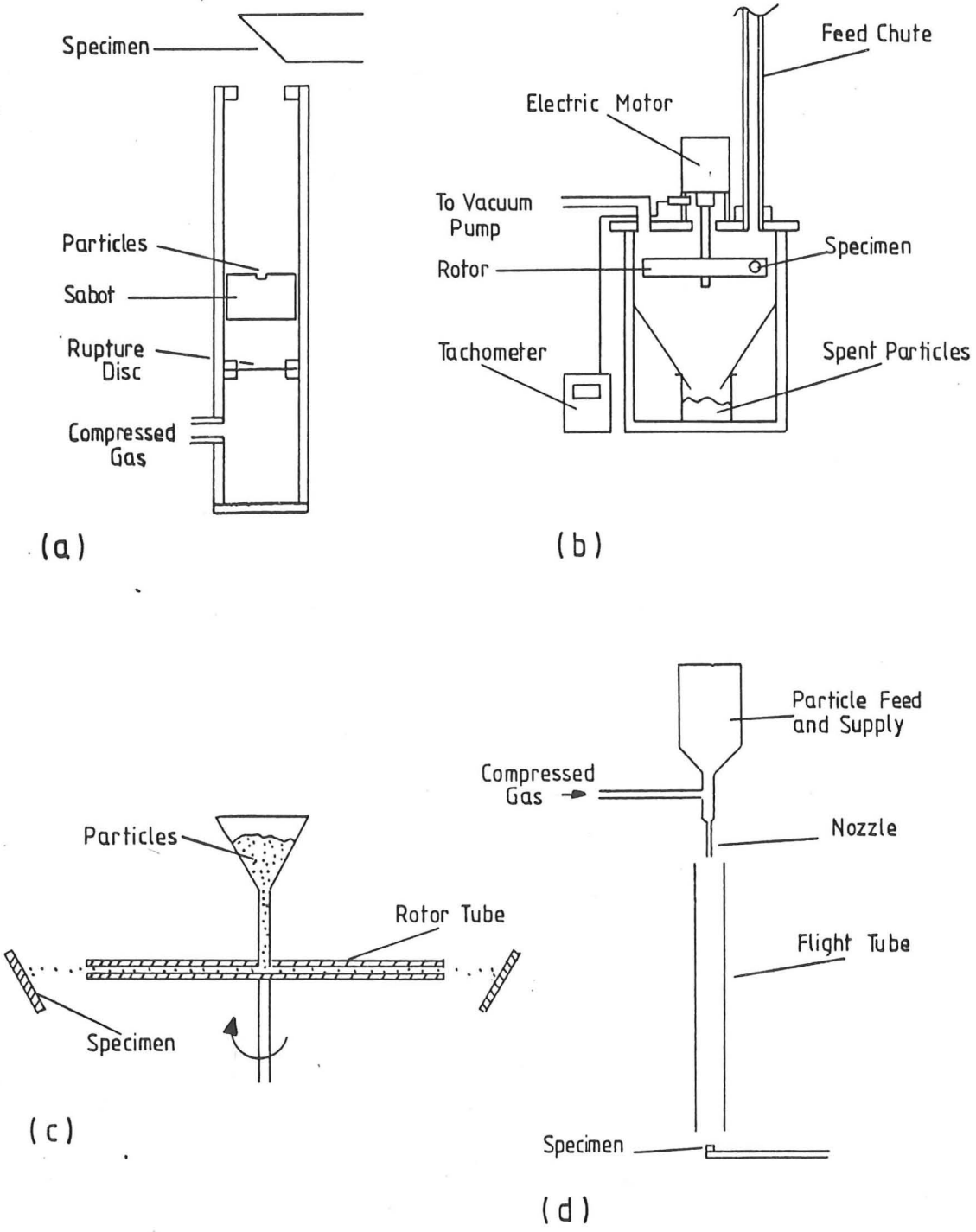

Figure 5.1 : Common types of erosion test apparatus

5.1.2 Multiple impact experiments

The rotating arm rig (Figure 5.1 (b)) is suitable for multiparticle experiments (Goodwin (1968)), Rickerby and Macmillan (1980), Towson (1980)). This apparatus consists of a rotor carrying two targets, spinning in an evacuated chamber. The erodent particles are dropped into the path of the targets. The chamber is evacuated to enable high velocities to be reached, free from air resistance. A further advantage is that it also ensures that the particles are not falling in turbulent conditions, and so impact at a controlled angle. It is not possible, with this apparatus, to control the orientation of the particle on impact.

Another apparatus based on a rotor spinning in an evacuated chamber, is the 'Slinger' erosion tester (Kosel et al (1979)). In this apparatus (illustrated in Figure 5.1 (c)), abrasive particles are fed into the centre of a tubular rotor rotating in a horizontal plane. The particles accelerate to the end of the tube and leave the rotor to strike specimens positioned at various angles around the sides of the evacuated chamber. The chamber may be evacuated, as with the whirling arm rig, to enable high velocities to be obtained with the absence of air resistance, and also to prevent particles being deflected by turbulence. The angle of impact will vary across the specimen, due to angular divergence of the particles leaving the rotor.

Alternative erosion test methods involve entraining particles in a stream of fluid directed onto the target surface.

The gas blast erosion tester uses a jet of compressed gas to carry a stream of particles onto the target (Figure 5.1 (d)) (Ives and Ruff (1979),

Gulden (1979), Brass (1977)). The gas is commonly compressed air, although the use of an inert gas is sometimes favoured to prevent surface oxidation of the target (Brown and Edington (1981a). The compressed gas and entrained particles are passed through an accelerating nozzle which allows the particles to reach the gas velocity, before striking the target. The nozzle's internal diameter is commonly in the range 1mm to 5mm. Neilson and Gilchrist (1968) utilised a novel form of gas blast erosion tester, in which in the place of a tubular nozzle, the particles were accelerated through a chute (termed a two-dimensional convergent nozzle by Neilson).

It is possible to present the target at a variety of angles to the nozzle, and by varying the gas pressure the velocity of particles leaving the nozzle can be controlled.

One of the major disadvantages of this type of apparatus is the lack of control of impact angle and velocity at impact. The gas jet striking the flat target surface will be deflected and will therefore deflect the path of the entrained particles. Some particles may, as a result, be deviated away from the target; the scale of the effect will depend on the momentum of the particles.

A variant of this type of apparatus is used by Sherman et al (1979). Their 'dust erosion tunnel' was a modified wind tunnel which blasted heated air carrying dust particles onto wedge shaped specimens. Whilst suffering the disadvantages of control problems, this apparatus enables experimental conditions approaching actual operational conditions to be achieved. As such, its use for materials selection for aircraft components was demonstrated by Sherman. Similar hot gas blast apparatus was used to

study erosion-corrosion behaviour (Barkalow et al (1979)).

Free falling projectiles have also been used for erosion studies (Iturbe et al (1979)). Their experiments involve multiple impacts on a single area, in a study of impingement fatigue.

5.2 AIR BLAST EROSION RIG

It is evident from a survey of the literature that this form of erosion test rig is becoming established as standard. It offers several advantages over the other common designs, such as flexibility of operating conditions, and ease of operation. The air blast rig allows testing over a range of impact angles 10^{o} to 90^{o}, and a wide range of erodent types (size from 10μm to 1mm) can be discharged at velocities in the range 10ms^{-1} to 100ms^{-1}.

Recently a standard practice for conducting erosion tests has been published (ASTM (1983)). The apparatus constructed in the course of this work was designed in accordance with the principles stated in this standard, but differs in certain details. The design follows more closely that of the erosion rig used at the Lawrence Berkeley Laboratory, University of California, described by Lapides and Levy (1980).

Figure 5.2 is a schematic diagram of the air blast erosion test rig.

The erosion rig is charged with a pre-weighed quantity of erodent, which is fluidised in a swirl chamber. The particle feed rate is controlled by varying the pressure of the air feed to the swirl chamber, and also by varying the inclination of the chamber itself. Earlier experiments were

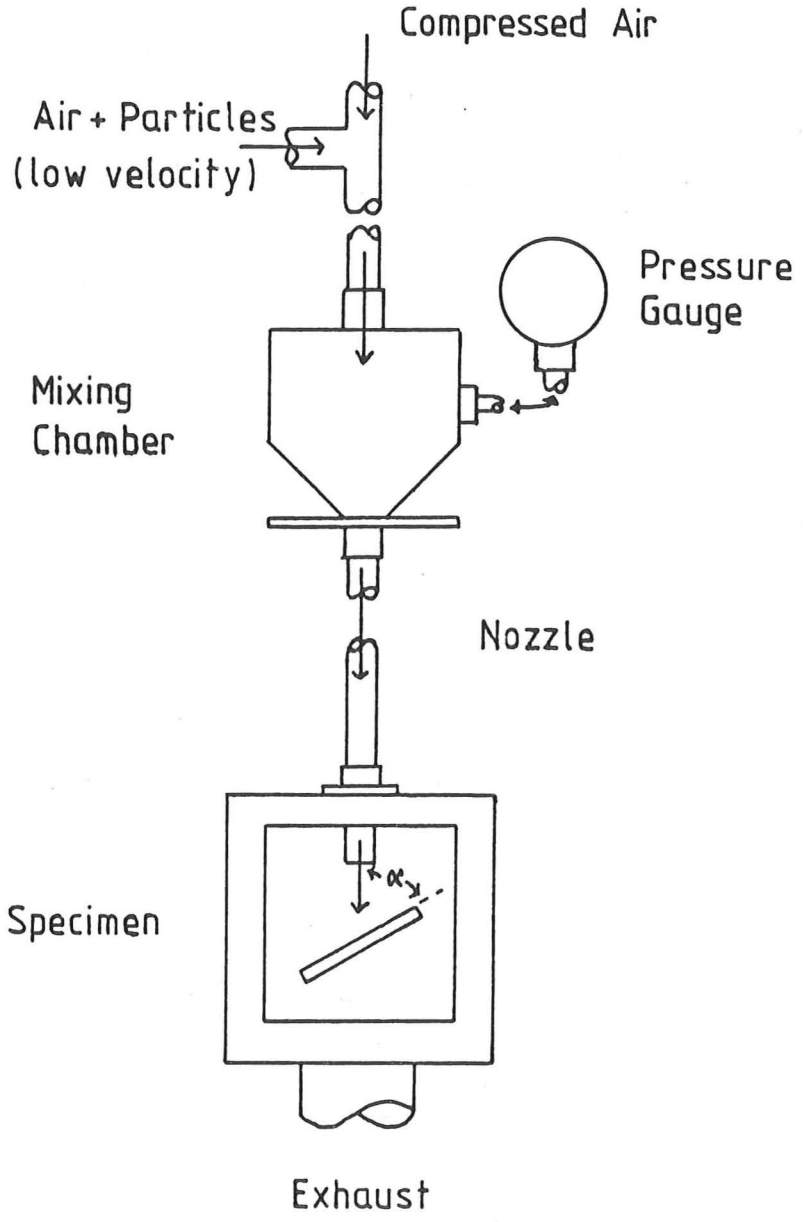

Figure 5.2 : Schematic diagram of the air blast erosion test rig

conducted using a vibrating tube to meter the erodent powder, similar to the system reported by Lapides and Levy (1980). The swirl chamber method was found to be a significant improvement over this system, allowing a much wider range of erodent types to be dispensed at steady and controlled rates. The particle feed rate is maintained in the range 10g to 50g per minute, depending upon the erodent type and size. Early experiments revealed no great sensitivity of erosion rate to particle feed rate, but indicated that for each erodent type and size an optimum feed rate exists to maintain stable flow conditions. Consequently for each series of experiments stable flow conditions were determined, and then adhered to.

The use of pre-weighed erodent increments was at variance with the ASTM standard, which advocates constant, well defined feed rates and timed experiments. The incremental method was chosen because it offered the maximum degree of control over the discharge rate, verified by the very good reproducibility seen in the experimental results.

The ASTM standard also differed in the details of the nozzle dimensions. The suggested dimensions are 1.5mm inner diameter and 50mm in length. The erosion test rig was designed with a much larger nozzle, 4.76mm i.d. and 30mm length, and avoided the use of a supply tube from the particle mixing chamber. The larger internal diameter results in a greater area of erosion damage on the specimen, and thus for a given mass of material removed a shallower erosion pit is created. This has the advantage of maintaining the geometry of impact over tests involving the discharge of several kilogrammes of erodent. Similar tests with smaller nozzle diameters resulted in deep erosion pits, leading to a change in the geometry of impact

so that the target material offered a range of impact angles to the impinging particles. (Chapter 6 section 6.4.1 discusses this effect, and reports the results of other workers using smaller nozzles.)

The use of a longer nozzle connected directly to the mixing chamber was favoured, as it provides a simple and efficient method of accelerating the entrained particles. The simplified geometry also allows the system to be analysed in terms of a simple fluid mechanical model. Ninham and Hutchings (1983) analysed the fluid flow in this system and constructed a microcomputer model which could be calibrated to predict particle velocities.

In accordance with the ASTM procedure the abrasive is used only once. The exhaust gas is filtered before venting to the atmosphere.

5.2.1 Experimental procedure

(a) Erodent preparation

Spherical erodent were mechanically sieved, using an Endecotts sieve shaking machine (type EFL 2 Mark 2). The sieves were 20cm in diameter, were charged with a maximum of 500g of erodent powder, and were shaken for over one hour. The chosen sieved fraction was weighed to 0.01g accuracy on a top pan balance, into 25g or 50g increments.

Angular abrasive was either used in the as-received size distribution, or sieved by hand using a brushing technique.

Optical microscopy was used to check the size distribution of prepared erodent. No attempt to define a statistical size range was made, the methods described above being adopted to ensure that each increment of erodent used in testing was in a readily reproducible form.

(b) Erosion testing

Before each test the nozzle diameter was inspected for wear and the nozzle replaced if necessary, angle of impact and height of nozzle from the specimen surface were selected. An initial charge of erodent was directed at a dummy specimen to ensure that the eroded region was centred on the specimen, and also to ascertain the optimum erodent fluidising and metering conditions.

Each specimen was polished to a standard surface finish, being finally wet ground with 1200 grit silicon carbide paper.

Each specimen was weighed on an analytical balance (Sartorious model 2474) to 0.01mg prior to testing. The air pressure at the mixing chamber was maintained constant throughout the erosion test. The specimens were cleaned with a jet of compressed air and weighed after each increment of erodent had been discharged.

Typical specimen dimensions are : 5mm thick, 65mm long and 20mm wide.

5.3 PARTICLE VELOCITY MEASUREMENT

5.3.1 Survey of existing methods

Ponnaganti et al (1980) examined and compared the various techniques commonly used for particle velocity measurement in erosion testing.

There are three main types of technique: photographic, laser and mechanical. These will be briefly reviewed here.

The computer model of particle and gas flow, described by Ninham and Hutchings (1983), is a method of velocity estimation rather than measurement. This method of velocity estimation requires knowledge of particle size and particle drag force. For irregular particles these factors are determined from experimental measurements of particle velocity. In this way the model is calibrated for a given particle system, using measurements of velocity, and then used to estimate the variation of particle velocity with gas pressure. The discussion in this section will be limited to direct methods of particle velocity measurement.

(a) Photographic techniques

There are several methods of producing a series of images on film, at controlled time intervals.

The simplest is the use of multiple flash illumination. This technique is most useful for single particle or very low density streams. The photograph is examined to identify a single particle in two positions, which correspond to two consecutive exposures at a known time interval. From the geometry of the experiment and the magnification of the enlargement, the distance and time measurements yield the particle velocity.

Although the simplest of the photographic techniques, this method involves careful setting up and does not rapidly yield results, even using Polaroid film. It is unreliable for all but the lightest flux of particles.

A more complex method involves the use of high speed cameras. High speed photography has proven a valuable tool in the investigation of the dynamics of single particle impacts (Hutchings et al (1976)). Its use in multiple impact studies has not proven so successful. In practice there is a size limit to the particles which can be measured and again a limit to the flux of particles from which reliable results can be obtained. The cost of the camera, and the ease of setting up are important considerations. As with multiple flash, the result is not rapidly obtainable.

The streaking camera technique is a third alternative photographic method. Here a rotating drum and lens-mirror systems cause the image of the particles to move across the film in a direction parallel to the axis of rotation of the drum. Figure 5.3 gives camera details and a sample result. This method can examine heavier fluxes of particles, but velocity measurements are neither conveniently nor rapidly obtained.

(b) Laser techniques

Ponnaganti et al described in some detail the laser doppler anemometer (LDA) an instrument developed to measure fluid velocity by injecting very small light-scattering particles into the stream (Ponnaganti et al (1980)).

The main components of an LDA system are the laser, optical transmitter, photomultiplier tube and signal processor. The principal of the method is illustrated in Figure 5.4. The laser light is split into two beams, focussed in the particle stream, and at the intersection of the two beams stationary interference fringes are produced. A particle passing through the measuring volume will scatter light with a frequency proportional to its velocity component normal to the fringes. Used in conjunction with a small

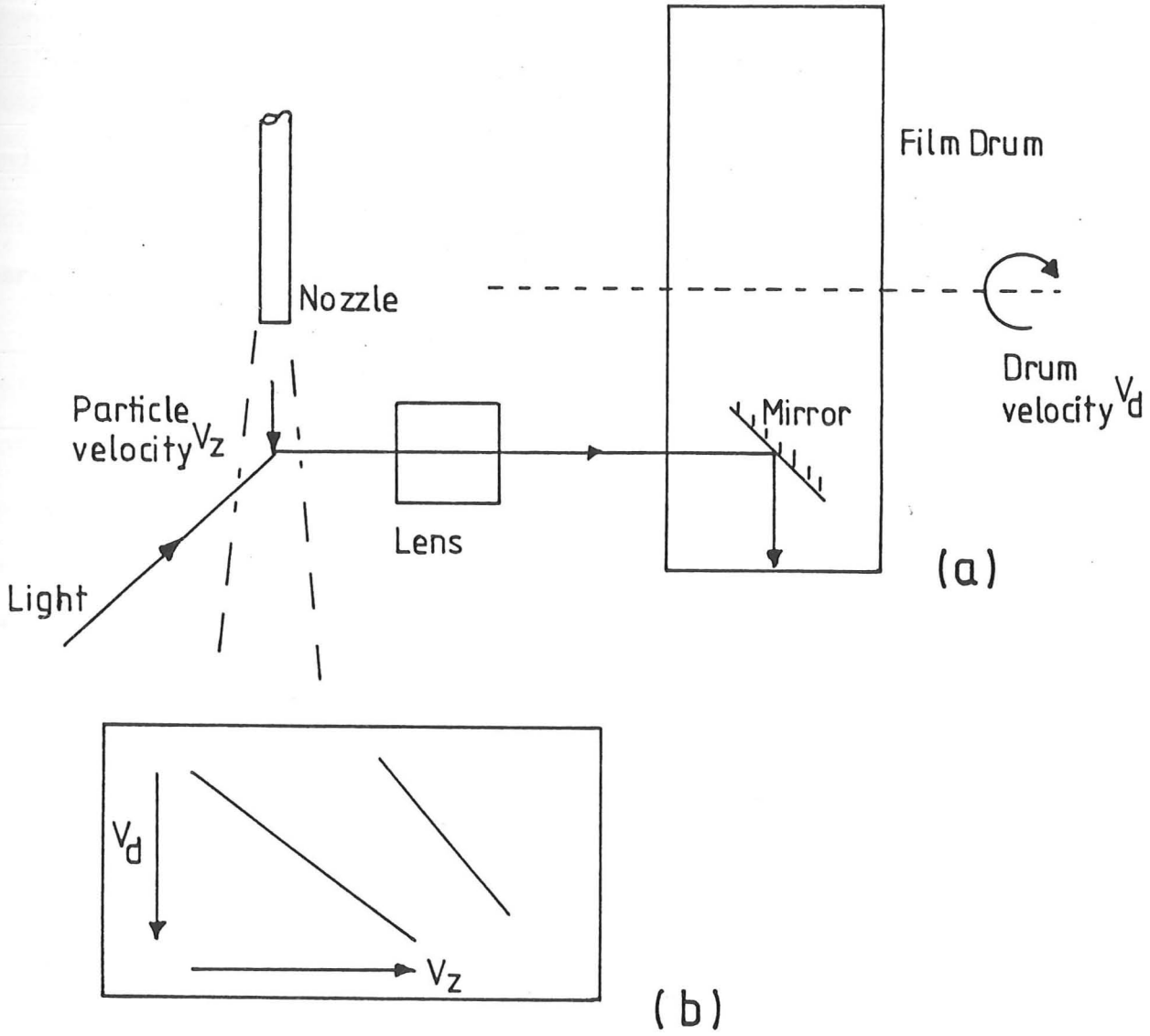

Figure 5.3 : (a) Streaking camera : (b) Photograph

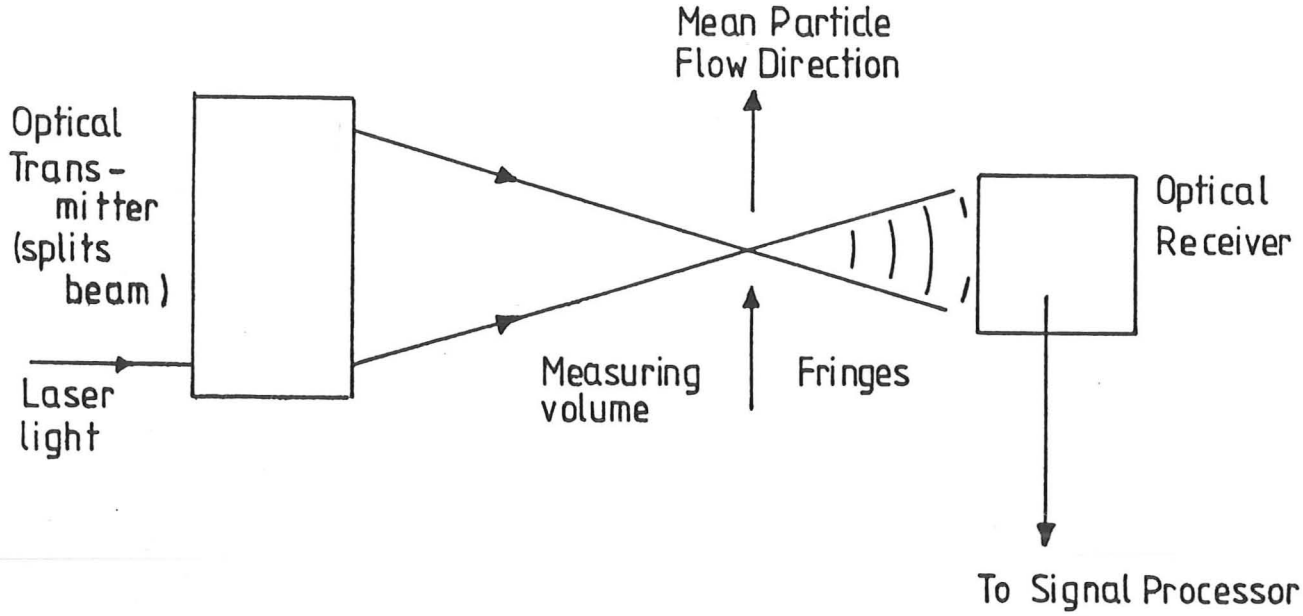

Figure 5.4 : Laser doppler anemometer

computer the system can determine the velocity of large numbers of particles, and produce statistical surveys of this data rapidly and accurately. The measuring volume can be selected to examine in great detail the flow of the particles impacting the target.

This technique is accurate, rapid and provides statistical surveys of particle velocities. A large number of measurements can be made during an experiment, at several different sites within the stream leaving the nozzle, and rebound velocities can also be measured. (In interpreting the results of this method it must be remembered that it is the velocity normal to the plane of the twin beams that is measured.) The cost of the complete system is however its one major disadvantage.

(c) Mechanical methods

A W Ruff and L K Ives (1975) described the only technique in this category. Their method was developed specifically to furnish erosion experimenters with a robust, simple, inexpensive system of particle velocity measurement.

Figure 5.5 illustrates this method. The average velocity of the particles is calculated from the spacing of the discs, their angular velocity and the angular displacement of the erosion marks on the second disc.

The major disadvantage in this method is its lack of accuracy, especially if there is a wide range of velocities, producing a broad erosion mark on the second disc. There is also some concern arising from the influence of the motion of the discs on the air stream. It is possible that aerodynamic effects will complicate the geometry, requiring a correction to be made to the measured angle of displacement before the velocity can be calculated.

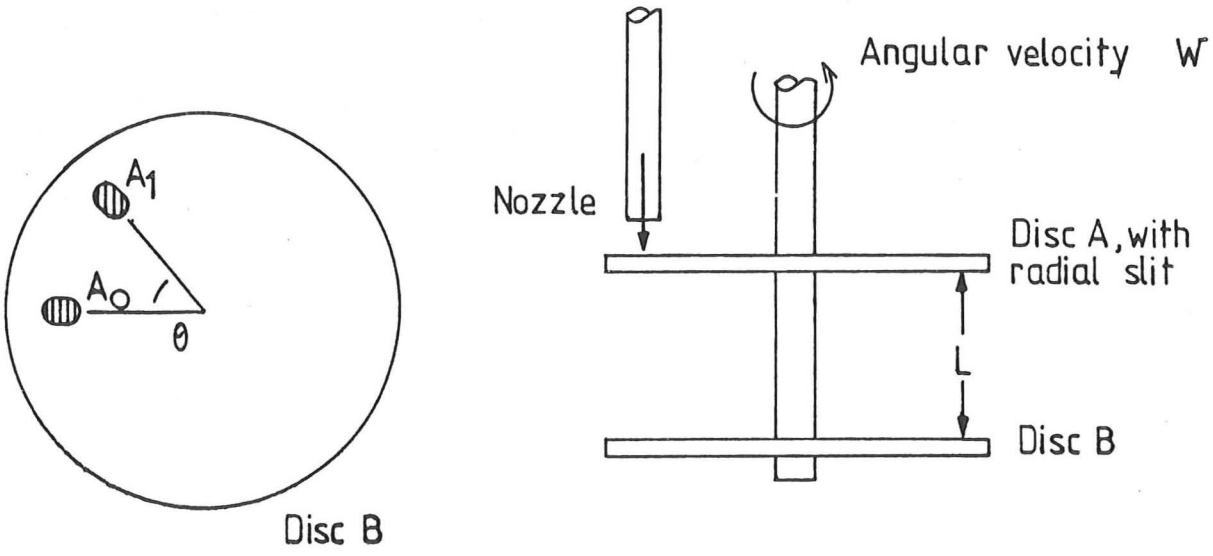

A_o Produced with discs stationary

A_1 Produced with discs rotating, angular velocity w

Velocity of particles V

$$V = \frac{2\pi wL}{\theta}$$

Figure 5.5 : Double disc method

(d) Summary of existing methods

Problems arise in the use of any of the methods described above.

The photographic techniques are neither rapid nor robust.

The LDA system is accurate, rapid and capable of measuring large numbers of particles. However it is very expensive, complicated to set up, and not very robust.

The double disc method is simple to use, but lacks accuracy. The technique can be improved, for instance by reversing the direction of rotation of the discs and making a second erosion mark. This avoids the problem of determining the exact position of the shadow of the slot with the discs stationary, and effectively doubles the accuracy of the method. The inaccuracies resulting from a spread of particle velocities, and possible aerodynamic deflections still remain.

5.3.2 Principles of cross correlation

The above discussion shows the need for a simple, inexpensive and robust system of particle velocity measurement. Ideally the system would collect data from a large number of particles, and preferably the data would be in the form of electrical signals to allow rapid computer processing and possible statistical evaluation.

An obvious method of measuring particle velocities is to measure time of flight between two sensors spaced a known distance apart. Assuming such a system could be developed the problem arises of how to determine the time of travel of one particle between the two sensors. A simple ON/OFF switching

by the sensors, ON as the first sensor detects a particle and OFF when the next sensor detects, will not produce the relevant information. In the real situation measuring small particles at high velocities, a significant number of particles may avoid detection altogether, or be detected by the first sensor and not the second. To ensure acceptable accuracy the sensors must be placed as far apart as possible, consequently unless the particle flux is extremely light there will be a 'train' of particles between the sensors. Switching a timer ON as the first sensor detects, and OFF at the next signal from the second sensor will clearly produce an inaccurate, and smaller, time of flight than the true value.

The technique of cross-correlation was developed to deal with this type of problem. Beck (1981) and Henry (1979) discussed cross-correlation at length. Figure 5.6 is adapted from Beck (1981) and conveniently illustrates the principles of cross correlation as applied to flow meters. Two sensors, A and B, produce signals x(t) and y(t). (x(t) denotes the intensity of the signal at time t.) A variable time delay is introduced in the x(t) record, of magnitude τ. Values of x at discrete times (t-τ) are then combined (for instance by multiplication) with corresponding values of y, (at time t). The results of all the individual combinations are then summed (or integrated) to produce a value $R_{xy}(\tau)$. The time shift τ is then altered and the process repeated to produce $R_{xy}(\tau_1)$.

The process can be thought of in terms of bringing the two traces into consonance as τ is changed. At a certain value of τ, τ^*, the x and y traces will be in perfect register, resulting in a maximum value $R_{xy}(\tau^*)$. Continuing the cross correlation procedure (further increasing τ) will then result in the two traces becoming increasingly out of register. At any

given stage, $\tau^* - \tau$ will control the degree of register of the two traces. Figure 5.6 provides an illustration of the result which may be generated by cross correlation, τ^* is the value of τ which maximises $R_{xy}(\tau)$, and corresponds to the mean time of flight between sensors A and B.

5.3.3 Development of a twin light beam cross correlation method of particle velocity measurement

As mentioned in the preceding section, cross correlation methods have been applied in the past to particle flow measurement. The aim of the present study was to produce a device which could be attached to the erosion rig, which would generate signals in a form that could be accepted by a micrcomputer for processing by cross correlation methods. Initially a transient recorder was available for data storage, but a long term aim was to use the microcomputer to collect, as well as to process the data.

5.3.3.1 Signal generation, amplification and processing

Various types of electrical transducer are available which can detect the movement of small particles in air, in close proximity. Types available include light sensitive devices, and capacitance or electrodynamic transducers. Beck (1981) gave details of the operation of capacitance and electrodynamic transducers. Green et al (1978) gave details of a non-correlation method, utilising capacitance sensors. The capacitance and electrodynamic methods respond, not to individual particles, but to localised groups of particles. These denser regions in the particle flow provide the fluctuations in the electrical properties of the gas/particle stream, which give rise to the signals. Early experiments with a solid state light emitting diode/phototransistor pair showed that this type of device was

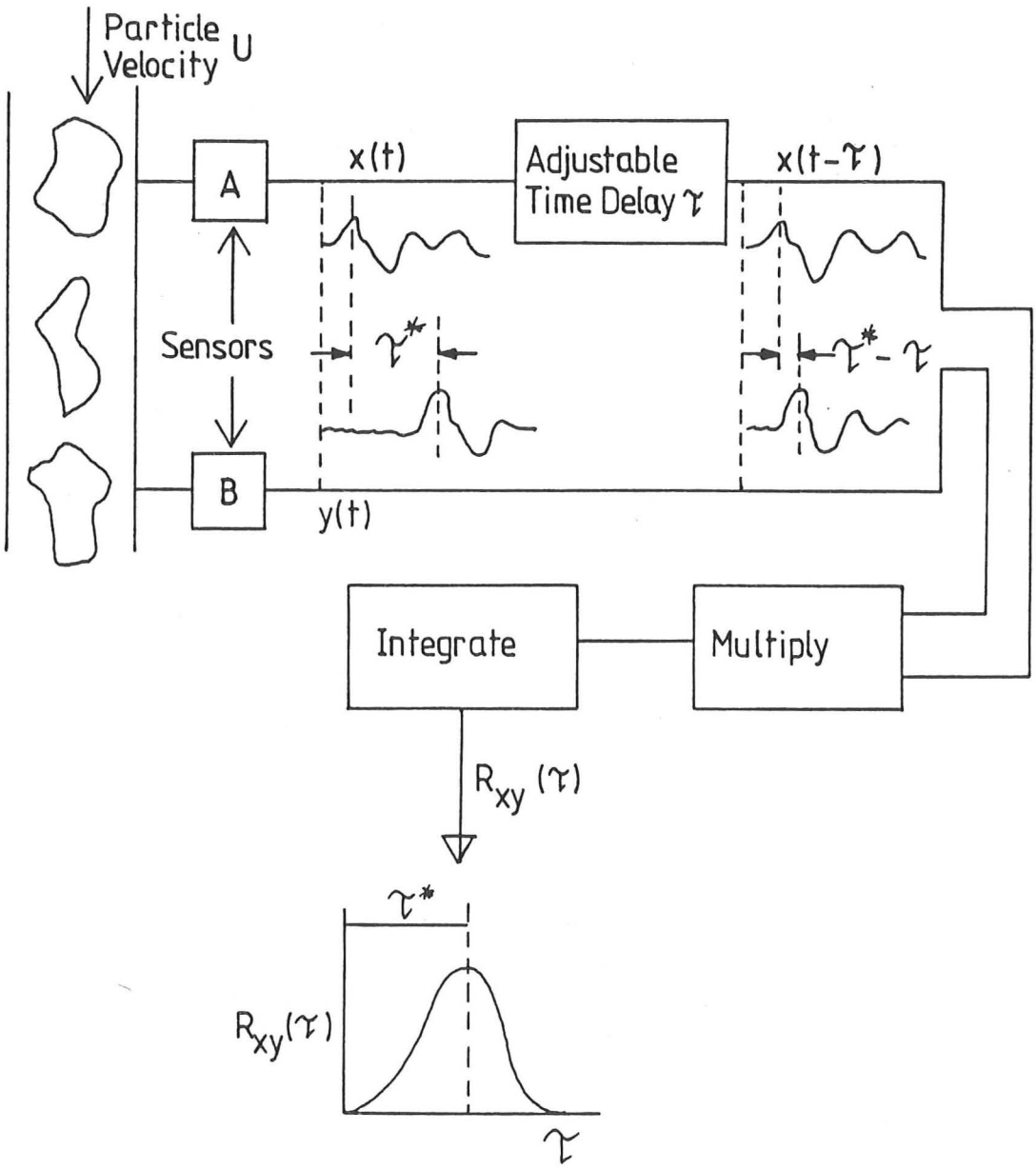

Figure 5.6 : Principles of cross-correlation

sensitive enough to detect a single erodent particle, and fast enough in response to be used in a particle velocity measurement system.

(a) Signal generation

Early experiments utilised a device comprising an infrared LED (light emitting diode) and a phototransistor encapsulated in a plastic mount (Texas Instruments L138). Although the sensitivity and response time of this device were adequate, the light beam was found to be divergent and the phototransistor poorly focussed. This resulted in unreliable detection of particles not travelling through the centre of the beam. Later experiments were carried out with a focussed phototransistor (L14F1 *) and a high intensity infrared LED (SE4352-003*). Although providing a great improvement, this system was still not reliable in the detection of off-centre particles.

In order to increase the efficiency of off-axis particle detection, it was necessary to generate a beam of light which was wide enough to cover the whole stream of particles. In order to ensure that the two light beams were set at a precise distance apart, measured along the direction of flow, the beams must be of uniform width across their whole length. By producing as thin a slot of light as possible, the detection of smaller particles would be enhanced. Figure 5.7 illustrates schematically the system which has successfully been utilised for particle velocity measurements. Light from a high intensity LED (SE4352-003) is first diffused by passing through a length of 3mm diameter single strand optical fibre. (Plastic optical fibres were used to minimise the absorption of infrared, which was essential for the detection of glass-ballotini). After passing through 0.5m of this

* (Footnote) Supplied by R S Components Ltd, London EC2P 2HA

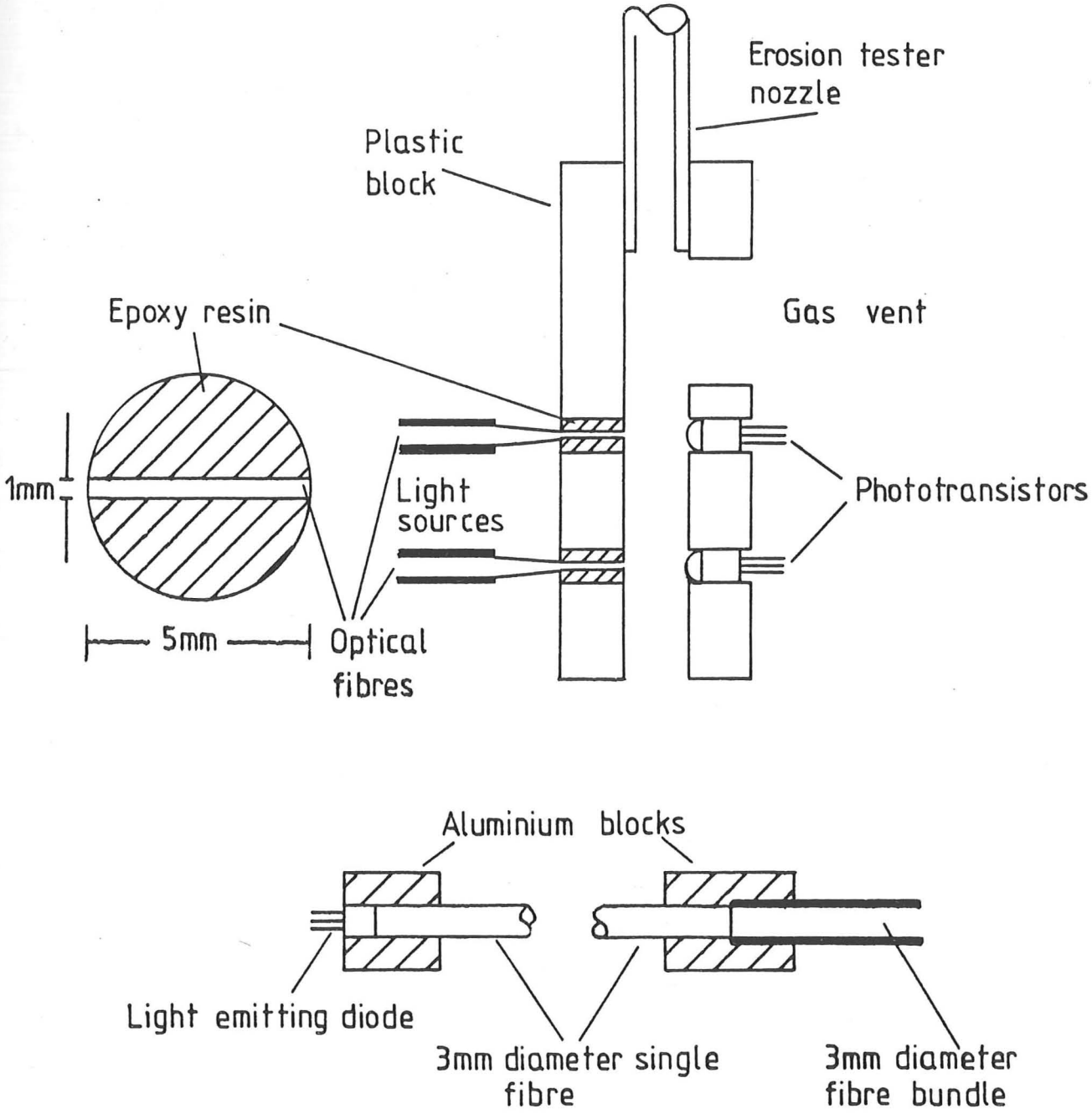

Figure 5.7 : Light sources and sensors for particle velocity measuring system

fibre the light was in the form of a very uniform 3mm diameter beam. This beam was then passed into 3mm diameter multifilament optical fibre, the opposite end of which was fanned out to produce a rectangular face 5mm x 1mm. The beam was directed at a lens capped phototransistor (L14F1). Two light sources and two phototransistors are held in position in a Perspex block (polymethylmethacrylate), which was attached to the nozzle of the erosion test rig.

(b) Signal amplification and processing

In order to develop an efficient correlation system, it is essential to process the signals generated by the sensors, prior to storage and subsequent manipulation. A simple circuit to amplify the signal from one sensor is illustrated in Figure 5.8; a typical trace of output voltage versus time is also sketched. This circuit utilises the solid state LED/ phototransistor pair, used in the early experiments described in the previous section.

Examination of the schematic output trace highlights the two main problem areas. First, as discussed in the previous section, with this early system not all particles were reliably detected. As the sketch trace indicates some particles result in large pulses, whereas others generate only very small pulses, if indeed they register at all. The design of the sensor finally adopted does much to improve on this. The electronic signal processing described below has the effect of further minimising the differences between individual pulses, by converting the signal into a digital form.

The second need for signal processing is shown by the complexity of each individual pulse, on the schematic trace. The significant information signalled by the sensor, for the purpose of cross correlation, is whether

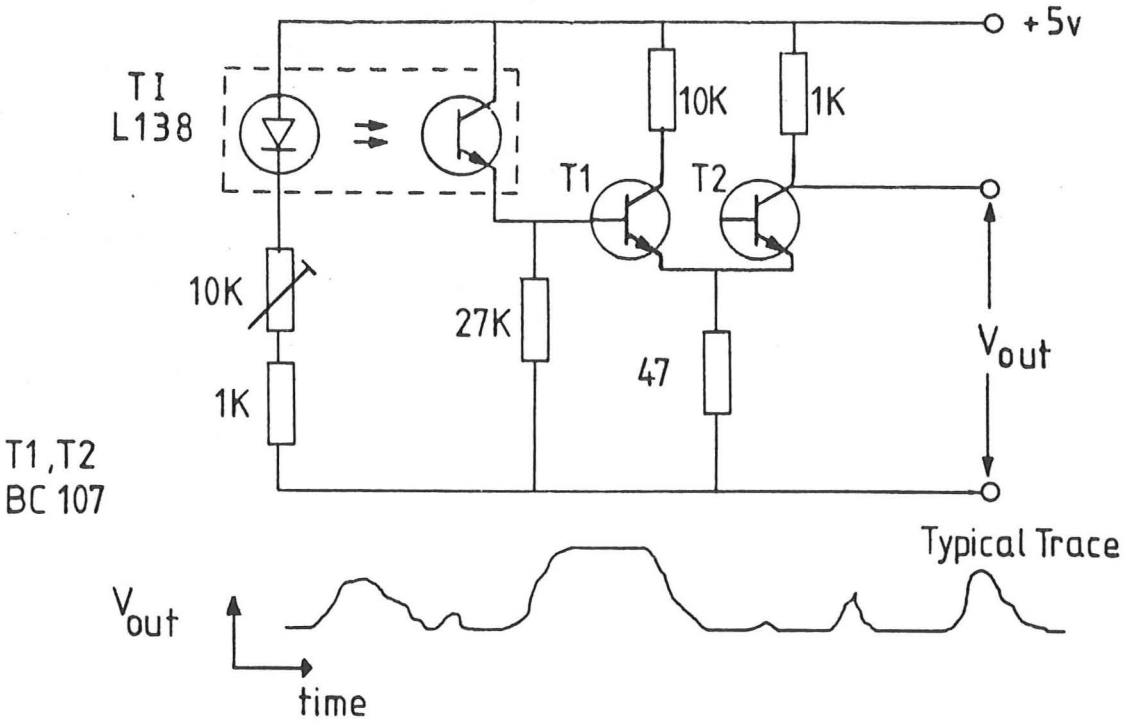

Figure 5.8 : Details of preliminary sensor circuit

the light beam was interrupted or not. The signal output in Figure 5.8 provides much redundant information concerning the degree of interruption. By simplifying the signal before storage, more efficient use is made of the limited storage space available.

Figure 5.9 details the circuitry used. Figure 5.9 (a) shows the circuit which converts the signal from the phototransistor into a series of binary pulses. It is possible to adjust the sensitivity of this circuit to select the smallest change in input voltage which will result in the output transition from 0 to 5v, i.e. from binary 0 to 1. An LED indicator is provided to show the output state. Before making a velocity measurement both sensor circuits can be set so as to be on the point of maximum sensitivity.

The sensitivity of the phototransistor and the signal generating circuit gives rise to operating problems. The stroboscopic effect of neon lights in the laboratory was easily detected, even with the sensors LED set at high brightness. Thus the sensor device must be shielded, in the erosion chamber. The LED brightness can then be adjusted to a low level, enabling the sensitivity of the phototransistor to be maximised.

The extreme sensitivity of the phototransistors and associated circuitry makes it essential to stabilise the power supplies to the LEDs. The occurance of voltage fluctuations can result in spurious signals occurring simultaneously on both sensor outputs. Figure 5.9 (b) gives details of the LED power supply circuit. The power supply is adjustable to allow the LEDs brightness to be matched to the phototransistors maximum sensitivity.

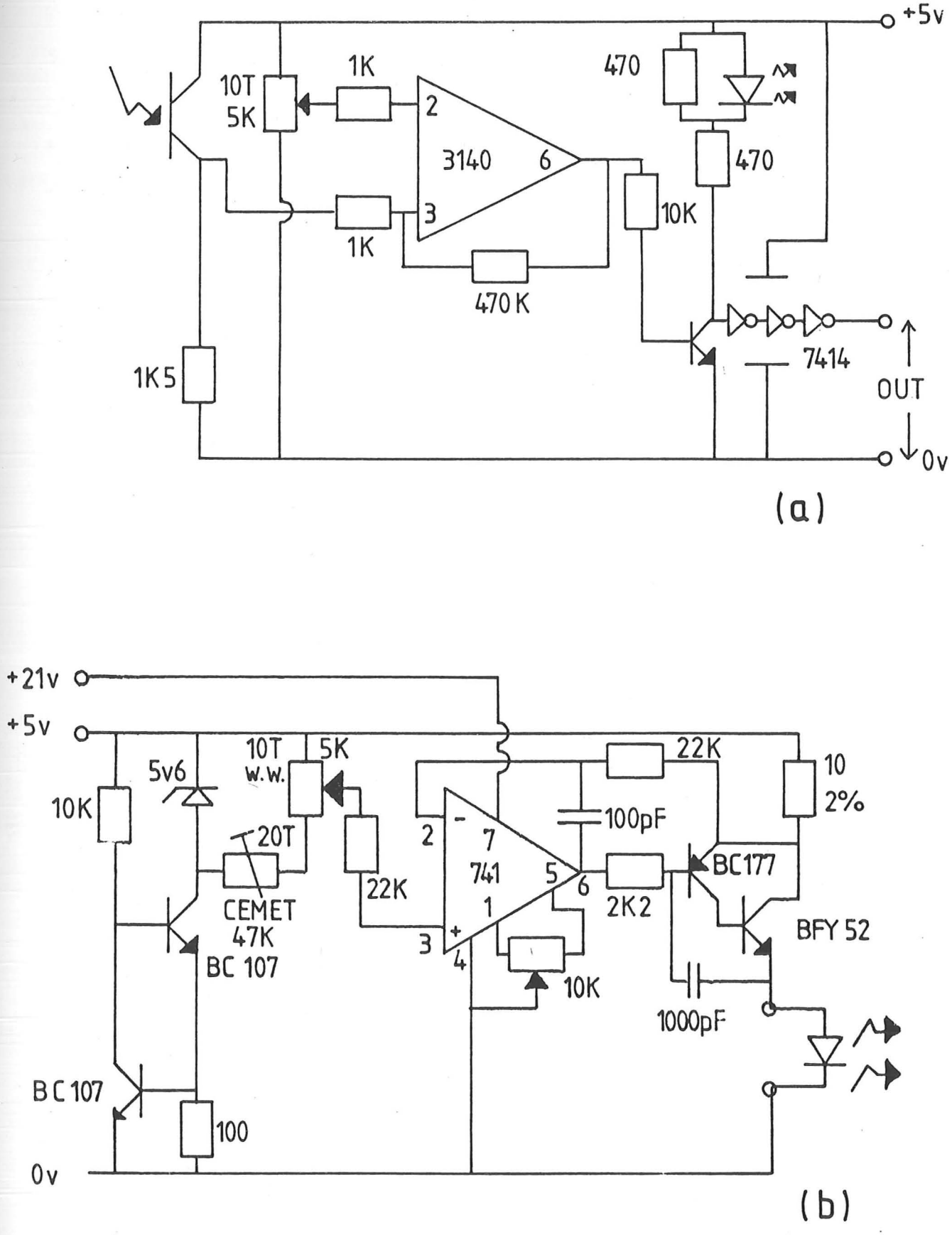

Figure 5.9 : Electronic circuit for velocity measuring system :

(a) signal generating circuit

(b) constant current supply for sensor LED

5.3.3.2 Data transfer

Figure 5.10 shows the equipment used to collect and store the data, and to calculate the velocities of the particles.

The transient recorder (Data Lab DL922) sweeps the input signal at a given rate, and stores the signal in digitised form. Using two channels, each of 1024 data points, signals produced by the sensors over a known time interval can be recorded, displayed on an oscilloscope (CRO) or read into a microcomputer. Figure 5.10 shows a schematic CRO display of a typical data store in the transient recorder.

To read the data into the microcomputer (a Commodore PET) the transient recorder is connected to the PET user port. Data is transferred using a conventional system of 'handshaking'. Handshaking is a method of ensuring that each individual byte of information is reliably sent and received, and involves the use of control signals.

The data transference can be controlled by the use of a BASIC language program; however this process takes approximately 45 seconds to load the 2048 data points stored in the transient recorder. To reduce this time, a machine code routine was written (reproduced in Appendix 3A) to control the data loading; this process can load the 2048 data points from the transient recorder into the microcomputer memory in less than one second.

The machine code routine is based on standard memory read/write operations. The methods used to address the 2048 data points requires some explanation. (Zaks (1980) should be consulted for details on machine code programming

techniques.) The Commodore PET has a 6502 central processor unit. The internal registers and the accumulator of the 6502 can hold only single byte (8-bit) numbers (i.e. maximum decimal value of 255). Available indexing techniques allow for a sequence of 256 addresses to be allocated. The data transference requires a sequence of 2048 addresses to be allocated, or alternatively two 1024 sequences.

In order to index a sequence of 2048 data points the machine code routine for data transfer is actually rewritten each time a data point is loaded. The memory locations which contain the destination addresses for the transferred data are updated after each data point is stored. A flow diagram is provided in Appendix 5A to illustrate this technique.

5.3.3.3 Microprocessor cross correlation

In section 5.3.2 the technique used by Beck was described. Beck (1981) utilised the data as generated by a sensor, in his velocity measurement system.

In the previous section it was argued that by digitising the signal, more efficient storage of the relevant information could be achieved. It is important to note that cross correlation will work on both the 'raw' data, as well as on processed signals. At each stage in the development of this velocity measurement system, the cross correlation technique has been verified by the use of simulated data. Data sets have been generated, by the microcomputer itself or by the use of signal generators, which have a known time shift between the two signals. Identification, by means of cross correlation, of this known shift provided verification of the technique. Further verification came from performing cross correlation on random data sets.

Henry (1979) noted the problems involved in using unprocessed signals from the sensors. In cross correlation techniques he summed up by saying that such signals contain 'Too much data - not much information'. He described a technique of encoding a digitised signal which extracts the relevant information from the original complex signal. Essentially Henry's method was to store the positions of the leading and trailing edges of the digitised block-wave data, as generated by the signal processor described in the previous section. He achieved this by feeding the signal from the sensor into a sensitive Schmitt trigger device, which in turn generated interrupt signals causing a computer to read a clock. The encoded signal of clock readings was then cross correlated.

The present work differs from that of Henry, in that the digitised signal itself, and not an encoded form, is cross correlated. This has the disadvantage of being less efficient in storage, but by allowing the use of Boolean operators the correlation routine is simplified and more rapid.

Figure 5.11 is a flow diagram representing the operations required to perform cross correlation. The combination operation on x and y, which is the central feature of the process described in this flow diagram, can be any one of a number of mathematical operations. If subtraction is chosen as the combination operation, then when the two signals are shifted into register, $R(\tau)$ will be at a minimum. If multiplication is chosen, a maximum in $R(\tau)$ will indicate the shift required to bring the signals to register.

The 6502 processor chip requires a number of instructions to complete a multiplication; addition and subtraction are less complex operations but still require more than one instruction. To complete a cross correlation

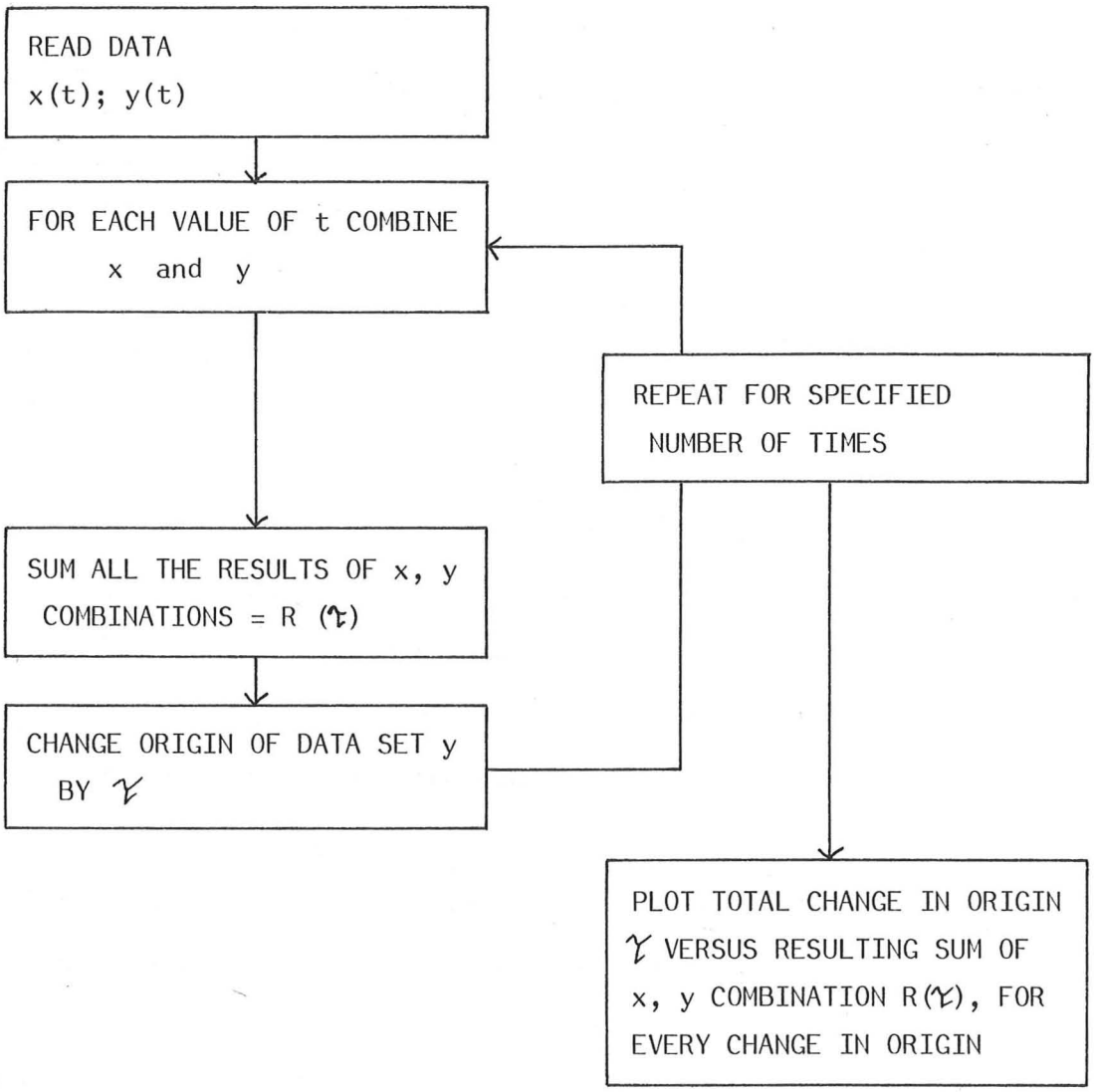

Figure 5.11 : Flow diagram illustrating method of computing cross-correlation

many thousands of combinations are carried out and thus an economy of only a few instructions will yield a significant saving of time. The function AND was chosen, since it requires a single command instruction. The AND truth table is :

$\wedge$	0	1
0	0	0
1	0	1

In the data transfer routine (see Appendix A) logical functions are used to ensure that the data is stored in a binary form, and the use of the 'AND' function in cross correlation ensures that a non-zero result is obtained only when both values are non-zero. In this way a maximum in $R(\tau)$ indicates the shift required to bring the signals into register.

The cross correlation program is described in Appendix 5B, and the machine-code program which accomplishes this is listed.

The data transfer and cross correlation programs described above must be incorporated into a BASIC program. The BASIC program is used to calculate starting addresses, to set counters and to read results into arrays. It is the BASIC program which finally calculates the velocity of the particles, from the results of the cross correlation, and information on the sensor spacing and transient recorder operating conditions. A listing of the BASIC program, together with brief notes of explanation, is also provided in Appendix 5B.

5.3.3.4 Results

Figures 5.12 (a) to (f) present the results obtained for 600μm particles accelerating under gravity, and under an applied pressure in the erosion rig of 0.05 bar. The results are in the form of $R(\gamma)$ versus γ plots, allowing the shift corresponding to the best register of the two signals to be identified. For clarity the results are plotted as continuous curves. However, it should be noted that non-integral shifts are not calculated by the program.

The velocity measured for particles falling under gravity can be compared with a theoretical velocity for objects falling an equivalent distance in vacuum. The measured velocity was $2.53ms^{-1}$ and the theoretical velocity $3.32ms^{-1}$. If the effects of falling through a confined tube in air are considered the result appears reasonable. Other experiments gave computed results in the range 2.47 to $2.83ms^{-1}$.

Computer modelling of the gas/particle flow in the erosion rig (Ninham and Hutchings (1983)) predicted a velocity of $20.81ms^{-1}$ for the particles accelerated by a pressure of 0.05 bar. The range of $15.05ms^{-1}$ to $18.96ms^{-1}$ reported in Figure 5.12 is not significantly different from the prediction. The large range of velocities measured is partly due to the particle size distribution, and also partly due to the difficulty of regulating such a low pressure at the erosion rig mixing chamber.

Attempts to measure the velocity of particles accelerated by gas at higher pressures were unfortunately unsuccessful. This was largely due to instability of the electronics generating the processed signal. The response time of the sensors was shown to be sufficient for the range of velocities

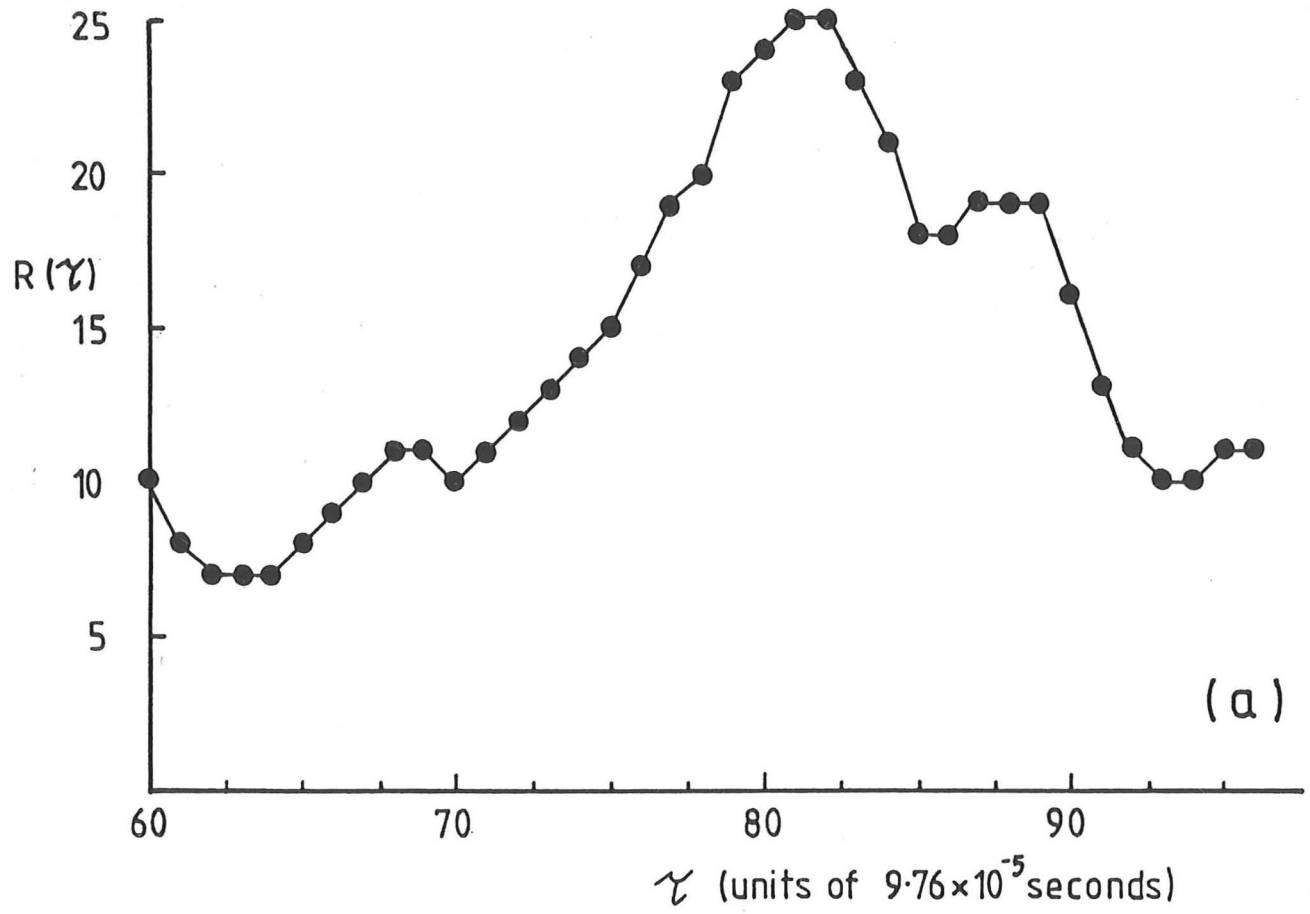

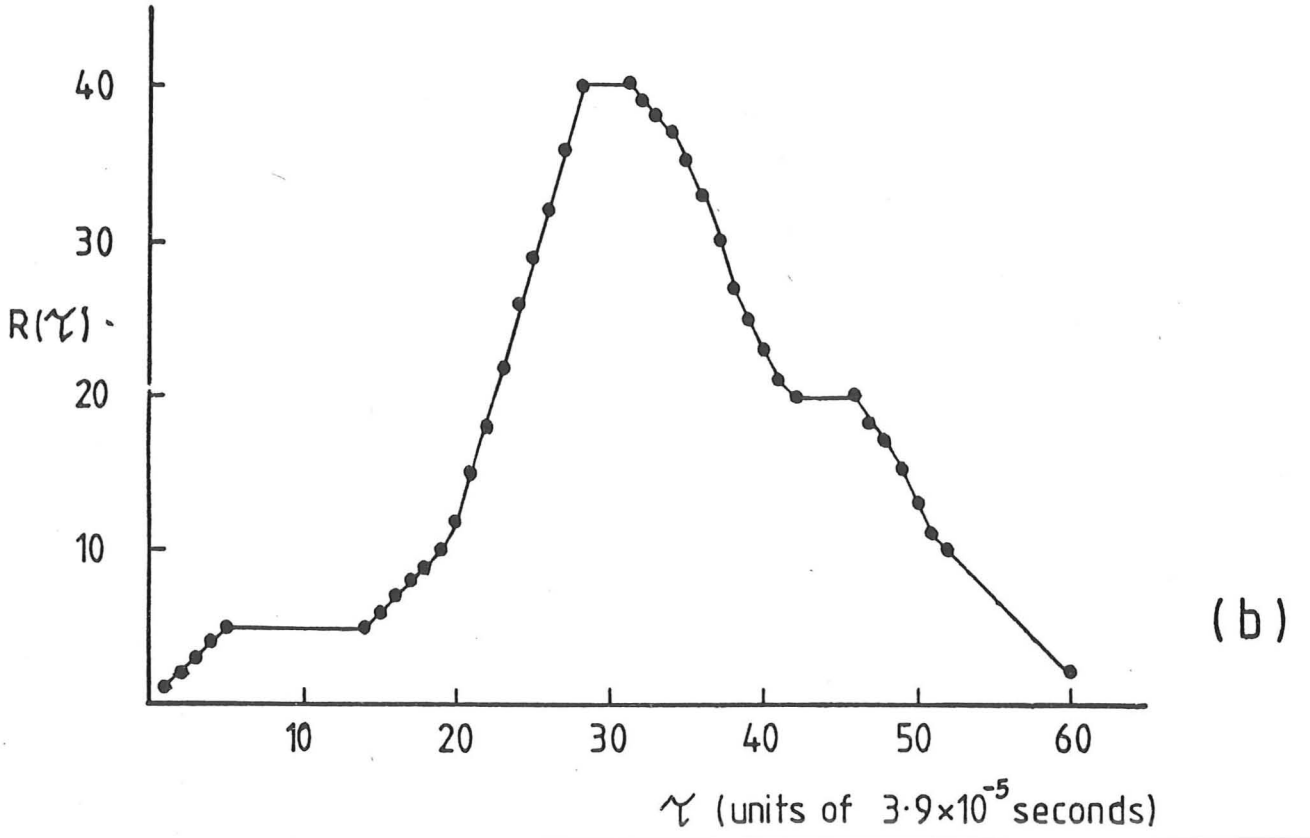

Figure 5.12 : (a) Analysis for free falling particles, measured velocity 2.53ms^{-1}

(b) Analysis for particles accelerated by 0.05 bar gas pressure, measured velocity 17.07ms^{-1}

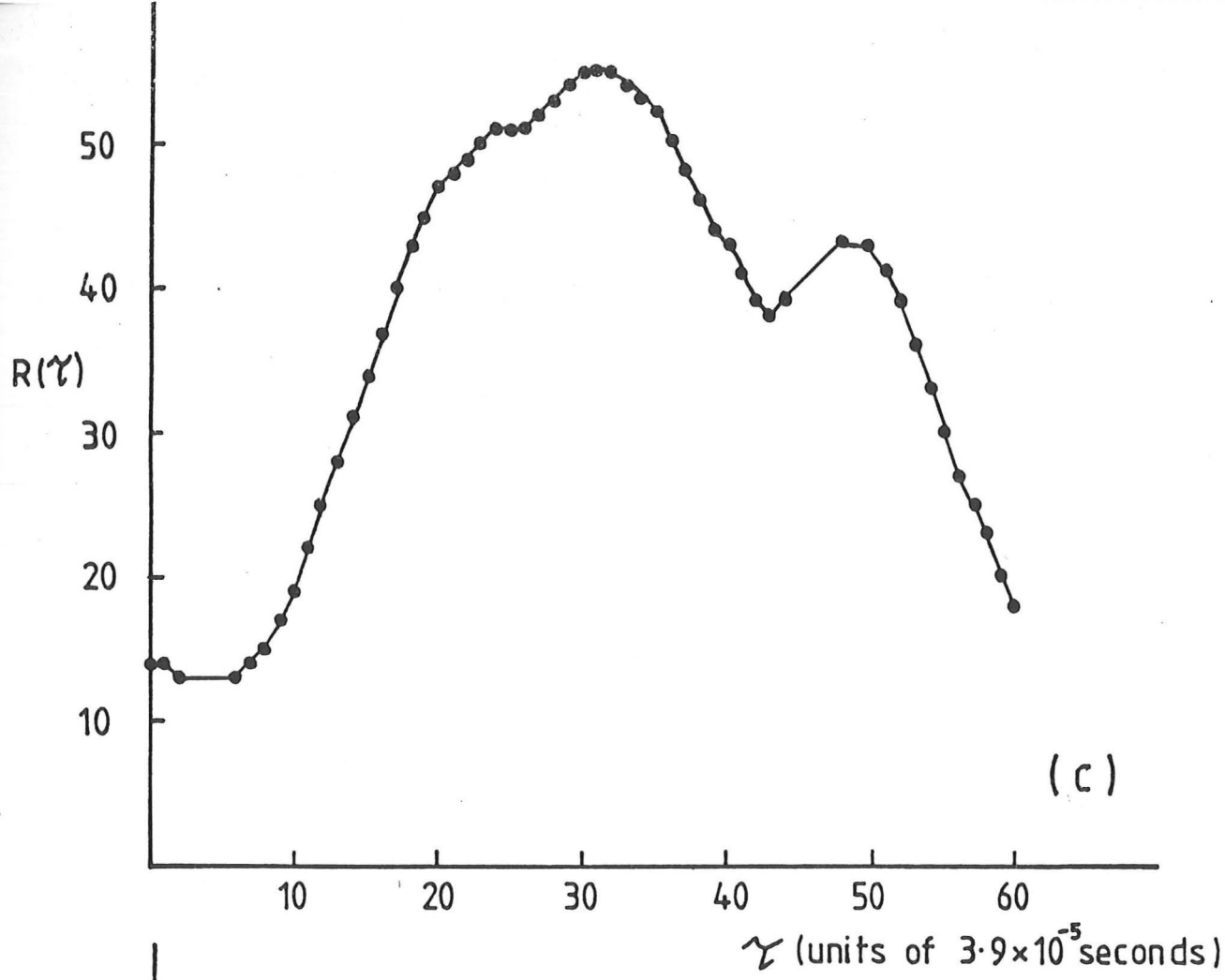

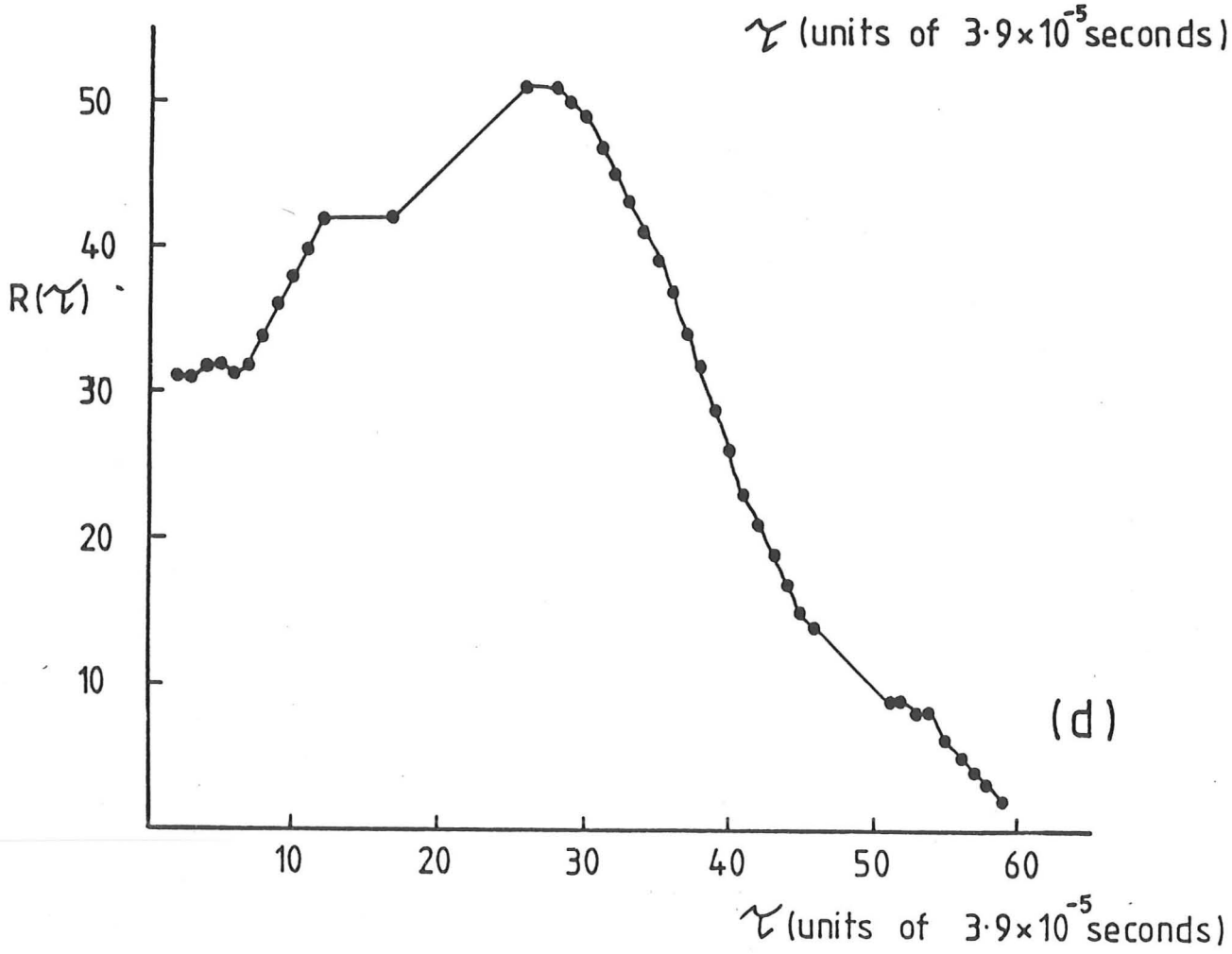

Figure 5.12 : Analysis for particles accelerated by 0.05 bar gas pressure, measured velocities

(c) $16.52 ms^{-1}$ (d) $18.96 ms^{-1}$

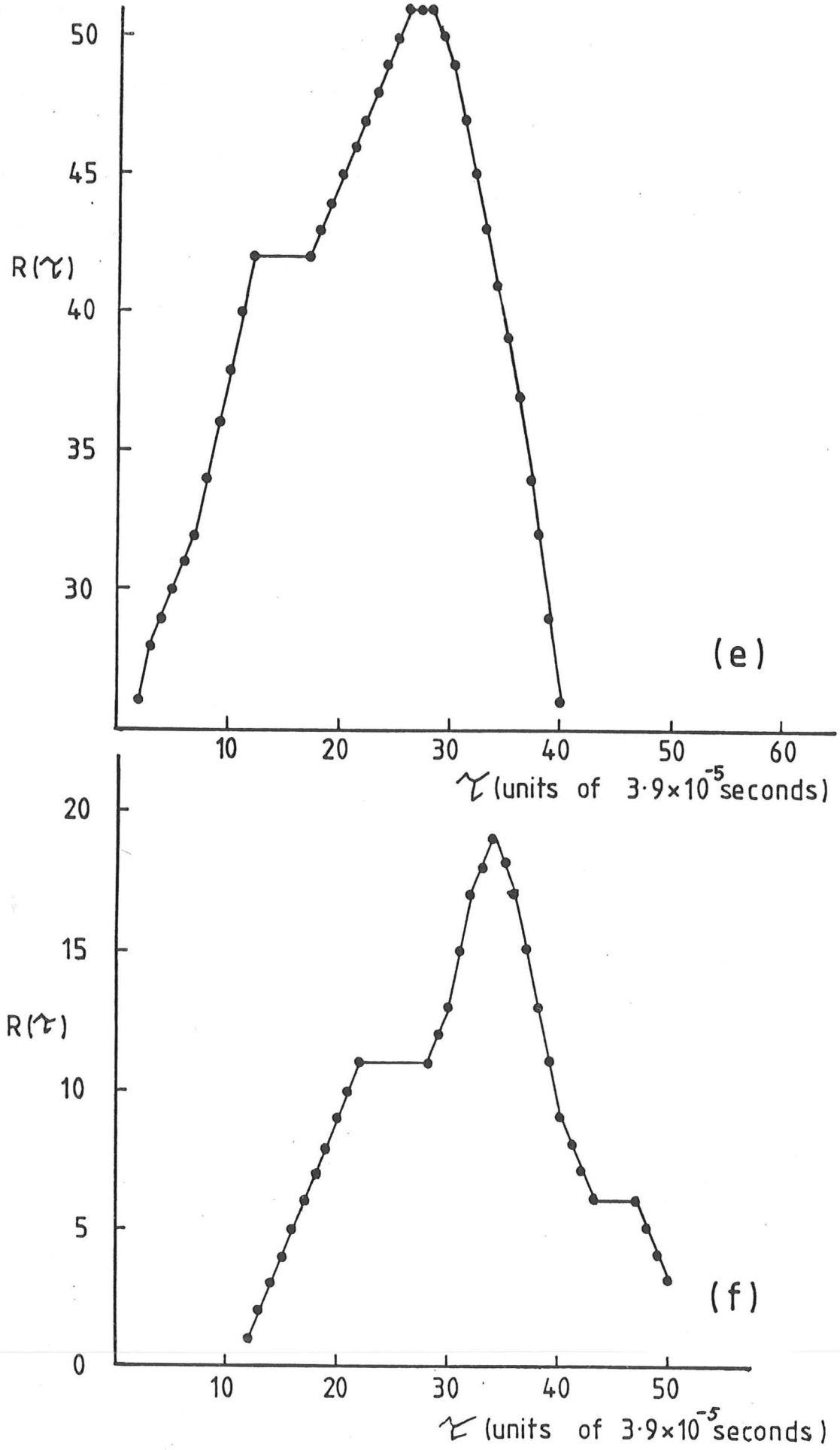

Figure 5.12 : Analysis for particles accelerated by 0.05 bar gas pressure, measured velocities

(e) 18.96ms^{-1} (f) 15.05ms^{-1}

achieved by the erosion tester, by using a signal generator to switch the LEDs. The processed signal was recorded and matched accurately the output of the signal generator. More experimentation is required to identify the cause of the electronic instability under operating conditions.

5.3.3.5 Suggestions for further modifications

The electronic signal processor must be investigated, and the cause of instability removed.

The software and data storage facilities, although adequate, also show scope for improvement. Firstly the BASIC program, as listed in Appendix B, contains many elements which will be redundant once the system is proven. It should be a simple matter to streamline the system to the extent that once a small number of parameters have been entered by the user, the cross correlation procedure will be fully automatic. Results would be generated directly as measured velocities.

There is scope for large improvements in the data storage, with the aim of eliminating the use of the transient recorder. The transient recorder is a sophisticated device, whose features are very much under-utilised in this application. It should prove possible to write a machine code routine which will enable the PET to load the processed signals directly via the USER port. The PET's CPU has an internal clock, and the times taken to perform any operation are invarient and are listed by the manufacturers.

Work has started on the development of this machine code routine. The logic used is similar to that of the data transfer program, but with an important difference.

The transient recorder sends the entire data store to the microcomputer as a string of 2048 bytes. If the two channels are utilised, the data is sent as two intermeshing binary sequences. The transient recorder was modified to ensure that the first byte sent was the first from channel one, the next byte, the first from channel two.

The PET user port is a single byte address. The two sensor signals are connected to the user port in such a way that each signal controls one bit. In this way it is possible to ensure that if the decimal number 3 (i.e. binary 11) is detected at the user port, then at the instant of loading both channels had the value 1. The loading of a zero (binary 00) would indicate both signals were low, while loading a 2 or a 1 (binary 10 or 01) would indicate only one of the channels was high. It is essential that regardless of the signal input, the machine code routine will scan the user port with a regular frequency. The use of NOP (no operation) codes in the routine ensures that a regular time interval elapses each time data is stored. The proposed machine code routine is listed in Appendix 5C. The timing of this routine has been checked by running a BASIC program with identical logic. Each step in the BASIC program which corresponds to a machine code element forces a counter to be loaded with a number proportional to the time taken to carry out the corresponding machine code process. NOP codes have been included in the machine code routine which result in the counter total being independent of the number on the user port.

This new routine has yet to be tested, awaiting the modifications to the electronic signal processor.

5.4 SUMMARY AND CONCLUSIONS

This chapter provides a description of the erosion test apparatus, and details of the experimental procedures. Alternative types of apparatus are described, and an explanation for the adoption of the particular design is given.

A survey of existing methods of particle velocity measurement has been completed. This survey highlights the need for a simple, robust and rapid method. A new system involving cross correlation has been developed.

Initial results of the cross correlation velocity measurement system are encouraging, and modifications and improvements are suggested.

The instability of the electronic circuits makes it impossible to use the system in its present form to measure particle velocities in the experimental work reported in later chapters. Where it has been necessary to measure velocities either the double disc method, or the computer program of Ninham and Hutchings (1983) have been used. Absolute values of velocity have not been required, and the values quoted should be taken as reliable to within +/- 10%.

APPENDIX 5A

DATA TRANSFER PROGRAM

PROGRAM			CODE		
Location	Command	Address/number			
Ø37Ø	LDA	E84D	AD	4D	E8
Ø373	AND	#$Ø2	29	Ø2	
Ø375	BEQ	R:F9(A:Ø37Ø)	FØ	F9	
Ø377	LDA	E841	AD	41	E8
Ø37A	EOR	#$8Ø	49	8Ø	
Ø37C	AND	#$8Ø	29	8Ø	
Ø37E	STA	77FF	8D	FF	77
Ø381	LDA	Ø3ED	AD	ED	Ø3
Ø384	BEQ	R:Ø6(A:Ø38C)	FØ	Ø6	
Ø386	DEC	Ø3ED	CE	ED	Ø3
Ø389	JMP	Ø399	4C	99	Ø3
Ø38C	LDA	Ø3EE	AD	EE	Ø3
Ø38F	BEQ	R:1D(A:Ø3AE)	FØ	1D	
Ø391	DEC	Ø3EE	CE	EE	Ø3
Ø394	LDA	#$FF	A9	FF	
Ø396	STA	Ø3ED	8D	ED	Ø3
Ø399	INC	Ø37F	EE	7F	Ø3
Ø39C	BNE	R:Ø3(A:Ø3A1)	DØ	Ø3	
Ø39E	INC	Ø38Ø	EE	8Ø	Ø3
Ø3A1	LDA	#$ED	A9	ED	
Ø3A3	STA	E84C	8D	4C	E8
Ø3A6	LDA	#$CD	A9	CD	
Ø3A8	STA	E84C	8D	4C	E8
Ø3AB	JMP	Ø37Ø	4C	7Ø	Ø3
Ø3AE	LDA	#$ED	A9	ED	
Ø3BØ	STA	E84C	8D	4C	E8
Ø3B3	LDA	#$CD	A9	CD	
Ø3B5	STA	E84C	8D	4C	E8
Ø3B8	RTS		6Ø		

These details are provided for completeness. Zaks (1980) should be consulted for further programming details. (Notes : In conditional transfer - e.g. Ø375, 'R' refers to relative jump, and 'A' denotes the absolute address

resulting from jump. When the command is in the immediate mode, e.g. Ø373,#$ in column three indicates a number (not address) which is in hexadecimal).

DATA TRANSFER - FLOW DIAGRAM

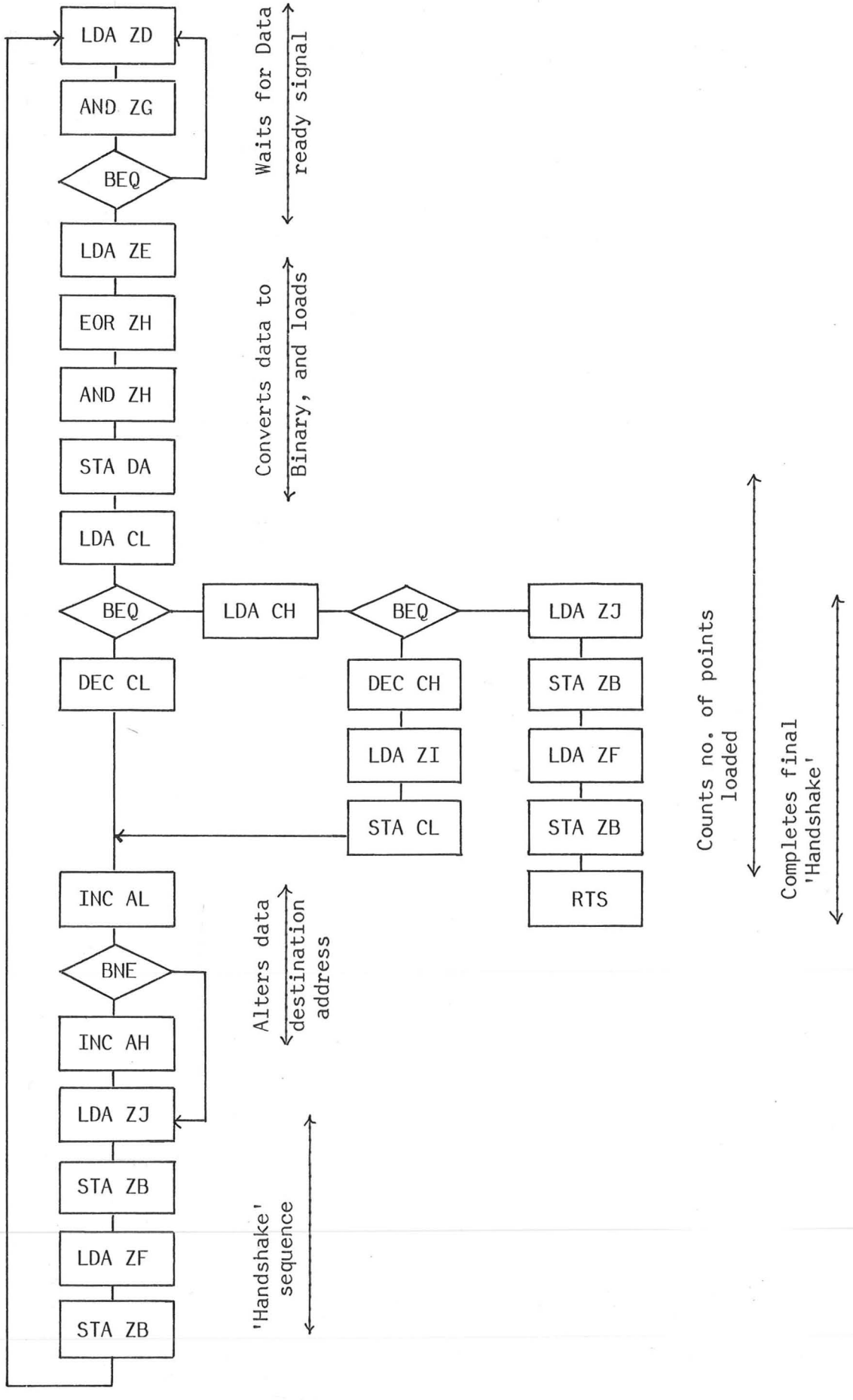

KEY TO TRANSFER FLOW DIAGRAM

Variable	Decimal value	Hexadecimal value
ZA	59459	E843
ZB	59468	E84C
ZC	59467	E84B
ZD	59469	E84D
ZE	59457	E841
ZF	2Ø5	CD
ZG	2	Ø2
ZH	128	8Ø
ZI	255	FF

CL/CH	Counter low/high
DA	Data destination address
AL	Location DA low
AH	Location DA high

APPENDIX 5B

CROSS CORRELATION PROGRAM

PROGRAM			CODE		
Location	Command	Address/number			
Ø35Ø	LDA	78ØØ	AD	ØØ	78
Ø353	AND	78Ø1	2D	Ø1	78
Ø356	BEQ	R:Ø5(A:Ø35D)	FØ	Ø5	
Ø358	INC	Ø3E8	EE	E8	Ø3
Ø35B	BEQ	R:45(A:Ø3A2)	FØ	45	
Ø35D	DEC	Ø3EA	CE	EA	Ø3
Ø36Ø	BEQ	R:2F(A:Ø391)	FØ	2F	
Ø362	INC	Ø351	EE	51	Ø3
Ø365	BEQ	R:12(A:Ø379)	FØ	12	
Ø367	INC	Ø351	EE	51	Ø3
Ø36A	BEQ	R:13(A:Ø37F)	FØ	13	
Ø36C	INC	Ø354	EE	54	Ø3
Ø36F	BEQ	R:14(A:Ø385)	FØ	14	
Ø371	INC	Ø354	EE	54	Ø3
Ø374	BEQ	R:15(A:Ø38B)	F0	15	
Ø376	JMP	Ø35Ø	4C	5Ø	Ø3
Ø379	INC	Ø352	EE	52	Ø3
Ø37C	JMP	Ø367	4C	67	Ø3
Ø37F	INC	Ø352	EE	52	Ø3
Ø382	JMP	Ø36C	4C	6C	Ø3
Ø385	INC	Ø355	EE	55	Ø3
Ø388	JMP	Ø371	4C	71	Ø3
Ø38B	INC	Ø355	EE	55	Ø3
Ø38E	JMP	Ø35Ø	4C	5Ø	Ø3
Ø391	LDA	Ø3EB	AD	EB	Ø3
Ø394	BEQ	R:ØB(A:03A1)	FØ	ØB	
Ø396	DEC	Ø3EB	CE	EB	Ø3
Ø399	LDA	#$FF	A9	FF	
Ø39B	STA	Ø3EA	8D	EA	Ø3
Ø39E	JMP	Ø362	4C	62	Ø3
Ø3A1	RTS		6Ø		
Ø3A2	INC	Ø3E9	EE	E9	Ø3
Ø3A5	JMP	Ø35D	4C	5D	Ø3

(See notes after listing in Appendix 5A for further information.)

CROSS CORRELATION - FLOW DIAGRAM

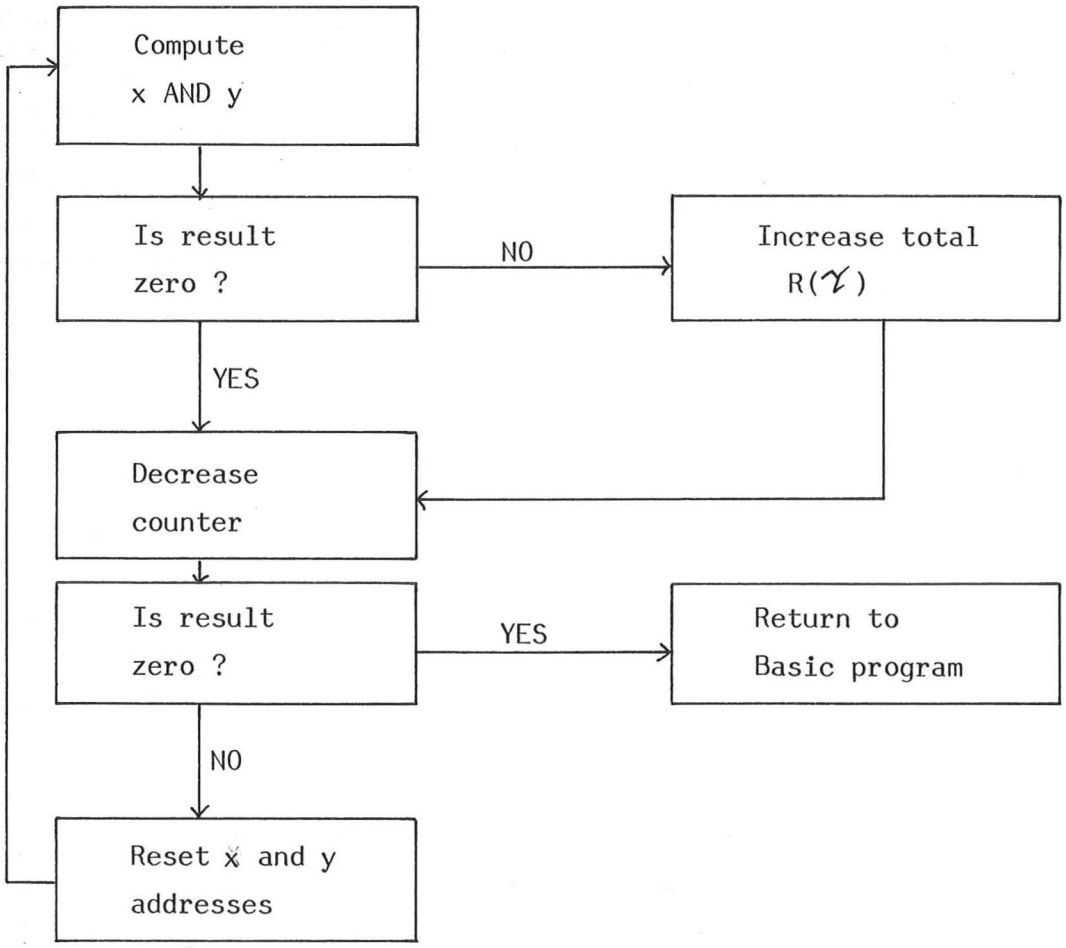

The BASIC program then computes the initial x and y addresses for the next shift τ, and re-enters the machine code routine. After each shift the memory locations containing R(τ) are read into an array for BASIC access.

LISTING OF CROSS CORRELATION BASIC PROGRAM

```
100 POKE53,118
110 DATA173,77,232,41,2,240,249,173,65,232
120 DATA73,128,41,128,141,255,119,173,237,3,240,6
130 DATA206,237,3,76,153,3,173,238,3,240
140 DATA29,206,238,3,169,255,141,237,3,238
150 DATA127,3,208,3,238,128,3,169,237,141
160 DATA76,232,169,205,141,76,232,76,112,3
170 DATA169,237,141,76,232,169,205,141,76,232,96
180 IFDT=1GOTO200:DIMT(73)
190 DIMT(73)
200 FORI=1TO73:READT(I):POKE(879+I),T(I):NEXT
210 IFDT=1GOTO470
220 ZB=59468:ZJ=237:ZF=205:ZE=59457:ZD=59469:ZG=2:ZA=59459:ZC=59467:NP=2048
230 DIMX(NP):DIMP(NP/2):DIMQ(88)
240 ZX=0
250 PRINT"--------------------------------------------"
260 PRINT"PARTICLE SPEED MEASUREMENT"
270 PRINT"____________________________________________"
280 PRINT"TRANSIENT RECORDER":PRINT"DATA HANDLING PROGRAM"
290 PRINT"DO YOU WANT TO READ DATA FROM TRANSIENT"
300 PRINT"RECORDER OR FROM DISC ?"
310 PRINT"TYPE T OR D"
311 GETA$:IFA$=""THEN311
312 IFA$="T"THEN370
318 PRINT"   FOLLOW STEPS 1 TO 4 "
319 PRINT"   ---------------------"
320 PRINT"1) PLACE DISC IN DRIVE 0"
330 PRINT"2) TYPE L FOLLOWED BY THE "
340 DT=1
349 PRINT"   FILE NAME IN DOUBLE QUOTES THEN ,08 "
350 PRINT"3) AFTER .  TYPE X"
351 PRINT"4) AFTER READY TYPE GOTO 470"
352 SYS1024
360 REM LOADING FROM TR
370 POKEZA,0
380 POKEZB,PEEK(ZB)OR1
390 POKEZC,PEEK(ZC)AND227
410 PRINT" AFTER RECORDING SIGNAL WITH TRANSIENT RECORDER "
430 PRINT" PRESS SPACE BAR ON PET TO TRANSFER":PRINT"DATA":WAIT59410,4,4
440 PRINT"LOADING";NP;"DATA POINTS"
445 POKEZB,ZJ:POKEZB,ZF
450 POKE1005,255:POKE1006,7:POKE895,255:POKE896,119
460 SYS880
470 PRINT"DATA LOADED"
480 REM SCREEN DISPLAY DATA
490 INPUT"TYPE S FOR SCREEN DISPLAY,OTHERWISE N";A$:IFA$="N"THEN910
510 IFZX=1THEN520
511 GOTO10000
520 INPUT"WHAT INTERVAL (1-12) BETWEEN POINTS";XIN
530 INPUT"WHAT START POINT (0-2048)";A
540 IF(A+80*XIN)<2048THEN560
550 PRINT"START POINT TOO HIGH":GOTO530
560 PRINT"START POINT"A"INTERVAL"XIN
```

```
570 MX=255
580 X(0)=X(1)
590 FORI=0TO78STEP2
600 Y=.5*INT(P(I*XIN+A))
620 L=33688-40*INT(Y-1)+I/2
630 IFY=INT(Y)THENS=123
640 IFY>INT(Y)THENS=126
650 POKEL,S
660 NEXTI
670 FORI=1TO79STEP2
680 Y=.5*INT(P(I*XIN+A))
700 L=33688-40*INT(Y-1)+(I-1)/2
710 IFY>INT(Y)THEN780
720 S0=PEEK(L)
730 S=108
740 IFS0=123THENS=98
750 IFS0=126THENS=127
760 POKEL,S
770 GOTO830
780 S0=PEEK(L)
790 S=124
800 IFS0=123THENS=255
810 IFS0=126THENS=226
820 POKEL,S
830 NEXTI
840 PRINT"▓▓▓▓▓▓▓▓▓▓▓▓▓▓▓▓▓▓▓▓▓▓▓"
850 FORI=0TO3
860 PRINT"▓"TAB(10*I)"| "INT(A+20*I*XIN)
870 NEXTI
880 PRINT"▓DO YOU WANT TO PLOT AGAIN (Y/N)"
881 GETR$:IFR$=""THEN881
882 IFR$="Y"THEN510
890 GOTO1310
900 REM TRANSFER DATA TO DISC
910 PRINT"▓▓DO YOU WANT TO TRANSFER DATA TO DISC?"
920 PRINT"▓TYPE Y OR N FOR YES OR NO"
921 GETA$:IFA$=""THEN921
922 IFA$="Y"THEN940
930 GOTO 990
940 PRINT"▓▓▓▓▓    FOLLOW STEPS 1 TO 4"
941 PRINT"     ------------------------"
942 PRINT"▓▓1) PLACE DATA DISC IN DRIVE 0"
950 PRINT"▓2) TYPE S FOLLOWED BY THE FILE NAME IN"
960 PRINT"    DOUBLE QUOTES THEN ,08,77FF,7FFF"
970 PRINT"▓3) WHEN ▓.▓ APPEARS TYPE X"
971 PRINT"▓4) AFTER ▓READY▓ TYPE GOTO 990"
980 SYS(1024)
990 REM CORRELATION PROGRAM
1000 DATA173,0,120,45,1,120,240,5,238,232
1010 DATA3,240,69,206,234,3,240,47,238,81
1020 DATA3,240,18,238,81,3,240,19,238,84
1030 DATA3,240,20,238,84,3,240,21,76,80
1040 DATA3,238,82,3,76,103,3,238,82,3
1050 DATA76,108,3,238,85,3,76,113,3,238
1060 DATA85,3,76,80,3,173,235,3,240,11
1070 DATA206,235,3,169,255,141,234,3,76,98
1080 DATA3,96,238,233,3,76,93,3
1090 FORI=1TO88:READQ(I):NEXT
```

```
1100 FORI=1TO88:POKE(847+I),Q(I):NEXT
1110 PRINT"■■■■■■■COMPUTING CORRELATION"
1120 PRINT"■■■■■■■_____"
1140 INPUT"■■START AT STEP NO. (0-) ";SA
1150 INPUT"■■NO. OF STEPS ";SP
1160 S=SA+SP
1170 IF S<NP/2GOTO1190
1180 PRINT"■■TOO MANY STEPS !":GOTO1140
1190 P=SA:B=256:A=30718
1191 PRINT"■■■RUNNING MACHINE CODE PROGRAM"
1200 M=2*P+2:Y=NP/2-P
1210 K=INT(Y/B):G=INT((Y+K)/B):F=Y-G*B+G
1220 EV=A+M:H=INT(EV/B):L=EV-H*B
1230 POKE(849),255:POKE(850),119:POKE(852),L:POKE(853),H
1240 POKE(1000),0:POKE(1001),0
1250 POKE(1002),F:POKE(1003),G
1260 SYS848
1270 X(P)=B*PEEK(1001)+PEEK(1000)
1280 P=P+1:S=S-1:IFS=SAGOTO1370
1290 GOTO1200
1300 REM LIST RESULTS
1310 PRINT"■DO YOU WANT TO LIST RESULTS, Y OR N"
1311 GETB$:IFB$=""THEN1311
1312 IFB$="N"THEN1350
1320 INPUT"■■START AND FINISH POINTS S,F";SPT,FPT
1325 OPEN128,4
1330 FORI=SPTTOFPT:PRINT#128,"X("I")="X(I):NEXT
1331 CLOSE128
1335 PRINT"■■DO YOU WANT TO LIST AGAIN Y/N"
1336 GETA$:IFA$=""THEN1336
1337 IFA$="Y"THEN1320
1340 PRINT"DO YOU WANT TO CALCULATE VELOCITY Y/N"
1341 GETA$:IFA$=""THEN1341
1342 IFA$="Y"THEN1700
1350 PRINT"■■DO YOU WANT TO CORRELATE AGAIN"
1351 GETA$:IFA$=""THEN1351
1352 IFA$="Y"THEN1140
1360 RUN
1370 MAX=0:S=SA+SP:ZX=1:PRINT"■"
1380 FORI=SATOS:IFX(I)>MAXTHENMAX=X(I)
1390 NEXT
1400 MIN=MAX
1410 FORI=SATO(S-1)
1420 IF X(I)<= MIN THEN MIN=X(I)
1430 NEXT
1440 REM DISPLAY RESULTS
1450 PRINT"■■CORRELATION STARTED AT",SA
1460 PRINT"■■NO. OF STEPS",SP
1470 PRINT"■■MAXIMUM VALUE OF X =",MAX
1480 PRINT"■■MINIMUM VALUE OF X =",MIN
1490 J=0:RNG=MAX-MIN:BIG=0
1500 FORI=SATO(S-1):J=J+1
1510 P(I)=X(I)-MIN
1520 IFP(I)>BIGTHENBIG=P(I)
1530 NEXT
1540 FORI=SATOS:P(I)=P(I)*(49*0.8)/BIG:NEXT
1550 GOTO520
1700 INPUT"SWEEP A ON TR (IN MILLISEC)";SWA
1710 INPUT"NO. OF SHIFTS AT PEAK";NS
1720 INPUT"DISTANCE BETWEEN SENSORS (MM)";DIST
1730 VEL=DIST*1E-3/(NS*SWA*1E-3/1024)
1740 PRINT"VELOCITY IN M/S";VEL
1750 PRINT"DO YOU WANT TO TRY AGAIN"
1751 GETA$:IFA$=""THEN1751
1760 IFA$="Y"THEN1700
```

```
1770 RUN
10000 PRINT"TYPE Y FOR A SINGLE SCREEN PLOT"
10001 GETA$:IFA$=""GOTO10001
10002 IFA$="Y"GOTO10130
10005 PRINT"TYPE Y TO PLOT ALL DATA"
10009 GETA$:IFA$=""GOTO10009
10010 IFA$="Y"THEN10030
10020 INPUT"■■■HOW MANY PAGES OF POINTS (MAX 25)";V:GOTO10040
10030 V=25
10040 MS=32767+200:A=0:Z=1:X=40:L=70:K=320:R=30719:C=120/128
10050 B=A*40:PRINT"■■";B:POKEMS+1,90:POKEMS+121,90:POKEMS+321,90:POKEMS+441,90
10060 FORI=ZTOX
10070 N=MS+I:F=R+2*B+2*I:Q=PEEK(F)*C:POKEN+Q,L:Q=PEEK(F-Z)*C:POKEN+K+Q,L:NEXT
10080 A=A+Z:IFA=VTHEN10100
10090 GOTO10050
10100 PRINT"DO YOU WANT TO PLOT AGAIN Y/N"
10101 GETA$:IFA$=""THEN10101
10110 IFA$="Y"THEN10000
10120 GOTO910
10130 MS=32767+200:A=0:Z=1:X=40:L=70:K=320:R=30719:C=120/128
10140 PRINT"■■":POKEMS+1,90:POKEMS+121,90:POKEMS+321,90:POKEMS+441,90:E=0
10150 FORI=0TO2048STEP52:E=E+1
10160 Q=PEEK(R+I)*C:POKEMS+E+Q,L:Q=PEEK(R+I+1)*C:POKEMS+E+Q+K,L:NEXT
10170 GOTO10100
```

NOTES ON CROSS CORRELATION BASIC PROGRAM

Line number	Comments
100-200	Machine code program for data transfer is stored as DATA statements. Line 200 loads program into PET memory.
318-352	Routine for reading data from a floppy disc.
360-470	Routine to access machine code program to transfer data from the transient recorder.
480-890	Routine to display results of correlation on PET screen as a graph.
900-980	Routine for storing data from transient recorder onto floppy disc.
990-1100	Cross correlation machine code, stored as DATA statements. Line 1100 loads program into PET memory.
1110-1290	Sets variables for machine code program, runs cross correlation, reads results from PET memory.
1300-1337	Lists results of cross correlation.
1440-1550	Determines variables for screen display of correlation results, then accesses display routine (480-890)
1700-1770	Calculates velocity, from results of cross correlation.
10000-10170	Routine to display data in PET memory (from transient recorder, or floppy disc).

APPENDIX 5C

DIRECT SIGNAL INPUT ROUTINE

PROGRAM			CODE		
Location	Command	Address/Number			
Ø35Ø	LDA	E841	AD	41	E8
Ø353	BEQ	R:ØC(A:0361)	FØ	ØC	
Ø355	CMP	#$Ø2	C9	Ø2	
Ø357	BEQ	R:ØF(A:Ø368)	FØ	ØF	
Ø359	BCS	R:14(A:Ø36F)	BØ	14	
Ø35B	TAX		AA		
Ø35C	LDY	#$ØØ	AØ	ØØ	
Ø35E	JMP	Ø378	4C	78	Ø3
Ø361	LDX	#$ØØ	A2	ØØ	
Ø363	LDY	#$ØØ	AØ	ØØ	
Ø365	JMP	Ø376	4C	76	Ø3
Ø368	LDX	#$ØØ	A2	ØØ	
Ø36A	LDY	#$Ø1	AØ	Ø1	
Ø36C	JMP	Ø377	4C	77	Ø3
Ø36F	LDX	#$Ø1	A2	Ø1	
Ø371	LDY	#$Ø1	AØ	Ø1	
Ø373	JMP	Ø379	4C	79	Ø3
Ø376	NOP		EA		
Ø377	NOP		EA		
Ø378	NOP		EA		
Ø379	STX	77FF	8E	FF	77
Ø37C	STY	78ØØ	8C	ØØ	78
Ø37F	LDA	Ø3C5	AD	C5	Ø3
Ø382	BEQ	R:Ø6(A:Ø38A)			
Ø384	DEC	Ø3C5	CE	C5	Ø3
Ø387	JMP	Ø397	4C	97	Ø3
Ø38A	LDA	Ø3C6	AD	C6	Ø3
Ø38D	BEQ	R:2D(A:Ø3BC)	FØ	2D	
Ø38F	DEC	Ø3C6	CE	C6	Ø3
Ø392	LDA	#$FF	A9	FF	
Ø394	STA	Ø3C5	8D	C5	Ø3

continued overleaf

DIRECT SIGNAL INPUT ROUTINE - continued/2

PROGRAM			CODE		
Location	Command	Address/Number			
Ø397	LDA	Ø37A	AD	7A	Ø3
Ø39A	CLC		18		
Ø39B	ADC	#$Ø2	69	Ø2	
Ø39D	STA	Ø37A	8D	7A	Ø3
Ø3AØ	BEQ	R:Ø9(A:Ø3AB)	FØ	Ø9	
Ø3A2	CLC		18		
Ø3A3	ADC	#$Ø1	69	Ø1	
Ø3A5	STA	Ø37D	8D	7D	Ø3
Ø3A8	JMP	Ø35Ø	4C	5Ø	Ø3
Ø3AB	INC	Ø37B	EE	7B	Ø3
Ø3AE	LDA	Ø37B	AD	7B	Ø3
Ø3B1	STA	Ø37E	8D	7E	Ø3
Ø3B4	LDA	#$Ø1	A9	Ø1	
Ø3B6	STA	Ø37D	8D	7D	Ø3
Ø3B9	JMP	Ø35Ø	4C	5Ø	Ø3
Ø3BC	RTS		6Ø		

(See notes after listing in Appendix 5A for further information.)

CHAPTER 6 : THE EROSION OF ALUMINIUM ALLOYS BY SPHERICAL PARTICLES AT NORMAL IMPINGEMENT

6.1 INTRODUCTION

A literature survey and discussion providing a background to the series of experiments described in this chapter has been presented in Chapter 3 section 3.1. The conclusion of this preliminary study was that there was little agreement in the literature on the mechanism of erosion by particles at normal impingement. It was further concluded that an experimental programme involving detailed surface and subsurface observations was necessary to determine which, if any, of the proposed mechanisms operates.

Early in the programme of research reported in this chapter, the need for detailed information concerning the deformation and flow of subsurface material was recognised. A technique for introducing a marker layer beneath the surface of test specimens prior to eroding has been developed as a means of providing this information. The experimental evidence from detailed observations of the surface and subsurface features of specimens eroded under controlled conditions is used to construct a model of the erosion process.

6.2 EXPERIMENTAL DETAILS

(a) Materials

Three aluminium alloys were used in these experiments :

(i) A precipitation hardening alloy Al 6061 (1% Mg, 0.6% Si, 0.3% Cu) in both the fully hardened (T6, solution treated

quenched and aged) and annealed (Ø, annealed at 415°C for 3 hours, furnace cooled at 30°C per hour) conditions.

(ii) Commercial purity aluminium, Al 1100 and British Standard B.S. 1470 (0.15% Si, 0.01% Cu, 0.5% Fe, 0.05% Mn) in the as-received (work hardened) state and also in the form of a roll-bonded composite (see below).

(iii) A precipitation hardening alloy HS 15, (British Standard 1470, 4% Cu, 0.5% Mg, 0.5% Si, 1% Mn) in solution treated and aged condition.

The hardnesses of these materials were measured, the results listed in Table 6.1.

Table 6.1

Alloy	Condition	Vickers Hardness kg f mm^{-2} ($1 kgf mm^{-2} = 9.8 MPa$)	Indenter load (kg)
Al 6061	T6	108	2.5
Al 6061	0	40	2.5
Al 1100 (C.Pure Al)	as received (work hardened)	40	1.0
HS 15	solution treated and aged	140	2.5

(b) Erodent materials

Three types of abrasive particles were used :

(i) Soda glass beads (Ballotini, supplied by Abrasive Developments Ltd, Solihull). Three size ranges were used 212-250μm, 495-600μm and nominal 40μm.

(ii) Iron shot, sieved size range 600-700μm.

(iii) Leaded glass beads (Supplied by Jencon Sci, Leighton Buzzard), nominal size 600μm.

In general the larger erodent sizes were used for erosion testing to facilitate subsequent microscopic examination, since preliminary experiments had indicated that the scale of the surface features and of the subsurface deformation depended on the size of the erosive particles.

(c) Erosion testing

The erosion experiments were carried out using the air-blast erosion tester described in Chapter 5 section 5.2. A nozzle of 4.76mm internal diameter was used. The specimens, with the exception of those produced from roll bonded material, were cut from 5mm thick sheet, and were 65mm long and 20mm wide. The roll bonded material was cut to the same length and width but approximately 1.5mm thick. Testing produced a circular area of damage, (diameter approximately 8mm), in the centre of the specimen.

Experiments were performed using a range of particle velocities from 30ms^{-1} to 60ms^{-1}. The velocity was measured by the double disc method (detailed in Chapter 5, section 5.3.1 (c)). The subsurface features reported below were common to all specimens.

(d) Marker layer techniques

In the introduction to this chapter the need was discussed for a technique which would provide information on the deformation and flow of the material

beneath the eroding surface. A central element of the experimental programme was the development of a method of placing an inert marker layer on, or in, an erosion test specimen. The movement of such a marker layer, determined by the subsequent sectioning of an eroded specimen, would provide the required information.

(i) Plating techniques

Initial attempts at establishing an inert marker layer involved conventional electroplating techniques. Platings were produced on both eroded specimens, and polished surfaces. A wide range of electroplating conditions were evaluated. Several pre-treatments were also utilised, ranging from simple cleaning and degreasing to the use of vacuum deposition techniques producing conductive layers on the surfaces. None of the methods attempted proved successful for producing a marker layer of copper or nickel on an aluminium surface. Thick platings were not sufficiently adherent to remain attached to the surface during erosion testing. Thin platings, although visible after erosion when the surface was examined by a low power stereo optical microscope, were not visible on subsequent sectioning of the specimen.

(ii) Roll bonding techniques

Roll bonding is a solid state pressure welding technique which can be used for joining sheets of similar or dissimilar metals. Initially, pure copper foil was roll-bonded between two strips of commercial purity Al (B.S. 1470). However, the resultant composite was found to deform in an unusual manner during erosion. (Details of the behaviour of this composite specimen are

presented briefly in Chapter 7 section 7.3.6.) Clearly the copper foil was not behaving as an inert marker, and work involving this combination of materials was abandoned without any attempt to optimise the roll bonding procedure.

Roll-bonded composites of aluminium foil and aluminium strip were prepared, and evaluated by erosion testing. This composite specimen was found to behave in a manner identical to simple aluminium strip. Weight loss measurements revealed that the erosion rate, and incubation period were not modified by the composite structure of the specimen. Microscopical examination of surface and subsurface features revealed no differences in behaviour due to the presence of the foil. Examination of polished sections of eroded composite specimens revealed no trace of the foil. Conventional etching techniques (10% sodium hydroxide, or 2% HF 3% HCL 5% HNO_3 90% H_2O to resolve fine detail) were used to determine the position of the foil/strip welded interface. In this way the position of the marker foil could be identified as a pair of parallel lines on an etched section.

Test specimens of roll-bonded composite were prepared from three 1.55mm thick strips of commercial purity aluminium (B.S. 1470) and two 0.2mm thick strips of pure aluminium foil. Each surface to be bonded was lightly abraded using 1200 grit silicon carbide paper, and then degreased with methanol. The strips were soft-rivetted together, and the completed 'sandwich' annealed at 400^{o}C for 0.75 h. The bonding was completed by a single pass through a rolling-mill achieving a 70% reduction in thickness (equivalent to a natural strain of 1.15).

6.3 EXPERIMENTAL RESULTS

6.3.1 Weight loss measurements

The measurements of mass change during erosion revealed that in each case the specimen exhibited an initial 'incubation' period of negligible mass loss or slight mass gain before a linear dependence of erosion on abrasive mass became established. Figure 6.1 (taken from Hutchings (1981)) shows a representative cumulative mass loss curve. For this specimen, approximately 1.3 kg of glass beads had impacted the surface before 'steady state' erosion was established.

Table 6.2 presents full details of the erosion measurements and test conditions. A theoretical analysis of these results has been published (Hutchings (1981)). The data is reproduced here to illustrate the small differences in erosion rates measured for the alloys after different heat treatments, despite the large differences in hardness (a factor of 2.7). For example, the linear erosion rates (mass removed per unit mass erodent) for erosion by 600-700μm iron shot at 32ms^{-1} were 6.8×10^{-6} for 6061-0 and 6.1×10^{-6} for 6061-T6 alloy.

6.3.2 Surface features

Microscopical examination revealed that during the incubation the surface of the specimen became roughened, exhibiting surface undulations with wavelengths comparable to the diameter of the impacting spheres. Figures 6.2 (a) and (b) illustrate the typical appearance of the surface once steady state conditions had been reached. The even distribution of surface waves is notable : the surfaces of the hills and valleys are marked by

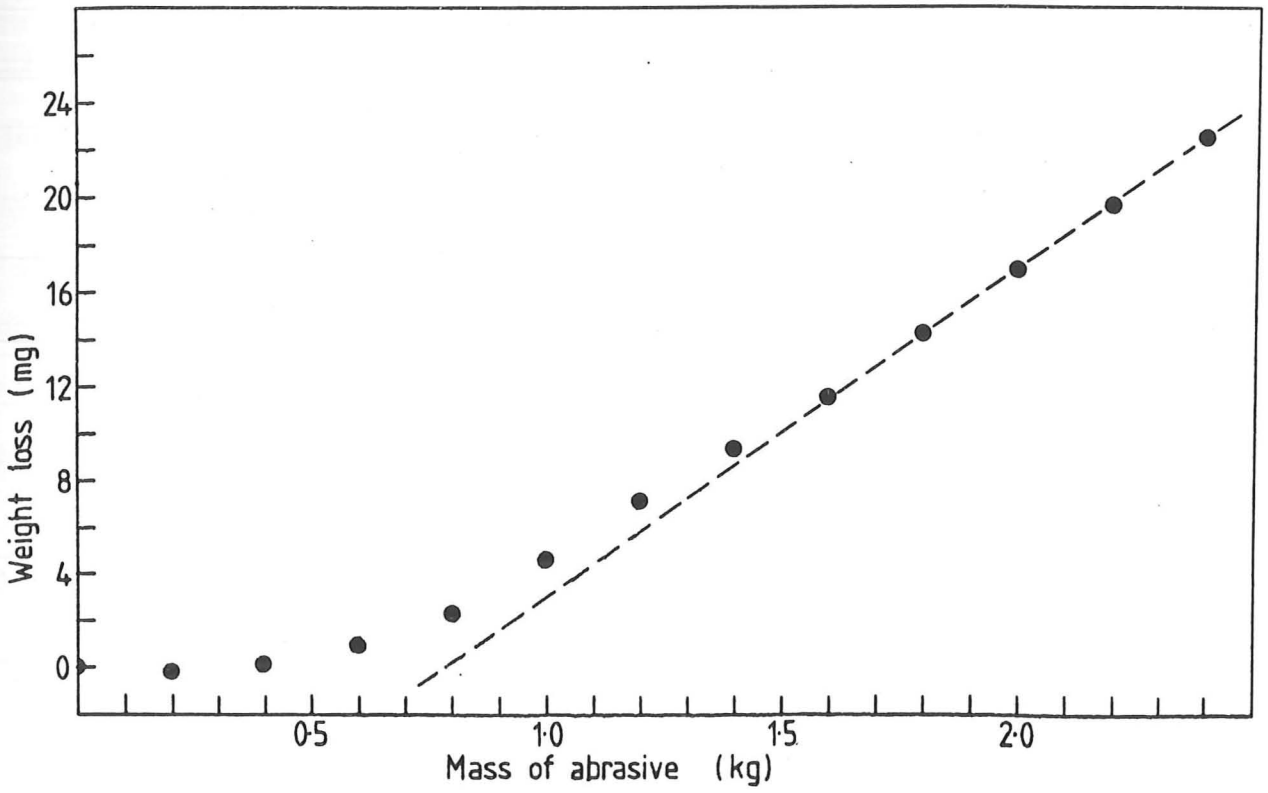

Figure 6.1 : Typical cumulative mass loss curve (broken line indicates steady state erosion). (After Hutchings (1981))

numerous smaller indentations, of spherical curvature, which represent the impacts of individual spheres. The jagged edges of flakes of material, which appear to be connected with the bulk over only part of their circumference, are clearly visible in Figure 6.2 (b). These flakes, ranging in size from considerably smaller than individual impact indentations to several times the size of an indentation, were seen on all the eroded surfaces, and form the source of the mass loss observed in the experiment.

6.3.3 Subsurface features

Specimens were sectioned and polished for metallographic examination : many of the subsurface features were visible without etching. Several features were common to all specimens and were found to occur when testing with both iron shot and glass beads as erodent.

Beneath the surface is a region, which in general follows the surface contours and which is clearly delineated by a sharp boundary from the bulk of the specimen. Examination of this region at higher magnification revealed an extremely disturbed microstructure, with many embedded particles and cracks. Figure 6.3 illustrates the extent of the subsurface layer for various alloys and erodent types. Over much of its extent the subsurface layer is of uniform thickness, approximately half the radius of the impinging spheres. At points where the surface rises to a peak (corresponding to the 'hills' visible in Figure 6.2 (a)), the thickness of the disturbed layer is much less, and occasionally the bulk material is found to be continuous right up to the surface.

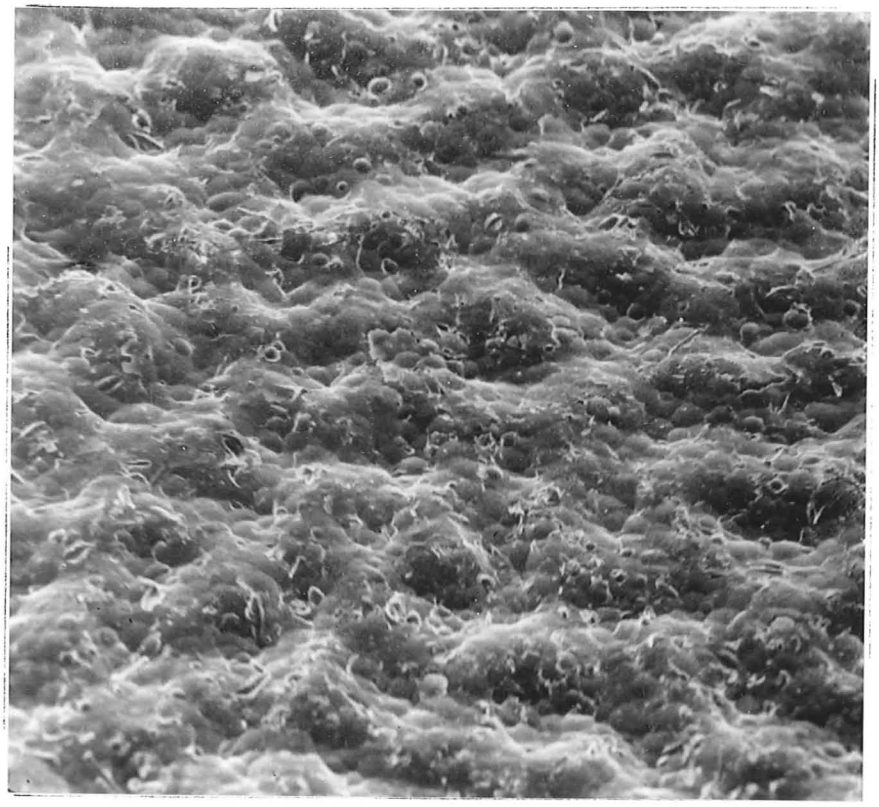

(a)

250µm

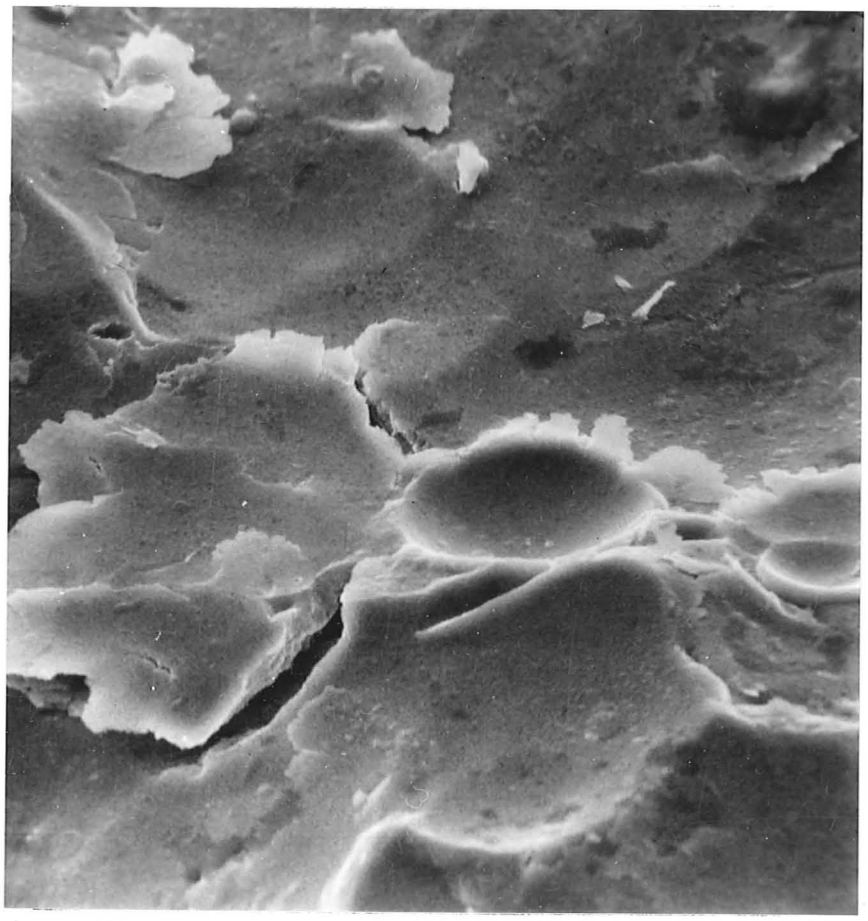

(b)

50 µm

Figure 6.2 (a & b) : SEM micrographs showing surface features of a specimen tested until steady state erosion was established. (This specimen was eroded by 212-250µm glass ballotini, impact velocity approximately 60ms^{-1}. The total weight of erodent used was 1.4kg.)

TABLE 6.2 : EROSION TEST RESULTS

	Specimen no. material and heat treatment	Erodent type steel 600-700μm	glass 212-250μm	glass 405-600 μm	Particle velocity ms^{-1}	Microhardness (20g load) averages $kgfmm^{-2}$ Sub-surface	Bulk	Linear erosion rate $\times 10^{-6}$ *	Total mass of erodent kg *	Average depth of subsurface layer μm
1	Al 6061-0	√			41	-	-	17.1	2.60	-
2	(annealed)	√			32	222	47	6.8	3.05	221
3	Al 6061-T6		√		40	250	101	2.9	3.25	30
4	(fully		√		50	260	126	5.1	3.60	37
5	hardened)		√		44	249	121	4.0	2.80	34
6			√		62	-	-	12.4	1.40	-
7				√	44	206	118	5.1	2.20	88
8		√			32	228	112	6.1	4.05	141
9		√			41	-	-	11.9	2.80	-
10				√	37	-	-	2.4	3.00	-
11				√	50	213	107	13.1	1.80	146
12			√		33	-	-	1.7	2.00	
13		√			47	260	124	22.6	1.60	128
14				√	50	204	103	13.9	2.40	114
15				√	56	-	-	22.1	1.60	-
16				√	30	250	120	2.5	3.60	57
17	1100-0	√			32	150	46	7.8	2.60	235
18	(annealed)	√			41	-	-	17.0	2.00	-

* Results from Hutchings (1981)

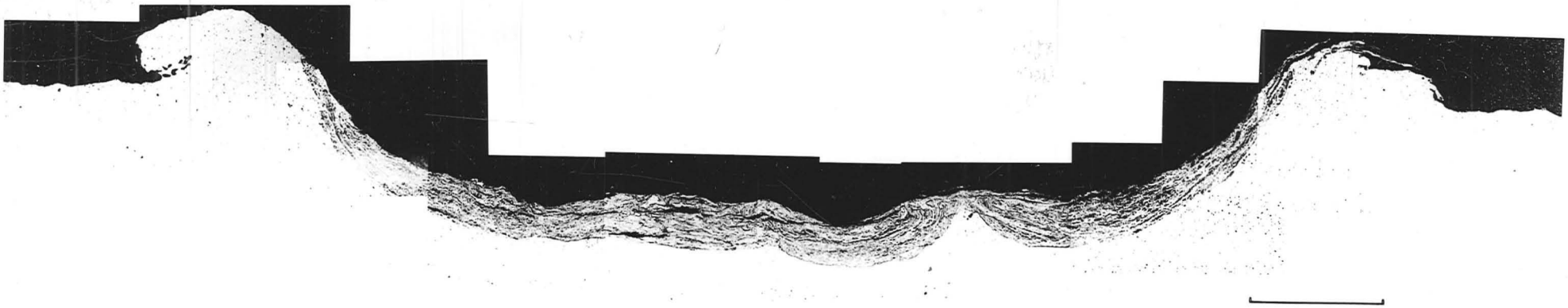

Figure 6.3 (a) :

Annealed commercial purity aluminium eroded by 600-700μm iron shot at 41ms^{-1}. Total weight of erodent 2.0kg. (Scale bar = 1mm)

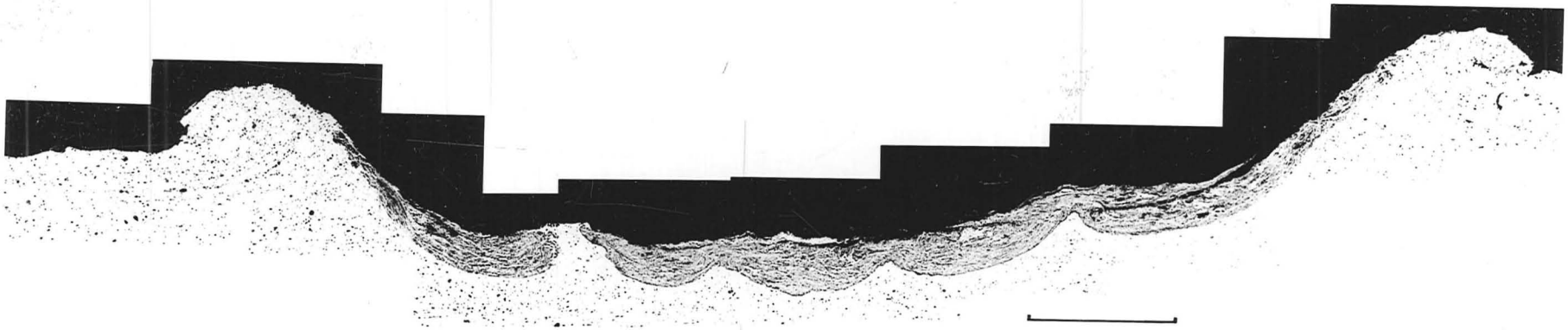

Figure 6.3 (b) :

Annealed 6061 aluminium alloy eroded by 600-700μm iron shot at 41ms^{-1}. Total weight of erodent 2.60kg. (Scale bar = 1mm)

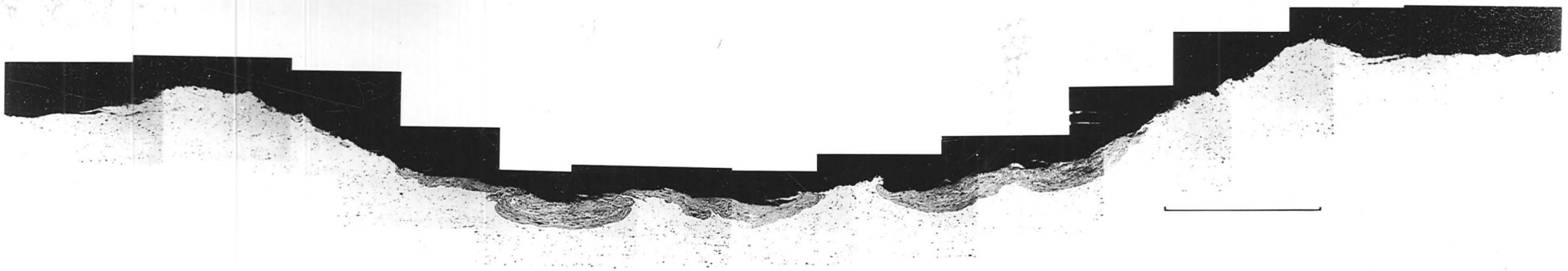

Figure 6.3 (c) :

Hardened (T6) 6061 aluminium alloy eroded by 600-700μm iron shot at 47ms^{-1}. Total weight of erodent 1.60kg. (Scale bar = 1mm)

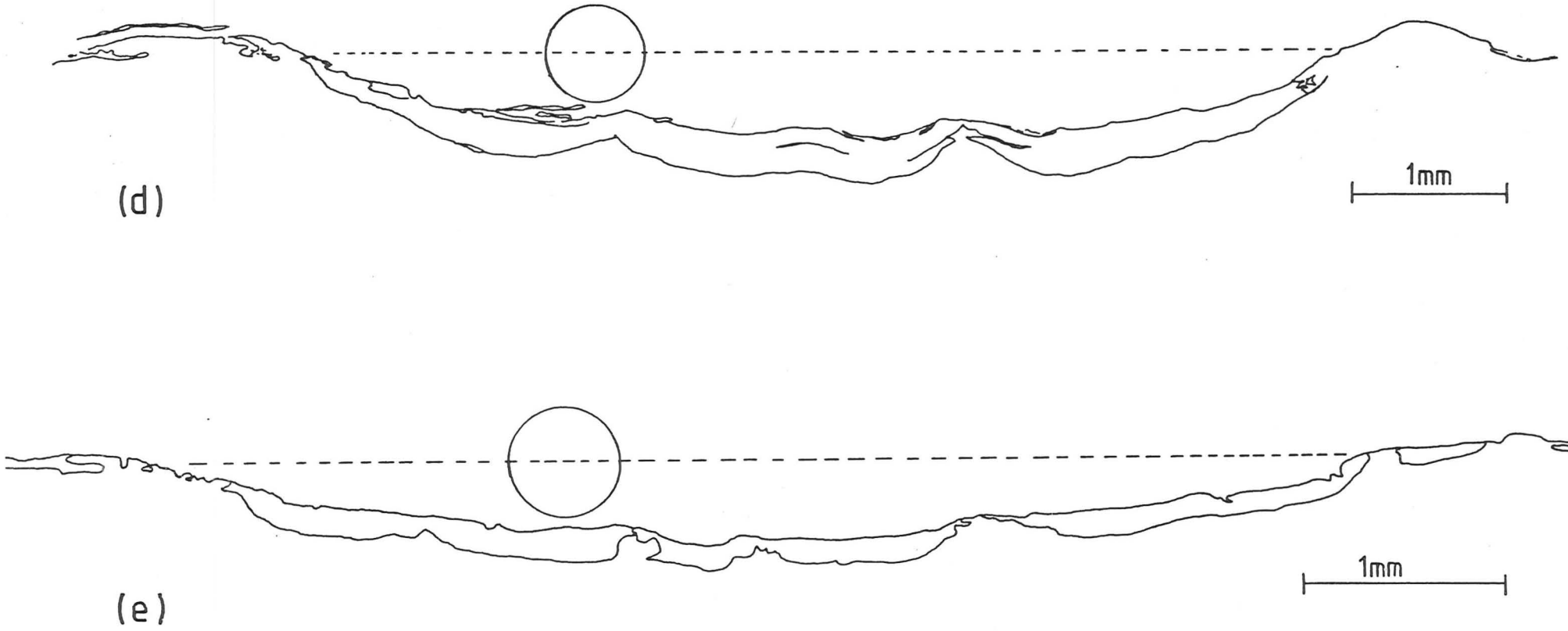

Figure 6.3 : Sections showing subsurface structure

(d) Annealed specimen (6061-0), eroded by 600-700μm iron shot, velocity 32ms^{-1}, total weight of erodent 3.05kg.

(e) Hardened specimen (6061-T6), eroded by 495-600μm glass beads, velocity 50ms^{-1}. total weight of erodent 2.40kg.

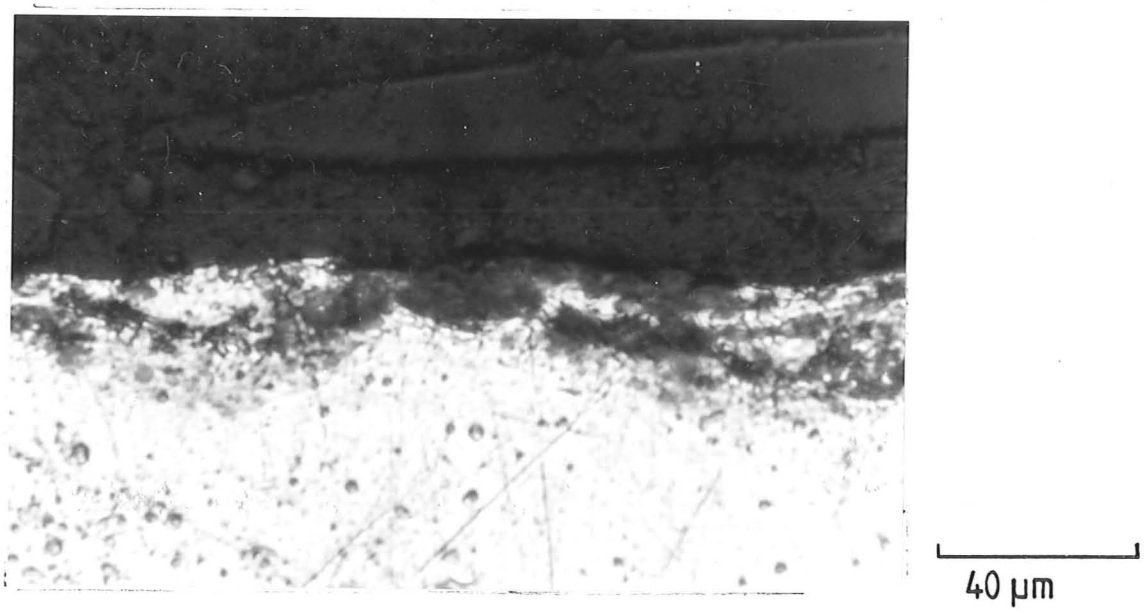

Figure 6.3 (f) : HE15 aluminium alloy eroded with 40µm glass beads

The subsurface structure is illustrated at higher magnification in Figures 6.4 (a) and (b), which show sections through specimens eroded by iron shot, and by glass beads, respectively. The disturbed layer consists of laminar regions of material, heavily deformed but otherwise similar in appearance to the bulk metal. In the case of the specimens eroded by glass beads, many of the particles embedded in the disturbed layer could be identified by polarised light microscopy as glass. Energy dispersive X-ray microanalysis of sections from specimens eroded by iron shot reveal a high concentration of iron within the layer, with no iron present (in detectable levels) in the bulk alloy. Figure 6.5 (a) presents these results in the form of a scanning electron microscope (SEM) micrograph; the figure caption explains the generation of this image. Figure 6.5 (b) is an SEM micrograph of the surface of a single iron shot particle; the surface oxide is clearly evident.

It was possible to recover glass fragments embedded in a specimen eroded by glass beads by dissolving the aluminium in 50% HCl. A non-eroded specimen was also dissolved and the insoluble residue weighed. By this technique the total weight of embedded glass could be estimated. A high speed centrifuge was used to enable the acid to be separated from the insoluble residue, which was washed repeatedly with acetone before being dried. Using this method the weight of glass recovered was found to be approximately equal to the maximum weight increase of the specimen during incubation. Kosel et al (1979) used a similar technique to quantify the amount of alumina fragments embedded in eroded pure nickel and copper specimens. They reported similar findings to the present work, with the chemical recovery method indicating the same weight as the maximum weight gain measured during incubation.

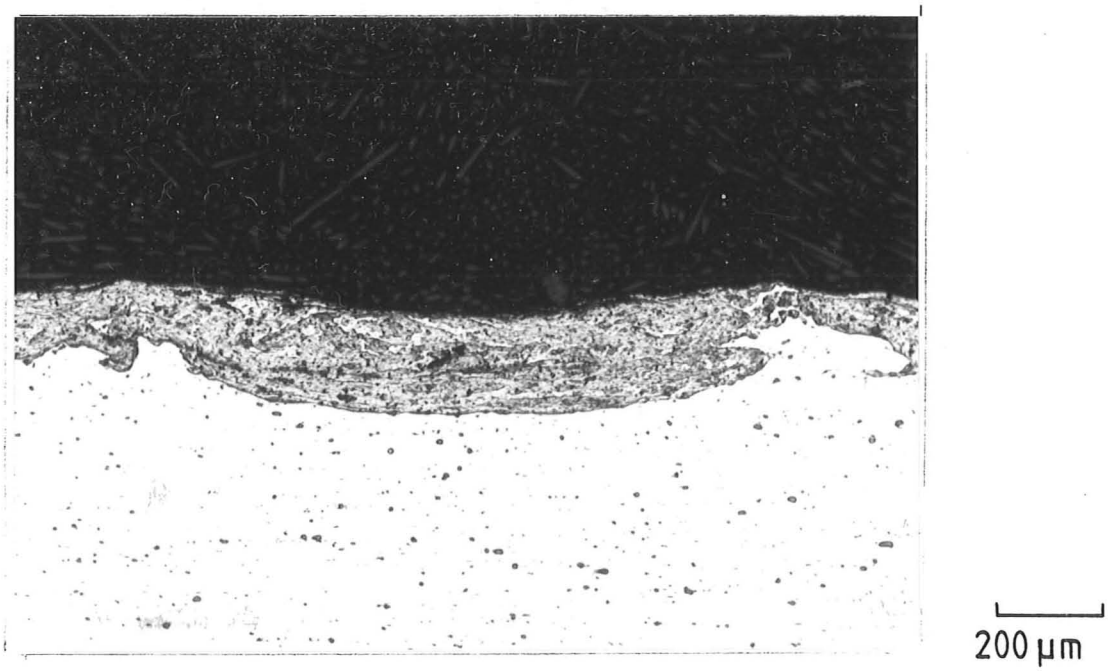

Figure 6.4 (a) : Optical micrograph, showing a section through a specimen of 6061-T6 eroded by 600-700µm iron shot at $32ms^{-1}$. Total weight of erodent 4.05kg.

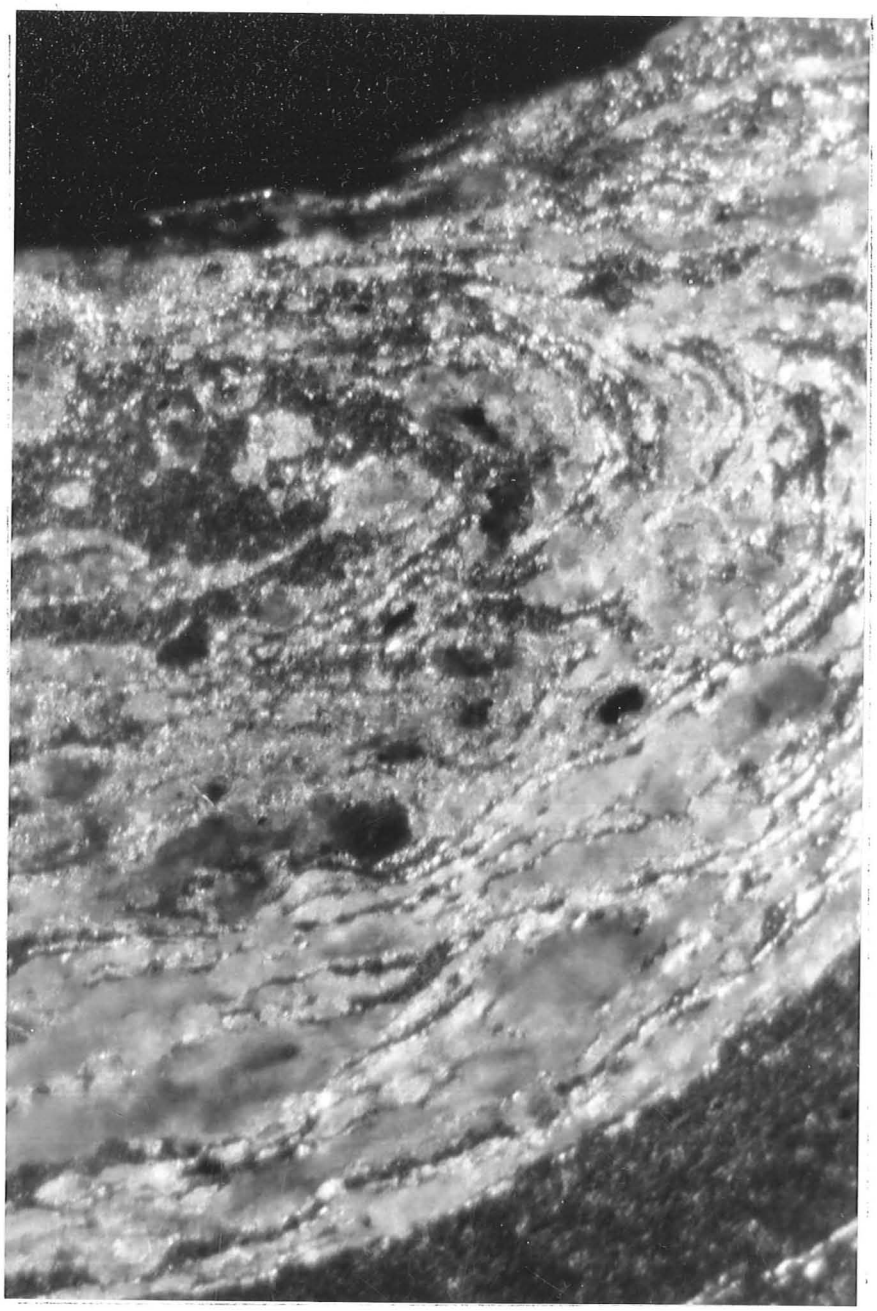

Figure 6.4 (b) : Polarised light micrograph, showing a section through a specimen of commercial purity aluminium eroded by 600μm glass beads at 58ms^{-1} (total weight of erodent 1940g). Note the laminar structure, and the contrast shown by the glass fragments.

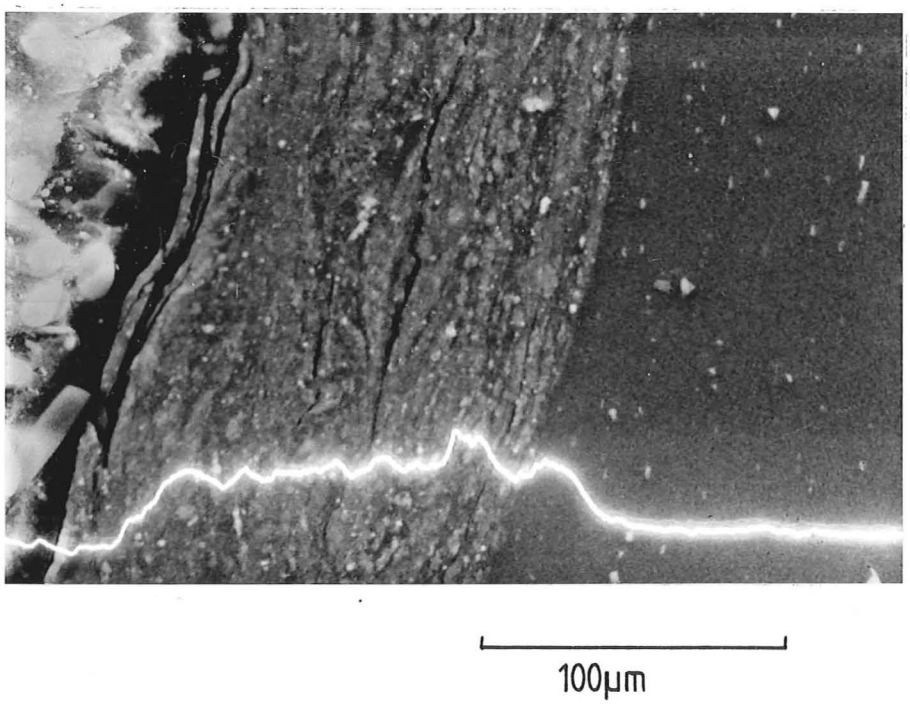

Figure 6.5 (a) : Scanning electron microscope micrograph of a section of an aluminium alloy (6061-T6), eroded by iron shot. The height of the white line is proportional to the intensity of x-rays, characteristic to iron, emitted whilst the electron beam scans a single line across the specimen. (The line profile slightly 'lags' the image.)

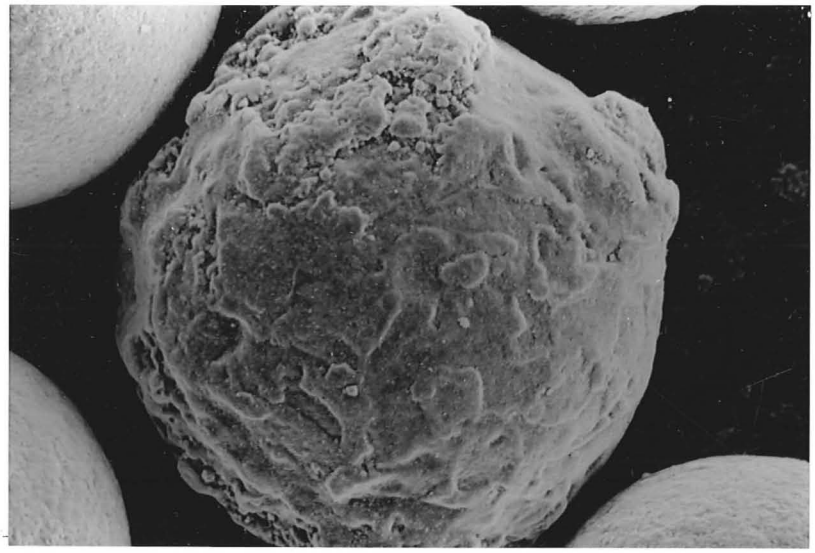

Figure 6.5 (b) : Scanning electron microscope micrograph of a single iron shot particle. (This particle is taken from a sieved fraction of smaller size than those used in the erosion experiments, but similar in shape and surface condition.) The particle illustrated is heavily oxidised; most particles examined showed surface oxidation to a lesser extent.

The largest difference they recorded between these two methods of measurement was a factor of 3.5

The measurements made in the present study indicate that the amount of glass present in the disturbed layer is approximately equivalent to only seven of the spherical glass beads. The specimen in question had been eroded by 1.6 kg of 600μm glass beads, a total of 5.7 million beads, each region of the specimen of area equal to the particle cross section will have experienced approximately 32000 impacts. Clearly only a small fraction of these impacts need result in fracture of the erodent particles in order to generate the fragments recovered from the disturbed layer.

By comparing sections of specimens eroded under identical experimental conditions, but with differing amounts of erodent, it is found that the depth of the disturbed layer is relatively constant once steady state erosion is established. (See Table 6.2 specimens no 11 and 14.)

Microhardness measurements on the sections revealed that the disturbed layer was markedly harder than the bulk material. For all the 6061 alloy specimens the hardness of the disturbed layer lay in the range of 200 to 250 $kgfmm^{-2}$ (Vickers, 20g indenter load). No significant difference was observed between the hardnesses of the layers formed in the precipitation hardened and in the annealed specimens. The change in the hardness across the boundary from the disturbed layer to the bulk metal was very abrupt, as illustrated by Figure 6.6, which shows micrographs of scratch hardness test specimens.

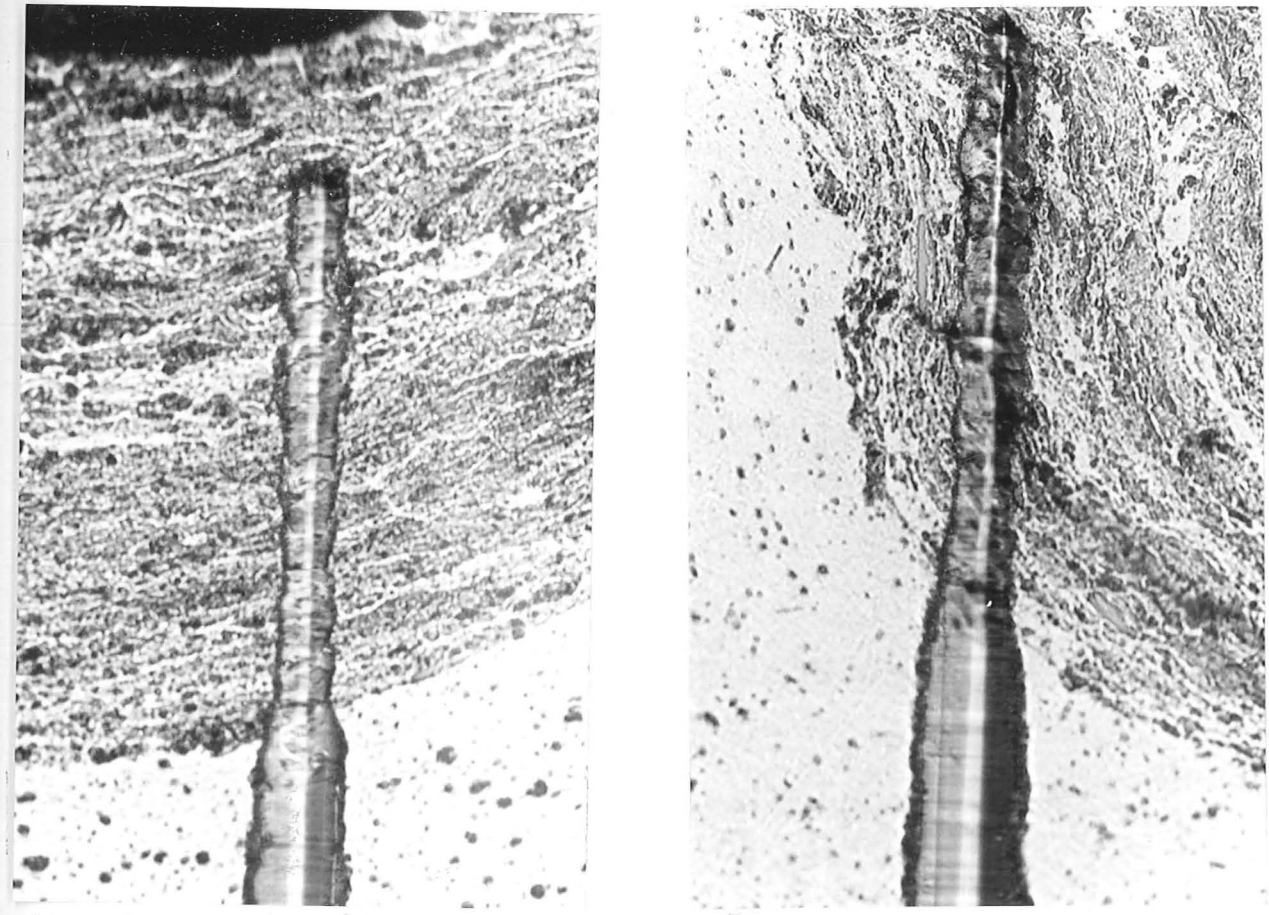

Figure 6.6 : Scratch microhardness test specimens.

(a) 6061 aluminium alloy, annealed, eroded with 2.60kg of 600-700µm iron shot at $32ms^{-1}$.

(b) Commercial purity aluminium, annealed, tested under identical conditions.

Note the immediate increase in scratch width as the boundary is crossed.

6.3.4 Roll Bonded specimens

As described in section 6.2 (d) above, the technique of roll bonding was used to place an inert aluminium foil marker layer beneath the surface of test specimens prior to eroding. A series of these specimens was eroded with increasing amounts of erodent and then sectioned for metallographic examination. In this way the development of the sub-surface layer, and its movement in the various stages of erosion could be determined. Figure 6.7 shows a cumulative mass loss curve for the roll bonded material; the stages at which the specimens were sectioned are indicated. Figures 6.8 (a) to (e) illustrate the sections at these stages. For clarity this information is reproduced in outline form, by the photo-reduction of tracings of the original photomicrographs. The erosion test produces a depression with circular symmetry, and these sections trace random diameters. Sectioning destroys the specimen, and therefore each section is from a separate specimen.

The important features which have been revealed by these experiments are as follows:

(i) In the earliest stages of erosion the surface appears rougher than when the subsurface layer is complete.

(ii) The subsurface structure is not fully developed until the maximum weight gain, in incubation, is achieved.

(iii) As erosion progresses, and the disturbed layer is pushed further into the bulk, only material very close to the boundary is disturbed. Thus we see that the marker layer is deflected only

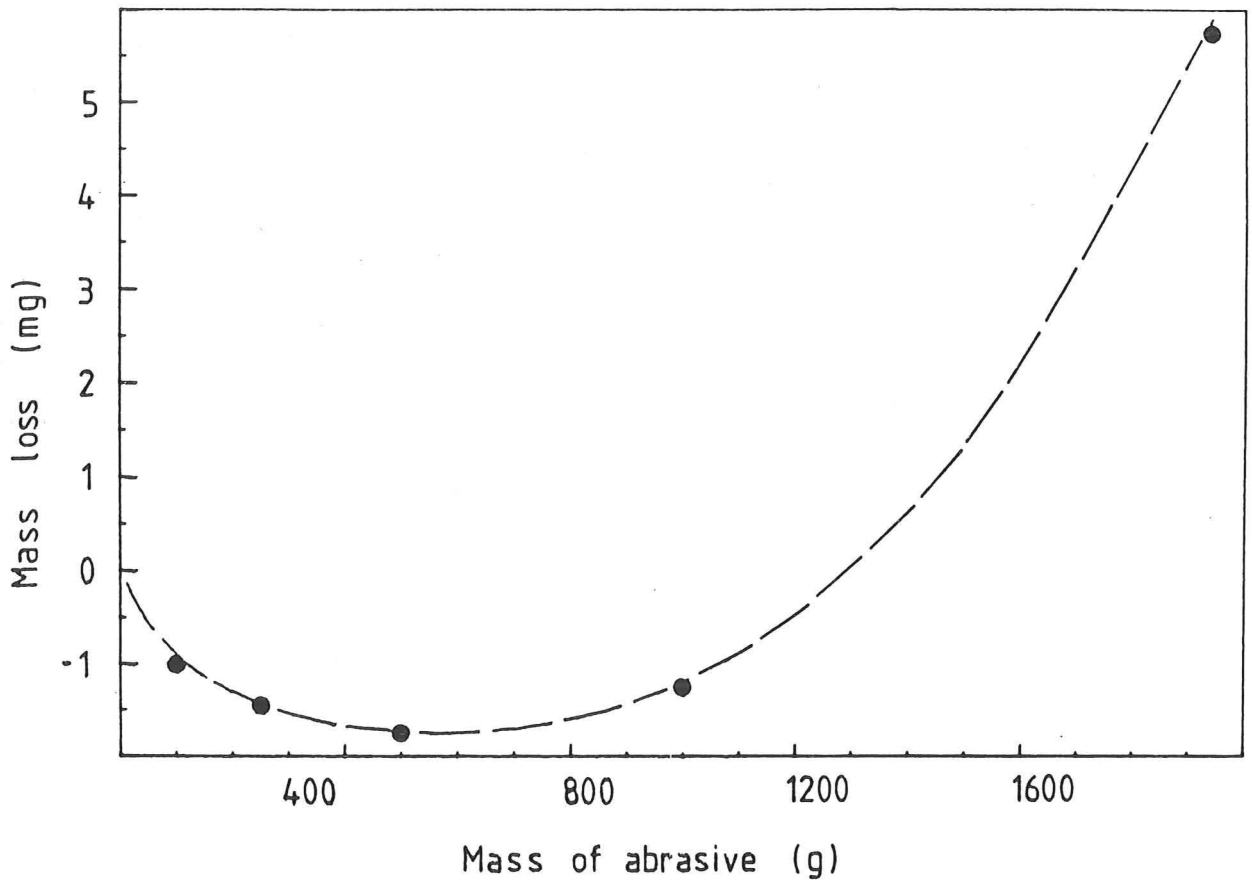

Figure 6.7 : Cumulative mass loss curve for roll-bonded material : ●, stages at which specimens were sectioned. Eroded by 600μm glass beads at approximately 60ms^{-1}.

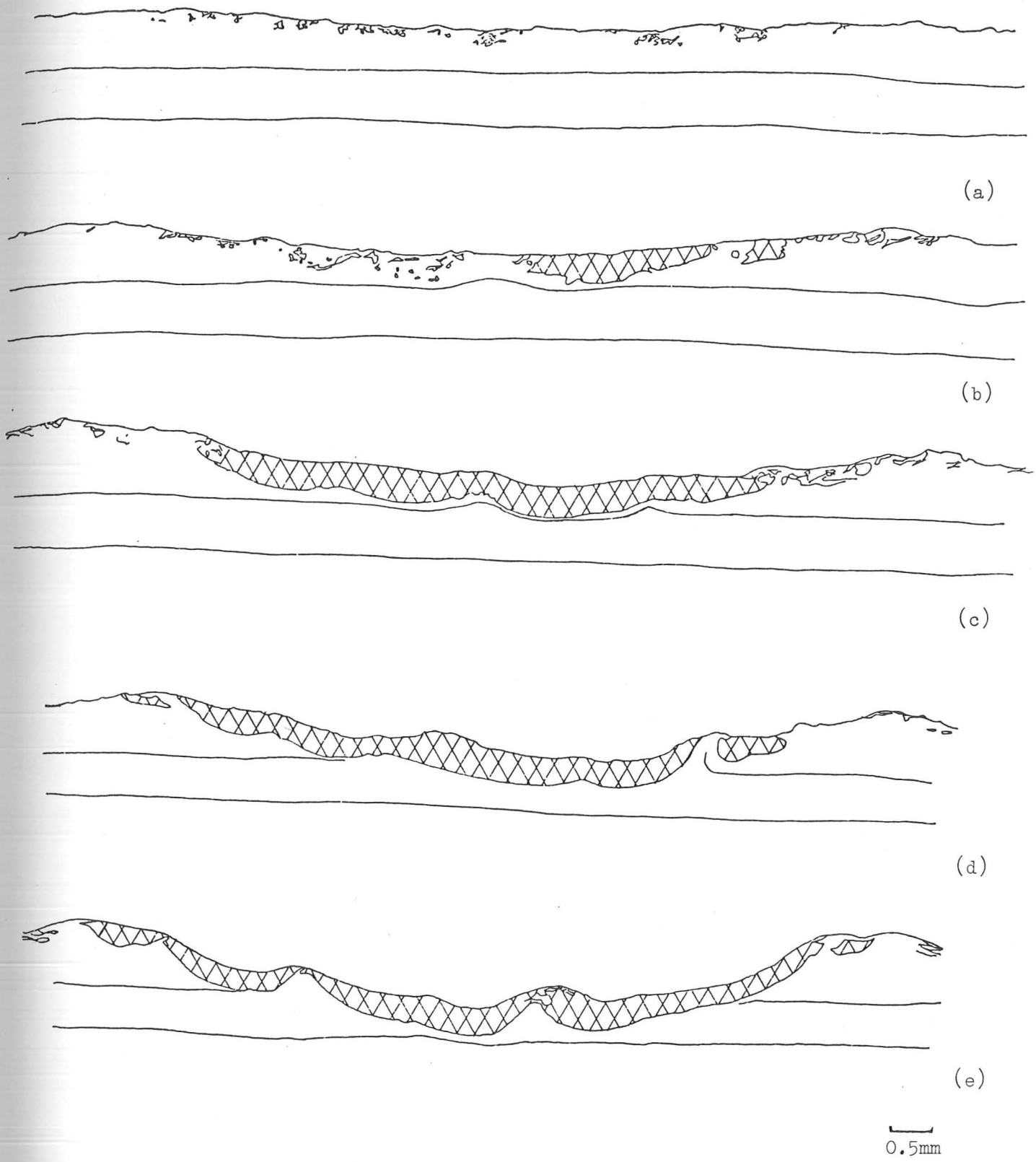

Figure 6.8: Sections of roll-bonded material eroded by 600μm glass beads.
The mass of erodent used in the tests was:
(a) 100g, (b) 250g, (c) 500g, (d) 1000g, (e) 1940g.

when it is within a certain critical distance of the boundary. (Typically not more than one quarter the depth of the disturbed layer.)

(iv) The marker layer is deflected so as to remain parallel with the boundary between the disturbed layer and the bulk.

(v) In order that the volume of metal between the two marker layers may be conserved in some regions the upper layer must be deflected upwards. This phenomenon is illustrated in Figure 6.8 (d), where the upper marker foil has ruptured beneath a surface 'hill'. Figure 6.9 shows magnified detail. In Figure 6.8 (e) there is no evidence of the marker layer beneath the left hand break in the disturbed layer, even though this is above the level of the original marker.

Figure 6.10 shows detail of another roll-bonded specimen illustrating additional features. Each marker layer has etched as two continuous lines showing the positions of the upper and lower surfaces of the foil. Beneath the centre of the surface trough, at the deepest point under the subsurface layer, the foil has become thinner, and etches as a single line. In the regions where the bulk material reaches the surface, under the 'hills', the foil shows signs of considerable thickening.

Figures 6.9 and 6.10 show details of the structure of the subsurface layer. Adjacent to the regions where the bulk material breaks through to the surface, the subsurface layer has a well developed laminar structure. Frequently, where the bulk material breaks through to the surface it can be seen to extend in thin flakes over the harder subsurface layer.

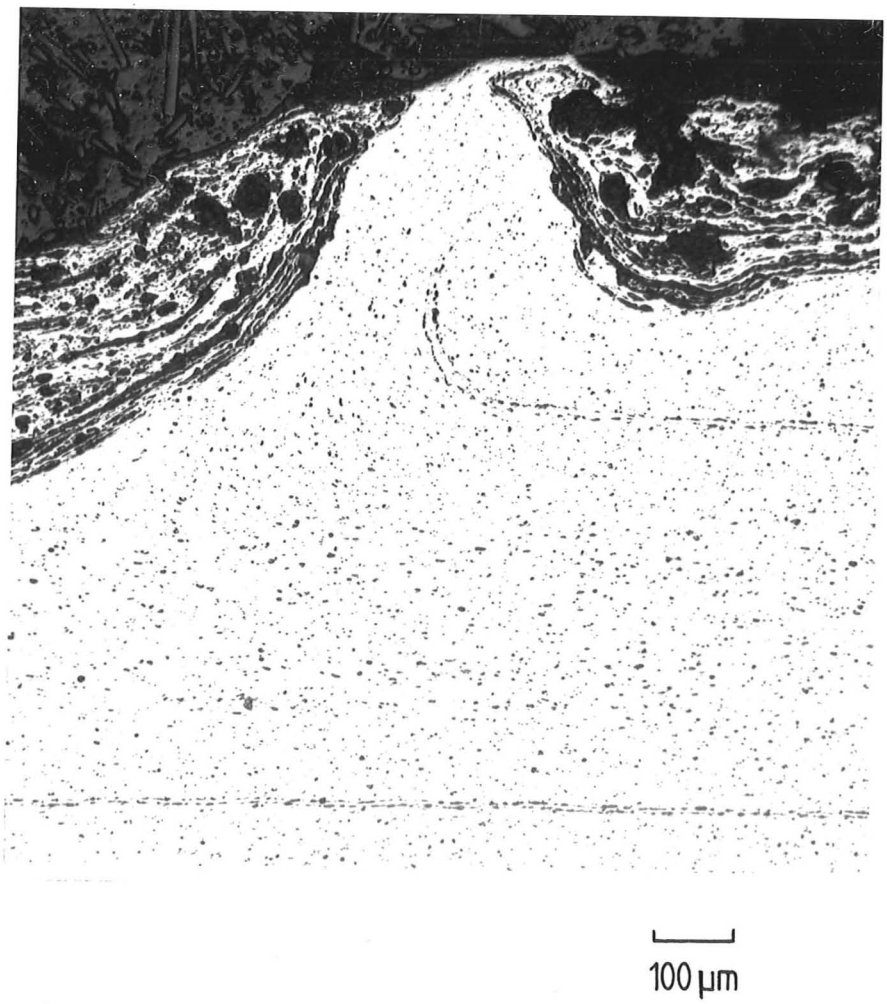

Figure 6.9 : Optical micrograph, from section of roll-bonded specimen shown in Figure 6.8 (d), giving detail of rupture in the marker foil.

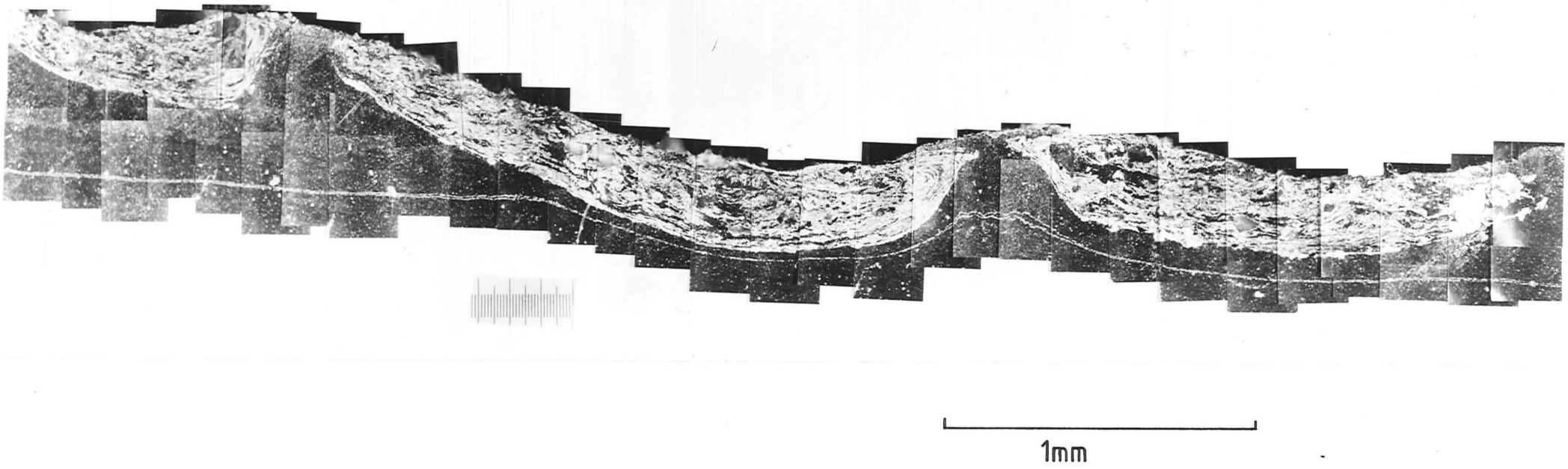

Figure 6.10 : Section of roll-bonded specimen showing distortion of marker layer. (Polarised light micrograph.)

6.3.5 Leaded glass erodent

A series of tests were conducted, using both conventional soda glass beads and leaded glass beads, to investigate the stability of the debris filled subsurface layer. These two erodent types were selected as being similar in mechanical properties, size and density, but due to differences in chemical composition easily distinguishable by energy dispersive x-ray analysis (EDAX). Figure 6.11 reproduces EDAX traces for the two glasses. It can be seen that the calcium peak is unique to the soda glass, the lead and potassium peaks unique to the leaded glass.

Three commercial purity aluminium (BS 1470) specimens were eroded under identical conditions, normal impingement, nominal 600μm erodent, particle velocity approximately 60ms^{-1}. It was estimated that under these conditions an exposure to 500g of erodent would ensure that the subsurface layer would be fully developed.

The first specimen was eroded by 500g of soda glass, the second by 500g of leaded glass and the third by 500g of soda glass followed by 500g of leaded glass. Following erosion testing the specimens were sectioned and polished and examined in the SEM. The subsurface layers were analysed by EDAX to determine which type of glass was present. The presence of leaded glass in the subsurface layer of specimen three would indicate that this layer is continually being removed and replaced, the observed stability of structure resulting from a balance between the rate of material removal and embedding of erodent fragments. The absence of leaded glass in the subsurface layer would indicate the stability of the layer, once established.

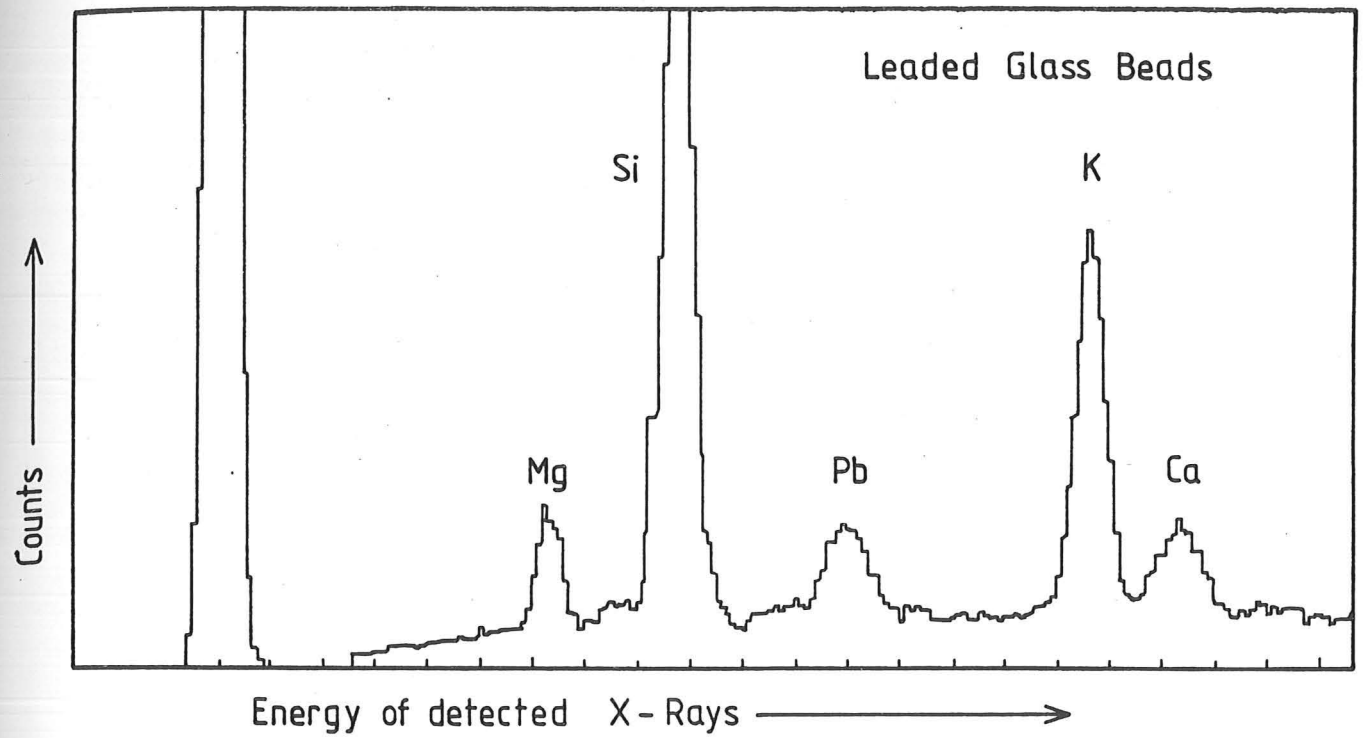

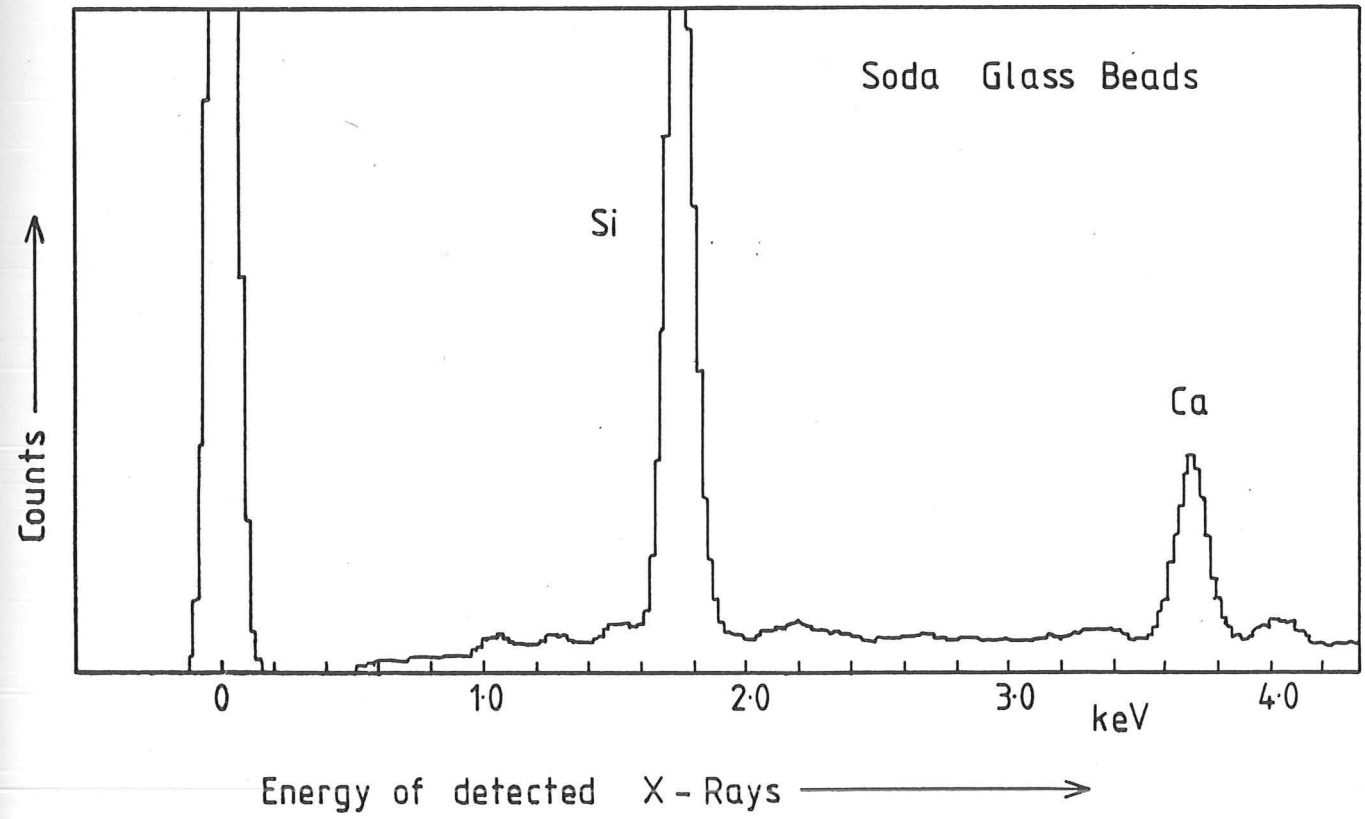

Figure 6.11 : Energy dispersive x-ray analyses of glass beads using a LINK system attached to an ISI scanning electron microscope

The experiment, as designed, was unsuccessful. No characteristic lead or potassium traces were obtained by EDAX from either specimen three, or specimen two. The concentration of the two marker elements averaged throughout the subsurface layer was below the detection level of the EDAX system. Attempts to analyse selected areas rich in glass fragments were also unsuccessful. The glass fragments, although clearly visible under optical examination, develop only very low contrast in the aluminium matrix under SEM examination. This is largely due to the fact that the atomic number of the dominant element in the glass, silicon, is very close to the atomic number of the aluminium matrix. Large differences in contrast are developed in the SEM between regions having large differences in 'effective' atomic number.

Some results were obtained, however, following detailed optical examination of the specimens. The erodent fragments in the subsurface layer of specimens eroded by soda glass were typically large, and dark coloured. The erodent fragments of leaded glass in the subsurface layer were generally smaller and lighter in colour. Figure 6.12 illustrates regions from the subsurface layer of each of the three specimens. Although this evidence is not conclusive, it indicates that some leaded glass has become embedded in the subsurface layer of specimen three. It is likely therefore that the subsurface layer is maintained by an equilibrium process of material removal and replacement. Material lost from this layer by the formation and detachment of flakes, is balanced by a continuing process of erodent fragment embedding.

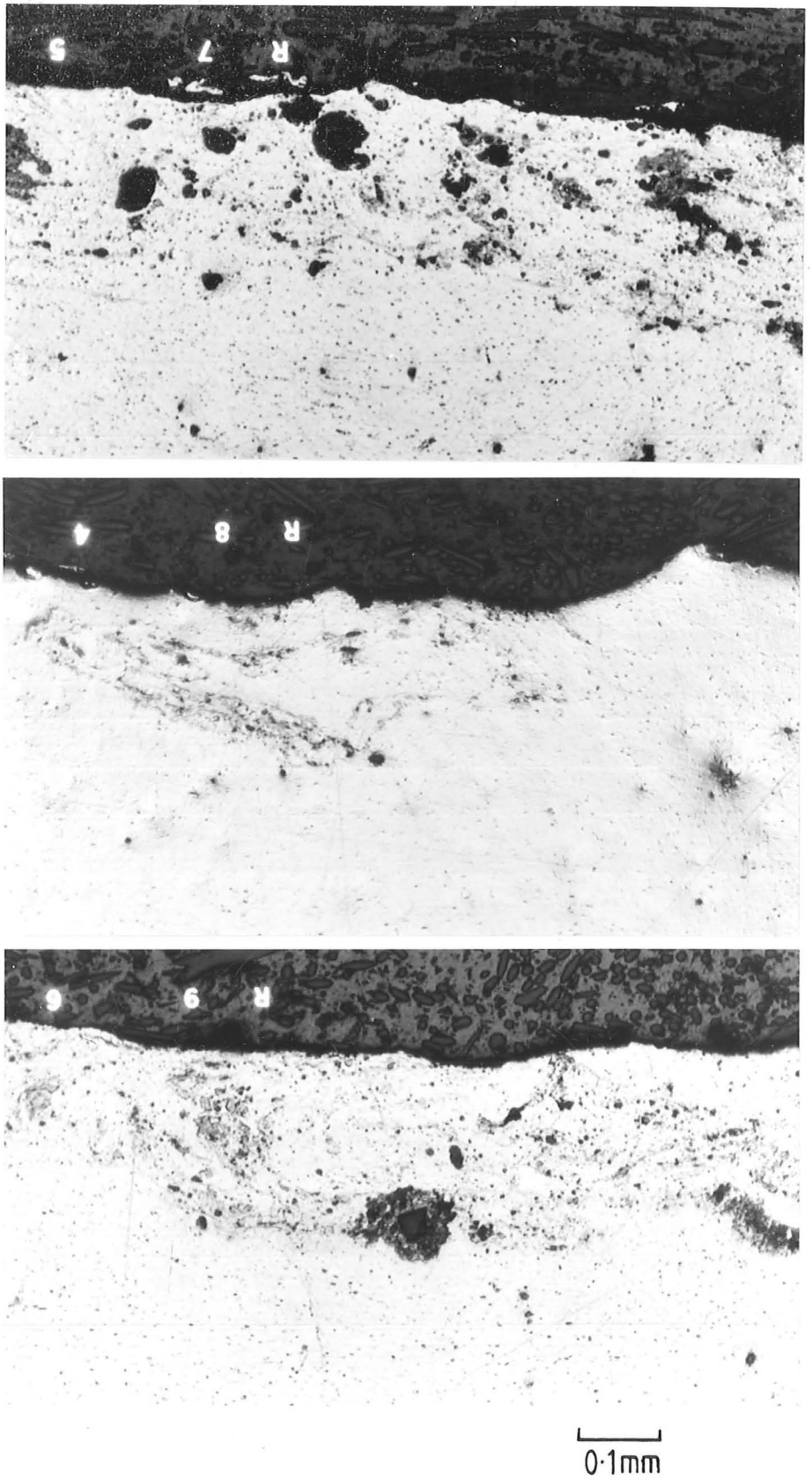

Figure 6.12 : (a) Aluminium eroded with soda glass beads, subsurface layer predominantly dark rounded particles.

(b) Aluminium eroded with leaded glass beads, subsurface layer predominantly fine grey particles.

(c) Aluminium eroded with first soda glass beads, then leaded glass beads. Note microstructure of subsurface layer is similar to (b), suggesting this layer has been renewed and contains fragments of leaded glass.

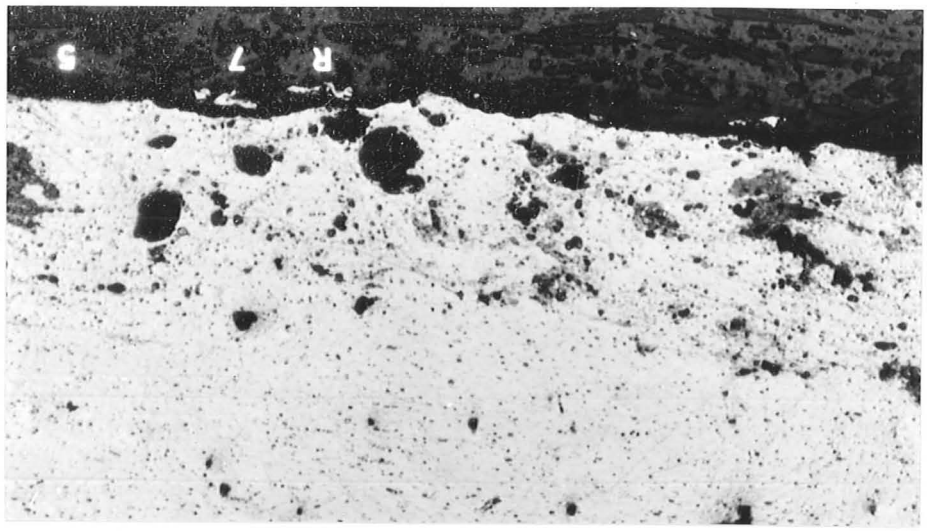

(a)

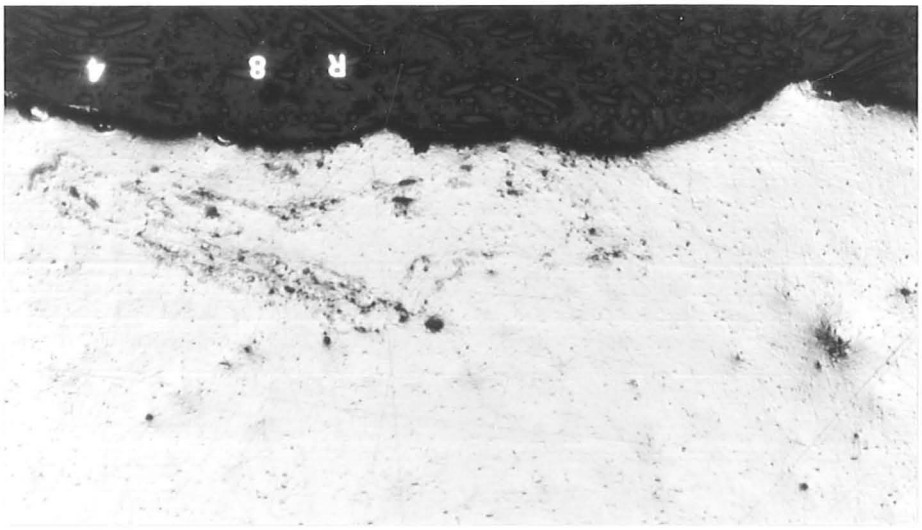

(b)

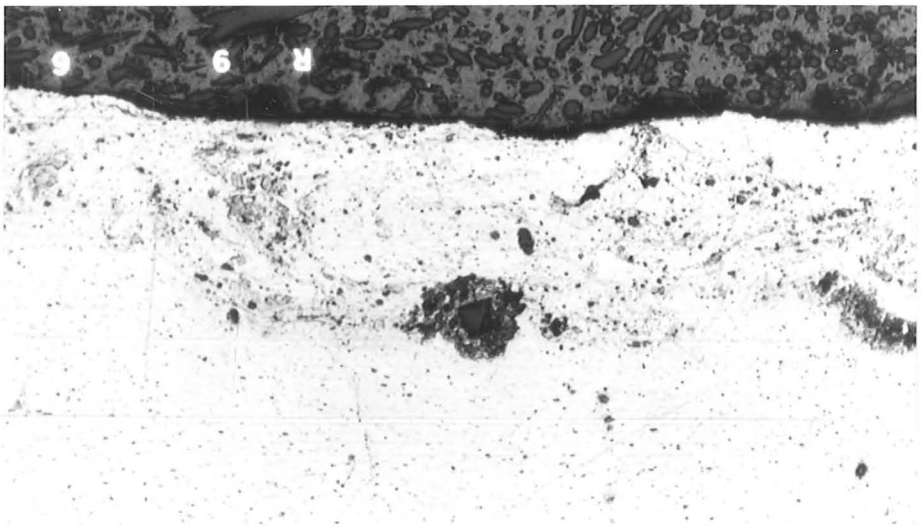

(c)

0·1mm

Figure 6.12 : (a) Aluminium eroded with soda glass beads, subsurface layer predominantly dark rounded particles.

(b) Aluminium eroded with leaded glass beads, subsurface layer predominantly fine grey particles.

(c) Aluminium eroded with first soda glass beads, then leaded glass beads. Note microstructure of subsurface layer is similar to (b), suggesting this layer has been renewed and contains fragments of leaded glass.

6.4 DISCUSSION

6.4.1 Comparison with earlier work

The results of the weight loss measurements, and of the surface examination are in good agreement with studies reported in the literature. Several previous investigators (Bellman and Levy (1981), Brown et al (1981b, d), Carter et al (1980) and Rickerby and Macmillan (1982)) have similarly concluded that the major source of erosive weight loss due to spherical particles at normal incidence involves the detachment of lamellar wear flakes.

There is, however, less agreement concerning the subsurface features. Whilst other workers have detected subsurface layers of highly disturbed material, containing embedded fragments of the eroding particles (Brown et al (1981b,d), Ives and Ruff (1979)), some investigators report the presence of a work-hardened layer free from embedded particles, (Bellman and Levy (1981), Rickerby and Macmillan (1982), Salik et al (1981a,b)).

Models have been suggested in which the impinging particles deform a thin surface layer which lies above this anvil-like work-hardened layer. It is not possible to discuss here the variety of models of this type; however, it can be observed that problems do exist in explaining the establishment and stability of the three-layered subsurface structure.

The results of Salik et al (1981b), in which 6061 aluminium eroded by normal impingement of glass beads showed no traces of embedded particles, apparently in contradiction to those above, require some comment. Salik et al stated that embedment occurs only at high impact velocities, but reported that the

particle speed was not measured. In the present study fragment embedment was observed for a range of particle velocities, from $30ms^{-1}$ to $62ms^{-1}$. Salik used extremely small (15μm) glass beads, and etched with a hydrofluoric acid etch after cross-sectioning the specimens. It is possible that such an etch might dissolve any fine glass fragments.

Two detailed mechanisms have been proposed by previous investigators for erosive wear involving the formation of a layer of highly disturbed material, containing fragments of the eroding particles. Ives and Ruff (1979) described a process where fragments from angular erodent particles were driven into the metal surface. Small fragments became buried when surface projections were deformed over them; large fragments may have fractured when impacted by impinging erodent, with the resultant fragments becoming further embedded. Ives and Ruff suggested that material which contained a high proportion of embedded fragments would be harder than the bulk material, and therefore might tend to become gradually higher than the average level of the surface. These higher regions would be expected to be weaker in shear than the surrounding metal however, and once exposed are therefore more susceptible to fracture and removal from the surface. In this way, they suggested, regions with high concentration of embedded particles will form the 'hills' of the rippled surface. This is at variance with the observations reported here for spherical particles, and also by Brown et al (1981b,d). It is also difficult to account, with this model, for the sharp boundary between the disturbed layer and the bulk. It must be concluded that, although the subsurface structures resulting from angular and spherical erodent are similar, it is not possible to explain the erosion observed in the present work with the model proposed by Ives and Ruff.

The second mechanism is suggested by Brown et al (1981b); this mechanism is further developed and extended to cover erosion by angular particles in a later paper (Brown et al (1983)). They suggested that embedding is concentrated in the valleys for two reasons. First, because the impact density is highest in the valleys as particles ricochet from the hill sides. Material is fed into the valleys by particles in glancing impact with the hill sides. This flow of material is continued across the valley floor and at its centre folds down into the subsurface layer. Flow is continued within the subsurface layer by shearing processes which cause material close to the lower boundary with the target bulk to flow upwards towards the hills. In this way, they suggested a convection-like cycle of flow is established within the disturbed subsurface layer. The shearing processes ensure that this layer is fundamentally weak and heavily cracked, resulting in material loss by flaking from the valley floor.

In the model of Brown et al the eroded surface is assumed to be considerably rougher than is observed in the present work. The hill and valley structure they suggested is much more pronounced, with slopes much steeper than those shown in Figure 6.10. The structures described in this work cannot be explained by this model. The surface slopes are low, and the impact angles vary only a little from 90^{o} (estimated from Figure 6.10 to be $90^{o} \pm 12^{o}$). No sphere impacting the specimen perpendicularly to the main plane of the surface could possibly rebound to strike the specimen again (except perhaps after collision with an incoming particle), and the glancing impacts necessary to drive the flow processes described by Brown et al will not occur. (Footnote).

(Footnote)

In addition to surface roughening, there is another effect which can cause the true angle of particle impact to differ from the angle between the nozzle and the initial surface plane of the specimen. As material is lost from the surface a depression is formed; if the nozzle of the erosion rig is small in diameter, the experiments may, in order to achieve measurable weight losses, allow the ratio of the depth of the depression to its radius to approach or even exceed unity. Rao et al (1982, 1983) showed sections of 6061-T6 aluminium alloy eroded with 20μm glass beads (velocity 60-80ms^{-1}) using an erosion tester with a 1.18mm diameter nozzle. Estimates from these sections gave the range of effective impact angles as 50^{o}-90^{o} for a nominally 'normal' impact nozzle/specimen configuration. (They reported other tests with ranges as large as 25^{o}-90^{o}). In this case the ratio of depression depth to radius is approximately 0.6. Rao showed how the surface features of the tested specimens reflect the range of true impact angles. Brown et al (1981b,d) used a 3mm diameter nozzle, and Bellman and Levy (1981) used a 4.76mm nozzle. To minimise the range of true impact angles the present work also uses a 4.76mm nozzle; the increased area of the depression results in longer incubation times and gives a more accurate measurement of specimen mass increase.

Brown et al also suggested that the higher density of impacts on the valley floor forces the pocket of embedded material down into the bulk of the target, extruding material backwards into the hills. It was suggested (Brown et al (1983)) that the ridge of material surrounding the eroded area on each specimen is similarly the result of backwards extrusion. The ridge effect was also noted in the present study (see Figure 6.3 (a) to (e)).

In their later paper (Brown et al (1983)) the role of the embedded fragments was further explored. It was suggested that the increased density of poorly conducting fragments below the eroded surface decreases the heat flow away from the impact sites. This effect, they suggested, increases the temperature of the near surface layers. Thermal softening of the valley floors then leads to increased flake formation, via a forging-extrusion process.

As discussed above the suggestion of a higher impact density on the valley floors is questionable. It is possible however that such a process does drive the extrusion which results in the establishment of ridges around the eroded area. Whilst the model of Brown et al is disputed, the backward extrusion mechanism does accord with the observations reported above. It also, as will be shown below, provides a good explanation for the origin and stability of the hill and valley structure.

6.4.2 Model for erosion by spheres at normal incidence

It is suggested that during the incubation period fragments of oxide, both from the erodent particles (if they oxidise readily) and from the metal itself, become embedded in the surface. The repeated impacts of erosive particles at random positions on the surface work-harden the surface, leading to pile-up of metal around the indentations caused by individual

particles (as observed around hardness indents in work-hardened metals). Material piled up in this way will be pressed down again by later impacts, trapping and embedding any particle fragments or oxide on the surface. Hardened both by the embedded debris, and by work-hardening of the aluminium matrix, the disturbed layer is considerably harder than the bulk material, and being heavily strained is less ductile. Continued battering of the surface by impinging particles presses this 'raft' of harder material on to the underlying bulk metal. Eventually, at points of weakness, the raft becomes indented from below by bulk material which is under compressive stress and is being forced upwards by a backward extrusion process. This flow is driven by the impact forces on the rest of the hard raft. The bulk material which is pushed upwards is extruded through a break in the raft, and then becomes smeared out by particle impact, forming a new layer on the top of the raft. A schematic diagram of the process envisaged is shown in Figure 6.13. A point at which complete penetration of the raft has occurred is seen in Figure 6.9, and points at which the raft has been indented from below, but at which complete penetration has not occurred are visible in Figure 6.8 (e). Figures 6.8 (d) and 6.8 (e) (extreme right) and 6.10 show material breaking through the raft, and being smeared out onto the surface. This continuing process of extrusion and smearing builds up the deformed layer resulting in the laminar structure, illustrated in Figures 6.4 (b), 6.6 (a) and (b) and 6.9. It is the removal of this smeared material, the surface flakes illustrated in Figure 6.2 (b), that accounts for the measured weight losses. The experiments with leaded glass beads indicate that material is also lost by failures within the disturbed layer. The continual extrusion of bulk material up to the surface replaces material lost from the disturbed layer in this manner. In every case the indentation, and corresponding thinning, of the hardened raft occurs at a hill on the surface. As shown by the deflection of the marker layers in Figure 6.8 (a)

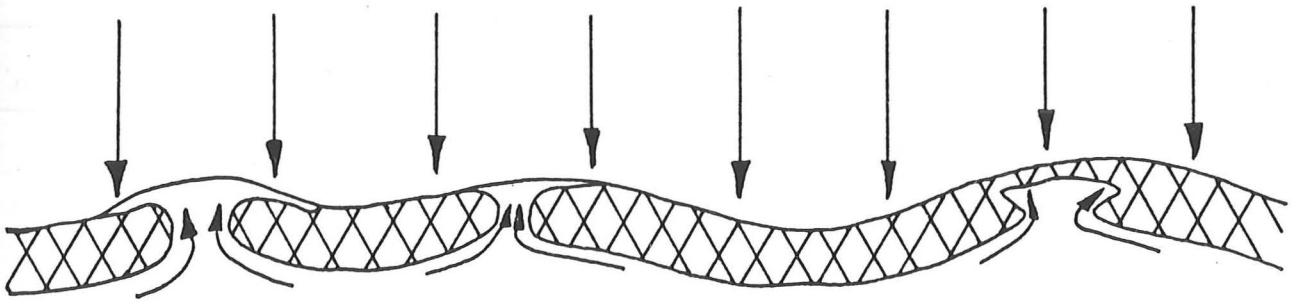

Figure 6.13 : Schematic diagram illustrating the 'backward extrusion' mechanism proposed

to (e) the flow from the bulk material into the hills is confined to the areas close to the boundary of the disturbed layer. It is suggested that slip at this boundary ensures that the disturbed layer remains clearly delineated from the bulk. Further support for the flow pattern illustrated in Figure 6.13 comes from the deflection of the bands of precipitates observed in the rolled aluminium alloy (visible in Figure 6.6 (b)).

Since the eroded material is removed as flakes from the disturbed layer, the properties of this raft of heavily deformed metal, containing embedded particles and oxide, will be as important in determining the erosion rate as the properties of the bulk metal. It is significant that in these experiments, where similar steady-state erosion rates were measured for the annealed and the precipitation hardened alloys, the hardness of the disturbed layers formed in these materials were also found to be very similar. This observation suggests a plausible explanation, at least for normal impact, for the reported insensitivity of the erosion rate of metals to their heat treatments, which was discussed in Chapter 1 (section 1.2.3 (a)).

It may be that disturbed layers formed on alloys with different heat treatments, or even on different alloys of the same base metal, all have similar mechanical properties. The design of materials with maximum erosion resistance, under these conditions, will require an understanding of how the properties of the bulk material affect the properties of the subsurface layer developed. Minimum erosive weight loss will be achieved by the rapid formation of a subsurface layer which is not only resistant to surface flake detachment, but also resistant to indentation by the backward extrusion of the material below. Further investigation in this area is needed.

While these experiments were performed with spherical particles, the mechanism proposed above could also operate to some extent with angular grit particles at normal incidence. Embedment has been observed in erosion with angular grit (Ives and Ruff (1979), Sargent et al (1980), Brown et al (1983)). Erosion rates are, however, higher than with spherical particles; metal can be removed by other mechanisms involving local plastic flow, gouging and cutting. For some materials, for example mild steel as reported in Chapter 8, the micromachining mechanisms may be the major wear mechanism when erosion is caused by angular grit.

6.5 CONCLUSIONS

Detailed observations of the surface and subsurface features of aluminium alloys eroded by glass beads at normal incidence have led to the proposal of a new mechanism for erosive weight loss. A novel technique utilising roll-bonding to place marker layers underneath the specimen surface has provided evidence of the pattern of flow of metal during erosion. Previously proposed models of the erosive wear process at normal impact have been examined and rejected in the light of these observations.

During the early stages of the erosion tests a complex subsurface structure is established. This involves the development of a layer of extremely disturbed microstructure of a laminar form, containing many embedded particles and cracks. This layer is considerably harder than the bulk material, and the continued battering of the surface by the erosive stream forces it into the softer bulk. The resultant compressive stresses force this bulk material upwards, causing it to indent the hard 'raft' of composite

material from beneath in what can be described as a backwards extrusion process. This extrusion breaks the surface at the ripple peaks (or hills), supplying material to replace that which is removed from the disturbed layer as flakes.

CHAPTER 7 : DEFORMATIONS ASSOCIATED WITH EROSION

7.1 INTRODUCTION

In this chapter consideration is given to the magnitude of the stresses and strains developed by erosion.

In section 7.2 the technique of upper bound limit analysis is used to model the back extrusion mechanism identified in the previous chapter. By assuming a plane strain process an estimate is made of the force required to cause the proposed flow of material, and energy balance methods then allow an estimate of the resulting erosion rate to be made.

It is found experimentally that initially flat metal specimens will develop a degree of curvature if one face is exposed to particle impact. The direction of this curvature results in the eroded area being deflected towards the direction of the impinging particles. Analyses are available for the elastic deformation of plates under various loading conditions.

In section 7.3 the measured curvatures of eroded disc specimens are compared with values using these analyses. In this way it is shown that the deformation of the specimens, caused by the residual surface stresses, involves stresses and strains in excess of the elastic limit.

7.2 UPPER BOUND LIMIT ANALYSIS

7.2.1 Introduction

Upper bound limit analysis is a technique which provides an estimate for the load required to cause plastic deformation in a given situation. This

estimate will be either correct, or an overestimate of the load required; a complementary, lower bound, analysis provides an underestimate. Johnson and Mellor (1973) can be consulted for details of the development of limit analysis, and provide proofs. Calladine (1969) presented a simpler introduction to the topic. A detailed review of limit analysis is presented by Avitzur (1977).

Calladine states the upper bound theorem thus :

'If an estimate of the plastic collapse load of a body is made by equating the internal rate of dissipation of energy to the rate at which external forces do work in any postulated mechanism of deformation of the body, the estimate will be either high, or correct.'

A simple illustration will serve as an introduction to the technique, as applied to plane strain deformation problems.

Figure 7.1 (a) shows a boundary between two rigid blocks of material, A and B. Material in block A is moving to the left, passing through the boundary, to emerge with a new velocity. The change in velocity and resultant distortion of the material is illustrated by a single parallelepiped of material, sketched before and after crossing the boundary XX.

Figure 7.1 (b) illustrates the relative velocities. Vector oa represents the velocity of the material at the right of XX, and is of unit length. ob represents the velocity of the material at the left of XX, and ab thus represents the velocity change on passing through XX.

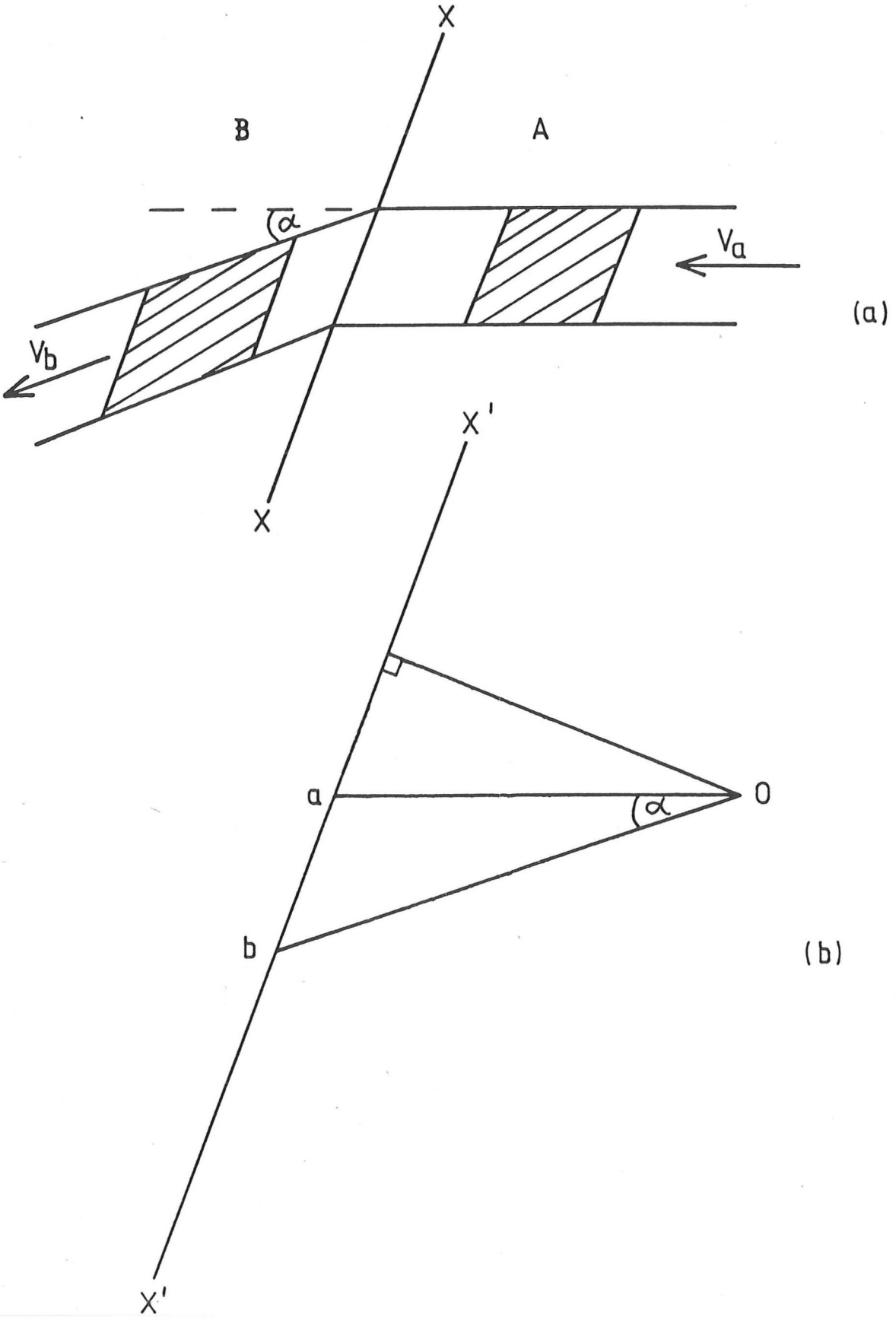

Figure 7.1 : Principles of the upper bound theorem
(a) Flow across a discontinuity
(b) Velocity diagram

It can be shown that the rate of energy dissipation per unit depth (assuming XX is the line resulting from a plane intersecting the plane of our diagram) is given by :

$$\frac{dw}{dt} = k \cdot l_{AB} \cdot v_{ab}$$

where: $\frac{dw}{dt}$ is the rate of energy dissipation per unit depth, assuming the diagram illustrates a plane strain situation.

k is the shear yield stress

l_{AB} is the length of XX, the boundary between block A and Block B.

v_{ab} is the velocity change on passing through XX, i.e. $\underline{ab}$

In order to extend this method to a real problem, for example, indentation by a punch, a system of shear discontinuities such as XX is postulated. The rate at which work is done by material crossing each discontinuity is calculated. The results are summed and equated to the rate at which work is done by the external forces, enabling an estimate of the external force to be obtained.

7.2.2 Application of upper bound limit analysis to a model of the mechanism of erosion

In Chapter 6 a model for the erosion of ductile materials by solid spherical particle impingement was described. This model involves the back-extrusion of ductile material through breaks in a hard surface raft.

Figure 7.2 (a) shows the mechanism in a simplified form; here a rigid raft is pressed by the force of the impinging particles into the softer bulk material. In order to apply the upper bound limit analysis we must

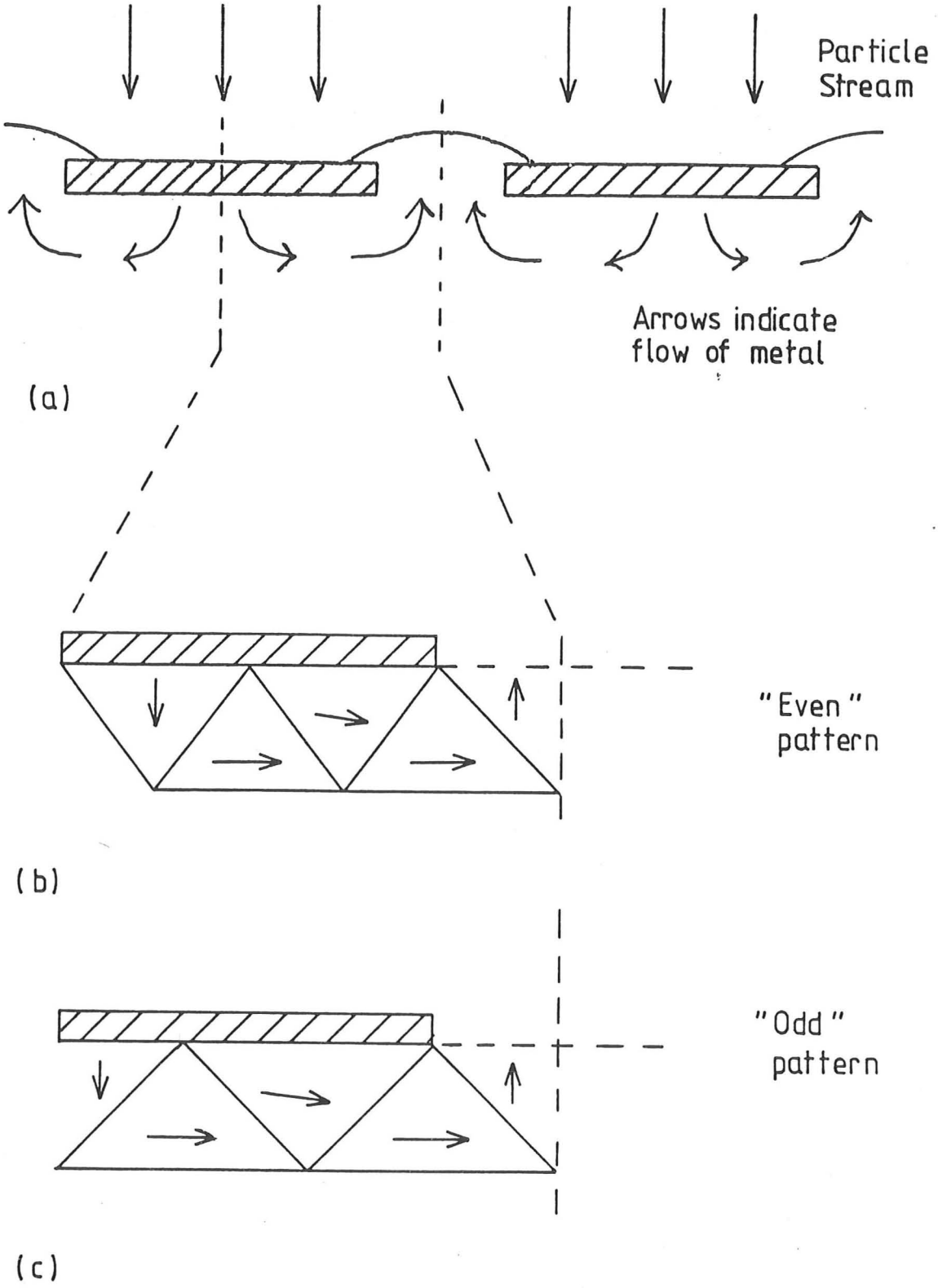

Figure 7.2 : Upper bound theorem applied to back extrusion process

postulate a pattern of discontinuities, as described above. Figure 7.2 (b) and (c) show two possible types of pattern; that shown in Figure 7.2 (b) has an integral number of triangular blocks under the raft and this group of patterns will be referred to as 'even'. The alternative, Figure 7.2 (c), with an extra half triangular block will be referred to as 'odd'.

Figure 7.3 shows a simple 'even' pattern, with two triangular blocks (n=2, where n is the number of whole triangular blocks in contact with the raft). This diagram is labelled to show the notation adopted; the velocity diagram (or 'hodograph') is also given.

In considering the movement of blocks in contact with the raft relative to the raft, it is possible to include a 'friction' term to describe the resistance to slip across this interface.

The general expressions obtained from consideration of these diagrams are:

for 'even' series

$$\frac{PW}{k} = 2nl_{0A}V_{0a} + V_{0bi}\left(n\, l_{0Bf} + \frac{n(n-1)}{2}\, l_{0Bi}\right) + l_{Bfc}\, V_{bfc} + \left[nWV_{pa}\right]$$

for 'odd' series

$$\frac{PW}{k} = (2n-1)\, l_{AiBi}\, V_{aibi} + V_{0bi}\,(l_{0Bf}\cdot n + (n-1)(W+w)) + V_{bfc}\, l_{Bfc} + \left[\frac{(n-1).2n}{(2n-1)} \cdot W \cdot V_{0bi}\right]$$

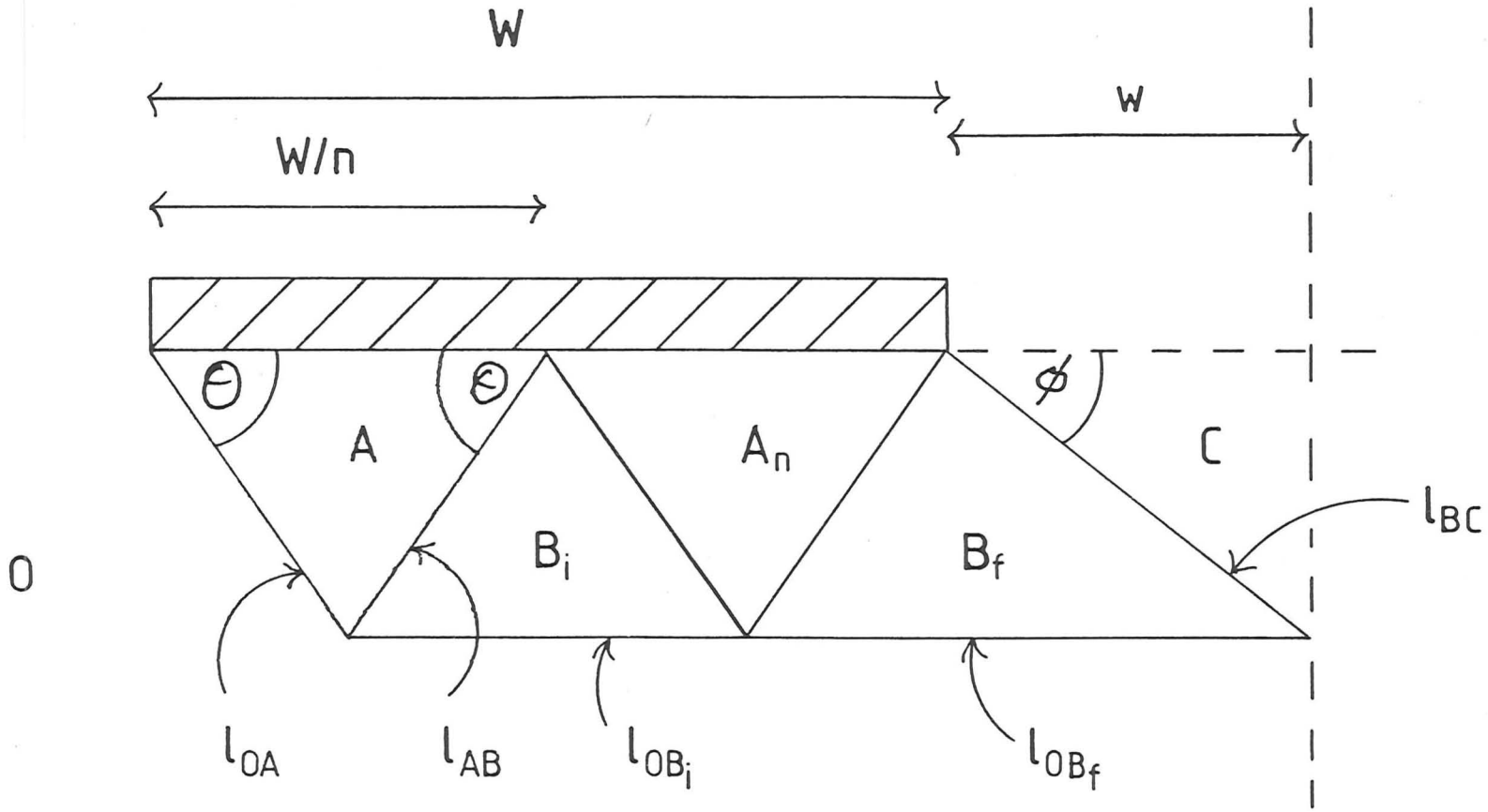

Figure 7.3(a) : Nomenclature used in analysis

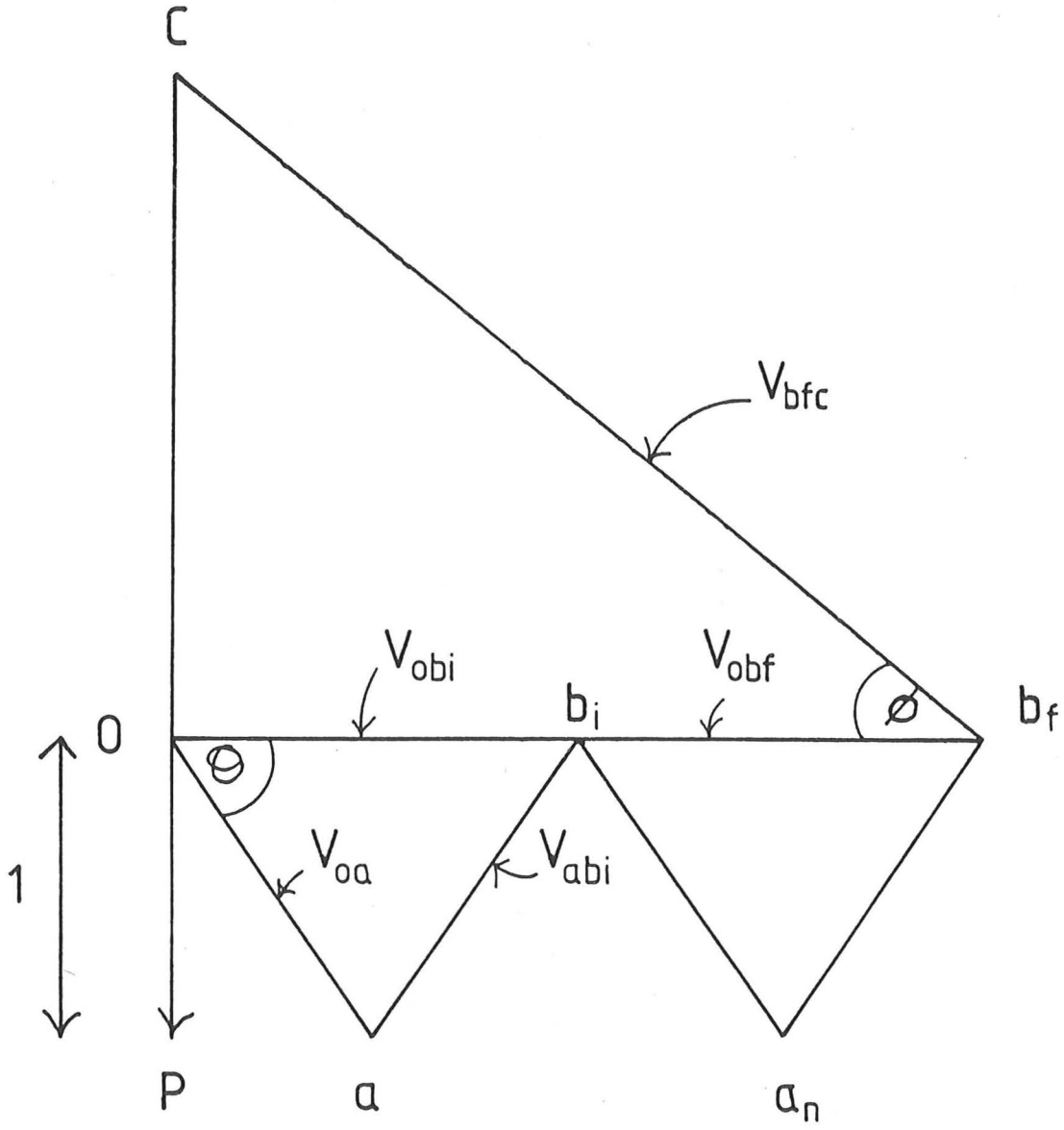

Figure 7.3(b) : Typical velocity diagram

These expressions follow the notation used in Figure 7.2. P is the pressure which must be applied to the hard raft in order to cause yielding of the underlying material. The final term in each expression ([....]) represents the interfacial friction acting along the under surface of the raft.

Simple geometry enables these expressions to be re-written in terms of the two angles θ and ϕ, and the ratio R(R = w/W). For the 'even' series :

$$\frac{P}{2k} = 0.5 \left(\frac{1}{\text{Sin } \theta \cos \theta} + \frac{n}{\tan\theta}(2R + 1) + \frac{2nR}{\cos^2\phi\tan\theta} + \frac{n}{\tan\theta}\right)$$

and $$\phi = \tan^{-1} (\tan \theta/2nR)$$

For the 'odd' series :

$$\frac{P}{2k} = 0.5 \left(\frac{1}{\sin\theta\cos\theta} + \frac{1}{\tan\theta}\left(\frac{(2n^2 - 2n + 1)}{(2n - 1)} + R(2n-1)\right) + \frac{(2n - 1)R}{\cos^2\phi\tan\theta} + \frac{(n-1)(2nR)}{(2n-1)\tan\theta}\right)$$

and $$\phi = \tan^{-1} (\tan \theta/R(2n-1))$$

As before, the last term in each equation for P/2k represents the contribution required to overcome the friction between the lower surface of the raft and the bulk material. There are obvious similarities between the expressions above; the differences only reflect the arbitrary classification into even and odd series.

Analytical methods could not be used to minimise these functions, and so the values of P/2k were evaluated numerically with a Commodore PET microcomputer. The procedure was to assign values to two of the three variables, for example, n and R, and to minimise the function by varying the third, θ, over

the range 0 to 90^{o}. The minimum value of P/2k was recorded, and then the value of n was increased, and the procedure repeated. The value n was an integer in the range 1 to 10. Once minimum values had been recorded for P/2k for each value of n, the value of R was increased and the complete procedure repeated. Values of R were selected in the ranges 0.1 to 1 in steps of 0.1, and 1 to 10 in steps of 1.

Figure 7.4 presents the results of this analysis. For each value of R, the minimum value of P/2k is plotted. (NB the abscissa scale is in two linear series 0.1 to 1 and 1 to 10). From this analysis the minimum value of P/2k is 2.828, occurring when R = 0.5, $\theta = 55^{o}$ and n = 1 in the 'even' series (neglecting the interfacial friction between the raft and the substrate). The same minimum value is found for the 'odd' series, and occurs when R = 1.0, $\theta = 55^{o}$ and n = 1. The friction term equals zero when n = 1, since there is no sliding across the lower surface of the raft.

If the Tresca yield criterion is applied to this result, the pressure required to drive the back extrusion process is, therefore, estimated at 2.828 times the uniaxial yield stress. This result can be compared with the result given by Johnson and Mellor (1973) for indentation by a flat frictionless punch (computed by the upper bound method); they found $P/2k = 2\sqrt{2}$ (= 2.828).

Tabor (1951) analysed the same indentation case, using slip-line considerations; he found $P/2k = (1 + \pi/2)$ (= 2.571). Thus it can be seen that by assuming the erodent particles impinge on a hard, rigid raft the analysis approximates the back extrusion process to that of simple indentation by a flat punch.

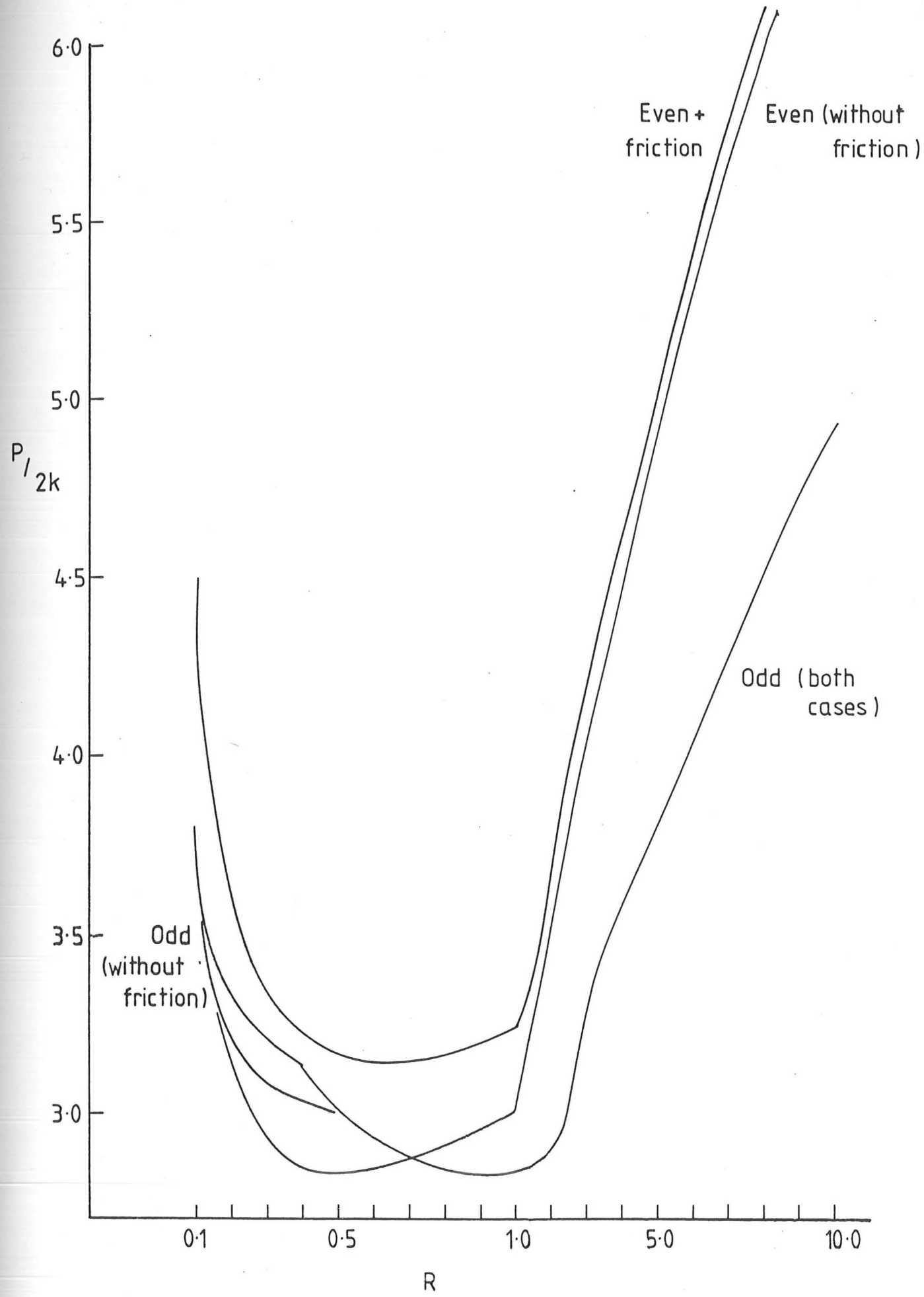

Figure 7.4 : Results of upper bound analysis

Fig. 7.4

This plot illustrates that in each case, both odd and even, a minimum value of P/2k can be identified.For each value of θ and n a minimum value was identified. This is plotted against the R value.

7.2.3 Estimation of the erosion rate

The method of energy balance can be applied to estimate the resultant erosion rate, using the estimate of the pressure required to drive the proposed erosion mechanism obtained in the previous section.

In Chapter 6 the observation that the thickness of the hard raft remains constant during steady state erosion was reported. It may, therefore, be assumed that the rate determining step for the removal of material from the surface is that of the delivery of material to the surface. The energy balance method can be used to determine the volume of material extruded by the impact, on the hard surface raft, of a single particle. The result of this calculation can then be used to obtain an expression for the dimensionless erosion rate (mass removed per unit mass erodent).

The kinetic energy (KE) of the impacting particle is given by :

$$KE = \tfrac{1}{2} mv^2$$

m = mass of particle

v = velocity of particle

The work done in extrusion is:

$$\text{Work} = PV$$

P = extrusion pressure

V = volume extruded

Equating available energy with work done :

$$V = \frac{1}{2}\frac{mv^2}{P}$$

Hence mass displaced $= \frac{mv^2}{2P} \cdot \rho_t$

ρ_t = density of the target material

The erosion (E) is therefore given by :

$$E = \frac{v^2}{2P}\rho_t$$

Substituting for P, $E = \frac{v^2 \rho_t}{2(2.828\sigma_y)}$

σ_y = uniaxial yield stress

This equation may be tested by referring to the example illustrated in Figure 6.7 (Chapter 6).

The uniaxial yield stress for the roll-bonded material was obtained by means of a standard tensile test. Strips of the roll-bonded material (as used in the erosion tests) approximately 1.5mm thick, 13mm wide with a 35mm gauge length were tested in an Instron testing machine. The crosshead speed was 1mm per minute, and the yield stress measured from a load/extension curve. The uniaxial yield stress measured this way was 105.5 MPa.

The particle speed in the erosion test was measured by the double disc method (see Chapter 5 section 5.3.1 (c)) as $57.5 ms^{-1}$. The density of commercial purity aluminium is 2.70×10^3 kgm^{-3} (Smithells (1976)).

The value of E obtained by substituting these values into the equation above is 1.50×10^{-2}. For comparison, the value of E measured experimentally was 1.15×10^{-5}.

7.2.4 Discussion

As a direct consequence of the energy balance approach used in this analysis (and in similar treatments by Finnie (1960) and Bitter (1963a,b)), it is predicted that erosion should be proportional to the square of the particle velocity. As discussed in Chapter 1, for ductile materials a velocity exponent of 2.4 is most commonly reported in the literature.

More significant, however, is the discrepancy of some three orders of magnitude between the predicted value, and the measured value of erosion rate. Finnie (1960) similarly found that only a small proportion of the energy delivered to the target surface by the impinging particle was used to remove material by the machining process he envisaged. He introduced a factor to allow for the considerable proportion (perhaps 90 percent) of particles which do not act in the idealised manner.

Rabinowicz (1979) derives an expression for erosion (volume removed per unit volume of abrasive) from equations describing abrasive wear. His analysis is vague in several areas, notably in his consideration of the dependence of erosion on angle of impact, which he incorporates simply by a factor β. This factor is assigned a value of one or 0.5, over three ranges of impact angle. Other parameters, predicted to be significant by his abrasive wear approach, are grouped together and described by the wear coefficient k_e. His equation:

$$\frac{Vr}{Va} = \frac{k_e \rho_a v^2 \beta}{gp}$$

Vr = volume removed

Va = volume of abrasive

k_e = wear coefficient

ρ_a = density of abrasive

β = constant, dependent on impact angle

g = gravitational constant (for dimensional consistency)

v = velocity of abrasive

p = penetration hardness of the target material

This equation is clearly similar to the equation derived above to describe normal impingement erosion :

$$E = \frac{v^2 \rho_t}{2(2.828\, \sigma_y)}$$

The significance of Rabinowicz's work to the present study, is that he collates the results of a number of workers and calculates values of his wear coefficient. These values lie in a range 1.2×10^{-3} to 160×10^{-3}, and, therefore, compare well with the overestimate of three orders of magnitude found in the present work.

It can be concluded from the work reported in the literature, and from this study, that simple energy balance methods result in both incorrect values of the velocity exponent and in very large overestimates of erosion. Given the weight of experimental evidence for the proposed mechanism, an explanation is, therefore, required for the inefficiency of the erosion process in practice. The upper bound analysis has shown clearly that sufficient energy is transferred to the target surface to drive the back extrusion process. The simple model assumed in the upper bound

Vr = volume removed

Va = volume of abrasive

k_e = wear coefficient

ρ_a = density of abrasive

β = constant, dependent on impact angle

g = gravitational constant (for dimensional consistency)

v = velocity of abrasive

p = penetration hardness of the target material

This equation is clearly similar to the equation derived above to describe normal impingement erosion :

$$E = \frac{v^2 \rho_t}{2(2.828\,\sigma_y)}$$

The significance of Rabinowicz's work to the present study, is that he collates the results of a number of workers and calculates values of his wear coefficient. These values lie in a range 1.2×10^{-3} to 160×10^{-3}, and, therefore, compare well with the overestimate of three orders of magnitude found in the present work.

It can be concluded from the work reported in the literature, and from this study, that simple energy balance methods result in both incorrect values of the velocity exponent and in very large overestimates of erosion. Given the weight of experimental evidence for the proposed mechanism, an explanation is, therefore, required for the inefficiency of the erosion process in practice. The upper bound analysis has shown clearly that sufficient energy is transferred to the target surface to drive the back extrusion process. The simple model assumed in the upper bound

analysis deviates from the observed erosion mechanism in certain areas, consideration of which may explain the overestimate of erosion rate.

First, while there is good evidence that the raft is significantly harder than the bulk material, the assumption that it is perfectly rigid (as in the analysis) is not well substantiated by the experimental evidence. There is evidence that the raft itself is deformed by the battering of the incoming particles. The energy dissipated in the plastic deformation of the hard raft itself will not be available for the back extrusion process.

Second, the simple model considered for the upper bound analysis considers only the particle impacts on the hard raft. This is obviously an over-simplification since the particles arrive in a uniform flux across the target surface. The analysis gave a minimum value for the extrusion pressure when the ratio of the width of the break in the raft to the width of the raft (R) was equal to 1.0 for the odd series, and equal to 0.5 for the even series.

The sections examined are random diameters of the circular area of damage. As a consequence it is not possible to make accurate measurements of the value of R observed experimentally. The surface examinations and sub-surface features revealed by sectioning are, however, consistent with R values in this range. The closer that R approaches unity, the more the back extrusion process will be opposed. In this way, impacts on the softer material which breaks to the surface will result in less energy being available to do the work of back extrusion. Such impacts will result in the smearing process which produces the surface flakes and builds up the hard subsurface raft.

A final fault of the model is the assumption of plane strain. Plane strain calculations have been found to be accurate in the analysis of many metal working processes; it is unlikely that the errors introduced by the adoption of this method will be as large as those discussed above.

7.3 BENDING OF SPECIMENS

7.3.1 Introduction

The impingement of rounded particles against a metal surface can result in the establishment of residual surface stresses. Such residual compressive stresses can considerably increase the fatigue life of components subjected to cyclic stress. The technique of shot peening, in which steel or cast iron shot or glass beads (0.1 to 2mm in size) are projected against metal surfaces, is successfully used to improve fatigue resistance. If enough residual stress is induced in a surface by peening, and the workpiece is sufficiently thin, appreciable bending will occur. This process, known as peen-forming, is utilised in the shaping of sheet for aircraft components. Details of both aspects of peening may be found in the conference proceedings edited by Niku-Lari (1982).

In the course of erosion testing it was noted that under certain conditions significant bending of the eroded specimens did occur.

Alderson and Tuitt (1974) reported similar observations of specimen bending during erosion testing. They found that erosion by low velocity particles resulted in the material in the eroded area rising; they termed this behaviour 'hump' formation. At higher velocities a depression was formed in

the target - termed a 'hollow'. They found that humps or hollows are formed when eroding steel or titanium sheet, and also a pure aluminium clad aluminium alloy (BSL 72).

7.3.2 Experimental procedure

Commercial purity aluminium strip (British Standard BS 1470) approximately 2.5mm thick, was rolled to achieve the following thicknesses : 0.90mm, 1.11mm, 1.39mm, 1.78mm and 2.255mm. Discs 22.35mm in diameter were punched out of the rolled strip, and then annealed at $400^{o}C$ for 12 h. The hardness of each disc was measured, to ensure that the anneal had completely relieved the residual stresses induced by the rolling; all the discs had hardnesses in the range 35.5 ± 0.3 $kgfmm^{-2}$ (Vickers hardness, using a 5kg load). The yield stress was measured, using a conventional tensile test procedure, to be 134 ± 2MPa (details of the tensile test are given in section 7.2.3 above).

Each disc was then eroded with a 500g charge of 600μm glass beads, at a velocity of approximately $60ms^{-1}$. Earlier experiments (reported in Chapter 6) had indicated that under these conditions the subsurface structure would be fully developed.

In order to ensure that the damaged area of the specimens remained concentric with the disc a jig was inserted into the specimen holder of the erosion tester. This was in the form of a dummy specimen on which was attached an aluminium plate (2.5mm thick). In the centre of the aluminium plate was a hole approximately 22.4mm in diameter, in which the test specimen was placed. All erosion testing was conducted at normal impingement, i.e. the aluminium plate/dummy specimen was set at 90^{o} to the nozzle of the tester.

After the erosion testing the deflections of each specimen were measured using a travelling microscope. Using this technique the deflection at the centre could be measured without difficulty to within 0.1mm. The thinnest specimens (i.e. 1.11 and 0.90mm thick) failed after only 250g of erodent had been discharged, and the tests were then abandoned.

Figure 7.5(a) shows the eroded discs, under oblique illumination. The increase in curvature with decreasing specimen thickness can be clearly seen. Figure 7.5(b) shows diametral sections through the specimens, after mounting and polishing.

7.3.3 The stresses developed during erosion

In order to apply simple analytical techniques in an investigation of the stresses developed by erosion, a number of assumptions must be made. Examination of the sections illustrated in Figure 7.5(b), together with similar observations reported in the previous chapter, indicates that at least three distinct layers exist beneath the eroded surface. Directly under the surface is a layer of highly disturbed material containing embedded debris. Beneath this is a layer of material which is back extruded during the erosion process. Experiments reported in the previous chapter indicate that bulk flow of material occurs within a region approximately one quarter the thickness of the embedded layer. Measurements of the subsurface features of the eroded aluminium discs indicate that in each case the subsurface layer of highly disturbed material containing embedded debris is approximately 0.2mm thick. Thus it may be estimated that the total depth of the first two subsurface layers is approximately 0.25mm. The remaining layer comprises the remaining bulk material. Figure 7.6 illustrates schematically the three layers.

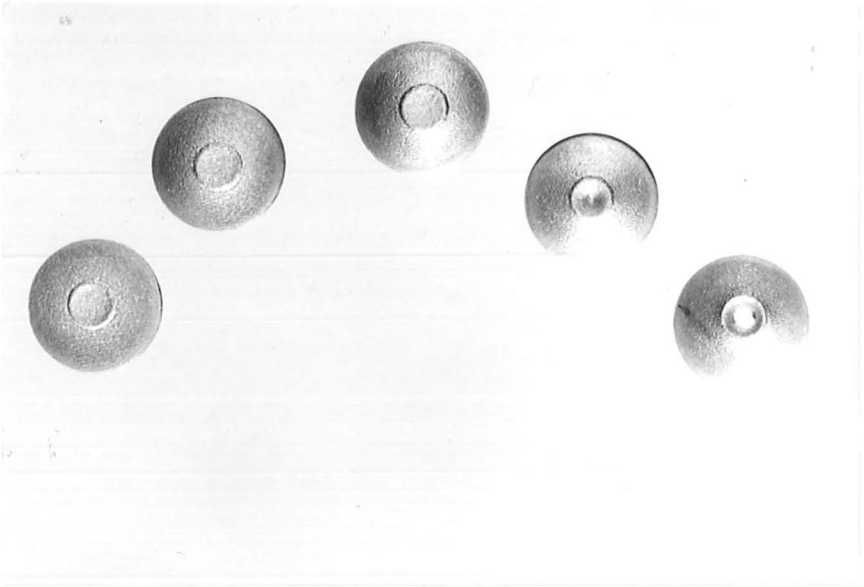

Figure 7.5 (a) : Aluminium disc specimens after erosion with 600μm glass beads (diameter of discs 22.35mm). Specimens are arranged in order of decreasing thickness

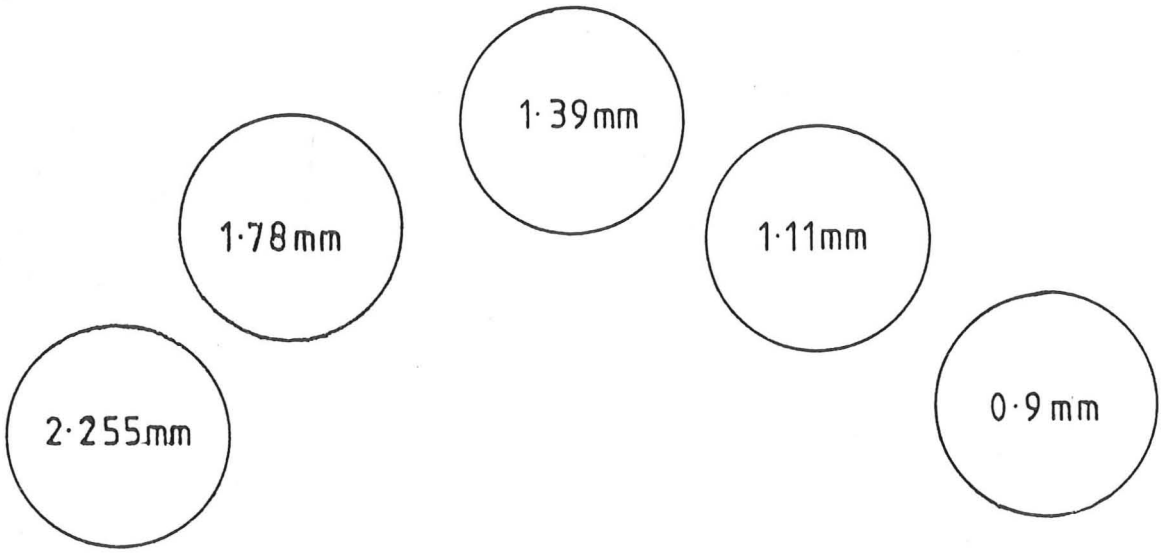

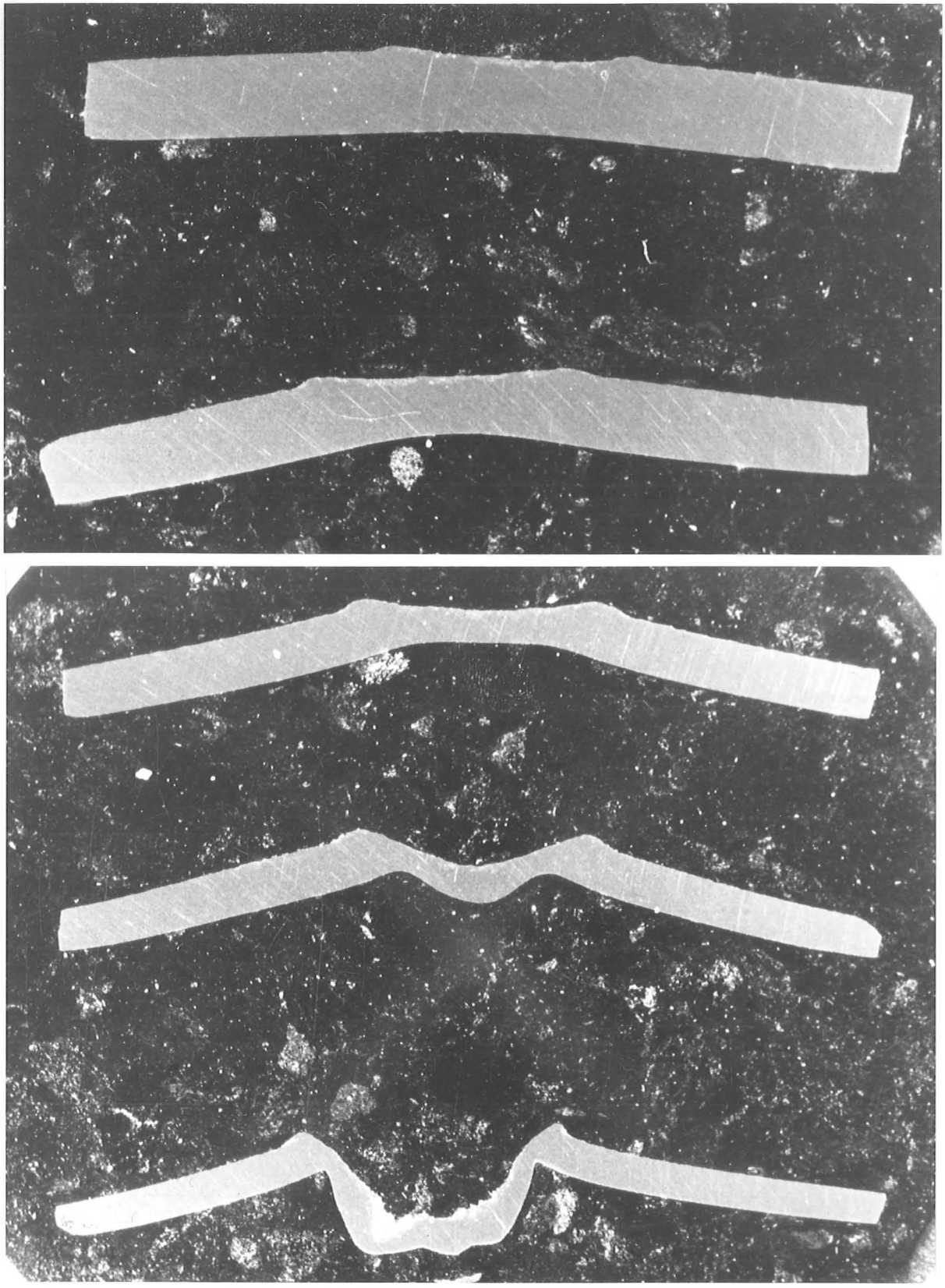

Figure 7.5 (b) : Sections of eroded discs

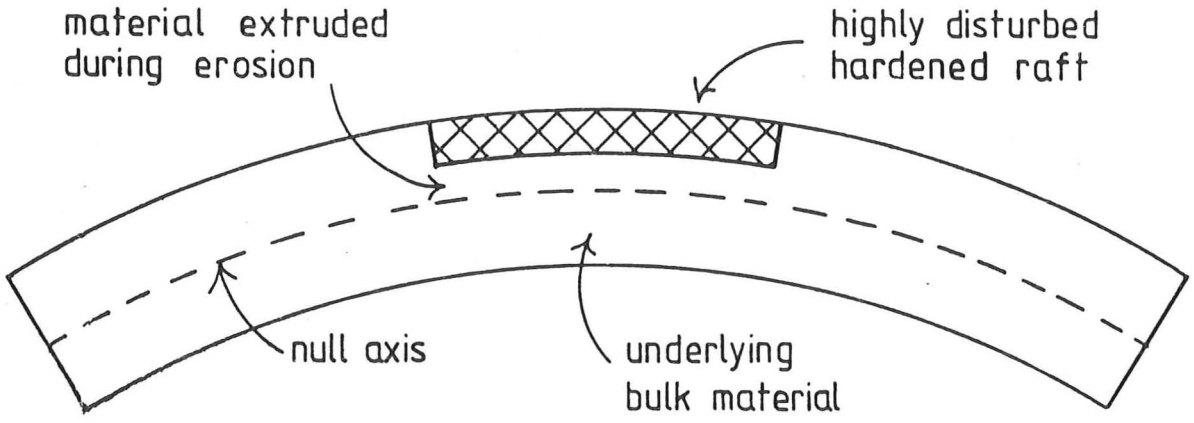

Figure 7.6 : Subsurface regions of eroded specimens
(schematic - not to scale)

A thorough analysis of the stresses within an eroded specimen would involve consideration of residual compressive stresses (resulting in the observed curvature), plastic deformation of material during extrusion, and elastic deformation of the remaining bulk material. A complete analysis of the plastic deformation of a disc under the action of residual compressive stresses is beyond the scope of the present study. Similar studies have been reported in the literature describing experiments in peen-forming and shot peening (Niku-Lari (1982)). These studies concluded that it was not possible to estimate the residual stresses directly from measured deformations; semi-empirical equations are produced requiring the determination of material coefficients by experimentation.

Analyses are available for the elastic bending of thin plates and shells (Timoshenko and Woinowsky-Krieger (1959)). The following assumptions are made, in order to use elastic bending theory, to estimate the stresses developed during erosion. First, it is assumed that the bulk material (that lying under the dotted line in Figure 7.6) suffers only elastic deformation. This deformation results from the residual stresses which are confined to the uppermost two layers. Second, it is assumed that the disc specimen is bent to a spherical surface. The radius of curvature of this surface can be determined by a measurement of the deflection of the centre of the specimen. The analysis will assume that the deflection of the disc results from pure bending (defined below).

The following analysis is taken from Timoshenko and Woinowsky-Krieger (1959), who made the initial assumptions:

(a) There is no deformation in the middle plane of the plate. This plane remains neutral during bending.

(b) Points of the plate lying initially on a normal-to-the-middle plane of the plate remain on the normal-to-the-middle surface of the plate after bending.

(c) The axial stresses normal to the plane of the plate are negligible.

The following notation will be used:

x, y, z	Rectangular coordinates (the xy plane is the plane of the plate)
r_x, r_y	Radii of curvature of the middle surface of the plate in xz and yz planes respectively.
σ_x, σ_y	Axial stress, parallel to x and y axes respectively.
ν	Poissons ratio
Mx, My	Bending moments per unit length of sections of a plate perpendicular to x and y axes respectively.
w	displacement, parallel to z axis, of the centre of the plate.
h	thickness of the plate
D	flexural rigidity of the plate
E	modulus of elasticity

In the case of pure bending of a prismatic bar it is assumed that cross sections of the bar remain plane during bending, and rotate only with respect to their neutral axes so as to be always normal to the deflection curve. Pure bending of plates requires the combination of such bending in two perpendicular directions. This will result in the middle surface being coincident with the neutral surface of the plate, a condition which is satisfied only if the middle surface of the bent plate is a 'developable' surface. If the middle surface undergoes some stretching during bending,

the plate is bent to a 'non developable' surface. The theory of pure bending can be applied in the instance of a disc bent to form a spherical cap provided that the thickness of the disc is small in comparison with the radius of curvature.

Figure 7.7 illustrates the simple case of the pure bending of a rectangular plate. In the particular case where $M_x = M_y = M$, for a plate of any shape, the bending moments are uniformly distributed along the entire boundary and the twisting moments vanish. The radii of curvature can be related to the bending moment as follows:

$$\frac{1}{r_x} = \frac{1}{r_y} = \frac{M}{D(1+\nu)}$$

It can be seen that in this special case the plate is bent to a spherical surface. The maximum normal stress acting on the xz or yz planes occurs at the surface of the plate (i.e. where z = h/2) and is given by the relationship:

$$(\sigma_x)_{max} = (\sigma_y)_{max} = \frac{6M}{h^2}$$

Finally the value of the flexural rigidity is given by:

$$D = \frac{Eh^3}{12\,(1-\nu^2)}$$

The radius of curvature of a spherical cap can be obtained by simple geometry, and is calculated from the central deflection and chord length 2a (a $\simeq$ radius of disc)

$$r \simeq a^2/2w$$

the plate is bent to a 'non developable' surface. The theory of pure bending can be applied in the instance of a disc bent to form a spherical cap provided that the thickness of the disc is small in comparison with the radius of curvature.

Figure 7.7 illustrates the simple case of the pure bending of a rectangular plate. In the particular case where $M_x = M_y = M$, for a plate of any shape, the bending moments are uniformly distributed along the entire boundary and the twisting moments vanish. The radii of curvature can be related to the bending moment as follows:

$$\frac{1}{r_x} = \frac{1}{r_y} = \frac{M}{D(1+\nu)}$$

It can be seen that in this special case the plate is bent to a spherical surface. The maximum normal stress acting on the xz or yz planes occurs at the surface of the plate (i.e. where $z = h/2$) and is given by the relationship:

$$(\sigma_x)_{max} = (\sigma_y)_{max} = \frac{6M}{h^2}$$

Finally the value of the flexural rigidity is given by:

$$D = \frac{Eh^3}{12\,(1-\nu^2)}$$

The radius of curvature of a spherical cap can be obtained by simple geometry, and is calculated from the central deflection and chord length 2a ($a \simeq$ radius of disc)

$$r \simeq a^2/2w$$

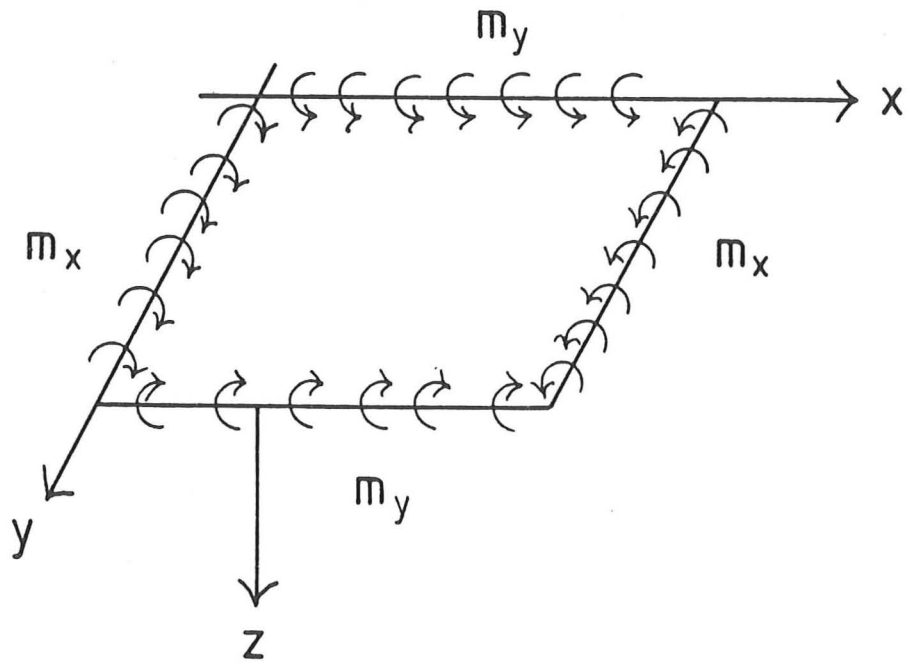

Figure 7.7 : Pure bending

This expression is accurate if w is small compared with the radius of curvature.

The values of the relevant parameters for the thickest disc eroded in these experiments are as follows:

$a = 11.16mm$

$h = 2mm$ (being 2.255mm, minus the deformed layers)

$E = 70.6$ GPa (Smithells (1976))

$\nu = 0.345$ (Smithells (1976))

$w = 600\mu m$

The resultant maximum normal stress is 1.04GPa. The significance of this result will be discussed in section 7.3.5 below.

An alternative approach is to fix the maximum stress at the elastic limit stress of the aluminium, and to work back to determine the resultant maximum elastic deflection. The yield stress of aluminium, used in these experiments, was measured to be 134MPa (details of the test technique are presented in section 7.2.3 above). The stress at the elastic limit (limit of proportionality) was approximately 80 percent of the yield stress.

The maximum elastic deflection, computed by this method, is $62\mu m$; the measured deflection, for comparison was approximately $600\mu m$. This result will be discussed in section 7.3.5 below.

7.3.4 Analysis of strains

If the eroded disc is assumed to be bent into the shape of a spherical cap, it is possible to produce an estimate of the maximum surface strain.

Referring to Figure 7.8, with α in radians, the arc length c is given by:

$$c = r\alpha$$

This is measured along the neutral plane, and is therefore assumed equal to the diameter of the undeformed disc.

The arc length c' is given by:

$$c' = (r + h/2)\alpha$$

This represents an original length plus a strain contribution dc:

$$c' = c + dc$$

Thus $$dc = \frac{h\alpha}{2}$$

and the strain at the surface of the bent disc is given by:

$$\frac{dc}{c} = \frac{h}{2r}$$

Table 7.1 gives the surface strains deduced in this way, for the measured central deflections of the eroded specimens.

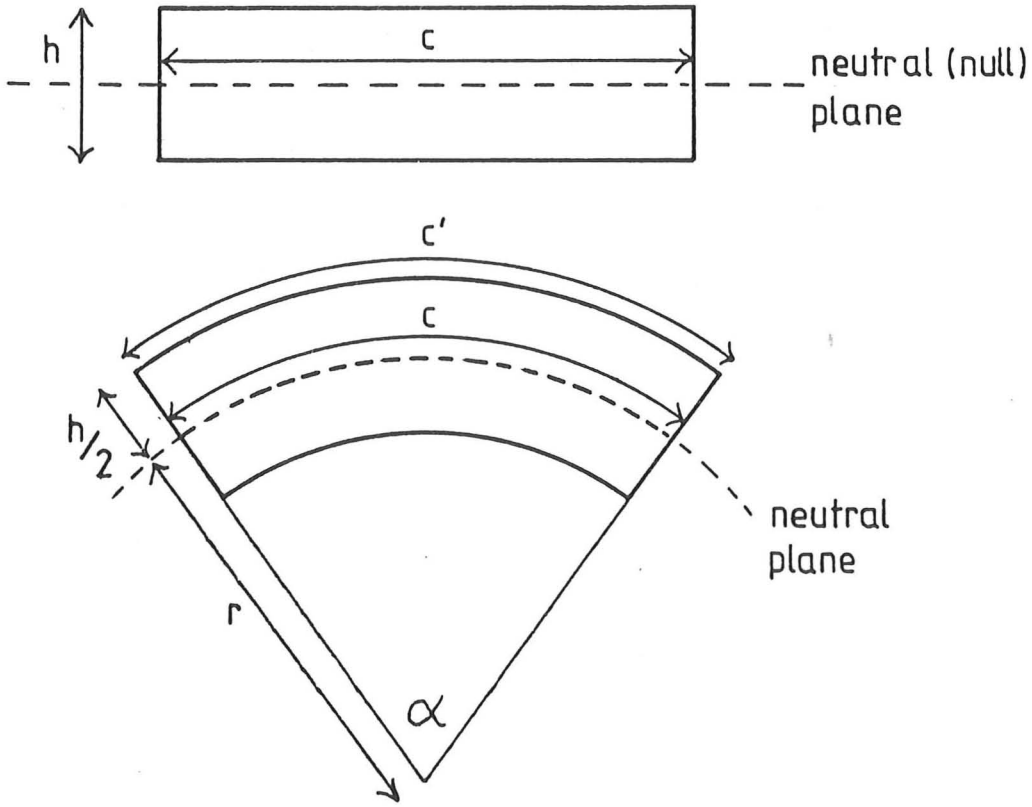

Figure 7.8 : Strains developed in a small element, with radius of curvature r.

Table 7.1 : Estimated Strains

All dimensions mm

h	2a	w	r	Strain %*
2.255	23.2	0.6	112	0.89
1.78	23.0	1.4	47.2	1.62
1.39	23.0	2.1	31.5	1.81

* NB : In accordance with assumptions listed in 7.3.3, strain is calculated from specimen thickness minus thickness of deformed layers.

As detailed in section 7.3.3.1 the yield stress of the aluminium used in these experiments was measured to be 134 MPa. The stress at the elastic limit was estimated to be 80% of the yield stress. Assuming a value of 70.6 GPa for the elastic modulus (Smithells (1976)) the strain at the elastic limit can be estimated to be 0.15%. This result is discussed in the following section.

7.3.5 Discussion

In order to estimate the stresses developed by erosion a number of assumptions have been made concerning the deformation of the eroded disc specimens. Primarily it was assumed that the bulk of the specimen was elastically deformed by the action of residual stresses confined to the highly deformed subsurface layers. The observations reported in Chapter 6 offered some justification for these assumptions, and the use of elastic deformation theories allowed the magnitude of the stresses resulting from erosion to be investigated.

The conclusion resulting from the application of the pure bending theory to the observed deformations is that these primary assumptions are not valid. First, application of the pure bending theory estimated that the maximum stress, developed on the top surface of the elastically deformed disc, was approximately one order of magnitude greater than the measured elastic limit stress. Further analysis indicated that the maximum elastic stress was developed in the specimen when the deflection at the centre of the specimen was one tenth of the measured value.

The analysis of strains resulted in a similar conclusion, when applied to the simple 'elastic' yielding disc situation. Estimated surface strains were approximately one order of magnitude greater than the strain computed from the measured elastic limit stress and a quoted value of elastic modulus.

This work indicates that the residual stresses developed in aluminium eroded with 600μm soda glass beads at 60ms^{-1}, are sufficient to cause permanent, plastic deformation of specimens up to 2.255mm thick. In all cases the measured deflections were too large to enable the bending stresses to be estimated using elastic theory. Clearly the deformed subsurface layers are subject to very high compressive residual stresses.

Further experimental evidence of the very high surface stresses involved in erosion was reported briefly in Chapter 6. During the development of the roll bonding technique for introducing a marker layer into test specimens, composite specimens with thin copper foil sandwiched in aluminium were produced. Full details are presented in Chapter 6, section 6.2. These specimens were produced with the objective of maximising the contrast of the marker layer, in the examination of polished sections.

An unusual failure mechanism was observed in these specimens in the early stages of the erosion tests. Figures 7.9 and 7.10 illustrate the eroded surface of the copper-aluminium composite after erosion with only 60g of glass beads at normal impact. In contrast, an aluminium specimen, eroded under identical conditions, would be expected to display incubation behaviour until $\sim$1000g of erodent had impacted the surface. The compressive stresses in the impacted surface have resulted in slip at the boundary of the copper foil (or within the foil itself).

The slip across this surface has caused the top strip of aluminium to buckle, to the extent of folding up the ridge of aluminium illustrated in section in Figure 7.9. . The complete ridge is illustrated in Figure 7.10, which shows the eroded surface before sectioning, under oblique illumination.

The use of elastic analysis was adopted after concluding that no suitable plastic analyses existed for the deformation observed in eroded specimens. Whilst the application of elastic theory has indicated that the deformation stresses are greater than the elastic yield stress, no detailed analysis was possible. Certain experimental methods of strain measurement do exist, however, which may prove useful in future work to investigate the deformation further. In addition, careful experimental design may enable alternative analyses to be adopted.

The use of an erosion test with a two dimensional convergent nozzle, such as used by Neilson and Gilchrist (1968), would enable the choice of a different specimen geometry . With this arrangement, rectangular specimens could be eroded along a centre line. The subsequent deformation would be

Figure 7.9 overleaf

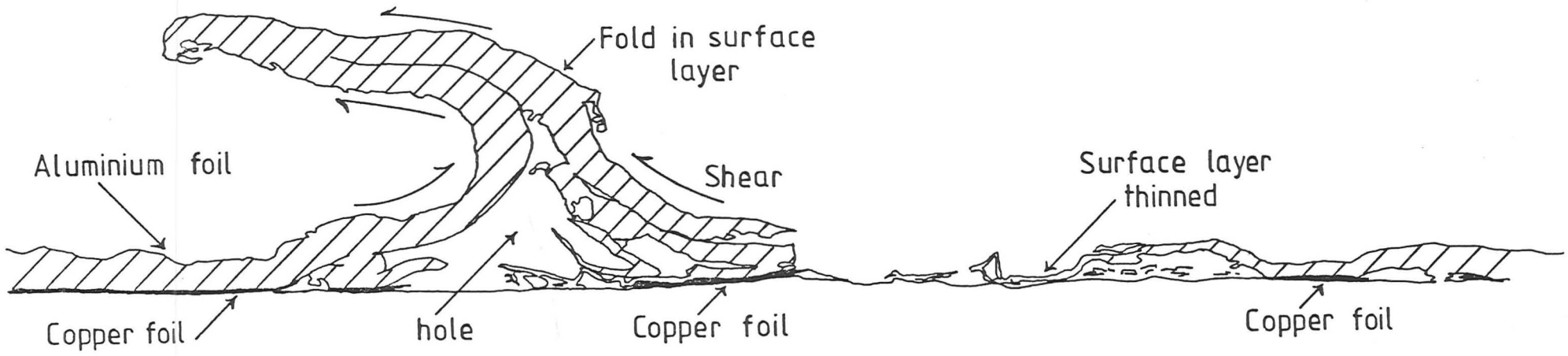

KEY to Figure 7.9 : Explanation of microstructure, the original surface layer is shaded

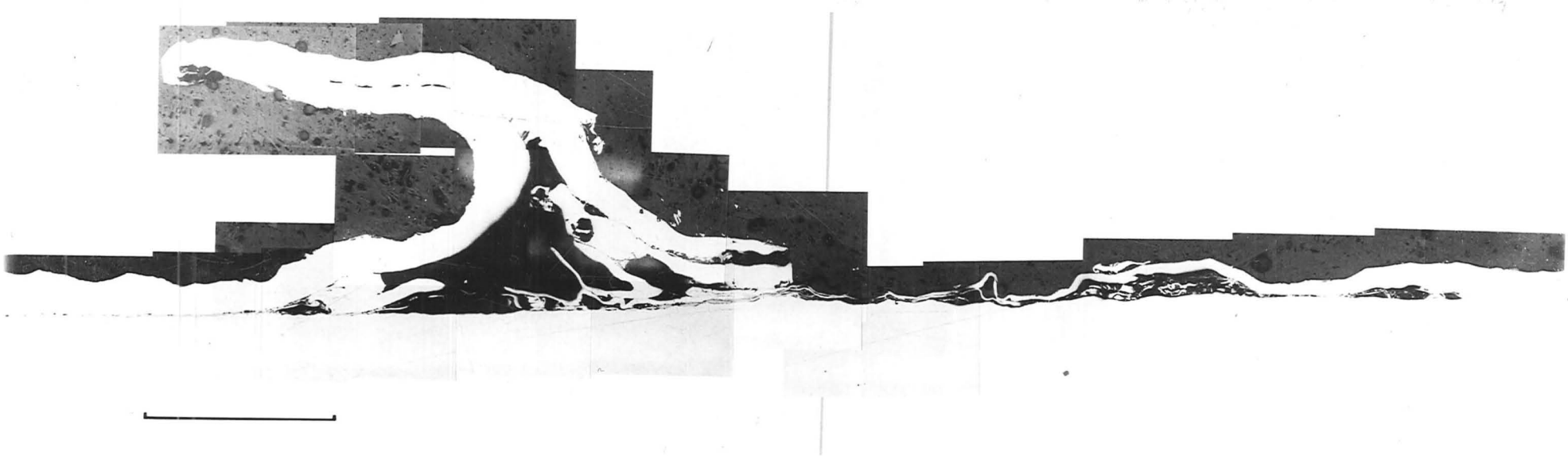

Figure 7.9 :

Section of aluminium/copper foil composite specimen eroded by glass beads. (Scale bar = 1mm)

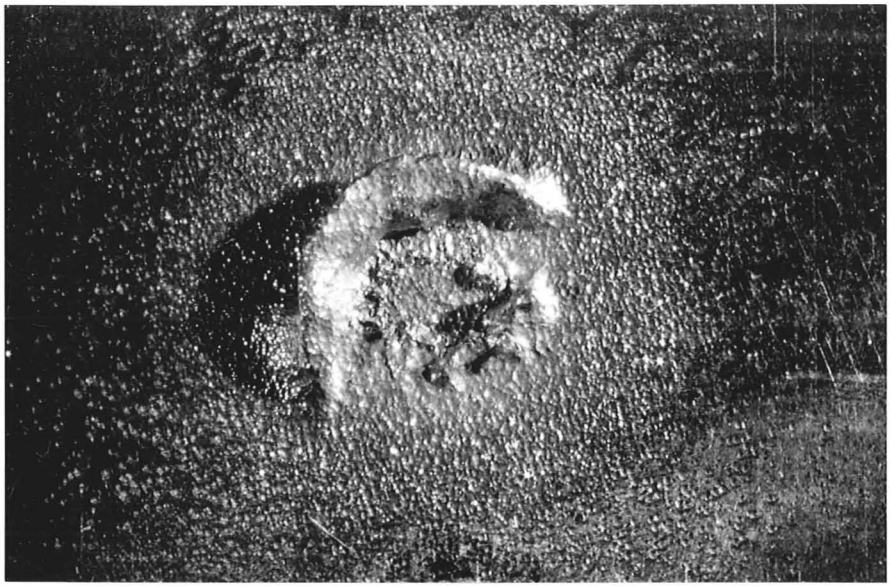

Figure 7.10 : Surface of aluminium/copper foil composite material after eroding with glass beads (oblique illumination)

suitable for analysis by beam bending theory, including 'plastic hinge' treatments. It would be necessary to support the edges of specimens eroded in this way, to prevent the relaxation of the subsurface stresses by material flow. Carter et al (1980) reported considerable flow across unsupported edges, in their work eroding the end faces of cylindrical specimens. A possible solution may be to erode a central strip across a rectangular specimen, and then to remove the uneroded edges.

The use of strain gauges would permit a direct measurement of the surface strains. There are several experimental methods available to investigate the strains developed on eroded specimens. First, a strain gauge rosette might be fixed in the centre of the back face of a disc specimen (of the type used in the present study) prior to eroding. A second alternative, again using a strain gauge rosette, would be to measure relaxation strains on the top face of an eroded specimen. A suitable technique would be to prepare a flat surface, and then to attach a rosette on to the eroded specimen. Once attached a hole would be drilled through the blank centre of the rosette configuration. The strain gauge would measure the relaxation strains introduced by this hole, allowing the residual surface stresses to be deduced. Other possible methods would measure the relaxation strains introduced by machining away (by mechanical or chemical methods) the disturbed layer containing the residual stresses.

7.4 CONCLUSIONS

The technique of upper bound limit analysis has been used to estimate the pressure required to cause material flow by the back extrusion mechanism proposed in Chapter 6. An estimate of erosion rate is generated from the

estimated extrusion pressure, using a simple energy balance technique. In common with the results of other workers using energy balance methods, this is found to give an incorrect prediction of the velocity dependence of erosion and also to greatly overestimate the erosion rate. Possible reasons for this overestimate are suggested, based on the experimental observations reported in Chapter 6.

The stresses and strains developed by erosion are investigated. The results suggest that considerable plastic deformation occurs as a result of the residual stresses developed within the eroded surface. Suggestions are made for further experimental investigations of the deformations resulting from erosion.

CHAPTER 8 : THE INFLUENCE OF ERODENT PARTICLE SHAPE ON THE EROSION OF MILD STEEL

8.1 INTRODUCTION

A survey of the literature presented in Chapter 1 section 1.2.4 concluded that little is known of the effect of particle shape on the erosion of ductile materials. Chapter 4 presented a survey of methods of shape measurement, and concluded that none presently available were suitable for the measurement of particles used in erosion testing, or taken from erosive environments.

This chapter describes a series of experiments investigating the effect of particle shape on the erosion of mild steel. The target material was selected as being a common engineering material. Three types of erodent material were selected. Two, spherical glass beads and crushed glass, were chosen as being similar in all respects, differing only in shape. In this way the effect of particle shape was isolated from other effects, such as particle hardness and frangibility. A third erodent material, angular silicon carbide, was incorporated as being a standard erodent type. This enabled useful comparisons to be made between the surfaces eroded in the present study, and also with results presented in the literature.

8.2 EXPERIMENTAL PROCEDURE

8.2.1 Erodent preparation

Three types of erodent particles were used :

(i) Soda glass beads, as used in the experiments described in Chapter 6, of sieved size range 95-105μm. Figure 8.1 (a) is an SEM micrograph, showing the beads to be smooth, perfect spheres.

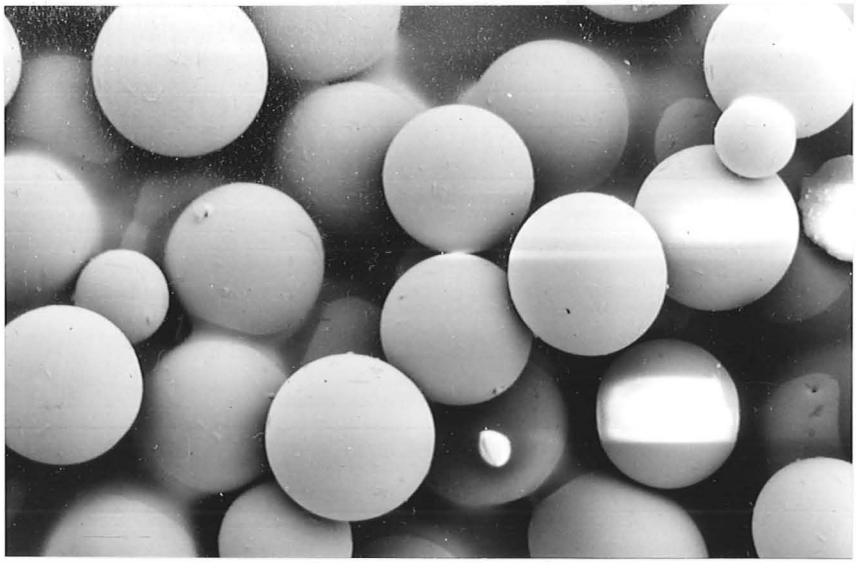

(a) Glass beads, sieved size 140/160 mesh (95-105μm)

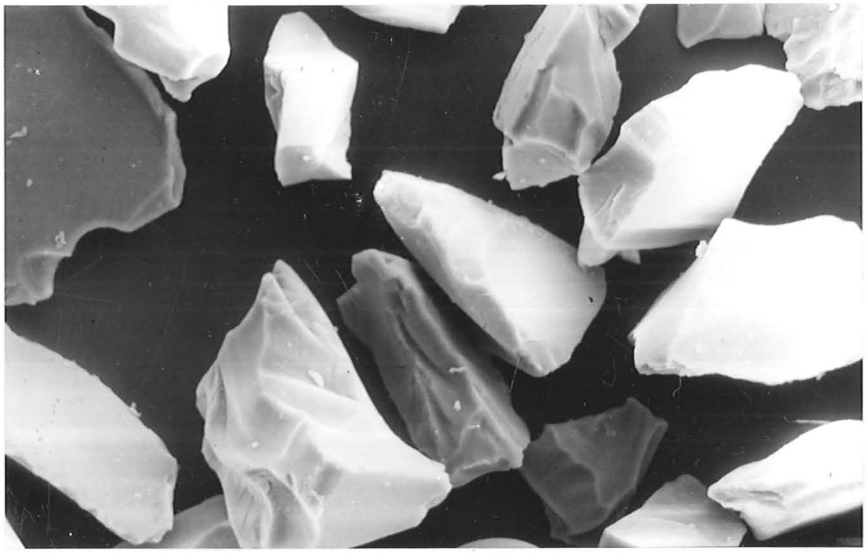

(b) Crushed glass, sieved size 140/160 mesh (95-105μm)

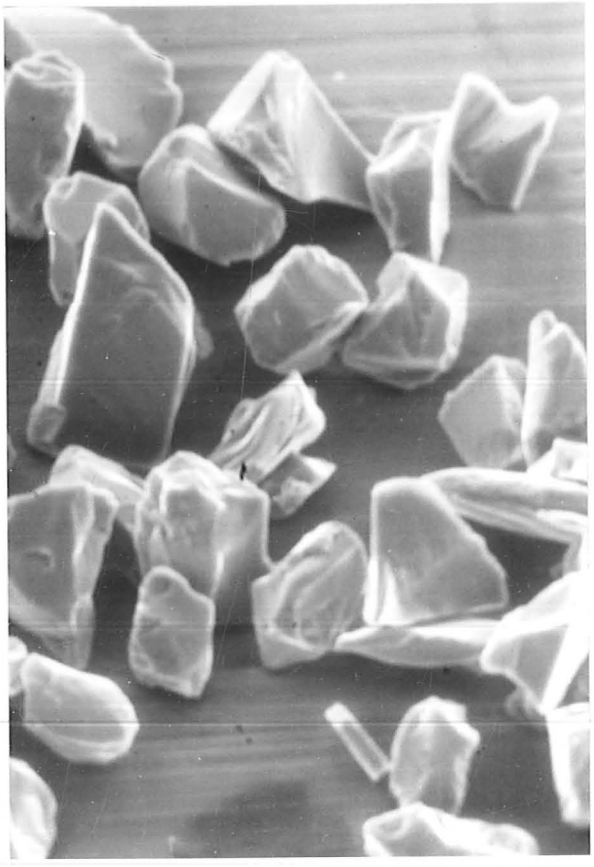

(c) Silicon carbide, sieved size 280 mesh (approximately 50μm)

Figure 8.1 : Scanning electron microscope micrographs of erodent particles

(ii) Crushed glass, of sieved size range 95-105μm. A mechanical mortar and pestle was used to crush large soda glass beads (minimum size 600μm) and the required size range extracted by sieving.

Details of the sieving procedures used for the spherical beads, and crushed glass, are presented in Chapter 5 section 5.2.1. Figure 8.1 (b) illustrates the appearance of the crushed glass particles.

The preparation of both types of erodent, (i) and (ii), from a common material source ensured that the particles differ only in shape. Size classification by sieving was selected as the most practical way of preparing the erodent types. It is acknowledged however that the large differences in particle shape between the two erodent types will, in some way, be reflected by differences in the statistical distributions of the masses of the individual particles.

(iii) Angular silicon carbide abrasive (manufactured by Carborundum) nominal size, 50μm. This material was used as supplied, sieved size 280 mesh.

8.2.2 Target material

All experiments were performed with mild steel specimens (composition : plain carbon steel 0.06% carbon), the Vickers hardness of which was measured as 170 ± 5 kgfmm^{-2} (indentation load, 10kg). Figure 8.2 is a micrograph illustrating the microstructure of this steel.

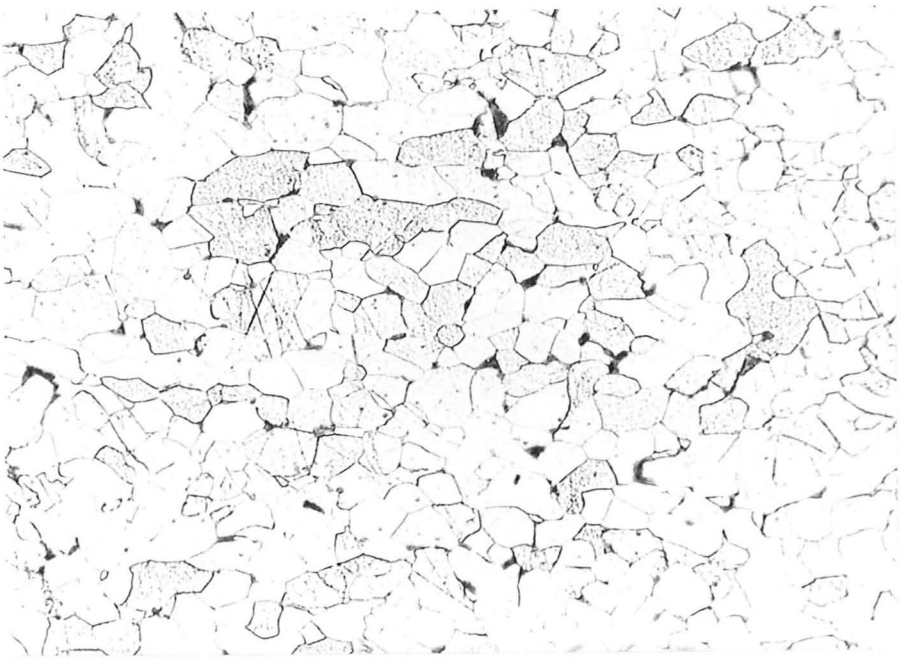

Figure 8.2 : Microstructure of mild steel. This microstructure is consistent with the very low carbon level analysed.

8.2.3 Erosion testing

Full details of the erosion test procedure are provided in Chapter 5, section 5.2.1. The gauge pressure at the mixing chamber (see Figure 5.2) was maintained at 10kPa for all experiments. Particle velocities were measured, using the double-disc method described in Chapter 5 section 5.3.1, as follows : glass beads $50ms^{-1}$, crushed glass $50ms^{-1}$, silicon carbide $55ms^{-1}$.

8.3 EXPERIMENTAL RESULTS

8.3.1 Weight loss measurements

(a) Erodent 140/160 mesh glass beads (size range 95-105μm)

Figure 8.3 (a) presents typical cumulative mass loss curves. Figure 8.3 (b) shows erosion (slope of mass loss curve at steady state, secondary stage) plotted against the angle of impact.

Two unexpected features are found in these results. First, the erosion is found to increase smoothly with angle of impact, reaching a maximum at normal impact. Second, the mass loss curve is bilinear for all impact angles except normal impact. In each case the initial slope (primary stage) is lower than that of the secondary stage.

(b) Erodent 280 mesh silicon carbide (nominal 50μm)

Figure 8.4 shows typical cumulative mass loss curves, and Figure 8.5 plots erosion versus angle of impingement.

Fig. 8.3

a) Shows typical results, each point represents the mean of several weighings. The lines are fitted by regression analysis.

b) Shows erosion versus impact angle. The two points for normal impact are thought to arise from minor alterations to the equipment. The larger value is directly comparable with the results at lower impact angles.

Figure 8.3 : Erosion of mild steel with spherical glass particles (140/160 mesh sieved size) at 50ms-1

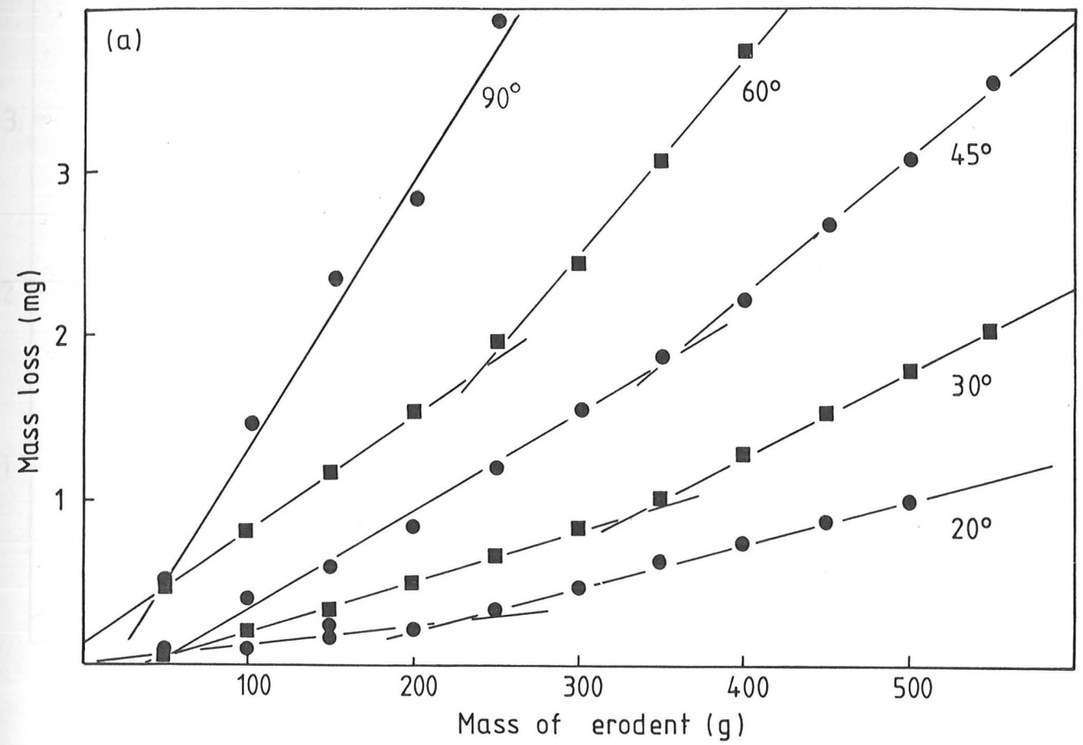

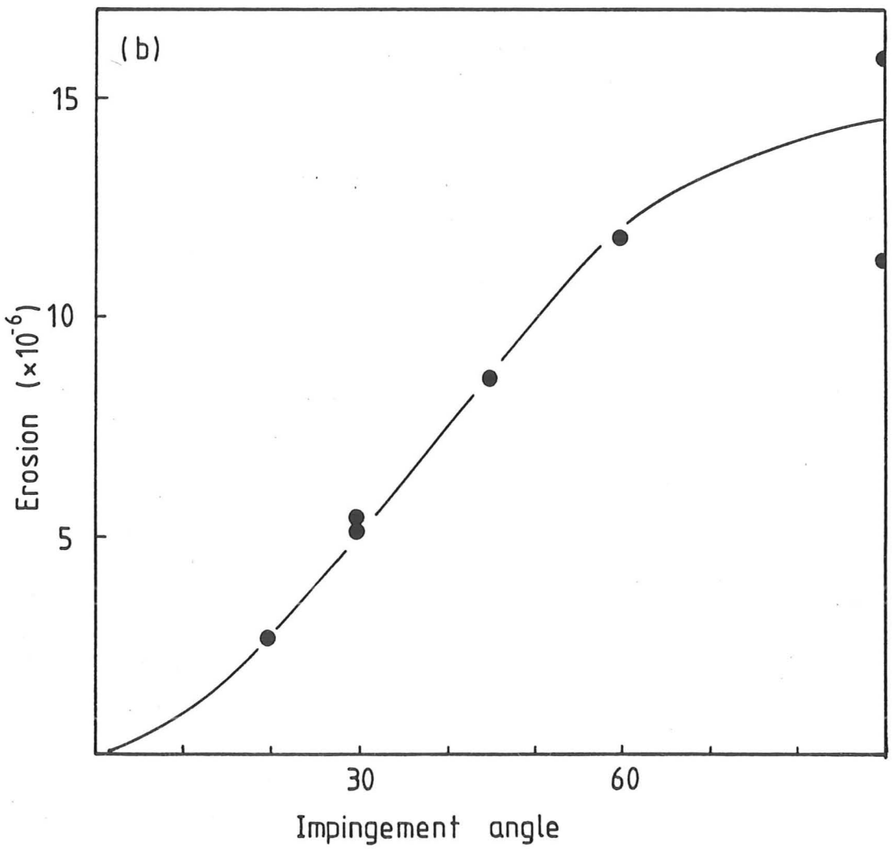

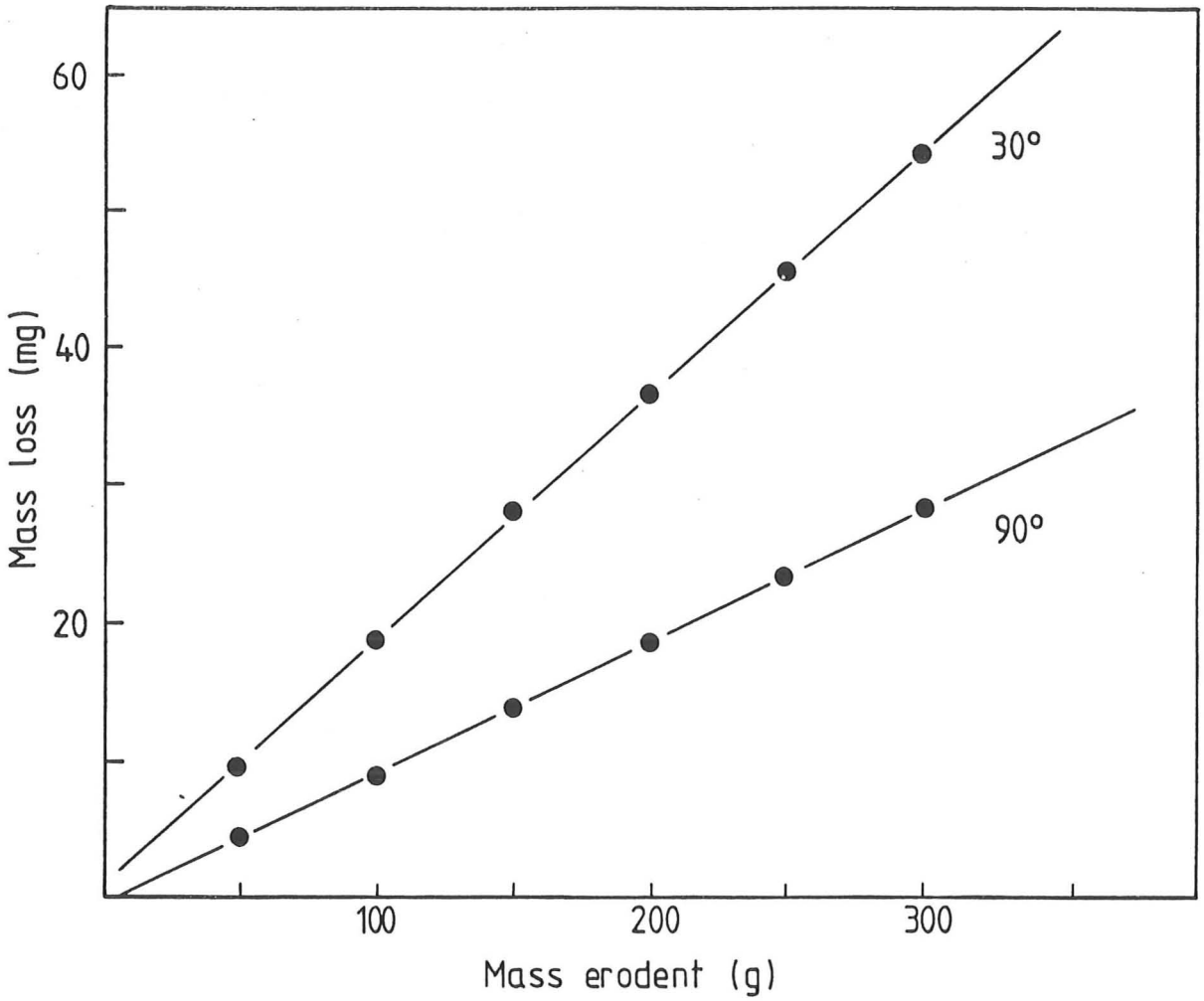

Figure 8.4 : Cumulative mass loss curve for mild steel eroded with 280 mesh angular silicon carbide at $55ms^{-1}$

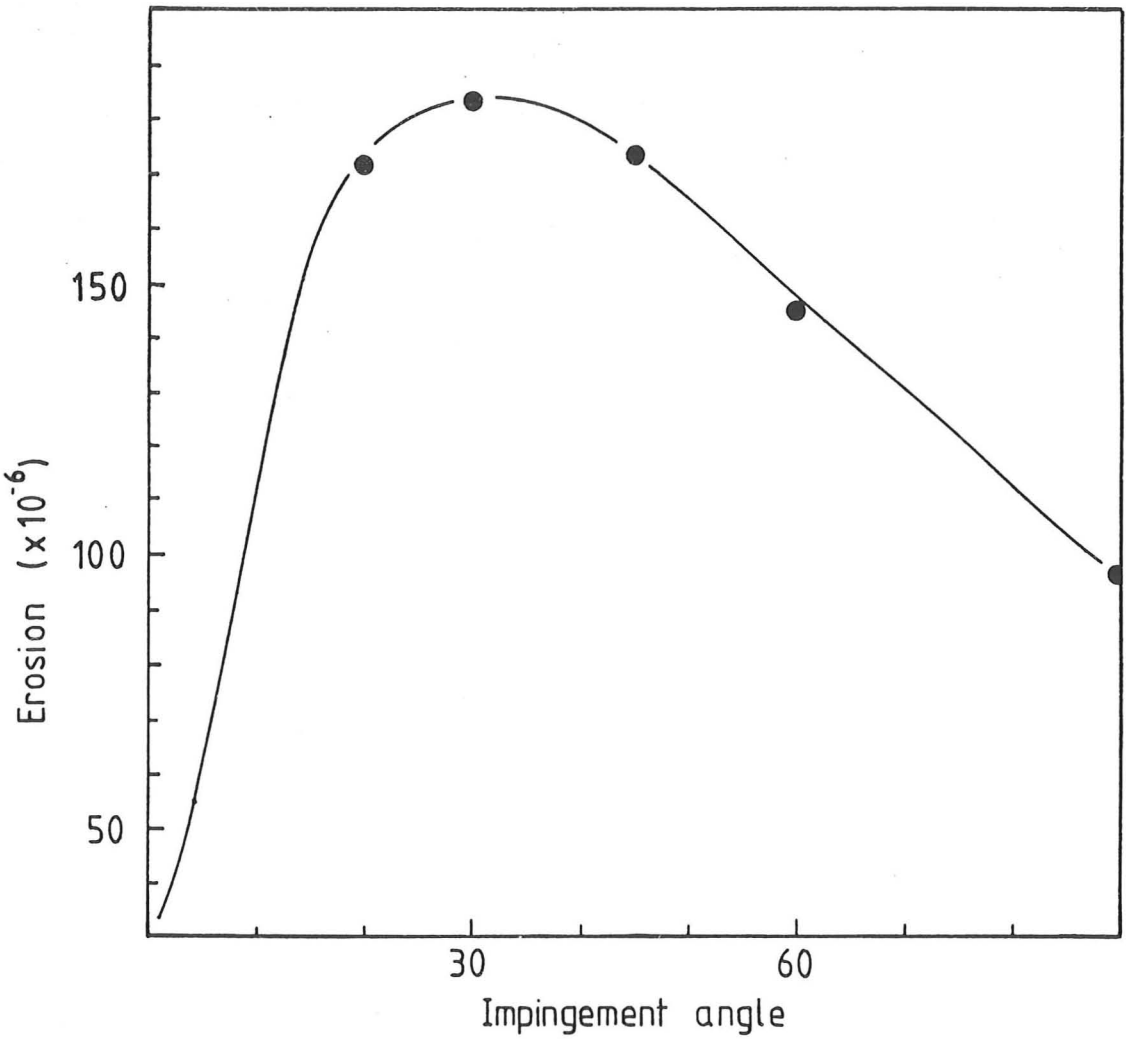

Figure 8.5 : Erosion vs impingement angle for mild steel eroded with angular silicon carbide (280 mesh) at $55ms^{-1}$

In these experiments steady state erosion was rapidly established. Maximum erosion is found at glancing angles (between 20^{o} and 30^{o}), and falls steadily away at higher impact angles.

Comparison with the results obtained with glass beads, (Figure 8.3) reveals an increase of approximately two orders of magnitude in erosion rate when using silicon carbide erodent.

(c) Erodent 140/160 mesh crushed glass (size range 95-105μm)

Two experiments were performed with this erodent; Figure 8.6 presents the cumulative mass loss curves.

The results are similar to those obtained with silicon carbide erodent. The erosion values are of similar order of magnitude, the mass loss curves show rapid establishment of steady state erosion, and the erosion at normal impact is less than that at oblique impact.

8.3.2 Examination of eroded surfaces

(a) Erodent 95-105μm glass beads

Figures 8.7 (a) to (e) illustrate the important surface features observed with these specimens. Figure 8.7 (a) shows detail from a mild steel specimen eroded at 20^{o} impact angle. Poorly developed ripples are present; this figure shows small flakes found 'downstream' of a surface peak. Smeared individual impact craters are visible across the whole surface.

Figure 8.7 (b) is a low magnification micrograph, showing the well developed rippled structure formed on the surface by 30^{o} impingement. Figure 8.7 (c)

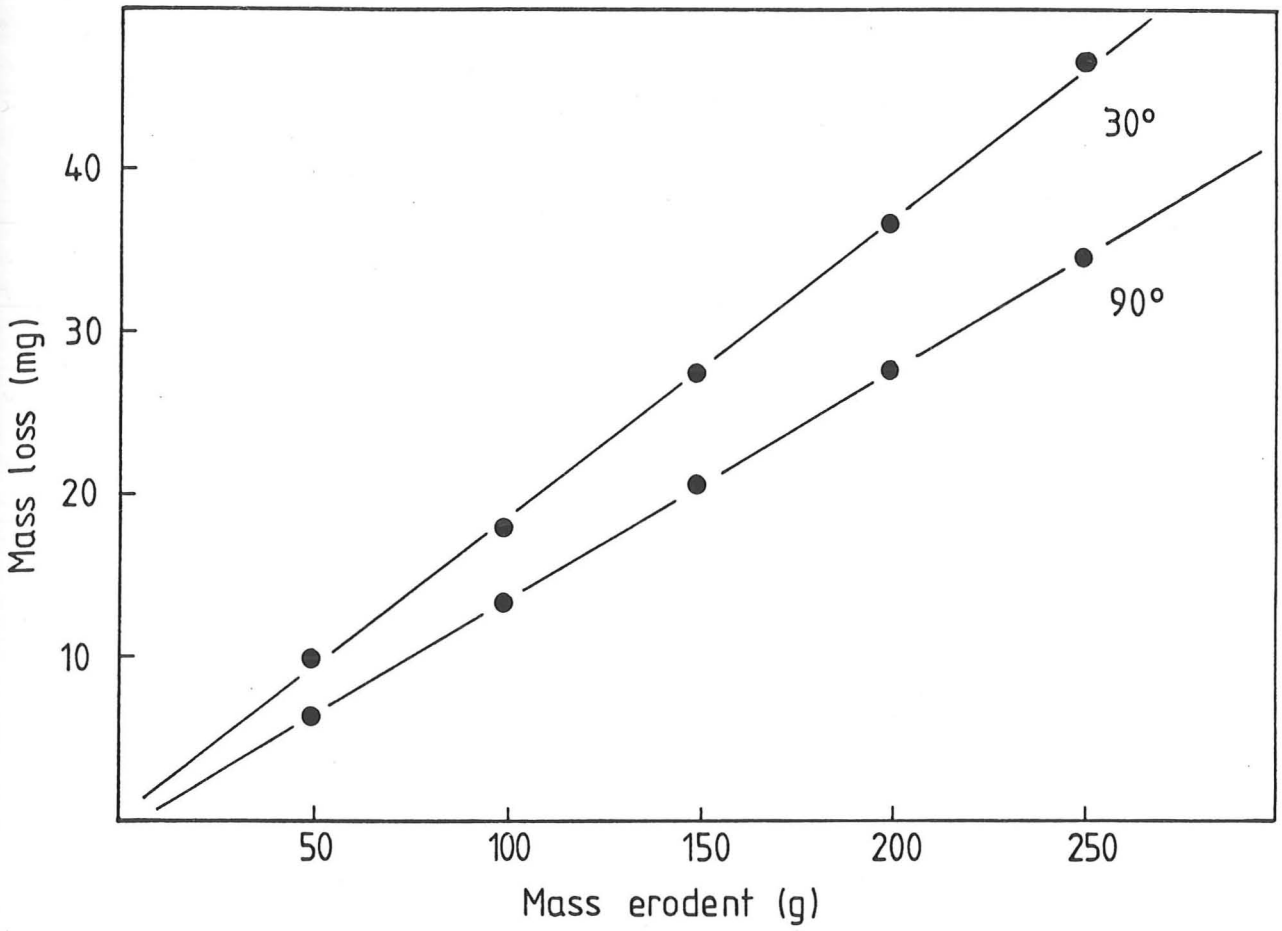

Figure 8.6 : Cumulative mass loss curve for mild steel eroded with angular glass erodent at $50ms^{-1}$

Erosion (slope of mass loss curve)

30^{o} impingement $E = 1.87 \times 10^{-4}$

90^{o} impingement $E = 1.39 \times 10^{-4}$

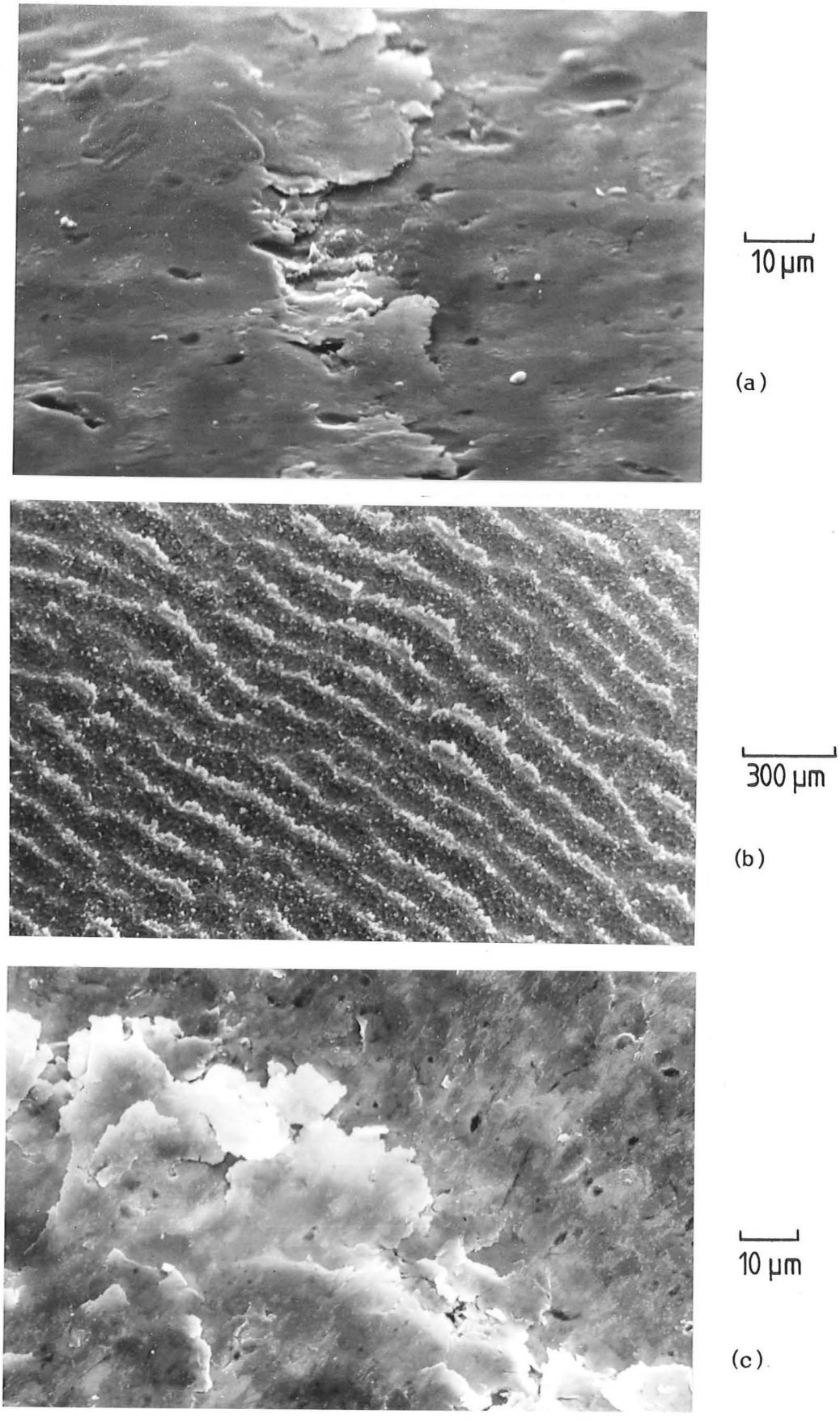

Figure 8.7 : Scanning electron microscope micrographs of eroded surfaces
Mild steel eroded with spherical glass erodent particles.
Angles of impingement : (a) 20^{o}, (b) 30^{o}, (c) 30^{o}.

(d)

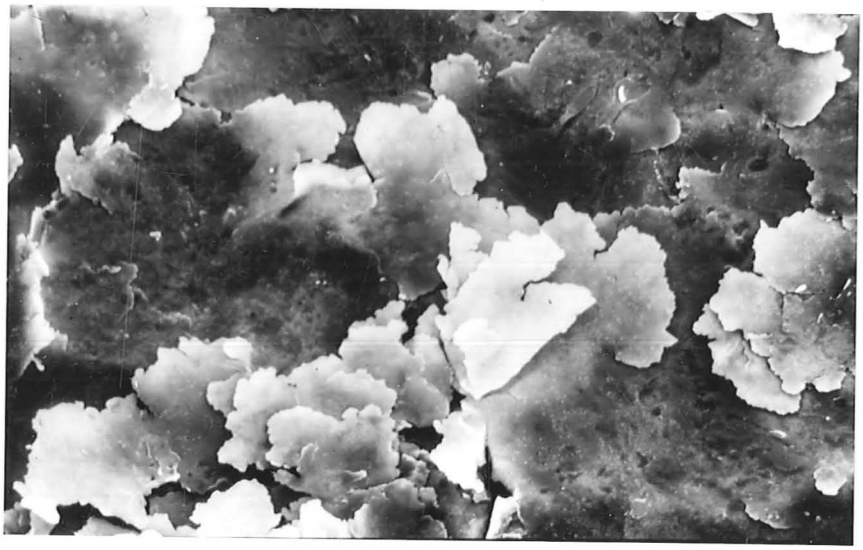

(e)

Figure 8.7 : Scanning electron microscope micrographs of eroded surfaces. Mild steel eroded with spherical glass erodent particles. Angles of impingement : (d) 45^{o}, (e) 90^{o}.

shows details of the surface ripple structure; flakes are found downstream of the peaks. These flakes are confined to the troughs, and point in the direction of the erodent flow up to the next peak.

Figure 8.7 (d) shows detail of a surface eroded by particles at 45^{o} impingement angle. As was the case at 30^{o}, surface ripples are well developed. Flakes are found in a similar position to those at 30^{o}, but now covering a larger proportion of the eroded surface area.

At 60^{o} impingement angle, much of the surface is covered with flakes which are oriented, aligned with the direction of flow of the erodent. There is some evidence of ripple formation, but these ripples are poorly developed. Figure 8.7 (e) gives detail of a surface eroded by spherical particles at normal impingement. The whole of the eroded surface is covered with flakes, randomly oriented.

(b) Erodent 50μm SiC, and 95-105μm crushed glass

Figures 8.8 (a) to (c) show surfaces eroded by silicon carbide particles at 20^{o}, 30^{o} and 90^{o} impingement respectively. Figure 8.9 shows a surface eroded by crushed glass at 90^{o} impingement.

In contrast to the surfaces eroded by spherical particles, when the erodent is angular there is little difference in the appearance of the eroded surface as the angle of impingement is varied. These micrographs support the conventional theories describing weight loss mechanisms, showing evidence of cutting and gouging. The surfaces eroded at glancing angles show more evidence of cutting processes, with gouging predominating at normal and near-normal impingement.

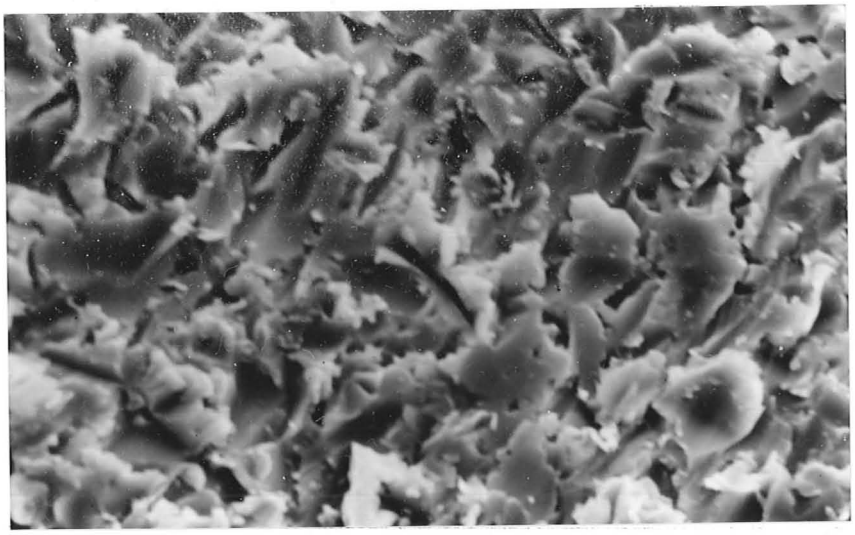

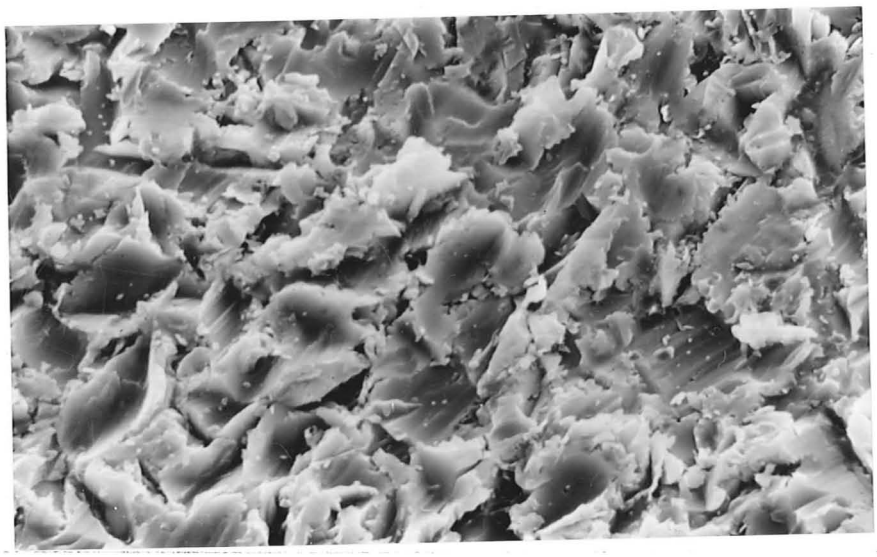

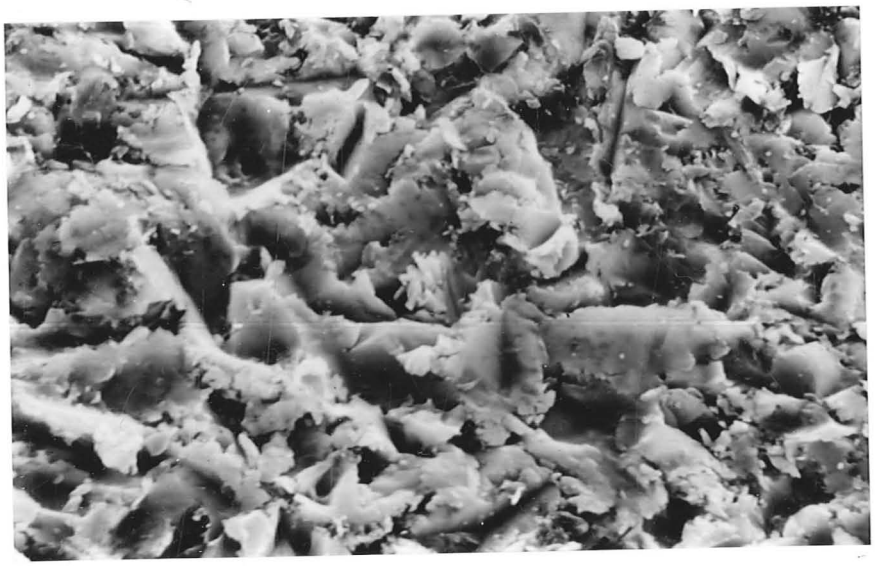

Figure 8.8 : Scanning electron microscope micrographs of mild steel surfaces eroded with angular silicon carbide. Angle of impingement : (a) 20^{o}, (b) 30^{o}, (c) 90^{o}.

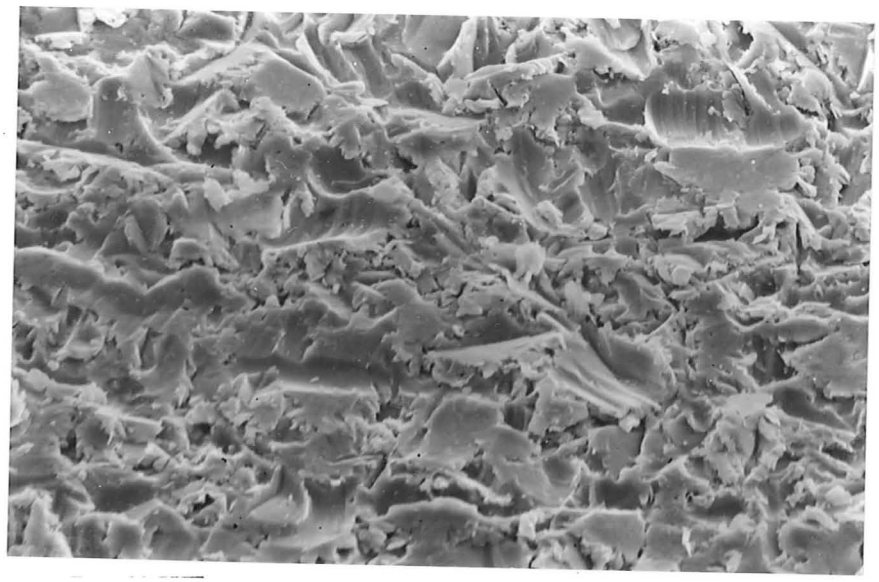

Figure 8.9 : Scanning electron microscope micrograph of mild steel eroded with angular glass at normal impingement.

8.4 DISCUSSION

8.4.1 Comparisons with earlier work

In Chapter 1 section 1.2.2 the effect of impact angle on the erosion of materials was discussed. It was concluded that the erosion behaviour of most materials can be classified in one of two ways, either 'brittle' or 'ductile'. This classification has become incorporated in the standard terminology for erosive wear (A.S.T.M. (1977)), and is summarised; 'With brittle erosion the maximum volume removal occurs at an (impact) angle near 90 degrees, in contrast to approximately 25 degrees for ductile erosion behaviour.'

Wellinger (1949) reported both ductile and brittle erosion behaviour in his study of the erosion of steels of differing hardnesses. Figure 8.10 presents Wellinger's results. A soft ($128 kgf mm^{-2}$ Vickers hardness), ductile steel was found to erode most at glancing ($\sim 30^{o}$) impact, whereas a harder, more brittle steel ($840 kgf mm^{-2}$ Vickers hardness) eroded most at near normal impact. (An intermediate behaviour was reported for a steel of moderate hardness, with maximum erosion occurring at approximately 60^{o} impact). Wellinger did not provide details of the abrasive used in these experiments. He provided micrographs of the eroded surfaces of the softer steel (these micrographs resemble Figures 8.8 and 8.9 of the present work), and described the surface damage as 'cutting'. Thus the work reported by Wellinger is in good agreement with the erosion of mild steel by angular abrasive as described above (section 8.3.2 (b)).

Sargent et al (1981) showed the effect of angle of impingement on the erosion of a range of plain carbon steels eroded by angular particles,

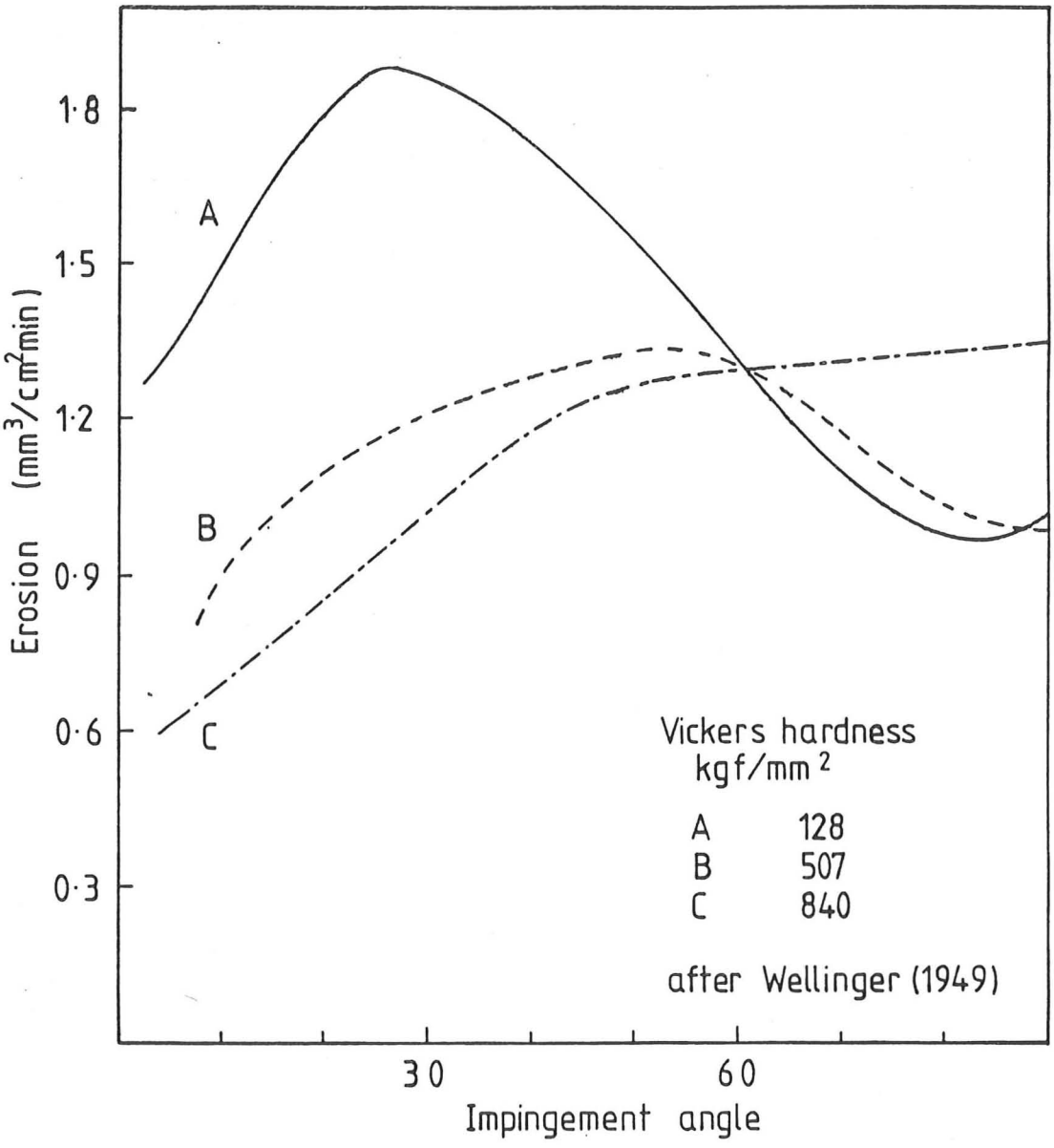

Figure 8.10 : Erosion vs impingement angle for steels of differing hardness

alumina and coal ash (45% silica, 27% alumina). In all cases he found the typical 'ductile' response.

Kleis (1969) reported maximum erosion at approximately 20^{o} impingement when low carbon steel was eroded by angular, alumina, abrasive. He found that the use of a more rounded slag as abrasive resulted in maximum erosion occurring at approximately 45^{o} impact angle.

Tilly and Sage (1970) investigated the angular dependence of the erosion of an aluminium alloy, using glass spheres and quartz as erodent. Their results are reproduced in Figure 8.11; they accounted for the differences in behaviour by the differences in hardness of the erodent materials. The glass spheres, they suggested, suffered greater fragmentation at normal impact, and hence significantly more erosion was caused by secondary erosion. (Full details of Tilly's two stage erosion mechanism are presented in Chapter 2 section 2.4). The choice of glass beads and crushed glass as erodent materials, in the present study, has eliminated the differences in hardness between erodent types. Further, the damage resulting from secondary erosion (as suggested by Tilly (1973)) is predominantly low angle cutting and gouging. The microscopic evidence presented in Figure 8.7 does not support the proposal that the wear resulting from erosion by glass beads is due to secondary erosion. A further discrepancy between the present study, and the results of Tilly and Sage, is revealed on examination of the relative magnitudes of the erosion caused by the two erodent types. In the present study the erosion by angular particles at 30^{o} impact was approximately twenty times greater than the erosion by spherical particles; at normal impact erosion by angular particles was approximately ten times greater than that by spherical particles. (Measured values, see Figure 8.3 and 8.6 : 30^{o} impact; crushed glass $E = 1.87 \times 10^{-4}$, glass beads $E = 5.06 \times 10^{-6}$; 90^{o} impact; crushed

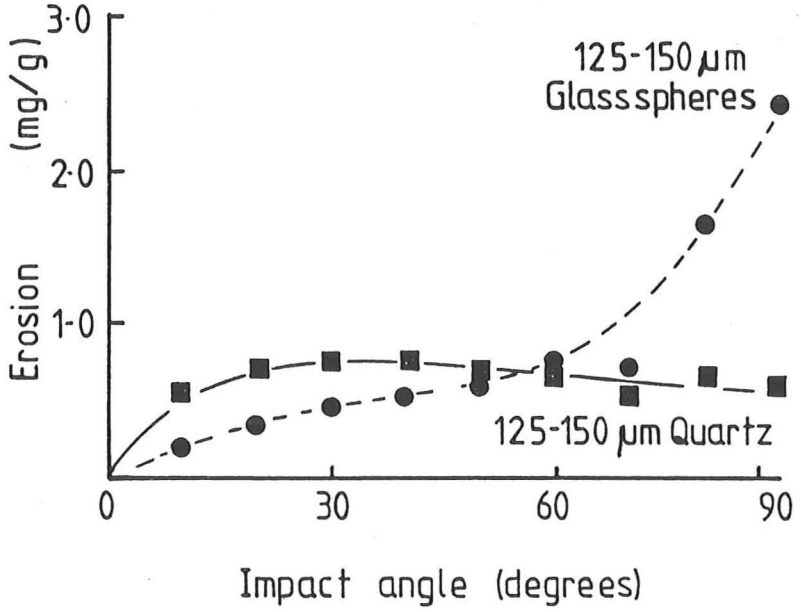

Figure 8.11 : Angle dependence for an aluminium alloy tested at 244ms^{-1}. (After Tilly and Sage (1970))

glass E = 1.39 x 10^{-4}, glass beads E = 1.45 x 10^{-5}). In contrast Tilly and Sage reported similar erosion for angular and spherical abrasives at 30^{o} impact, and approximately five times greater erosion by spherical abrasive compared with angular abrasive at normal impact.

The differences in the results reported by Tilly and Sage, and those of the present study may in part be due to the different target materials (aluminium alloy, and mild steel) and also the particle velocities used (244ms^{-1}, compared with 50ms^{-1} in the present study).

Further reports of a change of angular dependence in erosion are given by Gulden (1979), who reported a transition from 'ductile' to 'brittle' behaviour in steels, as a function of both heat treatment and impacting particle size. It is significant that she observed that 'Impact damage for brittle-type erosion response is not characterised by brittle fracture, but rather by intense localised plastic flow producing lips around the crater periphery'.

Salik and Buckley (1981a) did not present details of the angular dependence of erosion for their steel samples (1045 : 0.43-0.5%C, 0.6-0.3%Mn, $<$0.04%P, $<$0.05%Si), but in agreement with the results of the present study found that crushed glass particles eroded the steel an order of magnitude more rapidly than did glass beads. Raask (1969) similarly found in tests on mild steel that angular quartz particles were an order of magnitude more erosive than glass spheres of the same size. He concluded, '... with smooth particles the erosion rate is lower than with the quartz grains, where the cutting wear results in a high rate of metal loss'. In good

agreement with the present study he reported that for mild steel eroded with angular ash particles the angle of impingement for maximum wear was between 30^{o} and 45^{o}. He reported that the ash was approximately one third as abrasive as quartz grains (i.e. $\frac{\text{erosion wear by ash}}{\text{erosion wear by quartz}} \sim 0.2 - 0.4$) and that the abrasiveness of the ash is characterised by the amount of non-spherical particles in the material.

Green et al (1981) and Brown et al (1983) reported extensive surface ripples on plain carbon steels and aluminium alloy (1100) respectively, when eroded with angular abrasives. No evidence of surface ripple formation was detected in the present study on mild steel surfaces eroded by angular abrasives. Green used approximately 250μm silicon carbide particles, and Brown used approximately 210μm angular quartz particles. The silicon carbide used in the present study was approximately 50μm, and the crushed glass approximately 100μm. The absence of surface ripples on the surfaces eroded in the present study may result from the use of smaller particles; Brown et al suggested that there may be a threshold particle size for surface ripple formation.

Brown et al (1981b) reported details of a study of the erosion of pure α-iron using spherical glass particles. In contrast with the present study they reported that 'the dependence of the steady state erosion rate on the impact angle followed the classical form for ductile targets'. Whilst it is possible that the differences in results may simply reflect differences in target material properties, it must be noted that micrographs of surface features presented in Brown et al (1981b and 1981d)) are remarkably similar to Figure 8.7 above. Both reports (1981b and 1981d) concluded that in the case of erosion by spherical particles the major mechanism of material removal involves the formation and detachment of flakes or

platelets. This proposal is further developed in a later paper (Brown et al (1983)) where it is concluded that in the erosion of an aluminium alloy (1100) the establishment of surface ripples and the subsequent flake formation in the ripple troughs accounts for the material removal when eroding with both angular or spherical erodent.

In contrast with the work of Brown et al, Rao et al (1982) reported details of experiments with an aluminium alloy (6061-T6) and a steel (1045: 0.46%C, 0.8%Mn, 0.04%P, 0.05%S) eroded with crushed glass and also with glass beads. Rao used unconventional testing techniques (full details are presented in Chapter 6 section 6.4.1) making simple comparisons of results impossible. However, Rao concluded that if the erodent was spherical glass beads the material removal process involved the formation of flake like debris. Erosion by crushed glass resulted in material being removed as small chips, leaving a jagged angular faceted surface which he suggested was characteristic of 'cutting wear'.

It can be concluded that although much of the work reported in the literature does accord with the observations made in the present study, there are certain notable exceptions. The work of Tilly and Sage (1970) differs significantly from that reported here. Further work repeating their experiments on aluminium, but using the erodents used in the present study, is necessary to explain the discrepancies.

8.4.2 Erosion mechanisms

(a) Angular particles

The results of the erosion tests on mild steel using silicon carbide as erodent are in good agreement with others reported in the literature.

Surface features, as illustrated in Figure 8.8 show that similar mechanisms of material removal operate at glancing, and near normal impingement angles. Conventional theories (see Chapter 2 section 2.5) involving cutting and gouging modes of material removal, describe the observed erosion behaviour. Cutting predominates at glancing angles, while the less efficient gouging action predominates at near normal impingement.

Comparison of the mass loss measurements (Figures 8.4 and 8.6) and surface features (Figures 8.8 and 8.9) indicates that the erosion process when crushed glass is used as the erodent is very similar to that occurring when silicon carbide is the erodent. Comparison of Figures 8.1 (b) and 8.1 (c) shows the similarity of particle shape between the two types of erodent. It is concluded that conventional 'ductile' erosion behaviour occurs when mild steel is eroded by angular particles.

(b) Spherical particles

A completely different erosion response is displayed when the erodent particles are spherical. The dependence of erosion on impingement angle exhibits a maximum at normal impingement, more typical of a 'brittle' material (compare Figure 8.3 (b) with Figure 8.10 curve c). The maximum erosion occurs when the surface is completely covered with flakes or platelets. This observation is in accordance with that of Brown et al (1981d) who concluded that the major mechanism of weight loss when α-iron is eroded with spherical glass beads involves the formation and detachment of flakes. The role of surface flake removal in the erosion of ductile materials is also well documented for aluminium alloys (Chapter 6 this work, also Rickerby and Macmillan (1982)) and for copper (Carter et al (1980)).

Other types of surface deformation detected in this work were smeared 'ploughing' craters at glancing impact angles (visible in Figure 8.7 (a)) and well developed surface ripples at impingement angles of 30^{o} and 45^{o} (Figures 8.7 (b) and (d)).

The low erosion rate at low impact angles may be explained by the fact that only a small fraction of the surface is covered with flakes, and the ploughing impact craters result in little weight loss (in contrast to the more efficient cutting of the surface by angular particles at glancing angles of impingement).

The development of surface ripples offers an explanation for the two-stage erosion curves seen in Figure 8.3 (a). Initially the whole surface of the specimen presents the same angle to the flow of particles. As the ripples develop, areas of the surface will present a higher angle to the particle flow. As concluded earlier, higher angles of impingement result in more efficient flake formation and removal, and consequently the development of ripples increases the erosion rate. Thus the true steady state, or constant erosion rate, is established only when the surface ripples are fully developed. The true steady state erosion rate is therefore greater than the initial erosion rate.

It has not been possible in this work to determine the detailed mechanism by which the surface flakes are formed. A model was proposed in Chapter 6 of this work, in which platelets are formed by the back extrusion of bulk material through breaks in a hardened subsurface layer. Detailed examination of polished sections of the mild steel specimens provided no evidence of the formation of such a hardened layer, or any embedding of erodent fragments. Brown et al (1981b) proposed an alternative model for

flake formation which also involved a hardened subsurface layer, or required the development of surface ripples, Brown et al (1981d). Although surface ripples were developed on specimens eroded at 30^{o} and 45^{o}, and to some extent on the 20^{o} and 60^{o} specimens, the specimens which had surfaces totally covered by flakes (normal impingement specimens) showed no sign of surface rippling. (A full description of the models proposed by Brown is provided in Chapter 6 section 6.4.1).

Bellman and Levy (1981) described a forging-extrusion mechanism, involving thermal softening of the surface. This mechanism is discussed in Chapter 2 section 2.7. No metallographic evidence was found in this work, however, of extensive heating of the eroded surfaces.

It is only possible at this stage to state that the flakes observed appear to be extremely thin in relation to their large surface area, and become detached only after undergoing very high plastic strains. There are signs of surface shearing as well as of forging actions on surfaces eroded at glancing impact. It is probable that individual impacts raise a lip of material around the impact crater, and that further impacts on this lip deform the raised material into flakes. The flakes may well become detached when the material is deformed beyond a limiting plastic strain, as suggested by Naim and Bahadur (1983).

8.5 CONCLUSIONS

This study of the sensitivity of the erosion of mild steel both to angle of impingement and to erodent type has provided important information on the role of particle shape in erosion.

To date, 'ductile' erosion behaviour has been associated with maximum erosion at glancing impact angles, and 'brittle' erosion behaviour associated with erosion increasing with angle, reaching a maximum at normal impact. These experiments have shown that one material, mild steel, can be made to exhibit both types of erosion behaviour, depending upon the shape of the erodent particles. Significantly, examination of the eroded surfaces shows that in each case the mechanisms of material removal involve plastic deformation of the mild steel, and in no case could the mechanism be described as 'brittle fracture'. Angular grit removes material by cutting and gouging processes, which are well documented in the literature. Spherical particles give rise to erosion behaviour with a maximum in erosion at normal impingement, which would be conventionally described as 'brittle'. Correlation of weight loss measurements with the observation of surface features shows that material is removed from the surface in the form of platelets or flakes. At normal impingement the formation of these flakes is maximised. The formation of surface ripples at lower angles of incidence is thought to modify the erosion behaviour, with ripples presenting areas of higher incidence angles. In these areas, flake formation, and hence material removal, is enhanced.

Care is clearly needed if a classification of erosion mechanisms as 'brittle' or 'ductile' is to be made on the basis of the angular dependence of erosion. In the present case, behaviour which would conventionally be termed both 'brittle' and 'ductile' was found, in both instances, associated with plastic deformation of the surface, with no evidence of brittle fracture. These observations suggest that some reconsideration of the conventional terms 'ductile erosion behaviour' and 'brittle erosion behaviour' may be necessary.

CHAPTER 9 : THE EFFECT OF ION IMPLANTATION ON THE EROSION RESISTANCE OF MILD STEEL

9.1 INTRODUCTION

A brief introduction to the technique of ion implantation was presented in Chapter 3 section 3.4. A survey of the literature indicated that ion implantation could be used to improve the resistance of metals to certain forms of wear. This chapter presents the results of an experimental investigation of the effect of nitrogen ion implantation on the erosion resistance of mild steel.

9.2 EXPERIMENTAL DETAILS

All experiments were performed on mild steel specimens (nominally to British Standard BS 970 En3B 0.16/0.24C, 0.35 max Si, 0.50/0.90 Mn, 0.05 max S and 0.05 max P) which were supplied by B P Research Centre (Sunbury-on-Thames). Figure 9.1 is a micrograph illustrating the microstructure of the steel.

The specimens were approximately 5mm thick, 65mm long and 20mm wide. One half (along the 65mm length) of each specimen had been ion implanted at U.K.A.E.A., Harwell. The remaining half had been left untreated to act as a control specimen. The ion implantation dose level was 8×10^{17} N (ions) per cm^2. The hardness of the untreated mild steel was measured to be 160 $kgfmm^{-2}$ (Vickers indentation load 10kg).

Figure 9.1 : Microstructure of mild steel (section of ion implanted specimen).

The erodent materials used were :

Soda glass beads (Ballontini, supplied by Abrasive Development Ltd., Solihull) in two sieved size ranges (95-105μm and 53-58μm). The glass beads are almost perfectly spherical.

Angular silicon carbide abrasive (manufactured by Carborundum) of nominal sieved size 40μm.

Angular silica flour (SF120, supplied by Buckland Sand and Gravel Co., Reigate, Surrey) of nominal sieved size 40μm.

The particle velocities were in the range 49-56ms^{-1}, measured using the double disc method (with the exception of the experiments with silica flour.)

Full details of the experimental procedure are presented in Chapter 5 section 5.2.1.

9.3 EXPERIMENTAL RESULTS

No consistent difference in behaviour was detected between the ion implanted specimens and the unimplanted steel controls, over the range of velocities and erodent types used.

Tests using glass beads as erodent showed no measurable difference between the erosion of the ion implanted and unimplanted control specimens. This result occurred for both sizes of glass beads (95-105μm and 53-58μm sieved size ranges) over the full range of impingement angles.

Tests using 40μm silicon carbide as erodent showed no difference in erosion behaviour on implantation, except for the case of normal impingement. The results for normal impingement showed significantly greater variation than usual, and indicated that ion implantation slightly decreases erosion resistance. The eroded surfaces were examined by scanning electron microscopy, and the surface morphology was found to be fully consistent with that reported in Chapter 8 for mild steel (unimplanted), eroded under identical conditions. No evidence was seen for a difference in behaviour between the ion implanted mild steel and the untreated control, eroded by silicon carbide at normal impingement.

A final test was conducted in which the specimens were eroded with 40μm silica flour at 20^{o} impingement. The gas pressure at the mixing chamber was set at the lowest possible value. This resulted in an impact velocity of 56 ms^{-1}, estimated with the computer program developed by Ninham and Hutchings (1983). Figure 9.2 reproduces the cumulative mass loss curves. The scatter of points is low, and the erosion rates (slopes of the curves after incubation) are identical for the ion implanted specimen, and for the untreated control. There is, however, a slight change in incubation behaviour. The ion implanted specimen had an incubation period some 25g greater than the unimplanted mild steel control (represented by the offset between the curves).

9.4 DISCUSSION

The marked increase in wear resistance achieved by ion implantation, which has been reported by many workers, has not been reproduced in this series of erosion experiments.

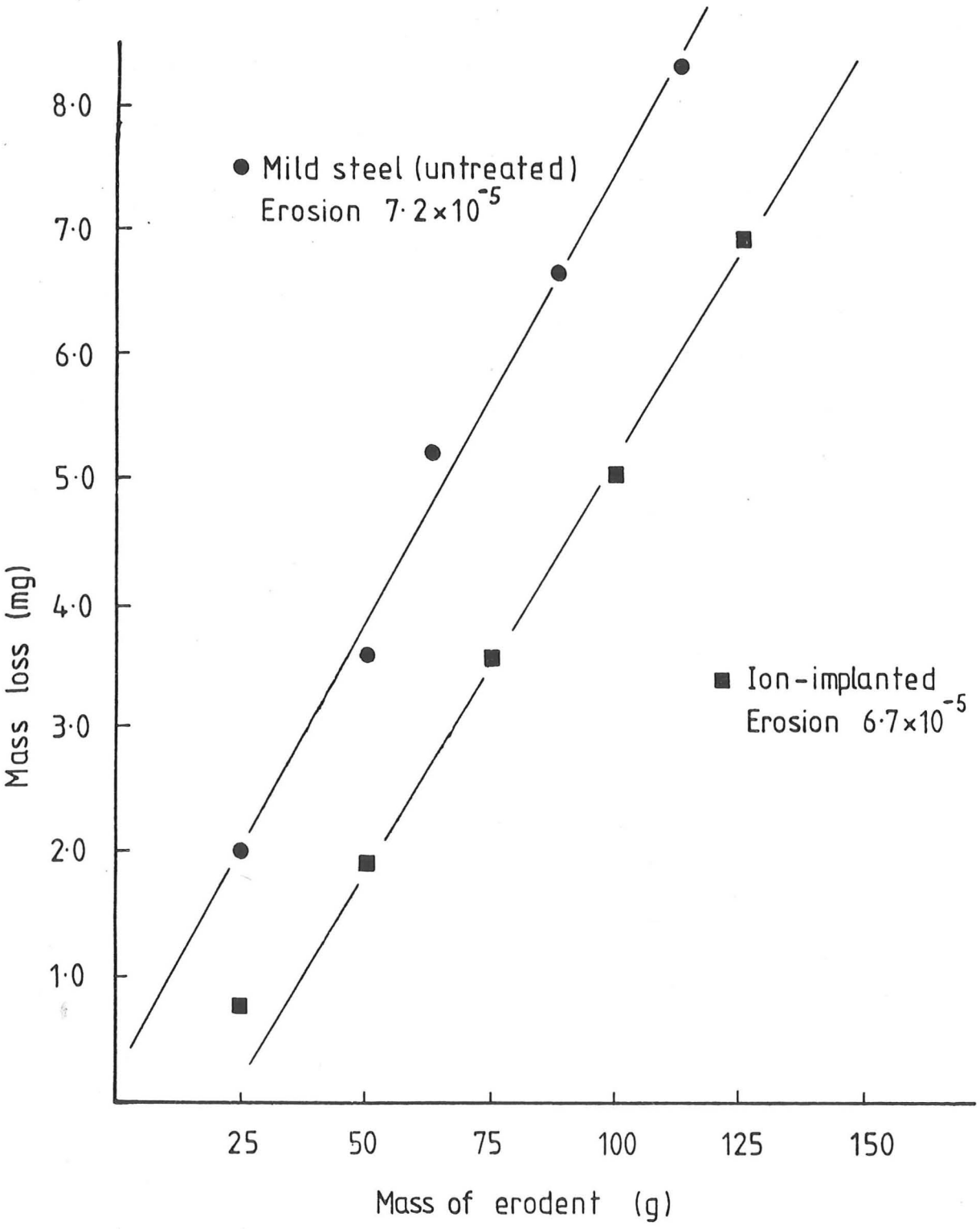

Figure 9.2 : Cumulative mass loss curve for ion-implanted mild steel, and control specimen

An investigation of the magnitude of the mass loss, and of the indentation parameters typical of these erosion tests, offers an explanation for the negligible effects of ion implantation.

9.4.1 Thickness of the ion implanted layer

There are two methods available for measuring the thickness of the nitrogen ion implanted layer. One method involves measuring the depth concentration profile of nitrogen, while the other involves ultramicro-hardness measurements.

The suppliers of the ion implanted specimens (B.P. Research Centre, Sunbury-on-Thames) provided the results of Auger depth concentration tests for a sample of the same steel after implantation to a dose level of 2×10^{17} N(ions) per cm^2. This is equivalent to one quarter of the dose level of the specimens which were used in the erosion experiments.

Auger spectroscopy involves scanning an electron beam across the surface of the specimen and analysing the energies of the electrons which are 'reflected' from the specimen. Some of the detected electrons result from elastic scattering of the scanning beam, while others will have been liberated from the surface by inelastic interactions. Such inelastic interactions will result in vacancies in the atomic orbitals of atoms lying very close to the surface. Electronic rearrangements within the surface will occur to fill these vacancies; these rearrangements result in the liberation of electrons (Auger electrons) with characteristic energies. The Auger electrons are very low in energy, and only those released from atoms within the uppermost few atomic layers will escape the surface and

be detected. In this way the Auger technique can be used to sample only the top few atomic layers, unlike alternatives such as energy dispersive x-ray analysis (EDAX) which sample large subsurface volumes (of the order of microns in diameter, Goldstein (1974)).

To construct a concentration versus depth profile, the surface is sequentially removed by argon ion bombardments ('sputtering') and Auger spectroscopy repeated on the newly created surface at each stage. Figure 9.3 is a plot of composition versus sputtering time for an ion-implanted mild steel specimen. The sputtering rate was 17.5nm min^{-1}, which allows an estimate of the thickness of the ion-implanted layer of 175nm to be made.

Samples of the materials used in the erosion tests with silica flour, both the ion-implanted and untreated control material were subjected to ultra-microhardness tests by Dr J B Pethica (Brown Boveri Research Centre, Baden, Switzerland). The method used in this work can detect a change of hardness as small as 20%, at indenter penetration depths as small as 30nm. Pethica et al (1982) estimated that at a penetration depth of 50nm the hardness measured will be due almost entirely to material within 200nm of the surface.

Figure 9.4 (a) illustrates the results of the ultramicrohardness measurements of the mild steel specimens. (For comparison the results of microhardness measurements of nitrogen ion implanted Armco iron, taken from Pethica et al (1982) are presented in Figure 9.4 (b)). It is not possible, from these results, to estimate the depth of the implanted layer on the mild steel specimens. The scatter in the results is thought to be due to surface oxidation and poor surface finish (before the ion implantation treatment). Since completing this work B P Research Centre have reported

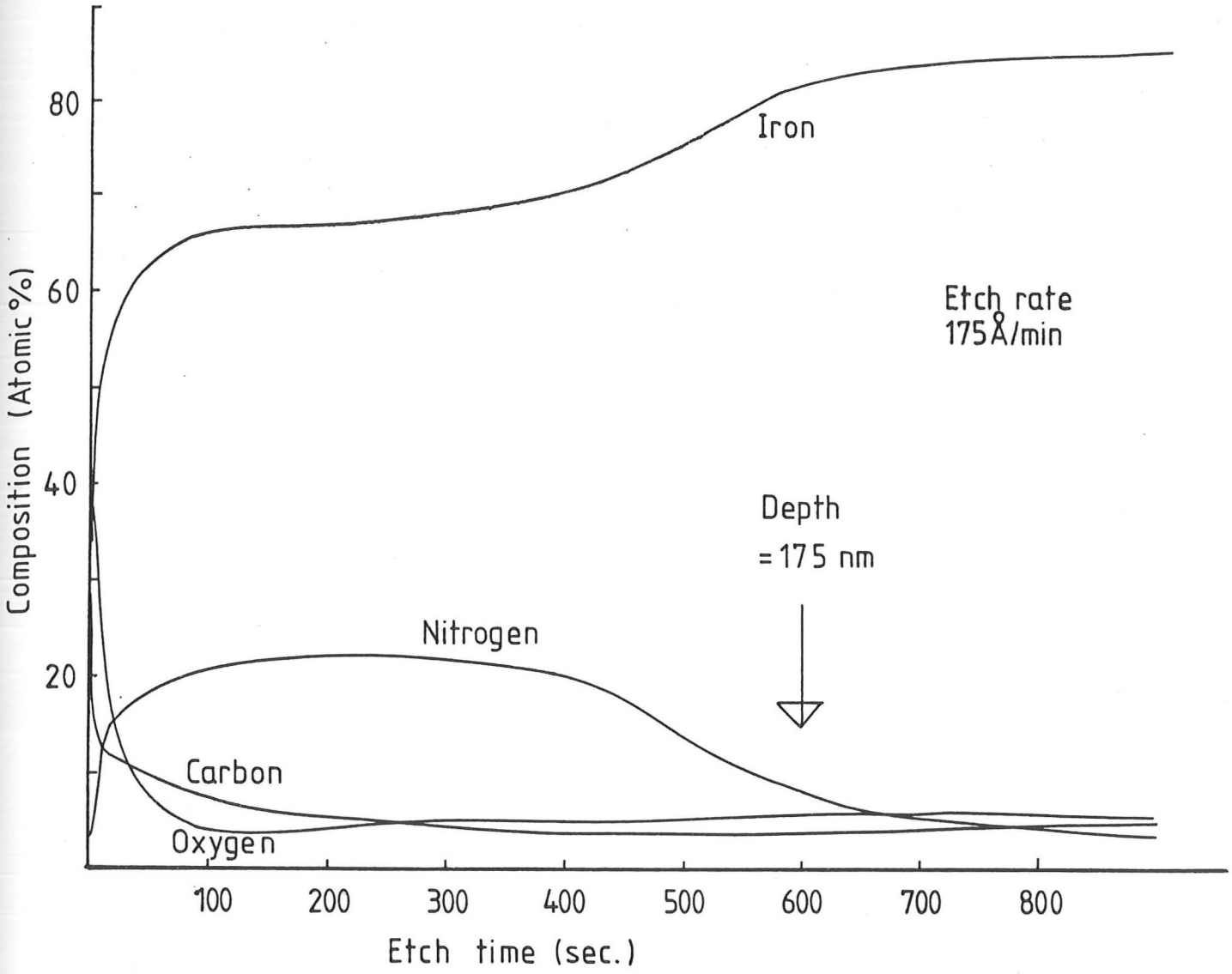

Figure 9.3 : Concentration depth profile for ion implanted mild steel (measured by Auger spectroscopy)

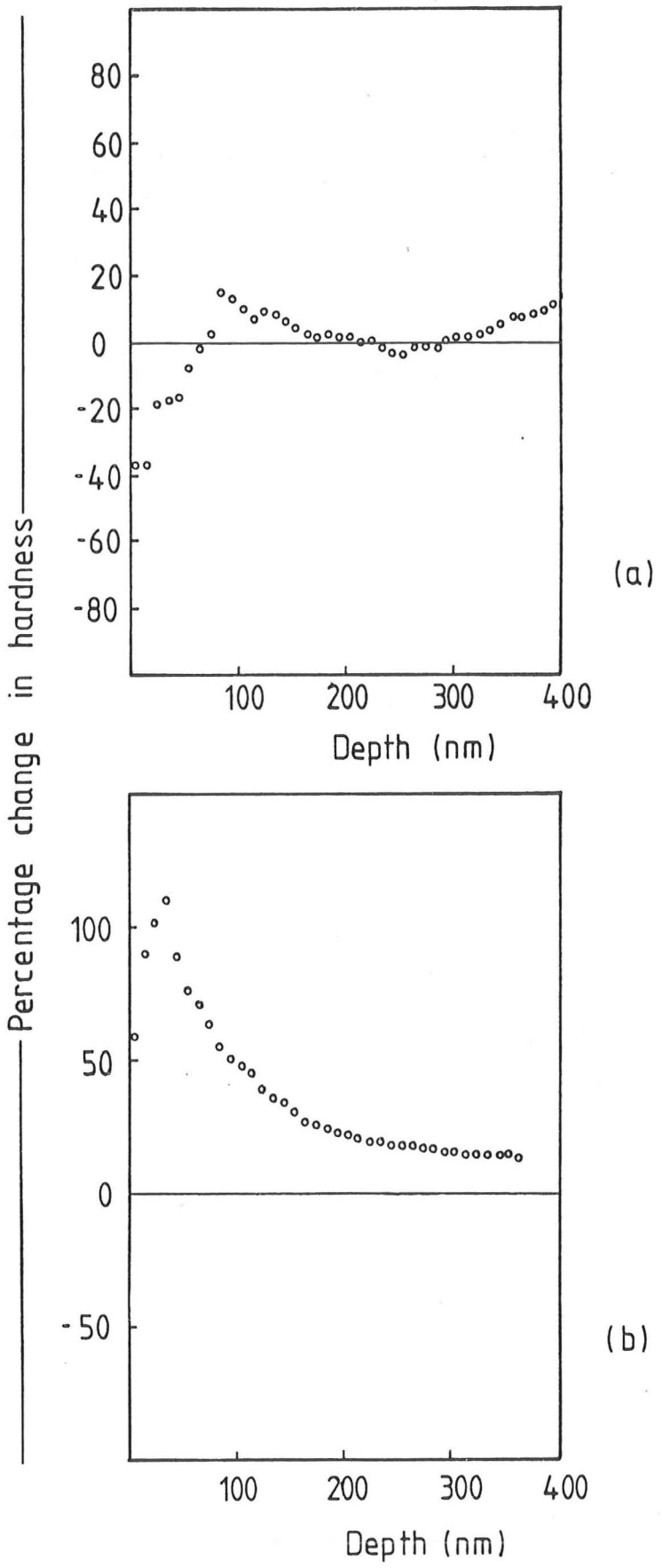

Figure 9.4 : (a) Ultramicrohardness survey of nitrogen ion implanted mild steel (dose rate 8 x 10^{21} ions/m^2)

(b) Ultramicrohardness survey of Armco iron nitrogen ion implanted (dose rate 3.5 x 10^{21} ions/m^2). After Pethica et al (1982)

that the results of independent tests on implanted specimens from the same batch indicate a low standard of control during implantation by their suppliers.

The ultramicrohardness results, and the anomalous results for normal impingement may be explained by poor specimen preparation. Insufficient specimens, from this treatment batch, were available to complete a full investigation. It was considered worthwhile to further investigate the effect of increased incubation; details are presented in the remainder of this discussion.

Pethica et al (1982) reported that for a range of materials, ion types and dose levels, the depth of the implanted layer is relatively insensitive to ion dose level. His measurements indicate that although maximum concentration or surface hardness may vary, for a range of materials and implantation conditions the thickness of the implanted layer is of the order of 100nm.

It is concluded from this, and from the results of Auger spectroscopy, that a value of 200nm may be taken as an estimate of the maximum thickness of the ion implanted layer for the specimens used in these experiments.

9.4.2 Estimate of the mass of the ion implanted layer

The erosion tests at normal impact concentrate the damage in a circular area on the surface of the specimen, which is approximately 8mm in diameter. At glancing angles of impingement the damaged area is elliptical,

and two distinct regions are visible within this area (this effect was reported by Lapides and Levy (1980)). The majority of the weight loss occurs within an inner ellipse, the area of which can be taken as approximately equal to the area of the damaged region under conditions of normal impingement. If it is assumed that the depth of the implanted layer is 2×10^{-7}m (discussed above), and that the density of the implanted layer is not significantly different from the density of mild steel (approximately 7.8×10^{3}kgm^{-3}, Smithells (1976)) it can be calculated that the mass of the implanted layer is approximately 0.08mg. From Figure 9.2 it is possible to estimate that this mass corresponds to the mass loss caused by only 7.5g of erodent impinging on the surface of the ion implanted specimen. The difference in incubation periods between the ion implanted specimen and the untreated mild steel control, is illustrated in Figure 9.2. The implanted specimen was eroded by 25g more erodent than the control specimen, before steady state erosion behaviour was established. Therefore, although the improvement to erosive wear resistance resulting from ion implantation is very small in this example, it appears that the mass loss process is influenced until a layer approximately three times the thickness of the implanted layer has been removed.

9.4.3 Indentation parameters

Figure 9.5 illustrates the geometry of indentation by a rigid sphere. From simple geometry, the following relationships may be derived.

$$h \simeq a^2/2r \quad \text{(for small h)} \qquad \ldots (1)$$

and

$$V \simeq \frac{\pi a^4}{4r} \qquad \ldots (2)$$

where V is the volume of the indent.

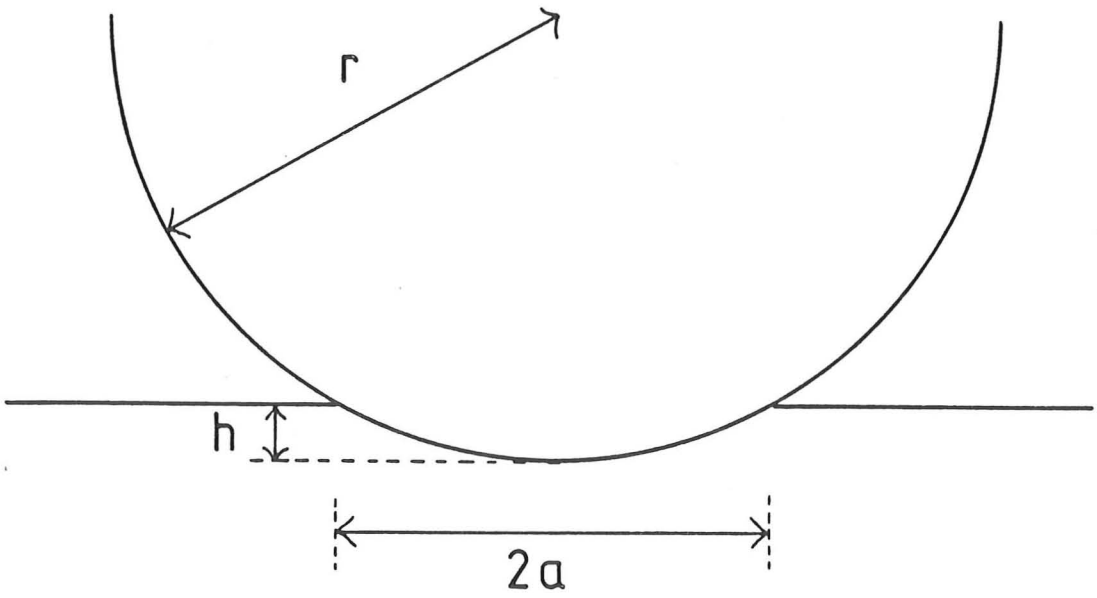

Figure 9.5 : Indentation geometry

By equating the initial kinetic energy of the impinging sphere with the work done in forming the indentation, it may be shown (Tabor (1951)) that:

$$a \simeq 2^{\frac{1}{2}} \, r \, v^{\frac{1}{2}} \left(\frac{2\sigma}{3P}\right)^{\frac{1}{4}} \qquad \ldots (3)$$

where v = velocity of spherical projectile

P = quasi-static indentation hardness (pressure to cause indentation)

σ = density of sphere

Using equations (1) and (3) we can estimate the depth of indentation for a given particle size, density and velocity impinging normally on to the target surface. For non-normal impacts an estimate of indentation depth can be made using the normal component of the particle velocity ($v \sin\alpha$, where α is the impingement angle), as the effective velocity causing penetration of the particles. This assumption follows Sheldon and Kanhere (1972), and is used to obtain a first approximation to the indentation depth.

Figure 9.6 plots the depth of indentation versus the particle velocity for a 40μm silica flour particle (which is assumed to be spherical) impinging at a range of angles, α, to the target surface.

The experimental conditions for the erosion tests using silica flour which were described in section 9.3 (results shown in Figure 9.2) are indicated in Figure 9.6 by the point labelled A. The analysis presented above predicted that the depth of indentation will be inversely proportional to the square root of the target surface hardness. The results of Pethica et al (1982) suggest that an estimate for the hardness of the implanted steel of double the untreated material hardness would be very optimistic.

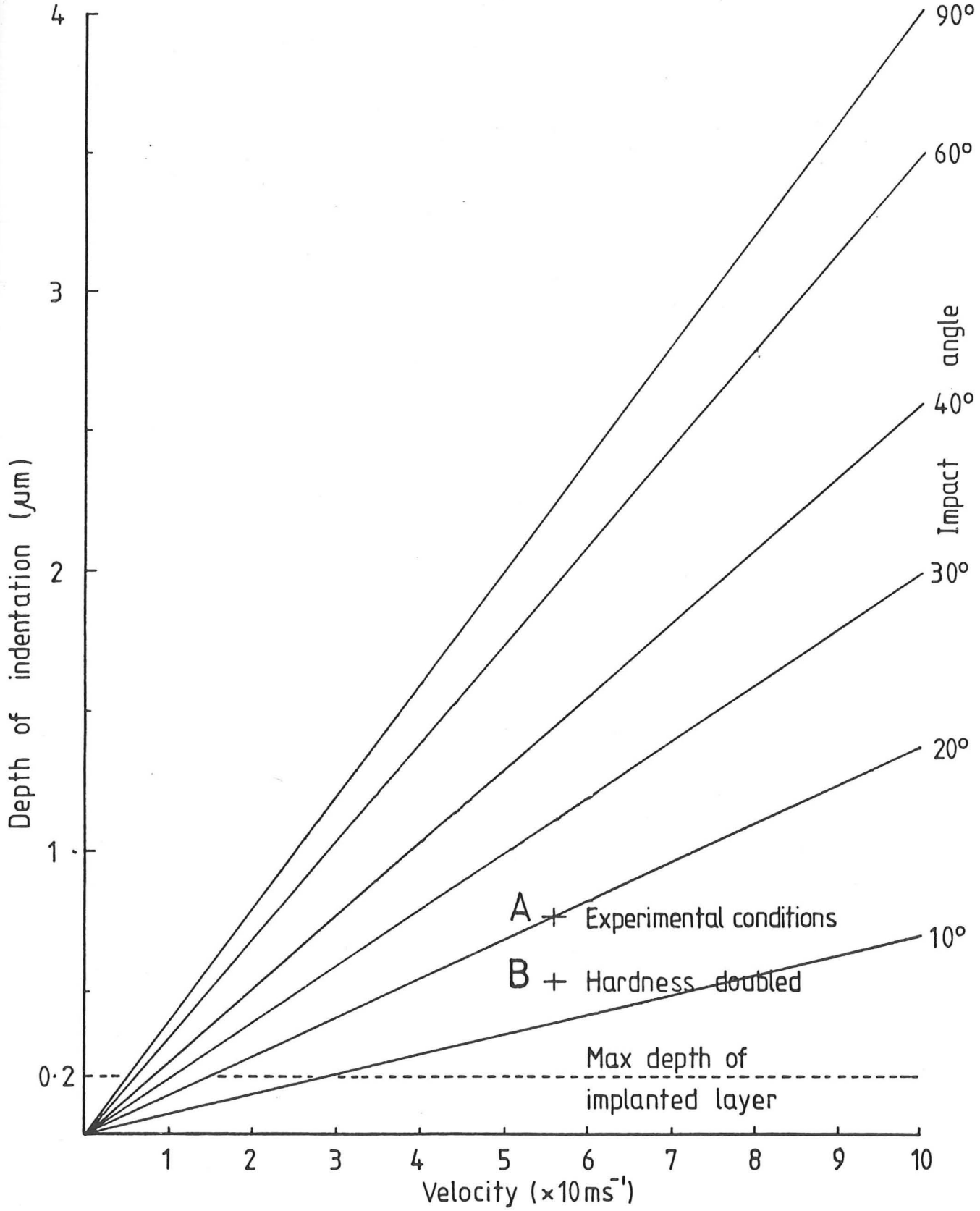

Figure 9.6 : Depth of indentation vs particle velocity (for 40μm silica particles)

Point B on Figure 9.6 indicates the estimated indentation depth, under the conditions of the erosion test using silica flour, assuming the implanted material was double the hardness of the untreated steel. Thus the true situation, representing the erosion of the ion implanted material will lie somewhere between the points A and B. Also included on this figure is a line showing the estimated maximum depth of the implanted layer (see section 9.4.1 above). It can be seen that the estimated thickness of the ion implanted layer is considerably less than the depth penetrated by the impinging particles.

9.4.4 Summary and general discussion

An estimate of the depth of the ion implanted layer has been used to compare the scale of the modification of the surface by ion implantation, with the scale of the surface damage caused by erosion.

First, the total mass of material affected by ion implantation has been shown to be negligible when compared with the mass of material removed from the surface by the action of only 100g of erodent. The results of experimental tests indicated that the complete ion implanted layer was removed during the earliest stages of incubation, and that the implantation of nitrogen ions had no effect on the steady state erosion of mild steel.

Second, the depth of the ion implanted layer is considerably less than the depth of penetration of the impinging particles, predicted by a simple model. The true significance of this observation, and its relevance to erosive wear, must be considered in the light of the following facts:

(i) The abrasive particles (silica flour) used in these experiments were not spherical. Consequently, the depth of penetration estimated by the model is probably an underestimate.

(ii) The assumption that the depth of penetration is independent of the component of the velocity of the particle resolved parallel to the target surface may prove invalid in the case of angular particles. The situation will be further complicated by the rotation of the particle during indentation.

(iii) The depth of indentation is only one measure of the scale of indentation damage. Tabor (1951) suggested that the volume of metal which is plastically deformed around an indentation is comparable with the volume of the indentation; this is for the simple case of the indentation of an 'infinite' block. The case under consideration in the present study is that of a hardened layer on the surface of softer bulk material. As reported above, Pethica et al (1982) suggested that at a penetration depth of 50nm the hardness measured will be due almost entirely to material within 200nm of the surface. Clearly, if the impinging particle is to interact only with material which has been hardened by ion implantation only penetration depths of 50nm or less will be tolerable. Inspection of Figure 9.6 reveals that this will only be achieved with particle velocities considerably less than $10ms^{-1}$ when eroding with 40μm spherical silica particles.

(iv) No consideration has been given to the actual mechanism of material removal. The information presented in Figure 9.6 suggests that ion implantation should be most effective in

increasing erosion resistance at glancing angles of impingement. However, it is known that, with angular erodent (see Chapter 8), maximum erosion occurs at glancing angles of impingement. Consequently, under these conditions, the complete ion implanted layer would be removed more rapidly.

(v) The formation of a hard surface layer may not be advantageous if such a layer were found to be brittle under erosive conditions. If Figure 8.10 (Chapter 8) is consulted, it can be seen that erosion increased with increasing hardness for steels of hardnesses in the range 128-840 ($kgfmm^{-2}$, Vickers) at near normal angles of impingement (Wellinger (1949)).

It can thus be concluded that while the model is clearly an over simplification of the true situation, in the erosion of ion implanted mild steel by angular silica flour particles, consideration of (i) to (v) above suggests that the scale of the implanted surface layer is indeed insignificant compared with the depth of penetration of the impinging particles.

9.5 CONCLUSIONS

Ion implanted mild steel specimens have been tested in an air-blast erosion tester in parallel experiments with mild steel control specimens. Mass loss measurements and scanning electron microscopy of the eroded surfaces revealed no significant change in erosive behaviour on ion implantation. Evidence of poor specimen preparation, and control of the implantation process, has been found (and independently reported by the supplier of the specimens).

Estimates are made of the thickness of the ion implanted layer, and of the depth of penetration of the impinging particles. The total mass of the implanted layer is estimated, and compared with experimentally measured erosion rates.

It is concluded that under the erosion conditions tested in this work, ion implantation does not significantly improve erosion resistance. The analysis of the indentation process suggests that if an increase in erosive wear resistance is to be achieved either the depth of the implanted layer, or its hardness (and preferably both) must be increased. It is unlikely that very large changes in these parameters will be achievable, and so ion implantation should only be considered as a surface treatment in mildly erosive environments. It is possible, for example, that for the case of very small particles travelling at low velocities, nearly parallel to the implanted surface, ion implantation may result in increased erosion resistance. A practical example of this type of erosion would be slurry erosion under conditions of laminar flow.

A similar conclusion has been reached by Shepard and Suh (1982) who found that in 'pin-on-disc' testing with low loads and under lubricated conditions, ion implantation increased the abrasive wear resistance of metals. However, under more aggressive conditions, for example high loads and dry sliding, ion implantation was found to have little effect on the abrasive wear resistance.

Shepard and Suh also tested specimens which had been surface hardened by ion nitriding. Jones et al (1973) described this process, which is also known as 'glow-discharge nitriding' or 'plasma nitriding'. Child (1979)

Estimates are made of the thickness of the ion implanted layer, and of the depth of penetration of the impinging particles. The total mass of the implanted layer is estimated, and compared with experimentally measured erosion rates.

It is concluded that under the erosion conditions tested in this work, ion implantation does not significantly improve erosion resistance. The analysis of the indentation process suggests that if an increase in erosive wear resistance is to be achieved either the depth of the implanted layer, or its hardness (and preferably both) must be increased. It is unlikely that very large changes in these parameters will be achievable, and so ion implantation should only be considered as a surface treatment in mildly erosive environments. It is possible, for example, that for the case of very small particles travelling at low velocities, nearly parallel to the implanted surface, ion implantation may result in increased erosion resistance. A practical example of this type of erosion would be slurry erosion under conditions of laminar flow.

A similar conclusion has been reached by Shepard and Suh (1982) who found that in 'pin-on-disc' testing with low loads and under lubricated conditions, ion implantation increased the abrasive wear resistance of metals. However, under more aggressive conditions, for example high loads and dry sliding, ion implantation was found to have little effect on the abrasive wear resistance.

Shepard and Suh also tested specimens which had been surface hardened by ion nitriding. Jones et al (1973) described this process, which is also known as 'glow-discharge nitriding' or 'plasma nitriding'. Child (1979)

reviewed many surface hardening methods, and produced results showing that surface hardening resulting from ion nitriding extended to depths in excess of 0.1mm (i.e. three orders of magnitude greater than that achieved by ion implantation). Shepard and Suh (1982) reported that under more aggressive abrasive wear conditions (i.e. dry sliding under heavy loads) surfaces treated by ion nitriding suffered less wear than those treated by ion implantation. They reported that a major advantage of the ion implantation process was the quality of the surface finish after treatment. Ion nitriding, although having the advantage of low cost, produced a roughened surface requiring machining.

It is concluded that in the case of mild steel, eroded by large particles (angular or spherical) at velocities in excess of $50ms^{-1}$, nitrogen ion implantation does not significantly increase erosion resistance. Under certain, very specific, erosion conditions, the ion implantation technique may prove useful, especially if the maintainance of surface finish is of primary importance. In general, however, an alternative (and possibly less costly) technique should be sought.

CHAPTER 10 : CONCLUSIONS

Detailed conclusions have been presented at the end of each chapter. The aims of this chapter are, first, to summarise the achievements of this work, and second, to outline the areas which seem most worthy of further study.

10.1 EROSION BY SOLID SPHERICAL PARTICLES AT NORMAL INCIDENCE

As a result of a careful experimental investigation a new mechanism has been proposed for the erosion of ductile metals under the conditions of normal or near normal impact of spherical or rounded particles. It is under these conditions that the accepted micromachining mechanisms fail to accurately describe the erosive wear of ductile metals.

The proposed mechanism involves the establishment of a hard subsurface layer containing fragments of oxide and erodent particles, and the back extrusion of bulk material through breaks in this layer. An analysis of the pressure required to drive this extrusion process was performed. An energy balance using this estimated pressure indicates, in agreement with previous investigations, that only a small fraction of the available kinetic energy of the impinging particles is needed to drive the postulated erosion process.

Further analyses of the observed deformations of eroded specimens indicate that considerable plastic deformation occurs in the bulk material underlying the hard subsurface layer. Suggestions are made for further experiments which will enable direct measurements of the subsurface residual stresses to be made.

Further work must now be done to investigate the range of erosion conditions over which this back extrusion process will operate. A greater understanding of the properties of the subsurface layer containing embedded debris may prove useful in developing materials with increased resistance to erosive wear. It is possible that the stable subsurface structure developed by erosion may be of use as a form of mechanical surface treatment. The practice of shot peening is already utilised as a means of producing residual stresses to increase the fatigue life of components subject to cyclic stresses. The additional hard layer of embedded debris may increase the resistance of the surface to other forms of wear. Khruschov (1974) reported that the impregnation of metal by abrasive grains had a substantial influence on its abrasive wear resistance.

10.2 PARTICLE VELOCITY MEASUREMENT

Considerable work has been carried out in developing a new, microcomputer-based device for measuring the velocity of the erodent particles in an erosion test. Complex problems, both of programming and of electronic circuit design, have been solved to allow preliminary measurements of particle velocity to be made. These results confirm the viability of the method, and suggestions are made concerning the improvements necessary before the technique can be employed for routine measurements at velocities of interest in erosion testing (up to, say, $200 ms^{-1}$).

10.3 THE EFFECT OF PARTICLE SHAPE ON EROSION

A detailed literature survey has been performed of the methods available for shape measurement. Conclusions are drawn from this survey, concerning the methods likely to prove useful in erosion studies.

Experiments have been performed in which mild steel is eroded by glass particles of two different particle shapes. Completely different erosion responses were observed for each erodent type.

Angular glass particles gave rise to a typically 'ductile' erosion response, with maximum erosion occurring at glancing angles of impingement. Examination of the surfaces of mild steel specimens eroded with crushed glass erodent particles suggested that the weight loss was due to a micro-machining process.

Spherical glass particles gave rise to a typically 'brittle' erosion response, with maximum erosion occurring at normal impingement. Examination of the surfaces of mild steel specimens eroded by glass beads suggested that the weight loss resulted from the formation and detachment of surface flakes.

The results have important consequences for the established methods of erosion testing and classification. First, it is possible that a similar change in erosion behaviour may accompany a change of particle size, particle hardness, or particle velocity. Care must be taken in the design of experimental programmes to ensure that such a transition is detected. The determination of the effect of impact angle on erosion is time consuming, but provides important information, which, together with examination of eroded surfaces, enables the weight loss mechanism to be identified. Second, both erosion responses observed in the tests on mild steel involved ductile deformation of the surface. Conventionally one response would have been classified as a brittle failure mode. This convention must now be questioned, and care taken in future in the classification of erosion response.

Finally, work must be done to correlate erosive behaviour with one of the suggested measurements of shape. Investigations into all aspects of erosion are confused by the inability to isolate the effects of erodent particle shape.

10.4 THE EFFECT OF ION IMPLANTATION ON EROSION

The implantation of mild steel surfaces by nitrogen ions has been shown experimentally to have little or no effect on its erosion resistance. An analysis of the dynamic indentation parameters is used to interpret this result. Alternative surface treatments, such as ion or plasma nitriding, which affect the surface to significantly greater depths, have been suggested as more effective for improving erosion resistance.

REFERENCES

The major conferences are abbreviated as follows :

Erosion by Liquid and Solid Impact : ELSI - nth

American Society for Mechanical Engineers International Wear conferences : Wear of Materials - Year

Full details of these conferences are given in the alphabetical list below.

M ALDERSON and D A TUITT
ELSI IV (1974)

D R ANDREWS and J E FIELD
J. Phys. D : Appl. Phys., 15 (1982) 2357-2367

P ASCARELLI
United States Army Materials and Mechanics Research Centre
Technical Report No. 71-47 (1971)

V ASHWORTH, W A GRANT, R P M PROCTOR
'IPAT 77' Conf. Ion Plating and Allied Techniques
CEP Consultants, Edinburgh, June (1977) 195-201

ASTM (1977) ANSI/ASTM G40-77
Standard Terminology relating to Erosion and Wear
American Society for Testing and Materials, Philadelphia

ASTM (1983) ANSI/ASTM G76-83
Standard Practice for Conducting Erosion Tests by Solid Particle Impingement.
American Society for Testing and Materials, Philadelphia

B AVITZUR
Ann. Rev. Mater. Sci. 7 (1977) 261-300

C BABU RAO and D K BHATTACHARYA and BALDEV RAJ
Pract. Met. 19 (1982) 699-712

R H BARKALOW, J A GOEBEL, F S PETTIT
ASTM Spec. Tech. Publ. 664 (1979) 163-192

M S BECK
J Phys. E : Sci. Instrum., 14 (1981) 7-19

J K BEDDOW
Testing and Characterisation of Powders and Fine Particles
Ed. J K Beddow and T Meloy, Heyden Press (1980) 44-176

J K BEDDOW, A F VETTER and K SISSON
Powder Met. Int. 8 No 2 (1976a) 69-76
Powder Met. Int. 8 No 3 (1976b) 107-109

R BELLMAN and A LEVY
Wear 70 (1981) 1-27

J C BEZDEK
Advanced Particulate Morphology
Ed. J K Beddow and T Meloy, CRC Press (1977) 121-140

J G A BITTER
Wear 6 (1963a) 5-21
Wear 6 (1963b) 169-190

L L BRASS
M.S. Thesis, Lawrence Berkeley Laboratory, University of California (1977)

B S Standard 1470 (1972)
Wrought aluminium and aluminium alloys for general engineering purposes - plate, sheet and strip. (British Standards Institution)

R BROWN and J W EDINGTON
Wear 69 (1981a) 369-382

R BROWN , E J JUN and J W EDINGTON
Wear 70 (1981b) 347-363

R BROWN and J W EDINGTON
Wear 71 (1981c) 113-118

R BROWN, E J JUN and J W EDINGTON
Wear of Materials (1981d) 583-591

R BROWN and J W EDINGTON
Wear 77 (1982a) 347-353
Wear 79 (1982b) 335-346

R BROWN, S KOSCO and E J JUN
Wear 88 (1983) 181-193

C R CALLADINE
Engineering Plasticity
Pergamon Press (1969) 104 -

G CARTER, M J NOBES and K I ARSHAK
Wear 65 (1980) 151-174

K S CHERNYAVSKII
Ind. Lab. USSR 44 No 9 (1978a) 1241-1251
Ind. Lab. USSR 44 No 12 (1978b) 1694-1698

H C CHILD
Surface Hardening of Steel
Engineering Design Guides 37, O.U.P. (1979) 21-22

A K COUSENS and I M HUTCHINGS
Wear of Materials (1983a) 382-389
ELSI VI (1983b) Paper 41

R DAVIES
Powder Tech. 12 (1975) 111-124
Testing and Characterisation of Powders and Fine Particles
Ed. J K Beddow and T Meloy. Heyden Press (1980) 138-

G DEARNALEY and N E W HARTLEY
Proc. 4th Conf. on Sci. and Ind. Applns. of Small Accelerators,
Denton IEEE New York (1976) 20-29

G DEARNALEY
NATO Advanced Study Institutes Series
Series B : Physics, Vol 47, Ed. A Perez and R Coussement
Site Characterisation and Aggregation of Implanted Atoms in Materials
Plenum Press (1978) 33-63

G DEARNALEY, P D GOODE and N E W HARTLEY et al
'IPAT 79' Conf. on Ion Plating and Allied Techniques,
London, CEP Consultants, Edinburgh (1979) 243-254

G DEARNALEY
J Metals Sept 35 (1982) 18-28

ELSI IV Proceedings of the Fourth International Conference on Rain Erosion and Associated Phenomena
Ed. A A Fyall and R B King
Meersburg Germany (1974)

ELSI V Proceedings of the Fifth International Conference on Erosion by Liquid and Solid Impact
Cavendish Laboratory, University of Cambridge (1979)

ELSI VI Proceedings of the Sixth International Conference on Erosion by Liquid and Solid Impact.
Ed. J E Field and N S Corney
Cavendish Laboratory, University of Cambridge (1983)

H E EXNER and E LINCK
Powder Met. Int., 9 No 3 (1977) 131-133

I FINNIE
Proc. 3rd National Congress of Applied Mechanics
American Society of Mechanical Engineers (1958) 527-532
Wear 3 (1960) 87-103

I FINNIE, J WOLAK, Y KABIL
J Mat. 2 No 3 (1967) 682-700

I FINNIE
Wear 19 (1972) 81-90
Corrosion-Erosion Behaviour of Materials
Ed. K Natesan AIME (1978) 118-126

H F FISCHMEISTER
Z Metallkunde 65 (1974) 558-562

A G FLOOK
Powder Tech. 21 (1978) 295-298
Proc. 2nd European Symposium on Particle Characterisation
Nuremberg (1979) 591-599

P S FOLLANSBEE, G B SINCLAIR and J C WILLIAMS
Wear of Materials (1981) 577-582

N GANE and J M COX
Phil. Mag. 22 No 179 (1970) 881-891

N GANE and M J MURRAY
ELSI V (1979) Paper 40

J I GOLDSTEIN
ASTM Spec. Tech. Publ. 557 (1974) 86-136

G F GONZALEZ-RIVAS
Bachelor's Thesis, Massachusetts Institute of Technology, (1981)

J E GOODWIN
National Gas Turbine Establishment, Pyestock, Farnborough
Note NT 698 (1968)

J E GOODWIN, W SAGE and G P TILLY
Proc. Inst. Mech. Engrs (London) 184 (1969) 279-292

R G GREEN, H K KWAN, R JOHN and M S BECK
J. Phys. E : Sci. Instrum. 11 (1978) 1005-1010

G M GREEN, R TAGGART and D H POLONIS
Metallography 14 (1981) 191-212

M E GULDEN
ELSI V (1979) Paper 31

N E W HARTLEY
J Vac. Sci. Techn. 12 (1975) 485-489

W J HEAD, L D LINEBACK and C R MANNING
Wear 23 (1973) 291-298

R M HENRY
IEE Correlation Processing, Conference Digest (1979) No 32, 3/1-4

H HERMAN, W W HU, C R CLAYTON et al.
IPAT 79 Proc.Conf.Ion Plating and Allied Techniques, London,
CEP Consultants, Edinburgh (1979)

H HERMAN
Nuclear Inst. and Methods 182/183 (1981) 887-898

I M HUTCHINGS
Wear 35 (1975a) 371-374
Ph.D. Thesis, University of Cambridge (1975b)

I M HUTCHINGS, R E WINTER and J E FIELD
Proc. R. Soc. Lond. A 348 (1976) 379-392

I M HUTCHINGS
J. Phys. D : Appl. Phys, 10 (1977) L179-L184
ELSI V (1979a) paper 36
ASTM Spec. Tech. Publ. 664 (1979b) 59-76
Wear 70 (1981) 269-281

E ITURBE, I G GREENFIELD and T W CHOU
ELSI V (1979) paper 30

L K IVES and A W RUFF
Wear, 46 (1978) 149-162
ASTM Spec. Tech. Publ. 664 (1979) 5-33

W JOHNSON and P B MELLOR
Engineering Plasticity, Van Nostrand Reinhold (1973) Chapter 13

C K JONES, D J STURGES and S W MARTIN
Metal Progress Dec (1973) 62-63

M H JONES and R LEWIS
ELSI V (1979) Paper 52

B H KAYE
Powder Tech. 21 (1978) 1-16

M M KHRUSCHOV
Wear 28 (1974) 69-88

I KLEIS
Wear 13 (1969) 199-215

I KLEIS, H UUEMOIS, L UKSTI, T PAPPEL
Wear 31 (1975) 403-408

T H KOSEL, A P L TURNER and R O SCATTERGOOD
Corrosion-Erosion Behaviour of Materials
Ed. K Natesan AIME (1978) 118-126
Wear of Materials (1979) 192-204

W C KRUMBEIN
J Sed. Pet. 11 No 2 (1941) 64-72

L LAPIDES and A LEVY
Wear 58 (1980) 301-311

G LEES
Sedimentology 3 (1964) 2-21

A LEVY
ELSI V (1979) Paper 39
Preprint no LBL 15240, Lawrence Berkeley Laboratory, University of California (1982)

G LEW, J K BEDDOW and A F VETTER
Powder Met. Int. 11 No 4 (1979) 165-168

J MAJI and G L SHELDON
ASTM Spec. Tech. Publ. 664 (1979) 136-147

S MALKIN
Wear 68 (1981) 391-396

B MANDELBROT
Fractals, Form, Chance and Dimension
W H Freeman, San Francisco, CA, USA (1977)

R A MAYVILLE
MS Thesis, Lawrence Berkeley Laboratory, University of California
LBL 7333 (1978)

A I MEDALIA
Powder Tech. 4 (1970) 117-138

T MELOY
Testing and Characterisation of Powders and Fine Particles
Ed. J K Beddow and T Meloy, Heyden Press (1980) 1-

D MILLS and MASON
ELSI V (1979) Paper 51

A MISRA and I FINNIE
Wear 65 (1981) 359-373

M NAIM and S BAHADUR
Wear of Materials (1983) 340-345

J H NEILSON and A GILCHRIST
Wear 11 (1968) 111-122

A NIKU-LARI
1st Int. Conf. Shot Peening Paris 1981
Ed. Niku-Lari Pergamon Press (1982)

A J NINHAM and I M HUTCHINGS
ELSI VI (1983) Paper 50

J B PETHICA, R HUTCHINGS and W C OLIVER
Proc. IBMM-82 Grenoble Sept (1982)

D POHL and F REDLINGER
Powder Met. Int. 9 No 4 (1977) 164-168

V PONNAGANTI, D E STOCK and G L SHELDON
Proc. Symp. 'Polyphase Flow and Transport Technology'
ASME San Francisco (1980)

C M PREECE and N H MACMILLAN
Ann. Rev. Mat. Sci. 7 (1977) 95-121

E RAASK
Wear 13 (1969) 301-315
ELSI V (1979) paper 41

E RABINOWICZ
ELSI V (1979) paper 38

P V RAO, S G YOUNG and D H BUCKLEY
NASA Tech. Memo 82933, National Technical Information Service,
Springfield, Virginia (1982)
Wear 85 (1983) 223-237

S B RATNER and E E STYLLER
Wear 73 (1981) 213-234

D G RICKERBY and N H MACMILLAN
ELSI V (1979) paper 29
Wear 60 (1980) 369-382
Wear 79 (1982) 171-190

D G RICKERBY
Wear 84 (1983) 393-395

S G ROBERTS and T F PAGE
Ion Implantation into Metals
Eds. V Ashworth, W A Grant and R P M Proctor
Pergamon Press (1982)

H C ROGERS
Ann. Rev. Mat. Sci 9 (1979) 283 -

A W RUFF and L K IVES
Wear 35 (1975) 195-199

A W RUFF and S M WIEDERHORN
Treatise on Mat. Sci. and Tech. 16 'Erosion'
Ed. Preece AC. Press (1979) 69-126

J SALIK and D H BUCKLEY
Wear of Materials (1981a) 592-596

J SALIK, D H BUCKLEY and W BRAINARD
Wear 65 (1981b) 351-358

L E SAMUELS and T O MULHEARN
J Mech. and Phys. of Solids 5 (1957) 125-134

G A SARGENT, M K KESHAVAN and H CONRAD
Microstructural Sci. 8 Ed. Stevens, Vander Voort and McCall (1980) 385-396

G A SARGENT, M K KESHAVAN, P K MEHROTRA and H CONRAD
Wear of Materials (1981) 613-618

S SARITAS, R P M PROCTOR, V ASHWORTH and W A GRANT
Wear 82 (1982) 233-255

A D SARKAR
Wear 87 (1983) 173-180

P O SCATTERGOOD and J L ROUTBORT
Wear 67 (1981) 227-232

H SCHWARZ and H E EXNER
Powder Tech. 27 (1980) 207-213

G L SHELDON and A KANHERE
Wear 21 (1972) 195-209

G L SHELDON
Trans. ASME J Eng. Mat and Tech. April (1977) 133-137

S R SHEPARD and N P SUH
Trans. ASME J. Lub. Tech. 104 (1982) 29-38

M M SHERMAN, E C ALEXANDER and A T HOPKINS
ELSI V (1979) paper 33

P G SHEWMON
ELSI V (1979) paper 37
Wear 68 (1981) 253-258

P G SHEWMON and G SUNDARARAJAN
Ann. Rev. Mat. Sci. (1983) 13 301-318

C E SMELTZER, M E GULDEN and W A COMPTON
Trans. ASME J Basic Eng. Sept (1970) 639-654

C J SMITHELLS
Metals Reference Book 5th edition
Butterworth and Co. Ltd. (1976)

G SUNDARARAJAN
Wear 84 (1983) 217-235

D TABOR
The Hardness of Metals, Clarendon Press (1951)
ELSI V (1979) Chairman's Message

G P TILLY and W SAGE
Wear 16 (1970) 447-465

G P TILLY
Wear 23 (1973) 87-96
Treatise on Mat. Sci. and Tech. 13 'Wear'
Ed. Douglas Scott Ac. Press (1979) 287-319

S TIMOSHENKO and S WOINOWSKY-KRIEGER
Theory of Plates and Shells, Engineering Societies Monographs McGraw Hill (1959)

S P TIMOTHY and I M HUTCHINGS
ELSI VI (1983) paper 43

P G TOWSON
MSc. Thesis, University of Cambridge (1980)

E E UNDERWOOD
Testing and Characterisation of Particles and Fine Powders
Ed. J K Beddow and T Meloy, Heyden Press (1980) 77

A K VIJH
Wear 39 (1976) 173-175

B VYAS
Treatise on Mat. Sci. and Tech. 16 'Erosion'
Ed. Preece (1979) 357-390

H WADELL
J. Geol. 40 (1932) 443-451
J. Geol. 41 (1933) 310-331

'Wear of Materials 1979', 'Wear of Materials 1981' and 'Wear of Materials 1983' all published by American Society for Mechanical Engineers, New York (1979, 1981 and 1983 respectively).

K WELLINGER
Z Metallkunde 40 (1949) 361-364

C D WOOD
U.S. Institute of Environmental Sciences.
Ann. Tech. Meeting (1966) 55-63

R ZAKS
Programming the 6502 3rd ed. Sybex Inc. (1980)

UNIVERSITY
LIBRARY
CAMBRIDGE